NATURE AND CHARACTERISTICS OF TROPOSPHERIC OZONE OVER JOHANNESBURG

ATHAM RAGHUNANDAN

Submitted in partial fulfilment of the requirements
for the degree of Master of Arts in the
School of Life and Environmental Sciences,
University of Natal

Durban
March 2002

PREFACE

The work described in this thesis was carried out in the School of Life and Environmental Sciences, University of Natal, Durban, from January 2001 to January 2003, under the supervision of Professor Roseanne D. Diab.

This study represents original work by the author and has not been submitted previously in any form to another University. Where use was made of work of others, it has been duly acknowledged in the text.

ACKNOWLEDGEMENTS

Undertaking a research project of this scope was a major task that I could not have accomplished without the assistance and commitment of many others.

My thanks are extended to:

Professor Roseanne D. Diab for her continuing support and guidance. She is an excellent, committed and inspiring supervisor who has shaped my thinking and has made the excitement and relevance of the field clear to me. I owe much to her for the arduous hours she spent critically reading and ensuring that the treatment of material was consistent throughout the write-up. Her thoughtful suggestions and comments have undoubtedly improved the quality and readability of the thesis.

Frank Sokolic (School of Life and Environmental Sciences, University of Natal, Durban) for his computing assistance on various occasions and allowing me the use of his programs concerning the computation of mean profiles and the conversion of ozone readings from parts per billion volume (ppbv) to Dobson Units (DU)

Fred Ellery (School of Life and Environmental Sciences, University of Natal, Durban) for teaching me how to run TWINSPAN (Two-Way Indicator Species Analysis) and the interpretation of output data

Marion Neal and Greg for their advice and insight on TWINSPAN and Isaak Abboy for his help with library resources

Aubrey Muswema (School of Life and Environmental Sciences, University of Natal, Durban) for assisting with the plotting of temperature profiles on tephigrams and the determination of stable layers

Charmaine John Kamadu, my girlfriend, for her continuing support and patience throughout

My family, friends and colleagues in our School for their encouragement

Gregory Scott (Council for Scientific and Industrial Research) for his help with the computation of standard deviations

The National Research Foundation (NRF) for providing funding for this research

National Oceanic and Atmospheric Administration (NOAA) Air Resources Laboratory (ARL) for the provision of the Hybrid Single-Particle Lagrangian Integrated Trajectory (HYSPLIT) transport and dispersion model and Real-time Environmental Applications and Display System (READY) website (http://www.arl.noaa.gov/ready.html) used in this research

MOZAIC (Measurement of Ozone and Water Vapor by Airbus In-Service Aircraft) for use of their data

The Almighty for His guidance

ABSTRACT

The aim of this thesis is to examine the nature and characteristics of tropospheric ozone over Johannesburg, South Africa. Ozone, water vapour and meteorological profile data, which form part of the MOZAIC (Measurement of Ozone and Water Vapor by Airbus In-Service Aircraft) database for the period 1995 to 2000 were utilized in this study.

The thesis is divided into two main parts. The first part deals with the computation of total tropospheric ozone. A clear seasonal cycle, with ozone peaking in September and October is found. It is suggested that the main reason for the spring maximum is biomass burning, combined with prevailing anticyclonic circulation patterns, which facilitate the build-up of ozone over the region. Variability in TTO is greatest in January, September and November and least during autumn and winter (April to July). The lower day-to-day variability in autumn and winter is a reflection of the more settled weather at this time. Interannual variability is least in January and April to June. The autumn and winter ozone values are more consistent and appear to represent background tropospheric ozone loadings on which the dynamic and photochemical influences of other months are superimposed.

High TTO events (>30 DU) occurred predominantly during September and October. Enhancements in the lower troposphere occurred mostly in September and seldom lasted for more than 1-2 consecutive days. It is suggested that these events are most likely due to effects of local surface pollution sources, either localised biomass burning or urban-industrial effects. An extended period of enhancement in the 7-12 km layer occurred from 14-17 September 1998 and again on 20 September 1998. The extended duration of this event suggests that it is due to an STE event. Confirmation of this was given in a case study of a particular MOZAIC flight on 16 September 1998 from Johannesburg to Cape Town.

The second part of the thesis deals with the classification of ozone profiles and is used to find pattern and order within the profiles. TWINSPAN (Two-Way INdicator SPecies ANalysis), a cluster analysis technique, was used to classify the profiles according to the magnitude and altitude of ozone concentration. Six distinct groups of profiles have been identified and their characteristics described.

The HYSPLIT (Hybrid Single-Particle Lagrangian Integrated Trajectory) trajectory model was used to relate the profiles to the origin of air masses, revealing clearly defined source regions. The mid-tropospheric peak in summer and the low to mid-tropospheric enhancement in spring is attributed to continental areas over central Africa and long-range transport while local sources are responsible for the winter low tropospheric enhancement. Reduced ozone values are due to westerlies bringing in clean maritime air.

The classification has highlighted three important findings. Firstly, it has emphasized the pronounced seasonality of ozone profiles. It is evident that seasons are dominated by particular patterns and by inference, the processes and transport patterns that shape individual profiles are seasonally dependent. Secondly, the widely recognized spring maximum in tropospheric ozone has been confirmed in this classification, but a new and equally high summer mid-tropospheric enhancement due to the penetration of tropical air masses from continental regions in central Africa has been identified. Thirdly, it is suggested that the computation of a mean profile and furthermore, extrapolation of trends based on a mean profile is meaningless, particularly for a location on the boundaries of zonally defined meteorological regimes.

LIST OF FIGURES

		Page
Figure 2.1	Geographical coverage of MOZAIC flights between August 1994 – July 1999. Red lines indicate percent in main directions (Source: MOZAIC-II: Technical Final Report, 2000: p 15)	7
Figure 2.2	Number of MOZAIC flights per year and main direction from Europe (August 1994 – July 1999) (Source: MOZAIC-II: Technical Final Report, 2000: p 14)	8
Figure 2.3	Number of flight hours per year achieved by MOZAIC operations (August 1994-July 1999) (Source: MOZAIC-II: Technical Final Report, 2000: p 14)	8
Figure 2.4	MOZAIC data recovery (%) between August 1994-July 1999 (Source: MOZAIC-II: Technical Final Report, 2000: p 14)	8
Figure 2.5	Front (left) and rear (right) view of the rack housing MOZAIC instrumentation (Source: MOZAIC website: http://www.aero.obs-mip.fr/mozaic/)	10
Figure 2.6	Removable probe plate pitot tube (top) and a Rosemount housing (bottom) (Source: MOZAIC website: http://www.aero.obs-mip.fr/mozaic/)	10
Figure 2.7	MOZAIC in-service instrumentation (Source: Marenco *et al.*, 1998: p 25637)	11
Figure 2.8	Plan of the MOZAIC ozone pumping system (Source: Thouret *et al.*, 1998a: p 25697)	12

Figure 2.9 Variations in the response of an ozone analyser over an operation period (March 28, 1996 to March 26, 1997) on board aircraft MSN-053 for three levels of the internal ozone generator (A, 0 ppbv; B, 80 ppbv; C, 510 ppbv). Accurate pre-flight and postflight calibrations, made at the laboratory, were in agreement within a 0.05% range (Source: Thouret *et al.*, 1998a: p 25698) 14

Figure 2.10 Aircraft intercomparisons (profiles):
(a) Paris 25/11/1994 – 50 min – AC49 / AC 51
(b) Frankfurt 04/03/1995 – 15 min – AC35 / AC53
(c) Osaka 09/06/1996 – 45 min – AC75 / AC 51
(d) Caracas 16/05/1999 – 90 min – AC35 / AC49
(Source: MOZAIC-II: Technical Final Report, 2000: p 17) 15

Figure 2.11 Cross section of the airborne MOZAIC humidity sensing device: humidity (Humicap-H) and temperature (PT100) sensors mounted in air sampling housing (Rosemount) (Source: Helten *et al.*, 1998: p 25644) 17

Figure 2.12 Mean uncertainty in percent RH of all 1995 MOZAIC relative humidity measurements (solid curve) as a function of static air temperature (bottom x axis). The corresponding altitude is indicated as the top x axis. The standard deviation of the mean is marked by the dashed curves. The region not covered by preflight and postflight calibrations (lower troposphere) is indicated with an estimated mean uncertainty (dashed/dotted line) (Source: Helten *et al.*, 1998: p 25650) 18

Figure 2.13 Relative humidity measured by MOZAIC humidity device, Lyman-Alpha hygrometer and cryogenic frost point hygrometer as function of flight time during descent of flight. Static air temperature (SAT, heavy line) and total recovery temperature (TRT, thin line) are shown in the upper panel of the figure (Source: Helten *et al.*, 1998: p 25651) 19

Figure 2.14 An intercomparison between static temperature (red line) and A340 static temperature (black dashed line) profiles for 20 September 1998 (Source: plotted from MOZAIC profile data) 24

Figure 2.15 A sample ozone profile as a function of barometric altitude (red line) and mid-layer altitude (black dashed line) for 28 August 1998 (Source: plotted from MOZAIC profile data) 28

Figure 2.16 5-day back trajectory HYSPLIT model results for 7 February 1996. Horizontal (top) and vertical (bottom) plots of back trajectories originating at 2.5, 5 and 7.5 km 30

Figure 3.1 Calculated zonal and annual mean fractional contribution to tropospheric ozone by industrial emissions and all fossil-fuel-related sources for the present day atmosphere (Source: Lelieveld and Dentener, 2000: p 3545) 34

Figure 3.2 Global distribution of lightning generated NO_x (Mg N) for (a) DJF, (b) MAM, (c) JJA, (d) SON and (e) the entire year. Values are based on LIS lightning measurements from 1988-2000 data and have a 0.5° resolution (Source: Bond *et al.*, 2002: p 1511) 38

Figure 3.3 Comparison of annual averages of nitrogen oxide emissions due to anthropogenic activity, biomass burning, soil release and lightning production in the tropics (Source: Bond *et al.*, 2002: p 1514) 38

Figure 3.4 Seasonal maps of the ratio of lightning nitrogen oxide production to the total from all four sources (anthropogenic activity, biomass burning, soil release and lightning) in the tropics. The values are given in percentages (Source: Bond *et al.*, 2002: p 1515) 39

Figure 3.5 Dependence of tropopause height (average) on time of year at Swan Island (17°N), Phoenix (33°N), North Platte (41°N) and International Falls (49°N) for the period 1946-1956 (Source: Staley, 1962: p 453) 45

Figure 3.6 Schematic representation of the mean circulation relative to the tropopause in the jet stream region, including a folded tropopause. J indicates the position of the jet stream (Source: Danielsen, 1968: p 517) 46

Figure 3.7 Conceptual model of the trajectories of ozone-rich air from the region of a tropopause fold in an upper-level trough behind a cold front and in the forward side of an anticyclone. L=low pressure; H=high pressure (Source: Danielsen, 1980: p 411) 47

Figure 3.8 A typical 200 hPa synoptic chart showing three types of cut-off low types: polar (P), subtropical (ST) and polar vortex (PV) and related jet streams (Source: Price and Vaughan, 1992: p 97) 48

Figure 3.9 Major circulation types governing the transport patterns of aerosols and trace gases within over and out of the southern African troposphere, together with the frequency of occurrence (bottom right) over the period 1988-1992 of, first the combined continental and ridging anticyclone classes (heavy solid line), second, the combined westerly waves/troughs and cutoff lows (light solid line), and third, easterly wave disturbances (dashed line). Surface flow over the oceans are given in isobars at mean sea level while contours of the 850-hPa surface are used over the land (Source: Tyson and Preston-Whyte: p 184) 50

Figure 3.10 Major low level transport modes likely to result in easterly or westerly transport from southern Africa or in recirculation within the anticyclonic system (Source: Garstang *et al.*, 1996: p 23723) 51

Figure 3.11 Daily variation of absolutely stable layers over Pretoria (southern Africa) during SAFARI-92. Stippled boxes indicate the height and depth of stable layers. Envelopes of continuous and discontinuous stable layers are indicated by cross-hatched regions enclosed by solid and dashed lines respectively. Light dashed lines depict the height of the 1200UT mixing depth. Circulation class for each day is shown by H (continental high), W (westerly disturbance) and E (easterly disturbance) (Source: Garstang *et al.*, 1996: p 23724) 52

Figure 3.12 Diagrammatic representation of the spatial extent of the 5-km absolutely stable layer (3 October 1992) and 3-km layer (6 October 1992) over southern Africa (Source: Garstang *et al.*, 1996: p 23725) 53

Figure 3.13 Ozone profiles observed at Cuiabá, Brazil, on (a) 18 September 1992 and (b) 2 October 1992 (after Kirchoff *et al.*, 1996) and at Ascension Island, South Atlantic Ocean, on (c) 9 September 1992 and (d) in September 1992 (after Thompson *et al.*, 1996). Absolutely stable layers are indicated by shading (Source: Swap and Tyson, 1999: p 68) 54

Figure 4.1 Mean monthly TTO (DU) above Johannesburg for the period 1995-1998 based on MOZAIC aircraft data. The vertical bars indicate two standard deviations on either side of the mean 60

Figure 4.2 Inter-annual variation in mean monthly TTO for 1995-1998. Dark blue = 1995; pink = 1996; green = 1997; light blue = 1998; red = mean 61

Figure 4.3 Monthly integrated TTO layers for 1995-1998. Dark blue = sfc-3 km; maroon = 3-5 km; cream = 5-7 km; light blue = 7-12 km layers 62

Figure 4.4 Ozone events with TTO greater than 30 DU. Dark blue = sfc-3 km; maroon = 3-5 km; cream = 5-7 km; light blue = 7-12 km layers 63

Figure 4.5 Percentage contribution of each layer for high ozone events with TTO greater than 30 DU. Dark blue = sfc-3 km; maroon = 3-5 km; cream = 5-7 km; light blue = 7-12 km layers 64

Figure 5.1 Mean vertical ozone concentration (ppbv) for the period 1995-2000: (a) spring, (b) summer, (c) autumn, (d) winter, (e) annual mean and (f) comparison of mean annual and seasonal profiles. Standard deviation bars for 150 m layers are given at 1050 m intervals 69

Figure 5.2 Distribution of ozone profiles at Johannesburg used in the TWINSPAN classification as a function of: (a) time of day and (b) season 72

Figure 5.3 Dendrogram showing the hierarchical classification of ozone profiles derived from the TWINSPAN cluster analysis for the first three levels of division. n=number of profiles. Eigenvalues are given in italics. The main categories selected for analysis are: 3a = single mid-tropospheric peak; 3b = steady tropospheric increase; 3c = reduced tropospheric ozone; 3d = lower tropospheric enhancement; 2c = pronounced layering; 2d = considerable tropospheric enhancement 73

Figure 5.4 Mean (solid red line) and individual values at 150 m height intervals (black dots) for ozone profiles in each group derived from the TWINSPAN cluster analysis at the first level of division. (a) Group 1a and (b) Group 1b 74

Figure 5.5 Mean (solid red line) and individual values at 150 m height intervals (black dots) for ozone profiles in each group derived from the TWINSPAN cluster analysis at the second level of division. (a) Group 2a, (b) Group 2b, (c) Group 2c and (d) Group 2d 74

Figure 5.6 Mean (solid red line) and individual values at 150 m height intervals (black dots) for ozone profiles in each group derived from the TWINSPAN cluster analysis at the third level of division. (a) Group 3a, (b) Group 3b, (c) Group 3c, (d) Group 3d, (e) Group 3e, (f) Group 3f, (g) Group 3g and (h) Group 3h 75

Figure 5.7 (a) Mean (solid red line) and individual values at 150 m height intervals (black dots) for ozone profiles and (b) a typical ozone profile (25 December 1996) in the single mid-tropospheric peak category 77

Figure 5.8 Composite of five-day back trajectory HYSPLIT model results for all days in the single mid-tropospheric peak category. Trajectories originating at 2.5 km are red, 5km blue, 7.5 km, green and 10 km, purple 79

Figure 5.9 (a) Mean (solid red line) and individual values at 150 m height intervals (black dots) for ozone profiles and (b) a typical ozone profile (23 December 1995) in the steady tropospheric increase category 81

Figure 5.10 Five-day back trajectory HYSPLIT model results for the steady tropospheric increase category. Trajectories originating at 2.5 km are red, 5km blue, 7.5 km, green and 10 km, purple 82

Figure 5.11 (a) Mean (solid red line) and individual values at 150 m height intervals (black dots) for ozone profiles and (b) a typical ozone profile (16 May 1997) for the reduced tropospheric ozone category 83

Figure 5.12 Five-day back trajectory HYSPLIT model results for the reduced tropospheric ozone category. Trajectories originating at 2.5 km are red, 5km blue, 8 km, green and 10 km, purple 84

Figure 5.13 (a) Mean (solid red line) and individual values at 150 m height intervals (black dots) for ozone profiles and (b) a typical ozone profile (12 August 1998) for the lower tropospheric enhancement category 85

Figure 5.14 Five-day back trajectory HYSPLIT model results for the lower tropospheric enhancement category. Trajectories originating at 2.5 km are red, 4km blue, 7.5 km, green and 10 km, purple 86

Figure 5.15 (a) Mean (solid red line) and individual values at 150 m height intervals (black dots) for ozone profiles and (b) a typical ozone profile (2 October 1998) for the pronounced layering category 87

Figure 5.16 Five-day back trajectory HYSPLIT model results for the pronounced layering category. Trajectories originating at 2.5 km are red, 6km blue, 7.5 km, green and 10 km, purple 88

Figure 5.17 (a) Mean (solid red line) and individual values at 150 m height intervals (black dots) for ozone profiles and (b) a typical ozone profile (8 October 1998) for the considerable tropospheric enhancement category. 89

Figure 5.18 Five-day back trajectory HYSPLIT model results for the considerable tropospheric enhancement category. Trajectories originating at 2.5 km are red, 5km blue, 7.5 km, green and 10 km, purple 90

Figure 5.19 Frequency distribution of ozone values within each of the 6 defined profile categories. Dark blue = single mid-tropospheric peak; red = steady tropospheric increase; pink = reduced tropospheric ozone; light blue = lower tropospheric enhancement; green = pronounced layering; brown = considerable tropospheric enhancement 91

Figure A.1 Individual ozone profiles in the single mid-tropospheric peak category for (a) 7 February 1996, (b) 17 January 1997, (c) 7 February 1997 (d) 25 December 1996, (e) 19 February 1997 and (f) 28 August 1998 119

Figure A.2 Individual ozone profiles in the steady tropospheric increase category for (a) 30 December 1998, (b) 23 December 1995, (c) 6 January 1999 (d) 16 December 1998, (e) 22 December 1998, (f) 18 November 1998, (g) 23 December 1998, (h) 17 November 1998 and (i) 5 February 1999 119

Figure A.3 Individual ozone profiles in the reduced tropospheric ozone category for (a) 26 March 1997, (b) 5 March 1997, (c) 8 May 1998, (d) 20 February 1998, (e) 29 March 1998, (f) 23 April 1997, (g) 3 May 1999, (h) 13 June 1997, (i) 6 July 1998, (j) 22 March 2000, (k) 29 December 1998, (l) 24 April 1996, (m) 1 May 1996, (n) 28 June 1998, (o) 12 June 1998, (p) 20 March 1998, (q) 2 May 1998 and (r) 16 May 1997 120

Figure A.4 Individual ozone profiles in the lower tropospheric enhancement category for (a) 15 December 1998, (b) 24 November 1998, (c) 11 December 1998, (d) 3 May 1995, (e) 22 May 1998, (f) 29 July 1998, (g) 12 August 1998, (h) 17 July 1998 and (i) 15 July 1998 121

Figure A.5 Individual ozone profiles in the pronounced layering category for (a) 2 October 1998, (b) 9 March 1999, (c) 20 September 1998, (d) 15 September 1998, (e) 14 September 1998, (f) 25 October 1998, (g) 21 August 1998, (h) 10 September 1998 and (i) 13 November 1998 122

Figure A.6 Individual ozone profiles in the considerable tropospheric enhancement category for (a) 11 October 1996, (b) 7 October 1998, (c) 25 October 1996, (d) 10 October 1997 and (e) 8 October 1998 122

Figure B.1 Inversion (red), isothermal (blue) and stable layers (grey) for ozone (solid line) and relative humidity (dashed line) profiles in the single mid-tropospheric peak category for (a) 7 February 1996, (b) 17 January 1997, (c) 7 February 1997 (d) 25 December 1996, (e) 19 February 1997 and (f) 28 August 1998 123

Figure B.2 Inversion (red), isothermal (blue) and stable layers (grey) for ozone (solid line) and relative humidity (dashed line) profiles in the steady tropospheric increase category for (a) 30 December 1998, (b) 23 December 1995, (c) 6 January 1999 (d) 16 December 1998, (e) 22 December 1998, (f) 18 November 1998, (g) 23 December 1998, (h) 17 November 1998 and (i) 5 February 1999 123

Figure B.3 Inversion (red), isothermal (blue) and stable layers (grey) for ozone (solid line) and relative humidity (dashed line) profiles in the reduced tropospheric ozone category for (a) 26 March 1997, (b) 5 March 1997, (c) 8 May 1998, (d) 20 February 1998, (e) 29 March 1998, (f) 23 April 1997, (g) 3 May 1999, (h) 13 June 1997, (i) 6 July 1998, (j) 22 March 2000, (k) 29 December 1998, (l) 24 April 1996, (m) 1 May 1996, (n) 28 June 1998, (o) 12 June 1998, (p) 20 March 1998, (q) 2 May 1998 and (r) 16 May 1997 124

Figure B.4 Inversion (red), isothermal (blue) and stable layers (grey) for ozone (solid line) and relative humidity (dashed line) profiles in the lower tropospheric enhancement category for (a) 15 December 1998, (b) 24 November 1998, (c) 11 December 1998, (d) 3 May 1995, (e) 22 May 1998, (f) 29 July 1998, (g) 12 August 1998, (h) 17 July 1998 and (i) 15 July 1998 125

Figure B.5 Inversion (red), isothermal (blue) and stable layers (grey) for ozone (solid line) and relative humidity (dashed line) profiles in the pronounced layering category for (a) 2 October 1998, (b) 9 March 1999, (c) 20 September 1998, (d) 15 September 1998, (e) 14 September 1998, (f) 25 October 1998, (g) 21 August 1998, (h) 10 September 1998 and (i) 13 November 1998 126

Figure B.6 Inversion (red), isothermal (blue) and stable layers (grey) for ozone (solid line) and relative humidity (dashed line) profiles in the considerable tropospheric enhancement category for (a) 11 October 1996, (b) 7 October 1998, (c) 25 October 1996, (d) 10 October 1997 and (e) 8 October 1998 126

Figure C.1 5-day back trajectory HYSPLIT model results for the single mid-tropospheric peak category for (1) 7 February 1996, (2) 25 December 1996 and (3) 17 January 1997. (a) Horizontal and vertical plots of back trajectories originating at 2.5, 5 and 7.5 km
(b) Horizontal and vertical plots of back trajectories originating at 10 km 127

Figure C.1 continued (1) 7 February 1997, (2) 19 February 1997 and (3) 28 August 1998. (a) Horizontal and vertical plots of back trajectories originating at 2.5, 5 and 7.5 km. (b) Horizontal and vertical plots of back trajectories originating at 10 km 128

Figure C.2 5-day back trajectory HYSPLIT model results for the steady tropospheric increase category for (1) 23 December 1995, (2) 17 November 1998 and (3) 18 November 1998. (a) Horizontal and vertical plots of back trajectories originating at 2.5, 5 and 7.5 km. (b) Horizontal and vertical plots of back trajectories originating at 10 km 129

Figure C.2 continued (1) 16 December 1998, (2) 22 December 1998 and (3) 23 December 1998. (a) Horizontal and vertical plots of back trajectories originating at 2.5, 5 and 7.5 km. (b) Horizontal and vertical plots of back trajectories originating at 10 km 130

Figure C.2 continued (1) 30 December 1998, (2) 6 January 1999 and (3) 5 February 1999. (a) Horizontal and vertical plots of back trajectories originating at 2.5, 5 and 7.5 km. (b) Horizontal and vertical plots of back trajectories originating at 10 km 131

Figure C.3 5-day back trajectory HYSPLIT model results for the reduced tropospheric ozone category for (1) 24 April 1996, (2) 1 May 1996 and (3) 5 March 1997. (a) Horizontal and vertical plots of back trajectories originating at 2.5, 5 and 8 km. (b) Horizontal and vertical plots of back trajectories originating at 10 km 132

Figure C.3 continued (1) 26 March 1997, (2) 23 April 1997 and (3) 16 May 1997. (a) Horizontal and vertical plots of back trajectories originating at 2.5, 5 and 8 km. (b) Horizontal and vertical plots of back trajectories originating at 10 km 133

Figure C.3 continued (1) 13 June 1997, (2) 20 February 1998 and (3) 20 March 1998. (a) Horizontal and vertical plots of back trajectories originating at 2.5, 5 and 8 km. (b) Horizontal and vertical plots of back trajectories originating at 10 km 134

Figure C.3 continued (1) 29 March 1998, (2) 2 May 1998 and (3) 8 May 1998. (a) Horizontal and vertical plots of back trajectories originating at 2.5, 5 and 8 km. (b) Horizontal and vertical plots of back trajectories originating at 10 km 135

Figure C.3 continued (1) 12 June 1998, (2) 28 June 1998 and (3) 6 July 1998. (a) Horizontal and vertical plots of back trajectories originating at 2.5, 5 and 8 km. (b) Horizontal and vertical plots of back trajectories originating at 10 km 136

Figure C.3 continued (1) 29 December 1998, (2) 3 May 1999 and (3) 22 March 2000. (a) Horizontal and vertical plots of back trajectories originating at 2.5, 5 and 8 km. (b) Horizontal and vertical plots of back trajectories originating at 10 km 137

Figure C.4 5-day back trajectory HYSPLIT model results for the lower tropospheric enhancement category for (1) 3 May 1995, (2) 22 May 1998 and (3) 15 July 1998. (a) Horizontal and vertical plots of back trajectories originating at 2.5, 4 and 7.5 km. (b) Horizontal and vertical plots of back trajectories originating at 10 km 138

Figure C.4 continued (1) 17 July 1998, (2) 29 July 1998 and (3) 12 August 1998. (a) Horizontal and vertical plots of back trajectories originating at 2.5, 4 and 7.5 km. (b) Horizontal and vertical plots of back trajectories originating at 10 km 139

Figure C.4 continued (1) 24 November 1998, (2) 11 December 1998 and (3) 15 December 1998. (a) Horizontal and vertical plots of back trajectories originating at 2.5, 4 and 7.5 km. (b) Horizontal and vertical plots of back trajectories originating at 10 km 140

Figure C.5 5-day back trajectory HYSPLIT model results for the pronounced layering category for (1) 21 August 1998, (2) 10 September 1998 and (3) 14 September 1998. (a) Horizontal and vertical plots of back trajectories originating at 2.5, 6 and 7.5 km. (b) Horizontal and vertical plots of back trajectories originating at 10 km 141

Figure C.5 continued (1) 15 September 1998, (2) 20 September 1998 and (3) 2 October 1998. (a) Horizontal and vertical plots of back trajectories originating at 2.5, 6 and 7.5 km. (b) Horizontal and vertical plots of back trajectories originating at 10 km 142

Figure C.5 continued (1) 25 October 1998, (2) 13 November 1998 and (3) 9 March 1999. (a) Horizontal and vertical plots of back trajectories originating at 2.5, 6 and 7.5 km. (b) Horizontal and vertical plots of back trajectories originating at 10 km 143

Figure C.6 5-day back trajectory HYSPLIT model results for the considerable tropospheric enhancement category for (1) 11 October 1996, (2) 25 October 1996 and (3) 10 October 1997. (a) Horizontal and vertical plots of back trajectories originating at 2.5,5 and 7.5 km. (b) Horizontal and vertical plots of back trajectories originating at 10 km 144

Figure C.6 continued (1) 7 October 1998 and (2) 8 October 1998. (a) Horizontal and vertical plots of back trajectories originating at 2.5, 5 and 7.5 km. (b) Horizontal and vertical plots of back trajectories originating at 10 km 145

LIST OF TABLES

		Page
Table 3.1	Seasonal changes of stratospheric mass (Source: Staley, 1962: p 453)	44
Table 3.2	Seasonal variation of median tropopause pressures (mb) over North America (Source: Reiter, 1975: p 462)	45
Table 4.1	Events showing enhancements as a function of layer. X denotes an enhancement	65
Table 5.1	Profiles in the single mid-tropospheric peak category as a function of season	77
Table 5.2	Profiles in the steady tropospheric increase category as a function of season	80
Table 5.3	Profiles in the reduced tropospheric ozone category as a function of season	82
Table 5.4	Profiles in the lower tropospheric enhancement category as a function of season	85
Table 5.5	Profiles in the pronounced layering category as a function of season	87
Table 5.6	Profiles in the considerable tropospheric enhancement category as a function of season	89
Table 5.7	Distribution of cases within each group by season	92
Table 5.8	Source regions of air masses associated with each ozone profile category as a function of height	94

TABLE OF CONTENTS

	Page
PREFACE	ii
ACKNOWLEDEMENTS	iii
ABSTRACT	v
LIST OF FIGURES	vii
LIST OF TABLES	xxi
CHAPTER 1: INTRODUCTION	1
1.1 Background	1
1.2 Aim and Objectives	3
1.3 The Scope of this Study	3
CHAPTER 2: DATA AND METHODOLOGY	5
2.1 Introduction	5
2.2 MOZAIC Data	5
2.2.1 The MOZAIC Program	5
2.2.2 Description of the MOZAIC Instrumentation	9
2.2.2.1 Installation	9
2.2.2.2 Operation of the Ozone Analyser	11
2.2.2.3 Operation of the Humidity Sensing Device and Temperature Sensor	16
2.2.3 Data Base	19
2.3 Total Tropospheric Ozone Methodology	21
2.3.1 Definition of Total Tropospheric Ozone	21
2.3.2 Computation of Total Tropospheric Ozone	21
2.3.3 Data Selection and Processing	22
2.4 Stable Layer Methodology	22
2.4.1 Definition of an Absolutely Stable Layer	22
2.4.2 Computation of Absolutely Stable Layers	23
2.5 Classification of Ozone Profiles	24
2.5.1 Rationale	24
2.5.2 Classification Technique	25
2.5.2.1 Hierarchical and Non-hierarchical Classification	25
2.5.2.2 TWINSPAN (Two-way indicator species analysis)	26
2.5.2.3 Input Data for TWINSPAN	27
2.6 Back Trajectory Modelling	27
2.6.1. Rationale	27
2.6.2. Hybrid Single-Particle Lagrangian Integrated Trajectory (HYSPLIT) Model	28
2.6.3. Description of the HYSPLIT (Version 4) Model	28
2.6.4. Input Data	29
2.6.5. Output Data	29
2.6.6. Limitations	30

CHAPTER 3: CHEMISTRY AND DYNAMICS OF TROPOSPHERIC OZONE 31
3.1 Introduction 31
3.2 Photochemical Processes 32
3.2.1 Sources Contributing to the Tropospheric Ozone Budget 33
3.2.1.1 Urban/Industrial Emissions 33
3.2.1.2 Biogenic Emissions 34
3.2.1.3 Lightning 37
3.2.1.4 Biomass Burning 40
3.2.2 Sinks Contributing to the Tropospheric Ozone Budget 42
3.2.2.1 Photolysis 42
3.2.2.2 HO_2/OH Catalysed Destruction 42
3.2.2.3 Surface Deposition 43
3.3 Dynamic Controls of Tropospheric Ozone Distribution 43
3.3.1 Stratospheric-Tropospheric Exchange 43
3.3.1.1 Mean Meridional Circulation 43
3.3.1.2 Movement of the Tropopause 44
3.3.1.3 Tropopause Folding 45
3.3.1.4 Cut-Off Lows 47
3.3.2 Synoptic Scale Circulations 49
3.3.2.1 Anticyclonic Circulations 49
3.3.2.2 Convection 53
3.4 Summary 55

CHAPTER 4: TOTAL TROPOSPHERIC OZONE 56
4.1 Introduction 56
4.2 Previous Research Results on TTO in Southern Africa 58
4.3 Total Tropospheric Ozone (TTO) over Johannesburg 60
4.4 Integrated Tropospheric Ozone in Layers 61
4.5 Elevated Ozone Events 62
4.6 Conclusion 66

CHAPTER 5: VERTICAL DISTRIBUTION OF TROPOSPHERIC OZONE 67
5.1 Introduction 67
5.2 Classification of Ozone Profiles 70
5.2.1 Classification Procedure 70
5.2.2 Characteristics of Ozone Profiles used in the Classification 71
5.2.3 Results of the Cluster Analysis 72
5.2.3.1 General Characteristics of Ozone Profiles in the Single Mid-Tropospheric Peak Category 76
5.2.3.2 Source Regions of Tropospheric Ozone for the Mid-Tropospheric Peak Category 78
5.2.3.3 General Characteristics of Ozone Profiles in the Steady Tropospheric Increase Category 80
5.2.3.4 Source Regions of Tropospheric Ozone for the Steady Tropospheric Increase Category 81
5.2.3.5 General Characteristics of Ozone Profiles in the Reduced Tropospheric Ozone Category 81

5.2.3.6 Source Regions of Tropospheric Ozone for the Reduced Tropospheric Ozone Category 83
5.2.3.7 General Characteristics of Ozone Profiles in the Lower Tropospheric Enhancement Category 84
5.2.3.8 Source Regions of Tropospheric Ozone for the Lower Tropospheric Enhancement Category 85
5.2.3.9 General Characteristics of Ozone Profiles in the Pronounced Layering Category 86
5.2.3.10 Source Regions of Tropospheric Ozone for the Pronounced Layering Category 87
5.2.3.11 General Characteristics of Ozone Profiles in the Considerable Tropospheric Enhancement Category 88
5.2.3.12 Source Regions of Tropospheric Ozone for the Considerable Tropospheric Enhancement Category 89
5.2.4 Comparison of Results as a Function of Category 90
5.2.4.1 Frequency Distribution of Ozone Values 90
5.2.4.2 Seasonality of Ozone Profiles 91
5.2.4.3 Source Regions 93
5.3 Summary 93

CHAPTER 6: CONCLUSION 95
6.1 Summary 95
6.2 Recommendations 98

REFERENCES 100

APPENDIX A 119

APPENDIX B 123

APPENDIX C 127

CHAPTER 1

INTRODUCTION

1.1 Background

Increases in ambient levels of tropospheric ozone as noted by many authors, for example Logan (1985), are of concern due to the important consequences for the global and local environment. Tropospheric ozone is acknowledged to be an effective greenhouse gas (Scholes and Andreae, 2000) and therefore plays a critical role in the control of climate (Zachariasse *et al.*, 2000). The importance of tropospheric ozone also stems from the fact that it is the primary source of hydroxyl (OH) radicals (Baldy *et al.*, 1996; Parsons *et al.*, 1996). According to Crutzen and Lelieveld (2001), OH acts as a major chemical scavenger or cleansing agent in the troposphere and thus plays a critical role in the atmosphere's ability to cleanse itself of a variety of gases such as methane (CH_4), carbon monoxide (CO), nitrogen dioxide (NO_2) and other atmospheric pollutants. Furthermore, elevated levels of surface ozone are very toxic and affect human health and vegetation negatively (Logan, 1985). One example of potentially negative effects is that on maize production in southern Africa. A substantial decline in maize production over the past few years in certain southern African countries has led to the establishment of the Cross Border Air Pollution Impact Assessment (CAPIA) project which is presently addressing the impact of ozone on maize production over the subcontinent (http://dbn.csir.co.za/capia/).

Satellite-based observations in the early 1990's, for example by Fishman *et al.* (1990, 1991), first drew attention to high levels of tropospheric ozone present over the South Atlantic Ocean between Brazil and Africa, extending across southern Africa towards the southern Indian Ocean. Ozone values within this giant plume were as high as those found in North America, Europe and Asia (Fishman *et al.*, 1990). Whereas the high northern hemisphere tropospheric ozone concentrations were most pronounced during the summer, the feature in the southern tropics was dominant during austral spring (September-November). These observations led to the launch of major scientific field campaigns such as the Southern African Fire-Atmospheric Research Initiative (SAFARI-92) and more recently SAFARI-2000. The SAFARI-92 program was the southern African component of the Southern Tropical Atlantic Region Experiment (STARE) program, and at the time was

the largest international experiment ever undertaken in the subcontinent's land/atmosphere system, providing an intensive analysis of the impact of biomass burning on atmospheric chemistry and the sources and fates of atmospheric chemicals (mainly pyrogenic emissions) over southern Africa and adjacent oceans. SAFARI-92 was based on extensive ground-based, aircraft, rawinsonde and satellite-based measurements (Andreae *et al.*, 1996; Lindesay *et al.*, 1996).

One of the main achievements of SAFARI-92 was the endorsement of a springtime enhancement in tropospheric ozone. High concentrations of ozone and ozone precursor gases originating from biogenic and soil emissions and biomass burning were transported into the tropical South Atlantic region and accounted for the observed tropospheric ozone maximum (Swap *et al.*, 1996; Thompson *et al.*, 1996a). Krishnamurthi *et al.* (1993; 1996) also drew attention to dynamic factors which could account for the ozone enhancement in this region. Over the southern African subcontinent the high concentrations of ozone were linked to the presence of absolutely stable layers and a dominant anticyclonic circulation which served to recirculate biomass burning products over the subcontinent over extended periods of time, thus allowing sufficient time for the buildup of ozone (Garstang *et al.*, 1996; Tyson *et al.*, 1996).

The SAFARI-2000 initiative built on the success of the SAFARI-92 and included continuous measurements, as well as intense field campaigns carried out from 1999 to 2001 (Otter *et al.*, 2002). Although SAFARI-2000 focussed more on aerosols, our knowledge of ozone distribution also improved. For example, Thompson *et al.* (2002) found that Lusaka (15.5°S, 28°E) was a regional collection point of very high tropospheric ozone originating from local and active burning areas within southern Africa.

There have been relatively few investigations of the vertical distribution of ozone in southern Africa (Logan, 1999). Long term ozonesonde records are only available for Irene (25°S, 28°E) and our knowledge of the vertical distribution of ozone stems from the early work of Zunckel *et al.* (1992a; 1992b), Diab *et al.* (1996a) and more recently Mari (2001). Shorter campaign measurements have been undertaken at Okaukuejo (19° S, 15° E) (Diab *et al.*, 1996a; Thompson *et al.*, 1996a) and recently at Lusaka (15.5°S, 28°E) (Thompson *et al.*, 2002). In addition, some aircraft measurements during SAFARI-92 using the airborne

Differential Absorption Lidar (DIAL) system provided vertical profiles of ozone from the surface to the tropopause at certain locations (Browell *et al.*, 1996).

It is within this context and in view of the paucity of investigations into the vertical distribution of ozone that this study is undertaken. The focus is on the vertical distribution of ozone over Johannesburg (26°S; 28°E) using aircraft profile data derived from the Measurement of Ozone and Water Vapor by Airbus In-Service Aircraft (MOZAIC) database for the period 1995 to 2000. Similar studies based on MOZAIC data include those of Newell *et al.* (1999) and Thouret *et al.* (1998), although this is the first time that a detailed investigation of the Johannesburg profiles has been undertaken.

1.2 Aim and Objectives

The aim of this thesis is to examine the nature and characteristics of tropospheric ozone over Johannesburg. Specific objectives are:

1. to investigate seasonal variations in total tropospheric ozone (TTO) and integrated ozone in four layers in the atmosphere
2. to focus on events of elevated TTO with a view to determining their origin
3. to characterise the vertical distribution of tropospheric ozone by means of a classification of ozone profiles
4. to identify the factors responsible for variations in the vertical distribution of ozone and in particular to determine the source regions of elevated ozone through back trajectory analysis

1.3 The Scope of this Study

A detailed description of the methodology applied, and the data used in this study are given in Chapter 2. This is followed by a review of the literature concerning the chemistry and dynamics of tropospheric ozone, in Chapter 3. This chapter pays particular attention to photochemical sources, such as urban/industrial emissions, biogenic emissions, lightning and biomass burning, that contribute to the tropospheric ozone budget. It also addresses stratospheric-tropospheric exchange mechanisms and dynamic controls of tropospheric ozone distribution. Chapter 4 presents the results of TTO variations and highlights days of

elevated TTO. Chapter 5 is concerned with the vertical distribution of ozone and presents the results of the classification of ozone profiles using a multivariate cluster analysis technique known as TWINSPAN (Two-Way Indicator Species Analysis). Chapter 6 presents conclusions drawn from the study and makes recommendations for future work. References and appendices are found at the end of the thesis.

CHAPTER 2

DATA AND METHODOLOGY

2.1 Introduction

The data used in this study are ozone and meteorological profile data for Johannesburg, South Africa (26°S; 28°E), for the period 1995 to 2000. The data were derived from the MOZAIC (Measurement of Ozone and Water Vapor by Airbus In-Service Aircraft) database. Full details of the data are given in section 2.2. The techniques used to compute total tropospheric ozone (TTO) and atmospheric stability layers are described in sections 2.3 and 2.4 respectively. The classification technique applied to ozone profiles is outlined in section 2.5 and the back trajectory analysis in section 2.6.

2.2 MOZAIC Data

2.2.1 The MOZAIC Program

At present, there is still a considerable lack of data describing the global distribution of ozone and water vapor. The acquisition of tropospheric and lower stratospheric ozone and water vapor measurements has been difficult for several reasons. Satellite instruments designed for ozone and water vapor measurements are unable to detect concentrations through cirrus clouds. They also have poor vertical resolution and accuracy in the troposphere. Ozone sounding stations or ozone lidars are few in number and are largely concentrated over continents in the northern hemisphere. Furthermore, the accuracy and precision of standard meteorological humidity sensors are not well known above 500 hPa. Dedicated aircraft campaigns using scientific aircraft as instrument platforms, or balloon sounding campaigns, have provided reliable information on the vertical and meridional distribution of ozone and water vapor. However, such campaigns are few in number and are usually conducted over a short period of time (Marenco *et al.*, 1998; Thouret *et al.*, 1998b). As a result the acquisition of reliable, high quality experimental data of tropospheric ozone and water vapor in both the northern and southern hemispheres is in high demand (Marenco *et al.*, 1998).

Aircraft present an interesting way of making *in situ* measurements as they provide data at high vertical and horizontal resolutions (Marenco *et al.*, 1998). Long-range passenger airliners are suitable platforms to perform measurements of ozone and water vapor in the troposphere and lower stratosphere on a regular basis during their routine in-service flights (Marenco *et al.*, 1998; Thouret *et al.*, 1998b).

The MOZAIC program was launched in January 1993 in an effort to collect experimental data to help understand the atmosphere and how it is changing under the influence of human activity. It involves a close partnership between European scientists, aircraft manufacturers (Airbus Industrie and its partners) and four European airlines (Air France, Austrian Airlines, Lufthansa, and Sabena) (Marenco *et al.*, 1998; MOZAIC-II: Technical Final Report, 2000).

MOZAIC consists of automatic measuring equipment installed on five Airbus A340 aircraft. The aircraft continuously measure concentrations of ozone and water vapor throughout their flights, across the globe (Marenco *et al.*, 1998; MOZAIC-II: Technical Final Report, 2000). Neither satellites nor radiosondes are able to supply such data (Marenco *et al.*, 1998).

MOZAIC-I, the first phase, extended from January 1993 to September 1996. It consisted of the development and installation of ozone and water vapor equipment aboard five A340 aircraft. Regular measurements recorded during in-service flights were used to compile a database of ozone and water vapor measurements collected between 0-12 km. MOZAIC-II, the second phase, which extended from October 1996 to September 1998, continued with ozone and water vapor measurements and their interpretation, but was also used as an opportunity to undertake a feasibility study of new airborne devices to measure total reactive nitrogen (NO_y) and carbon monoxide (CO). MOZAIC-III, the third phase, is currently in operation. It officially started on March 1, 2000. New devices were installed and it was planned that the aircraft would fly the whole set of instruments (ozone, water vapor, carbon monoxide and NO_y) for several years (Marenco *et al.*, 1998).

Laboratoire d' Aérologie Toulouse (LA/CNRS) is responsible for the overall co-ordination of the MOZAIC Project, the overall instrument control system as well as the development and adaptation of the ozone sensor. The Institute for Chemistry of the Polluted

Atmosphere/Jülich (KFA) is responsible for measurements of water vapor (Marenco *et al.*, 1998).

Regular data collection commenced in August 1994. By the end of July 1999, 11785 flights distributed across eight main directional routes (Fig. 2.1) had been successively completed. Figure 2.2 shows the number of flights per year as a function of the destination from Europe over this period. A total of 86291 flight hours had been covered by the end of July 1999. Figure 2.3 presents the yearly distribution of flight hours recorded (MOZAIC-II: Technical Final Report, 2000).

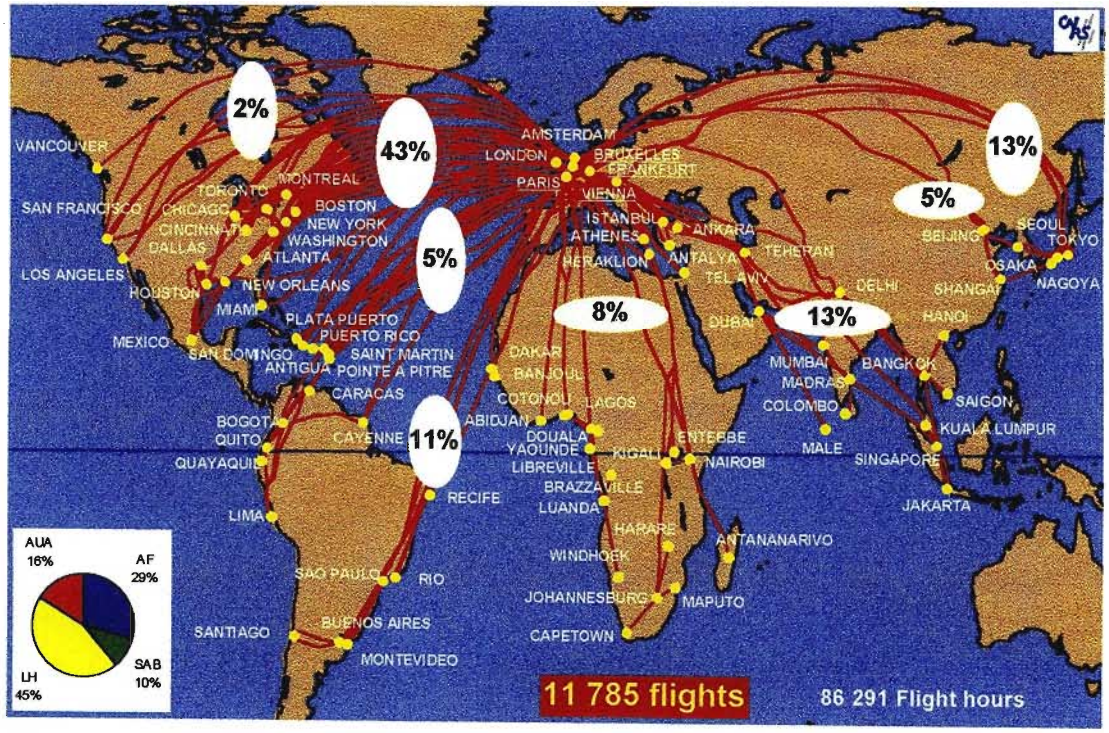

Figure 2.1: Geographical coverage of MOZAIC flights between August 1994 – July 1999. Red lines indicate percent in main directions (Source: MOZAIC-II: Technical Final Report, 2000: p 15)

Since the MOZAIC program makes use of long-range aircraft, 90% of the data were collected at cruise levels (Thouret *et al.*, 1998a; 1998b) and the remaining 10% were obtained during ascents and descents at airports (MOZAIC-II: Technical Final Report, 2000). Data recovery in MOZAIC-I was 85%. In MOZAIC-II the data recovery improved to 92%. The reason for this is that in 1997, a new data mass storage unit, Flash disks PCMIA cards (which are 100% shock resistant) replaced the Bernoulli disks used previously in MOZAIC-I. Figure 2.4 shows MOZAIC data recovery between August 1994 and July 1999 (MOZAIC-II: Technical Final Report, 2000).

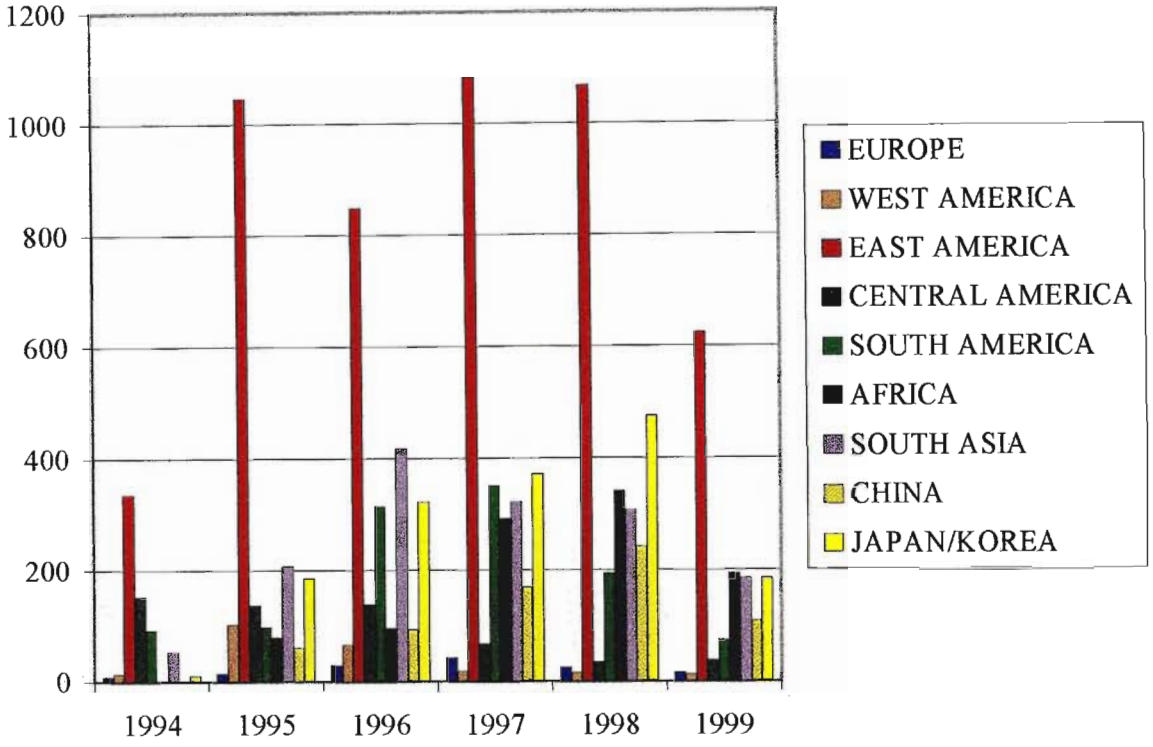

Figure 2.2: Number of MOZAIC flights per year and main direction from Europe (August 1994 – July 1999) (Source: MOZAIC-II: Technical Final Report, 2000: p 14)

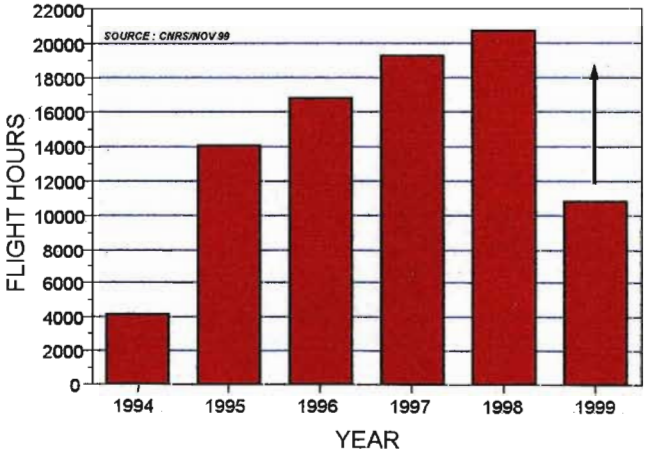

Figure 2.3: Number of flight hours per year achieved by MOZAIC operations (August 1994-July 1999) (Source: MOZAIC-II: Technical Final Report, 2000: p 14)

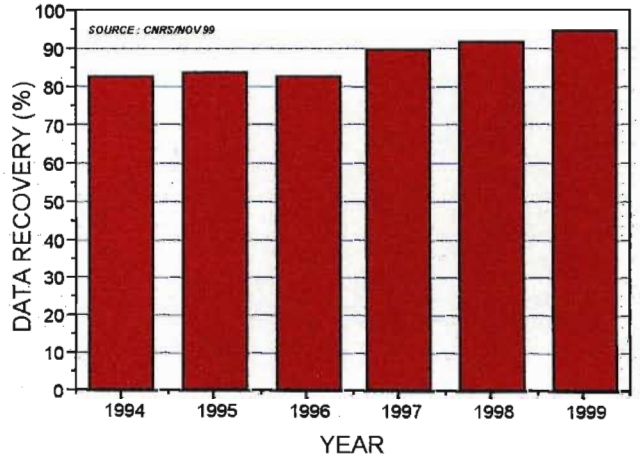

Figure 2.4: MOZAIC data recovery (%) between August 1994-July 1999 (Source: MOZAIC-II: Technical Final Report, 2000: p 14)

2.2.2 Description of the MOZAIC Instrumentation

2.2.2.1 Installation

The MOZAIC scientific instrumentation was specially designed to make automatic measurements of ozone, water vapor and temperature during routine flight operations aboard commercial A340 aircraft. It comprises a specially designed rack (Fig. 2.5) and a removable probe plate (Fig. 2.6). The rack is installed in the avionic compartment, an area where temperature (20°C) and the aircraft's internal pressure are controlled. Various shelves making up the rack are occupied by scientific equipment, including the ozone analyser and water vapor analyser, which are mounted on shock absorbers (Fig. 2.5). The probe plate is situated on the left side of the fuselage, 7 m away from the tip of the aircraft. It holds two air inlet probes, the pitot tube for ozone measurements and a Rosemount housing for humidity and temperature measurements. The pitot tube and water vapor sensor housing are suspended at distances of 7 and 10 cm respectively above the plate so that air sampling occurs safely outside the boundary layer of the aircraft, which is roughly 3 cm thick (as calculated by Aerospace engineers). External air sampling for ozone measurement occurs only after takeoff and before landing. This precautionary measure is taken in order to prevent the input line from contamination by dust and deposition of organic compounds from local pollution sources while the aircraft is on the ground (Marenco *et al.*, 1998).

The MOZAIC system is powered by the aircraft's power supply. A computer system and software is used to control the scientific instruments and store data (Fig. 2.7) (Marenco *et al.*, 1998). The MOZAIC software was developed to perform the following tasks: control of scientific instruments, acquisition of chemical parameters (ozone and water vapor measurements), acquisition of aircraft parameters, data storage, and system maintenance (MOZAIC-II: Technical Final Report, 2000). The software is also used to control an electronic interface which in turn controls the auxiliary devices which comprise pumping devices, electrovalves, mass flowmeters, an error detection system and various electronic transmitter units (Marenco *et al.*, 1998).

Measurements are recorded every 4 seconds during each flight. Data (ozone, relative humidity, temperature, and status of control parameters) and aircraft parameters (time,

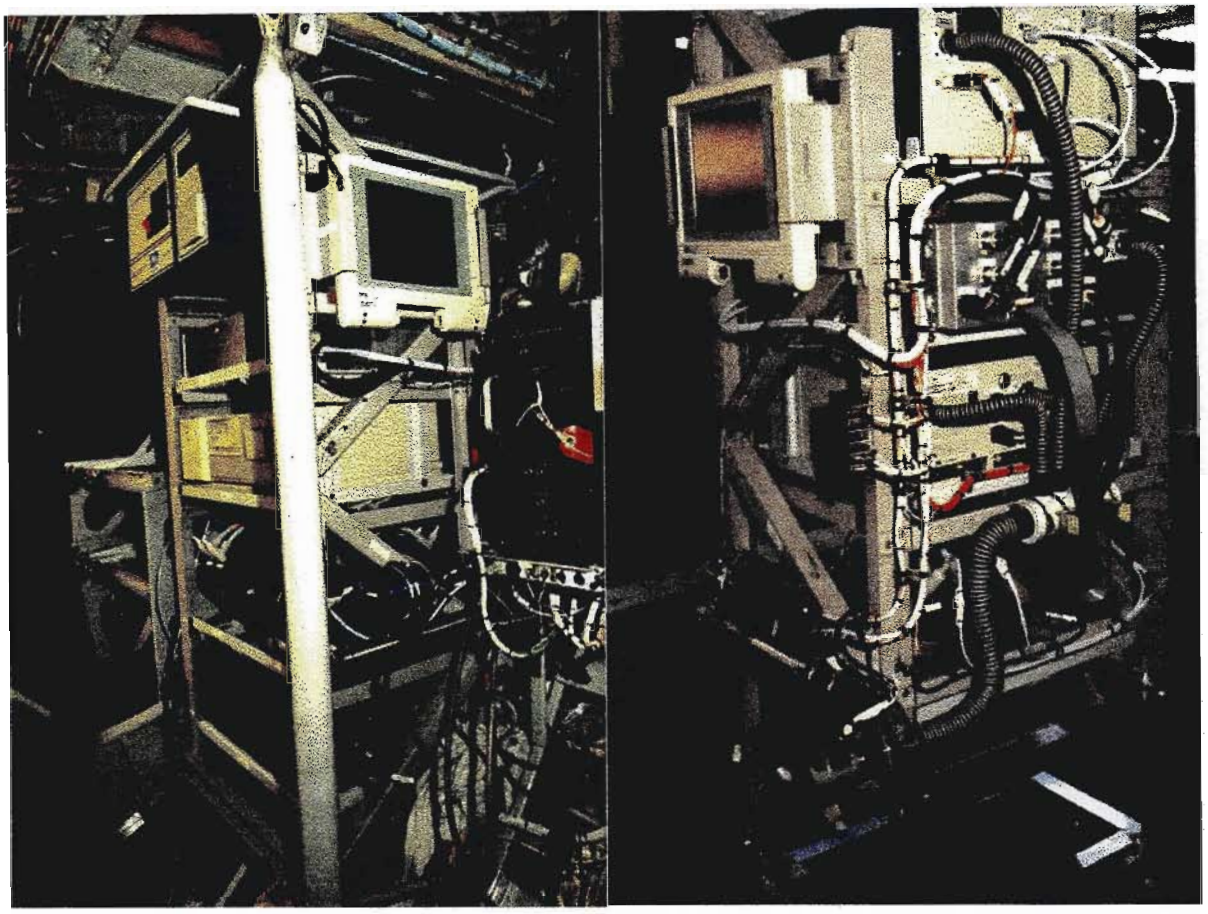

Figure 2.5: Front (left) and rear (right) view of the rack housing MOZAIC instrumentation (Source: MOZAIC website: http://www.aero.obs-mip.fr/mozaic/)

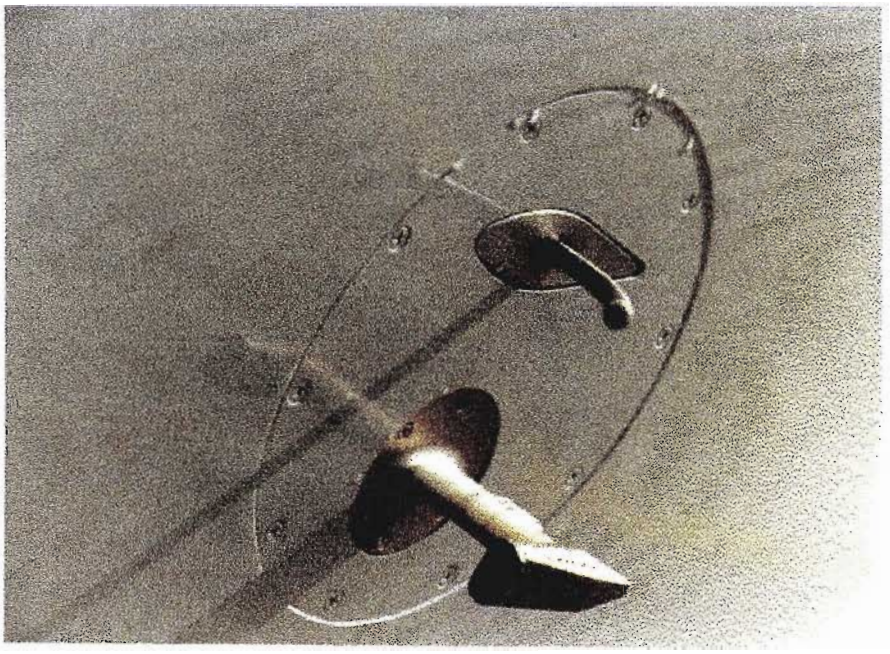

Figure 2.6: Removable probe plate pitot tube (top) and a Rosemount housing (bottom) (Source: MOZAIC website: http://www.aero.obs-mip.fr/mozaic/)

latitude, longitude, altitude, pressure, aircraft speed, wind direction, and velocity) from the Air Data Computer are stored on a detachable high capacity storage disk (Marenco *et al.*, 1998).

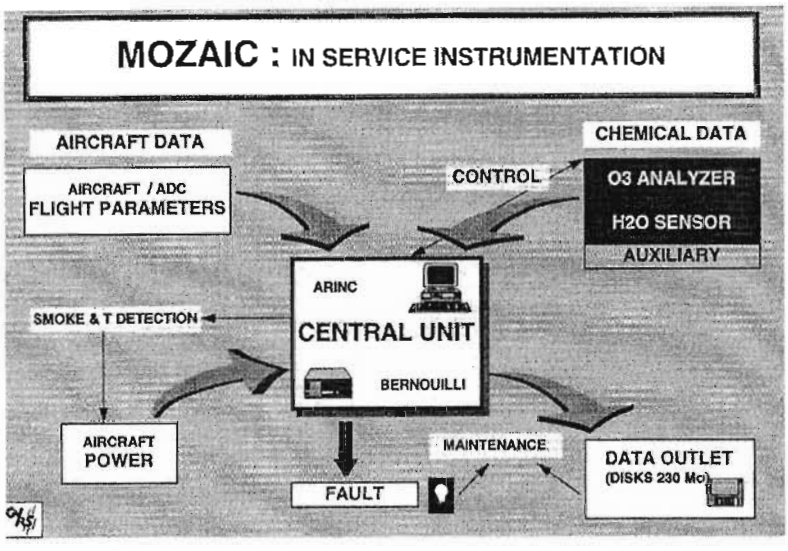

Figure 2.7: MOZAIC in-service instrumentation
(Source: Marenco *et al.*, 1998: p 25637)

The system operates automatically, without assistance from the flight crew. After approximately every 500 flight hours or on a (roughly) monthly basis, water vapor sensors and data disks are replaced. In addition, routine stopovers are used as an opportunity for maintenance crew of the airline to check the system's operation for malfunctions such as faulty lamps or error messages (Marenco *et al.*, 1998).

2.2.2.2 Operation of the Ozone Analyser

The ozone analyzer is a dual beam UV absorption instrument (Thermo-Electron, Model 49-103). It has a response time of 4 seconds. The analyser automatically corrects ozone concentration against influences of pressure and temperature. Laboratory tests and in-flight measurements have confirmed that the operating principle, electronic design and specifications behind this particular model give it excellent stability. Evaluations show that the analyser has an overall precision of 2 ppbv, noise of 1 ppbv, minimum detection limit of 2 ppbv and an accuracy of 2%. In this way, accurate and reliable measurements can be recorded over extensive durations. This corresponds to an upper limit of the error on the measurements, and studies of MOZAIC data have in fact shown better characteristics (Thouret *et al.*, 1998a).

The ozone measuring system is connected to the inlet probe with Teflon lines via auxiliary devices such as Teflon pumps and valves (Fig. 2.8). The inlet tube is composed of a stainless steel pipe that is lined with Teflon so that ozone destruction does not occur on the steel (Thouret *et al.*, 1998a).

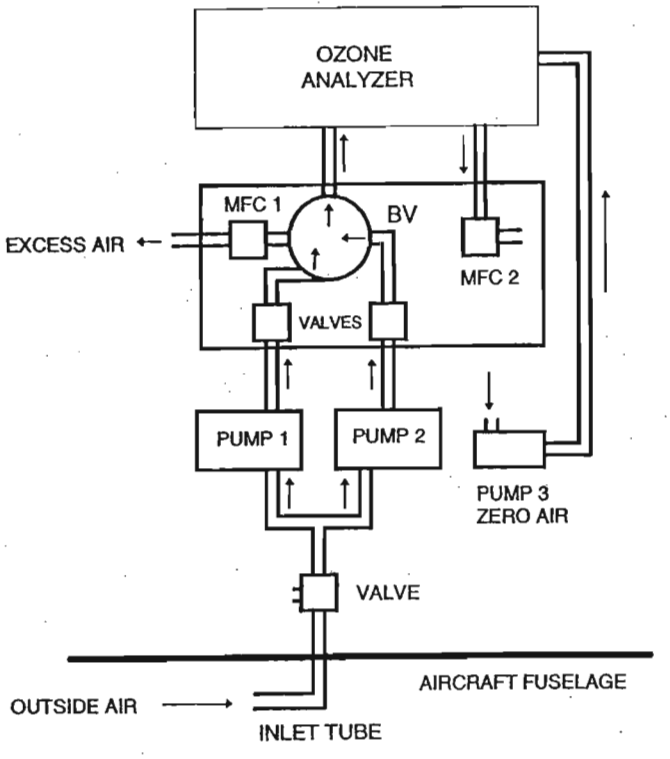

Figure 2.8: Plan of the MOZAIC ozone pumping system
(Source: Thouret *et al.*, 1998a: p 25697)

Figure 2.8 shows a plan of the MOZAIC ozone pumping system. PUMP 1 is a Teflon KNF Neuberger pump. It is used to draw ambient air through the analyser at a flow rate of over 2 litres per minute. Mass flow controllers (MFC 1 and MFC 2) are used to drive the pump. A Teflon flask (BV), with a volume of 100 cm^3, is positioned along the Teflon line just before the ozone analyser. It serves as a buffer volume to equilibrate the external air pressure with the internal aircraft pressure just before it enters the ozone analyser. If PUMP 1 malfunctions, PUMP 2, a second Teflon pump is automatically activated (Thouret *et al.*, 1998a).

The sampled air takes approximately 2 seconds to travel between the inlet and the ozone analyser. In this way, possible destruction of ozone within the lines is minimized. Laboratory tests have shown that total ozone losses occurring at the inlet, along the lines, through the pump, and buffer volume were below 1% (Thouret *et al.*, 1998a). During

aircraft ground maintenance, pumps and inlet Teflon lines are inspected on a regular basis for cleanliness and are replaced at regular intervals. A remote-controlled Teflon valve that is used to test outside air for ozone measurements is automatically triggered only when the aircraft has reached 20 m above ground level after takeoff and before landing in order to prevent the input line from contamination as mentioned earlier.

The MOZAIC system remains powered continuously especially since the aircraft are under intensive operation. This ensures that the ozone analyser is always equilibrated and ready to function at any given time. Thus any disturbance during the 1-hour warming-up period is avoided (Thouret *et al.*, 1998a).

At ground-based stations the ozone sensor has proved to be a highly stable device over many years of continuous service. During flight however, a special procedure is undertaken to determine whether there are any inconsistencies in instrument efficiency. This is accomplished by using the analyser's ozone generator in conjunction with a stream of "zero air" supplied by an auxiliary pump (PUMP 3) (Fig. 2.8), which pulls in ambient air from the electronic compartment through an ozone filter. The remote-controlled ozone generator is activated automatically at 2 hour intervals during cruise, just before takeoff, and after landing. References are executed at around three levels: 0, 80 and 500 ppbv (Thouret *et al.*, 1998a).

For in-flight conditions, precision of the internal ozone generators is estimated at 3%. This estimate takes into consideration the limited 5 minute time of activation, UV lamp stability, and auxiliary pump flow rate stability. Figure 2.9 depicts variations in the response of the ozone analyser over a flight period of one year (Thouret *et al.*, 1998a).

The MOZAIC program uses a total of seven ozone analysers. Five of them are in regular operation aboard their respective aircraft, the sixth one is kept as a spare instrument, while the seventh one acts as a reference analyser and remains at LA/CNRS. At the beginning of the program, all ozone analysers were intercalibrated against this reference analyser. Their factory calibrations, including pressure transducers (for pressure correction) agreed within the 0.5% range of the reference. All analysers were also tested for linearity within the 0-1000 ppbv range. The overall accuracy of the reference analyser calibration was estimated at 0.5% (Thouret *et al.*, 1998a).

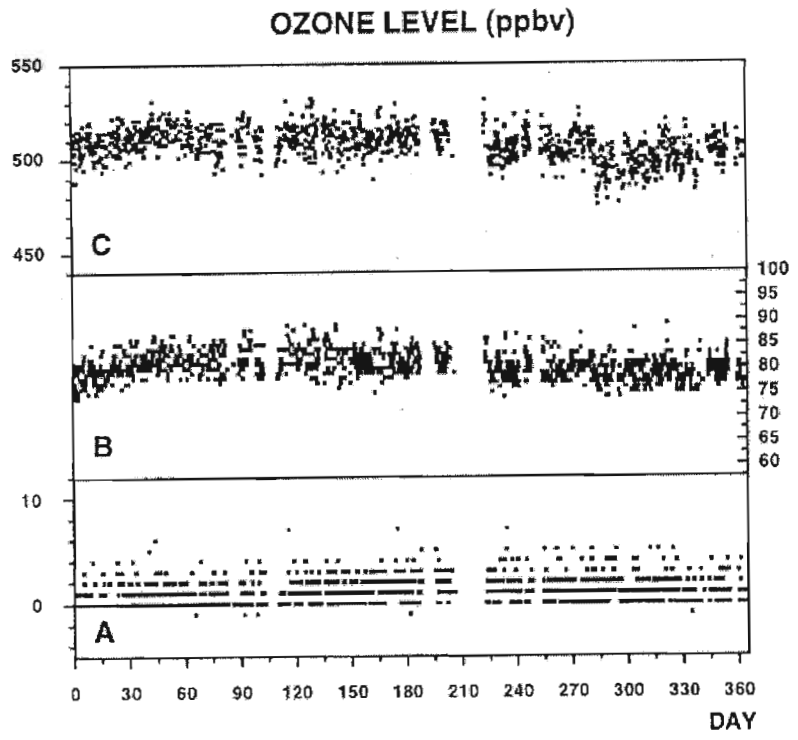

Figure 2.9: Variations in the response of an ozone analyser over an operation period (March 28, 1996 to March 26, 1997) on board aircraft MSN-053 for three levels of the internal ozone generator (A, 0 ppbv; B, 80 ppbv; C, 510 ppbv). Accurate pre-flight and postflight calibrations, made at the laboratory, were in agreement within a 0.05% range (Source: Thouret *et al.*, 1998a: p 25698)

After the first intercalibration, each ozone analyser was thereafter exchanged every year and recalibrated against the reference analyser. Except for the detection of three significant drifts, analyzer operations in general did not show signs of any extensive variation (less than 1%), between 1994 and 1997 (Thouret *et al.*, 1998a).

The purpose of the internal ozone reference is to identify the sequence of main events in the case where exceptional drift in calibration is noted. It is not used for accurate on-line calibration. The preflight and postflight calibrations are used in conjunction with main trends derived from the ozone reference to produce an average curve, which describes the evolution of the analyser efficiency. The data are corrected if necessary (Thouret *et al.*, 1998a).

A systematic flight inter-comparison programme was initiated to assess the consistency and repeatability of the ozone measurements recorded during MOZAIC flights. Flight comparisons between 2 or more MOZAIC aircraft are possible when aircraft are flying along similar trajectories or near the same airports, within a 3-hour interval. This permits

cross checks between different aircraft during cruise, and ascent and decent phases. Most inter-comparisons showed an excellent agreement if aircraft were sufficiently close in time (Thouret *et al.*, 1998a).

A multitude of tropospheric ozone profiles have been established within the vicinity of the respective airports for different combinations of ozone devices and aircraft. They have exhibited remarkable agreement both in profile structure (shape) and in the vertical distribution of ozone concentrations. Figure 2.10 presents four flight inter-comparison cases of ozone profiles recorded between 15 to 90 minutes apart at various airports. These comparisons confirm the ozone analyzer's data precision of ± (2 ppbv + 2%) and demonstrate that no bias exists between the different ozone devices used (Thouret *et al.*, 1998a).

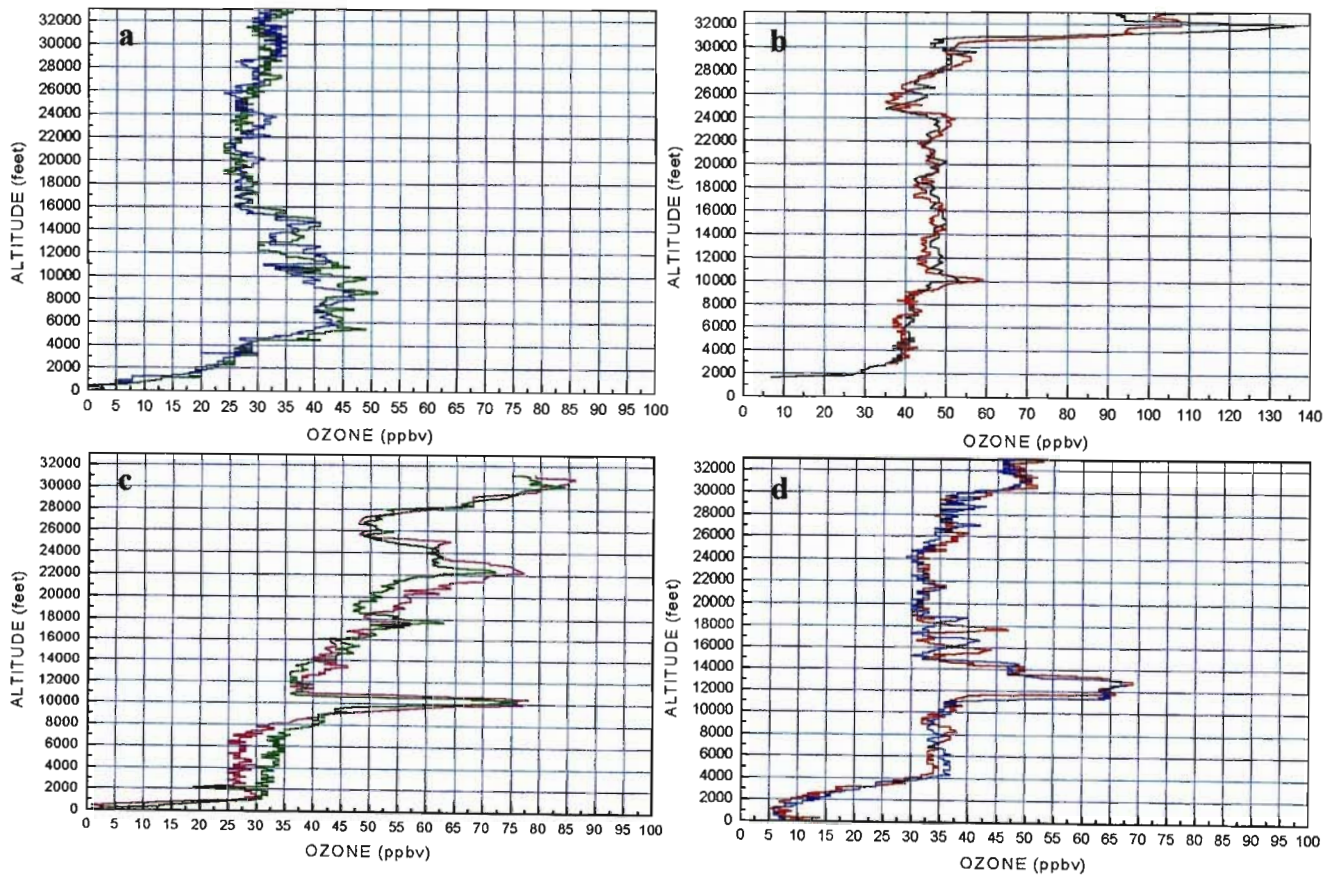

Figure 2.10: Aircraft intercomparisons (profiles):
(a) Paris 25/11/1994 – 50 min – AC49 / AC 51
(b) Frankfurt 04/03/1995 – 15 min – AC35 / AC53
(c) Osaka 09/06/1996 – 45 min – AC75 / AC 51
(d) Caracas 16/05/1999 – 90 min – AC35 / AC49
(Source: MOZAIC-II: Technical Final Report, 2000: p 17)

Flight inter-comparisons have also demonstrated that changes (if any) in the aircraft's boundary layer, perhaps caused by turbulence during ascent or descent have had no noticeable impact on measurements (Thouret *et al.*, 1998a). Similarly, anomalies have not been detected in the performance of the ozone system in extreme turbulence or when entering clouds (Cammas *et al.*, 1998).

It is concluded that MOZAIC ozone data are of excellent quality and are suitable for the generation of accurate and reliable ozone climatologies (Marenco *et al.*, 1998; Thouret *et al.*, 1998a; 1998b).

2.2.2.3 Operation of the Humidity Sensing Device and Temperature Sensor

Relative humidity and temperature measurements are recorded *in situ* using a special airborne sensing device AD-FS2, developed by Aerodata (Braunschweig, Germany). The sensing element is made up of two sensors, a capacitive sensor and a platinum resistance sensor. The capacitive sensor (Humicap-H ®, Vaisala, Finland) is used for measuring relative humidity, while the platinum resistance sensor (PT100) is used for measuring temperature at the humidity-sensing surface. Signals from the relative humidity (RH) and temperature sensors are sent to a microprocessor-controlled transmitter unit (HMP230, Vaisala, 1993), which in turn relays the signals to the automated data acquisition system. Both sensors are mounted in a special air sampling housing (Model 102 BX, Rosemount Inc., Aerospace Division, United States). The sensor housing is shown in Figure 2.11 (Helten *et al.*, 1998).

The sampled airflow is separated into two sub-flows within the housing inlet. The main flow passes straight through the main channel of the housing while the minor flow takes a right-angled turn, which leads into a smaller channel. Sampled air in the smaller channel makes contact with the sensing elements before it is expelled through a little outlet at the housing's lower back. The sensors are protected from water, dust and particles by the sharp right angle turn of the minor airflow. Tiny holes in the side walls of the housing suck out air originating from the internal boundary layer, thus minimizing internal boundary layer effects. In this way thermal or humidity influences (caused when sampled air flow makes contact with the housing walls) have negligible effects on the core of the sampled airflow. During ascent and descent, the time response of the MOZAIC sensor was found to be less

than 10 seconds near ground and under a minute at an altitude of 9 km (Helten *et al.*, 1998).

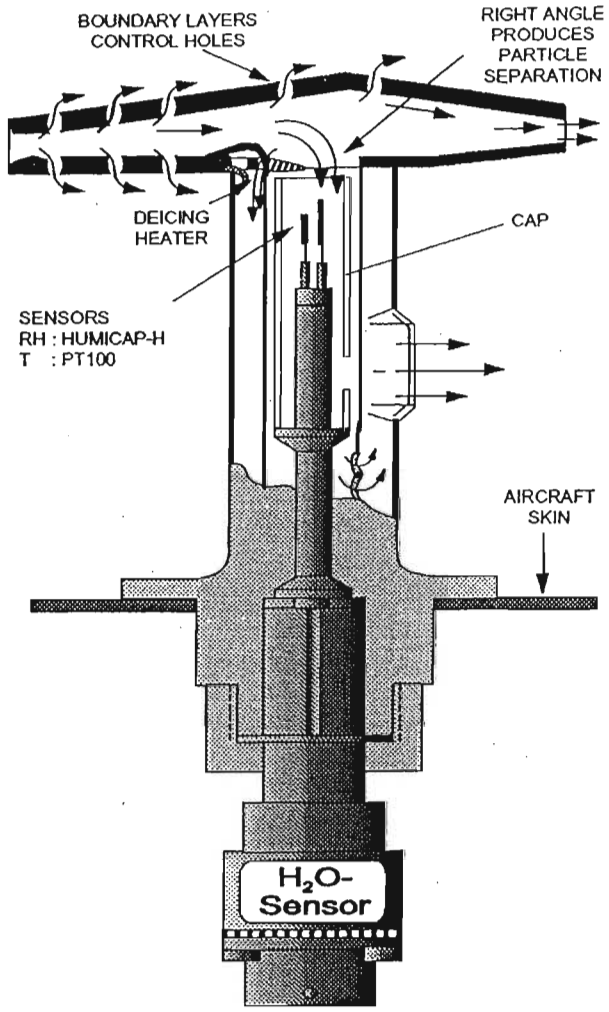

Figure 2.11: Cross section of the airborne MOZAIC humidity sensing device: humidity (Humicap-H) and temperature (PT100) sensors mounted in air sampling housing (Rosemount) (Source: Helten *et al.*, 1998: p 25644)

Very low temperature is typical at altitudes above 8 km. In these conditions, readings are usually in the lowest 10% of the sensor's range. Individual calibrations of each sensor are therefore a necessity. Each humidity sensor is subject to independent calibration in a laboratory at Jülich prior to installation aboard an aircraft and again after a period 500 flight hours. A sensor is only cleaned before a pre-flight calibration. Post-flight calibrations are performed without prior cleaning. An environmental simulation chamber is used to carry out the laboratory calibration. Temperature and pressure in the chamber are computer-controlled to simulate typical tropospheric conditions of pressure, temperature and water vapor concentration encountered up to an altitude of about 15 km.

Concentrations of water vapor are varied using independent temperature control in conjunction with the addition of saturated air released in small amounts. Air temperature inside the chamber can be varied from +30°C down to -70°C. Chamber pressure can vary between 100 and 1000 hPa (Helten *et al.*, 1998).

All measurements are subject to uncertainties. Uncertainty at high altitude ranges from ±7% RH (at –55°C, ~13 km) to ± 4% RH (-40°C, ~10 km) (Fig. 2.12). The uncertainty is within ±(4-6)% RH at lower altitude levels between -40°C (~9 km) and -20°C (lower troposphere). Uncertainty increases to ±8% RH near the surface where temperatures are above 0°C (Helten *et al.*, 1998).

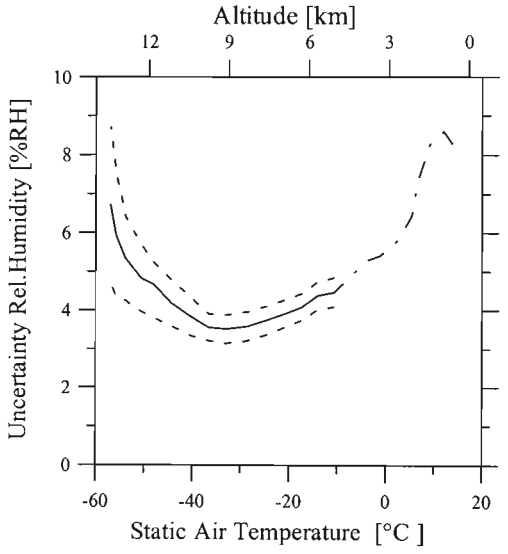

Figure 2.12: Mean uncertainty in percent RH of all 1995 MOZAIC relative humidity measurements (solid curve) as a function of static air temperature (bottom x axis). The corresponding altitude is indicated as the top x axis. The standard deviation of the mean is marked by the dashed curves. The region not covered by preflight and postflight calibrations (lower troposphere) is indicated with an estimated mean uncertainty (dashed/dotted line) (Source: Helten *et al.*, 1998: p 25650)

In March 1995 an in-flight comparison aboard a Falcon research aircraft was conducted between the MOZAIC humidity sensing device (AD-FS2) and two airborne reference instruments: a cryogenic frost point hygrometer and a Lyman-Alpha Fluorescence hygrometer. Tropospheric air masses sampled during the descent are shown in Figure 2.13 demonstrating that the MOZAIC sensing device agrees to within ±10% RH of both

reference instruments at temperatures below -10°C but measures drier values than the frost point hygrometer above -10°C (Helten *et al.*, 1998).

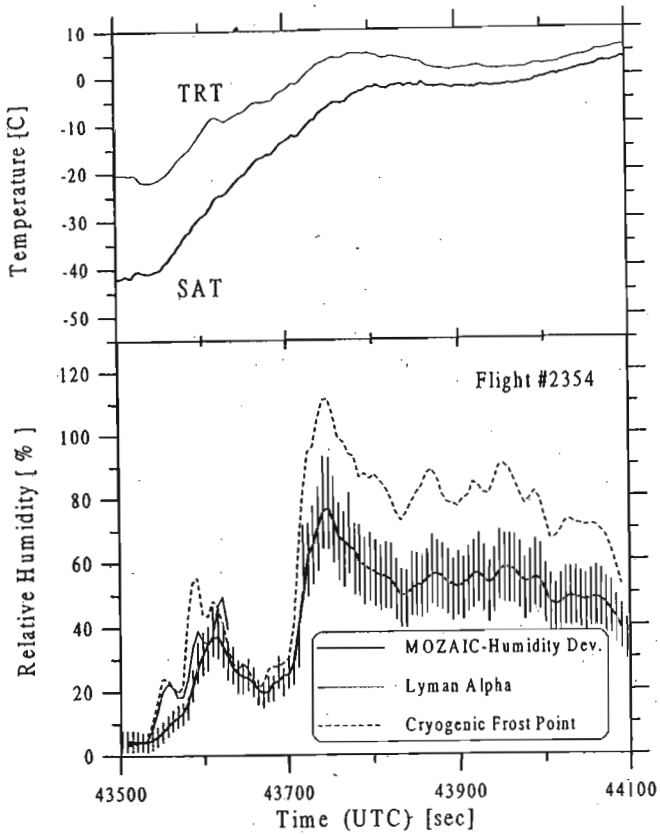

Figure 2.13: Relative humidity measured by MOZAIC humidity device, Lyman-Alpha hygrometer and cryogenic frost point hygrometer as function of flight time during descent of flight. Static air temperature (SAT, heavy line) and total recovery temperature (TRT, thin line) are shown in the upper panel of the figure (Source: Helten *et al.*, 1998: p 25651)

2.2.3 Data Base

MOZAIC data collected by the five MOZAIC aircraft are transferred to Meteo France, Toulouse once phases of calibration and validation are completed at the respective institutes responsible for instruments measuring ozone (LA/CNRS) and water vapor (KFA). The MOZAIC data are thoroughly reviewed by the processing team over an extended period of time to ensure that instrument errors, data processing errors and calibration errors are minimized. Numerical and visual checks are also done, and erratic values are finally filtered. Measurements are also evaluated against the response time of the ozone and water vapor devices (MOZAIC-II: Technical Final Report, 2000; Thouret *et al.*, 1998a).

The raw MOZAIC measurements are taken every 4 seconds, thus providing a horizontal resolution of about 1 km (at cruise altitude) and a vertical resolution of approximately 30 m (during ascent and descent). The raw observations of each flight are partitioned into 3 sets of data: ascent, cruise, and descent. Raw data of the ascent and descent profiles are averaged on a fixed altitude grid of 85 layers, each 150 metres thick. Thus all profiles are given on a constant pressure grid. For most applications, averaging by the above technique does not compromise the loss of important meso-scale information (MOZAIC-II: Technical Final Report, 2000).

MOZAIC profile data, which allow the study of vertical profiles recorded during ascent and descent phases of an aircraft near the vicinity of airports, were used in this study. A vertical profile is classified as the part of the flight, which occurs between the ground and the first stabilized level (i.e. when the aircraft levels off) or where pressure variations are less than 30 Pa (Thouret *et al.*, 1998a). The descent part of a flight is determined using a similar principle as the ascent, but in reverse (MOZAIC Readme_prof file).

A comparison of ozone climatologies was made between MOZAIC and the Ozone Sounding Network (OSN). Measurements made by both programs corresponded well. The MOZAIC climatology, which spanned 2-years (1994-1996) was generated from high-density data collected during ascents and descents at airports. The OSN climatology corresponds to measurements often more than 20 years in length from 8 locations of the OSN. The sonde data provide an extensive time series with lower frequency measurements (2-12 soundings per month), while the MOZAIC data provide higher frequency measurements (daily or weekly profiles) over a considerably shorter period (Thouret *et al.*, 1998a).

While differences exist in the nature of the two programs, a remarkable similarity is noted between climatologies derived from the two data sets. Seasonal and latitudinal variations of ozone were well represented by both data sets. Mean ozone concentrations in the free troposphere obtained from ozonesonde data exceed those derived from the MOZAIC program by approximately 3 to 13%, in a similar geographic location. These discrepancies are within the uncertainty range of both techniques (Marenco *et al.*, 1998; Thouret *et al.*, 1998a).

2.3 Total Tropospheric Ozone Methodology

2.3.1 Definition of Total Tropospheric Ozone

Total ozone (TO) is defined as the integrated amount of ozone in a vertical column of air extending from the earth's surface to the top of the atmosphere (Diab *et al.*, 1992; Zunckel *et al.*, 1992b). Total tropospheric ozone (TTO) is defined as the integrated amount of ozone in a vertical column of air in the troposphere i.e. between the surface and tropopause. Both TO and TTO are expressed as a thickness reduced to standard temperature and pressure (STP). This is given in Dobson Units (DU) where 1 DU is equivalent to 0.01 mm of ozone at STP (Combrink *et al.*, 1995; Diab *et al.*, 1992; Zunckel *et al.*, 1992).

According to Fishman *et al.* (1990), TTO constitutes 10-15% of the total column ozone. Lelieveld and Dentener (2000) state that the value is closer to the lower end of this range, viz. 10%. However, recent studies have found that there is a progressive increase in the level of tropospheric ozone on a global scale (Marenco *et al.*, 1994) and hence it is expected that the TTO component may be greater than 10%.

2.3.2 Computation of Total Tropospheric Ozone

TTO was computed from MOZAIC profile data which recorded ozone concentrations in parts per billion by volume (ppbv) at 150 m height intervals. Aircraft profiles were integrated from the surface to 12 km (above sea level) giving a TTO value in DU.

The method used to compute integrated tropospheric column ozone (or the column ozone amount in the troposphere) is based on ozone readings in ppbv at available levels and the conversion to DU at each level is estimated as follows:

$$O_{DU} = \left(\frac{\frac{O_{PPBV}}{10^{-9}} * P * \Delta H * 273.15 * 1000}{1013.25 * T_K} \right) * 100$$

...where O_{PPBV} = ozone concentration (ppbv)

O_{DU} = ozone in Dobson Units (DU)

T_K = temperature (K)

$\Delta H = \frac{\text{difference in height between 2 successive layers (gpm)}}{2}$

P = pressure (hPa)

The total column ozone is obtained by integrating the ozone profiles between the surface and 12 km.

Subsequently, TTO was subdivided into layers within the troposphere in order to undertake an analysis of the relationship between tropospheric ozone and stable layers in the atmosphere. The layers (surface-3 km; 3-5, 5-7 and 7-12 km) were selected based on the presence of absolutely stable layers as detected by Cosijn and Tyson (1996).

2.3.3 Data Selection and Processing

Of the 427 ozone profiles that were available over the period 1995-1998, a total of 381 profiles were finally selected for the computation of TTO. The remaining 46 were discarded due to continuous missing data over a vertical distance that exceeded 1050 m. Data were interpolated from the mean monthly profile if the height interval/s over which data was missing was less than 1050 m.

2.4 Stable Layer Methodology

2.4.1 Definition of an Absolutely Stable Layer

An absolutely stable layer is defined as a layer of air where the observed environmental lapse rate of temperature is less than the saturated adiabatic lapse rate. These thermodynamic conditions constrain free vertical movement of air except under conditions of strong convection. Thus stable layers prevent vertical transport of pollutants such as ozone and have the effect of trapping pollution between intervening layers (Cosijn and Tyson, 1996).

According to Cosijn and Tyson (1996), the stability structure of the atmosphere over southern Africa has a strong influence on the accumulation and dispersal of atmospheric pollutants. It is also responsible for controlling the horizontal transport of pollutants over vast distances.

Whilst studies undertaken by Anderson *et al.* (1996), Blake *et al.* (1996), Gregory *et al.* (1996), Heikes *et al.* (1996), Singh *et al.* (1996) and Talbot *et al.* (1996), have focussed on the role that inversions of temperature play in the vertical distribution of trace gases and aerosols, Swap and Tyson (1999) state that vertical transport and mixing in the troposphere is controlled more by stable layers, which are a less conservative measure of atmospheric stability than temperature inversions.

2.4.2 Computation of Absolutely Stable Layers

The MOZAIC data base records two temperature readings, the A340 static temperature, which is provided by the aircraft computer, and static temperature, which is recorded by the MOZAIC sensors. Since many of the sensor data were recorded as missing, the A340 static temperatures were used instead. A number of intercomparisons between static temperature and A340 static temperature profiles for the same flight were performed (where both were available) to establish whether there were differences between the two sets of readings. Figure 2.14 shows an example of an intercomparison for 20 September 1998. Excellent agreement between the two sets of readings is observed.

Each temperature profile was plotted on a tephigram. The gradient of each segment of the temperature profile (line between 2 successive temperature measurements) was compared with that of the saturated adiabatic lapse rate. If the gradient of the environmental lapse rate was less than that of the saturated adiabatic lapse rate, this layer of air was regarded as an absolutely stable layer.

Since the occurrence of stable layers were identified according to pressure levels on the tephigram, the corresponding equivalent height above sea level (barometric altitude) of each pressure reading was used to plot stable layers on a graph. The pressure and height readings referred to above are recorded simultaneously by the MOZAIC database. Temperature inversions (where temperature increases with height) and isothermal

conditions (where there is no variation of temperature with height) were distinguished from the absolutely stable layers.

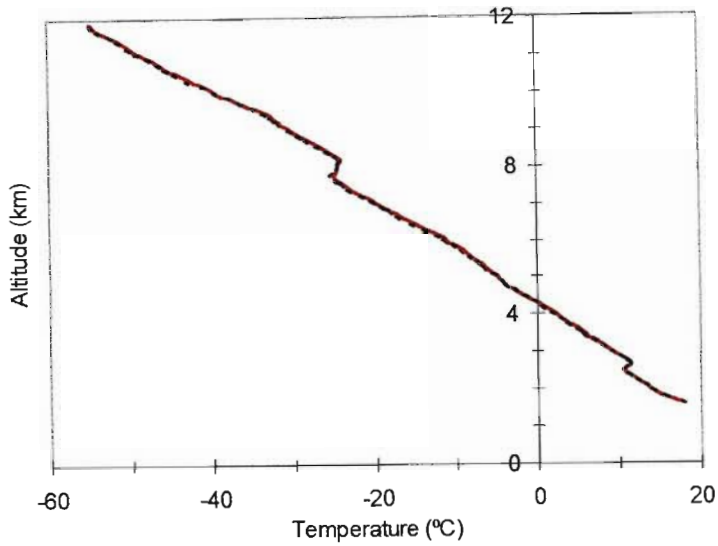

Figure 2.14: An intercomparison between static temperature (red line) and A340 static temperature (black dashed line) profiles for 20 September 1998 (Source: plotted from MOZAIC profile data)

2.5 Classification of Ozone Profiles

2.5.1 Rationale

Tropospheric ozone profiles display marked variation in their vertical structure on a day-to-day basis, in response to dynamic and photochemical processes. Not only do the altitudes and magnitudes of maxima and minima change but the vertical structure appears very irregular, sometimes exhibiting marked stratification with a single or double peak, and at other times exhibiting a uniform profile and absence of structure, indicative of a well-mixed atmosphere.

Different approaches have been used to analyze ozone profiles. The most common approach is the computation of mean ozone profiles averaged by season or year, together with some measure of variability about these means. These are sometimes difficult to interpret because of the counteracting influences inherent in the micro-structure and hence, computation of a mean profile has its limitations. Case study analysis on the other hand has been used to gain an understanding of processes operating but has not contributed very much to our knowledge of the frequency of occurrence of such events.

In this study an alternative approach to the analysis of ozone profiles is adopted. Specifically, a search for pattern and order in the ozone profiles is conducted, in which the objective is to develop a classification of ozone profiles. It is expected that this approach will offer important insights into the dynamic and photochemical processes responsible for the vertical structure of ozone. Classification was also undertaken to find out whether the source of this variability could be linked to a seasonal influence.

2.5.2 Classification Technique

2.5.2.1 Hierarchical and Non-hierarchical Classification

The central purpose of classification is to summarize large data sets such that similar entities are assigned to clusters (classes or groups). The resultant output from classification is either a non-hierarchical or hierarchical arrangement of cases. Non-hierarchical classification merely allocates each case to a cluster, grouping cases according to their similarity. Non-hierarchical classification mitigates noise, identifies outliers, and summarizes redundancy, but does not characterize relationships among clusters based on their similarity (Gauch, 1982). Hierarchical classification is similar to non-hierarchical classification in that it groups similar entities into classes, but additionally arranges these classes in a hierarchical manner, which can be graphically illustrated as a dendogram. Dendograms indicate relationships or show the relative similarity among classes or groups (Everitt, 1978; Gauch, 1982; Gauch and Whittaker, 1981; Sneath and Sokal, 1973).

Hierarchical classification techniques fall into three major categories, namely monothetic divisive, polythetic agglomerative, and polythetic divisive (Gauch, 1982). Monothetic divisive classification techniques start with the division of a single group containing all samples into a hierarchy of smaller and smaller groups based on the behaviour of a single variable. Polythethic agglomerative classification techniques consider each sample as a separate group and then progressively aggregate groups until all samples are contained within a single group. Polythethic divisive classification techniques start with the division of a single group containing all samples into a hierarchy of progressively smaller groups until each group contains a single sample or some specified number of samples (Gauch, 1982). It is the last classification technique which was applied in this study, and which is discussed in the next section.

2.5.2.2 TWINSPAN (Two-way indicator species analysis)

The cluster analysis program called TWINSPAN (Two-Way INdicator SPecies ANalysis) (Hill, 1979), that is often used in ecological applications to classify vegetation into communities, was used in this study. In vegetation studies, the samples are differentiated on the basis of species composition and abundance. In this study, the samples or cases were grouped according to the magnitude and altitude of ozone mixing ratios in a profile.

Although a wide variety of cluster analysis techniques are available, TWINSPAN was deemed appropriate as the classification divisions are based on indicator species, defined as those that occur in more than 80% of the samples of one group and less than 20% of the other group (Hill, 1979). Analogous to indicator species are the presence of ozone peaks at certain altitudes in this application. The cases (profiles) are divided successively into a hierarchy of smaller and smaller clusters until finally each cluster contains only one sample or a user-specified small number of cases. An advantage of TWINSPAN is that it has effective and robust properties with minimal computer requirements. Further, divisions at each level are automatic and impartial (Gauch, 1982).

A dendogram can be used to display the sample hierarchy generated by the TWINSPAN output (Gauch and Whittaker, 1981). Unlike any other hierarchical classification program, TWINSPAN intentionally assembles the two extremes on the ordination axes at each node in a manner whereby samples that have the closest resemblance are placed side-by-side in the dendogram's sample sequence (Gauch, 1982). This allows a single analysis to be viewed at a variety of levels, progressing from general to detailed, and expresses relationships among classified entities. The sample sequence for a series of samples is indicated along the abscissa. As one progresses from the origin, levels on the ordinate represent increasingly finer divisions of the samples into groups that are progressively more similar. Samples grouped at the top of the dendogram (level 0) are most dissimilar, whereas samples grouped at the bottom (e.g. level 6) are most similar (Gauch, 1982).

In this study the output was analyzed after three levels of division, since further sub-division represented minor, less meaningful divisions. The extent of similarity between groups is provided by an eigenvalue, which ranges between 0 and 1. A low value indicates a high degree of similarity between groups and an eigenvalue closer to 1 indicates a high

degree of difference. Therefore, high eigenvalues indicate divisions between samples that are markedly different, and which are therefore meaningful.

2.5.2.3 Input Data for TWINSPAN

In adapting the TWINSPAN program for this analysis, each ozone profile was regarded as a sample or case, in which the elevation was taken as equivalent to the species and the ozone concentration at that height as the species abundance. The TWINSPAN program does not permit missing data and hence only a total of 56 profiles (out of 516 profiles available over the period 1995-2000) with no missing values between the surface and 12 km were used. In addition, elevation levels had to be entered with a fixed interval between successive readings. Barometric altitude could not be used in this instance as it gives the precise height of an ozone reading and successive measurements do not occur at a fixed interval. Consequently, the mid-layer altitude for consecutive ozone readings which is constant for all profiles, was used instead.

A number of intercomparisons between ozone concentration as a function of mid-layer altitude and barometric altitude for the same flight were performed. Figure 2.15 shows an example of one such intercomparison for 28 August 1998. The black dashed line represents the vertical distribution of ozone concentration plotted against mid-layer altitude while the red line represents the vertical distribution of ozone concentration plotted against barometric altitude. An excellent agreement was found between the two profiles, indicating that mid-layer altitude could be substituted for barometric altitude.

2.6 Back Trajectory Modelling

2.6.1 Rationale

In this study, back trajectory analysis has been used to find the origin of air masses arriving at four selected tropospheric levels for each ozone profile used in the classification scheme (discussed in section 2.5). Back trajectory analysis can help to identify possible sources and important transport pathways of substances with atmospheric lifetimes shorter than a few weeks (Merrill, 1994).

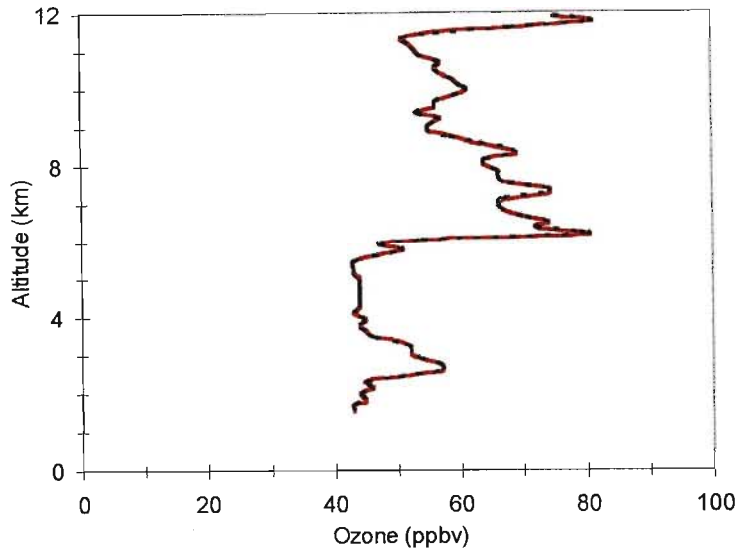

Figure 2.15: A sample ozone profile as a function of barometric altitude (red line) and mid-layer altitude (black dashed line) for 28 August 1998 (Source: plotted from MOZAIC profile data)

2.6.2 Hybrid Single-Particle Lagrangian Integrated Trajectory (HYSPLIT) Model

Back trajectory modelling was undertaken using the HYSPLIT (version 4) model, which was jointly developed by the National Oceanic and Atmospheric Administration (NOAA) and modified by the Australian Bureau of Meteorology (Draxler, 1998). The HYSPLIT model is the most recent version of a comprehensive system designed for computing simple air trajectories to highly elaborate dispersion and deposition simulations (Draxler, 1999b; Draxler and Hess, 1997; Heffter, 2002). It is an interactive model that can be accessed on the Real-time Environmental Applications and Display sYstem (READY) website: http://www.arl.noaa.gov/ready/hysplit4.html.

2.6.3 Description of the HYSPLIT (Version 4) Model

Traditionally, the modelling of atmospheric transport has been accomplished using either an Eulerian or a Lagrangian framework (Stein *et al.*, 2000). The technique employed by the HYSPLIT model calculation is a hybrid between the two approaches (Draxler and Hess, 1998; Heffter, 2002; Rolph *et al.*, 1992; 1993; Stein *et al.*, 2000), hence the "hybrid" component of the acronym refers to the application of both 'Lagrangian' and 'Eulerian' modeling frames of reference within the system (Draxler, 1999a).

Eulerian models, which are characteristically applied when complex emission scenarios are considered, solve the advection-diffusion equation on a fixed grid. Lagrangian models, which are characteristically favored when single-point-source emissions restrict computations to a few grid points, calculate advection and diffusion components independently (Draxler and Hess, 1998; Heffter, 2002; Stein *et al.*, 2000).

Hybrid models emerge as a third possibility for handling the transport and transformation of chemical species in the atmosphere, as they combine advantages of both Lagrangian and Eulerian features (Stein *et al.*, 2000).

2.6.4 Input Data

The meteorological fields used in the HYSPLIT model were four dimensional gridded fields from the National Centre for Environmental Prediction (NCEP). HYSPLIT calculates trajectories using various meteorological forecast models. In this study, Reanalysis archive data and FNL archive data was used for trajectories computed during 1995-1999 and 2000 respectively.

For this study, 5-day kinematic back trajectories were computed from Johannesburg (26.13°S; 28.24°E), at four standard heights (2.5, 5, 7.5 and 10 km), except for minor modifications in the mid-troposphere to take account of observed ozone peaks on particular days. Specifically, for categories 2c and 3d (in the classification scheme) the 5 km height was replaced by 6 and 4 km respectively, and for category 3c, the 7.5 km height was replaced by 8 km.

The kinematic approach was used as the meteorological model generates three-dimensional velocity fields that take diabatic and adiabatic factors into account (Draxler, 1996). Although trajectories can be calculated up to 13 days back, a maximum run time limit of 5 days was chosen as it would yield a more accurate calculation.

2.6.5 Output Data

Output data produced by the HYSPLIT model is in the form of back trajectory maps (Fig. 2.16) which depict the general path taken by air parcels before reaching their point of

origin. The aerial view (top panel) shows the horizontal movement of air parcels while the vertical view (bottom panel) shows the vertical movement of air parcels. Symbols along each trajectory indicate the relative position of the air parcel at 24-hour intervals. Height is given in meters above ground level.

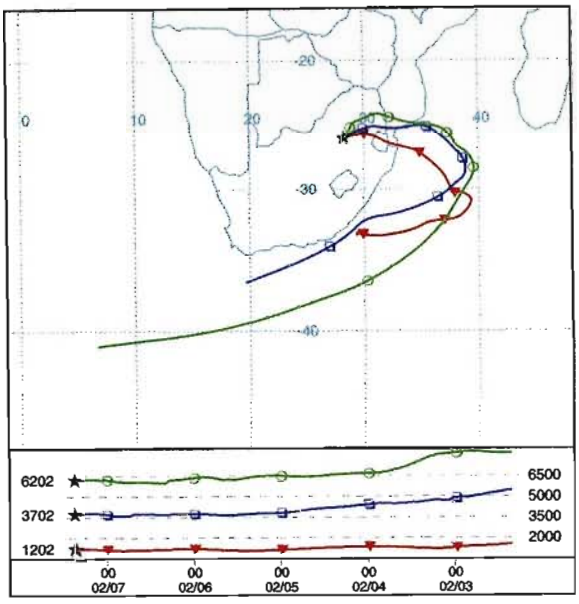

Figure 2.16: 5-day back trajectory HYSPLIT model results for 7 February 1996. Horizontal (top) and vertical (bottom) plots of back trajectories originating at 2.5, 5 and 7.5 km

2.6.6 Limitations

Back trajectory analysis has many sources of error and uncertainties as meteorological fields are known to fluctuate continually in time and space and are sometimes inadequately represented by a field defined at fixed locations and at fixed temporal intervals (http://www.arl.noaa.gov/slides/ready/traj/traj3.html). It must be remembered that back trajectories only offer an estimate of air movement. Thus, the primary application of trajectories should be a diagnostic tool used to evaluate the flow field at different atmospheric levels (Heffter, 2002). However, trajectories based on meteorological data that are routinely available are reasonably accurate under normal atmospheric conditions (Merrill *et al.*, 1986).

CHAPTER 3

CHEMISTRY AND DYNAMICS OF TROPOSPHERIC OZONE

3.1 Introduction

This chapter focuses on the role of photochemical and dynamical processes in the tropospheric ozone budget. Tropospheric ozone is known to vary markedly, both in the horizontal and the vertical in response to photochemical and dynamic processes operational in the atmosphere.

Tropospheric ozone makes up only ~10% of the total atmospheric ozone present in the atmosphere, while the larger portion, of the order of 90%, is present in the stratosphere. It plays an important role in the regulation of various oxidation processes in the atmosphere as it is responsible for the production of hydroxyl (OH) radicals (Lelieveld and Dentener, 2000). OH is produced by photodissociation of ozone in the presence of water vapor and controls the atmospheric lifetime of many gases (Levy, 1971).

Initially it was alleged that the ozone in the troposphere originated from the stratosphere through rapid intrusions of stratospheric air. Early analysis based on the observed ozone gradient with altitude led researchers to believe that tropospheric ozone was controlled by stratospheric-tropospheric exchange (STE) (Danielsen, 1968; Junge, 1962). This first analysis was suggestive of a source at the tropopause and a sink at the surface. In the 1960s, interest was directed towards tropospheric ozone formation by *in situ* photochemistry as it was recognised that extreme ozone episodes in urban areas during summer could be attributed to the breakdown of hydrocarbons (Leighton, 1961). Thus two contrasting schools of thought developed around the source of tropospheric ozone, where one supported the notion that ozone was transported from the stratosphere (Levy *et al.*, 1985), while the other favoured the role of *in situ* photochemistry (Chameides and Walker, 1976). However, it is now known that both dynamic and photochemical processes play a significant role in the tropospheric ozone budget.

Three-dimensional (3-D) global chemistry transport models (CTMs) which have been developed to account for both photochemical and dynamical processes highlight the

relative importance of STE but indicate that net *in situ* photochemical production is the major contributor to ozone levels in the troposphere (Lelieveld and Dentener, 2000).

The following sections examine the photochemical sources and sinks (section 3.2) and the stratospheric exchange processes (section 3.3) contributing to the tropospheric ozone budget.

3.2 Photochemical Processes

Ozone production and destruction in the troposphere occurs through a series of complex photochemical reactions. Nitrogen oxides ($NO_x = NO + NO_2$) serve as catalysts during *in situ* ozone formation (Crutzen and Lelieveld, 2001; Lelieveld and Dentener, 2000), for example in the oxidation of carbon monoxide (CO) to carbon dioxide (CO_2):

(R1) $CO + OH(+M) \rightarrow H + CO_2(+M)$

(R2) $H + O_2 + M \rightarrow HO_2 + M$

(R3) $HO_2 + NO \rightarrow OH + NO_2$

(R4) $NO_2 + hv \rightarrow NO + O \quad (\lambda \leq 400 \text{ nm})$

(R5) $O + O_2 + M \rightarrow O_3 + M$

net: $CO + 2O_2 \rightarrow CO_2 + O_3$. (adapted from Crutzen and Lelieveld, 2001)

The net result of the above catalytic chain of reactions is the oxidation of CO to CO_2 and ozone formation. (R3) is a critical step in the reaction chain because a deficiency of NO will lead to a loss of ozone as HO_2 will now react with O_3 instead:

(R6) $HO_2 + O_3 \rightarrow OH + 2O_2$ (adapted from Crutzen and Lelieveld, 2001)

with the following net result:

(R7) $CO + O_3 \rightarrow CO_2 + O_2$. (adapted from Crutzen and Lelieveld, 2001)

CH_4 and other hydrocarbons are also oxidised similarly. The possible net result of the oxidation of CH_4 to CO in NO_x-rich air is summarised as:

(R8) $CH_4 + 8O_2 \rightarrow CO + H_2O + 4O_3 + 2OH$ (adapted from Crutzen and Lelieveld, 2001) leading to a net production of O_3 and OH.

In contrast, the net result in NO_x-deficient air may be summarised as:

(R9) $CH_4 + OH + HO_2 \rightarrow CO + H_2 + 2H_2O$ (adapted from Crutzen and Lelieveld, 2001) with loss of OH and HO_2.

The above reactions emphasize that NO_x plays an important role, in that ozone production predominates in NO_x -rich air while destruction prevails in NO_x-deficient air (Crutzen, 1973). Photo-oxidation of CO, CH_4, and other hydrocarbons controlled by NO_x accounts for at least 90% of tropospheric ozone production (Lelieveld and Dentener, 2000).

3.2.1 Sources Contributing to the Tropospheric Ozone Budget

Emissions resulting from urban/industrial environments, biogenic sources, biomass burning, and lightning are regarded as some of the most important sources of ozone precursor gases in the troposphere. Each of these source categories will be examined in turn.

3.2.1.1 Urban/Industrial Emissions

In recent years, NO_x emissions resulting from the combustion of fossil fuels and industrial activities have become an important source of tropospheric ozone, particularly in the Northern Hemisphere, where large increases have been noted. Industrial and fossil fuel burning sources presently make up 20-30% of the tropospheric ozone column in Northern Hemisphere tropics and 10-20% in tropical and extratropical areas of the Southern Hemisphere (Fig. 3.1). The burning of fossil fuels accounts for more ozone being produced from industrial emissions than that of biomass burning at low northern latitudes (Lelieveld and Dentener, 2000)

Although smaller in magnitude than sources in the Northern Hemisphere, regions of intense industrial emissions in southern Africa are the Zambian copper belt mining operations and charcoal kilns in south-central Africa and the South African highveld. The

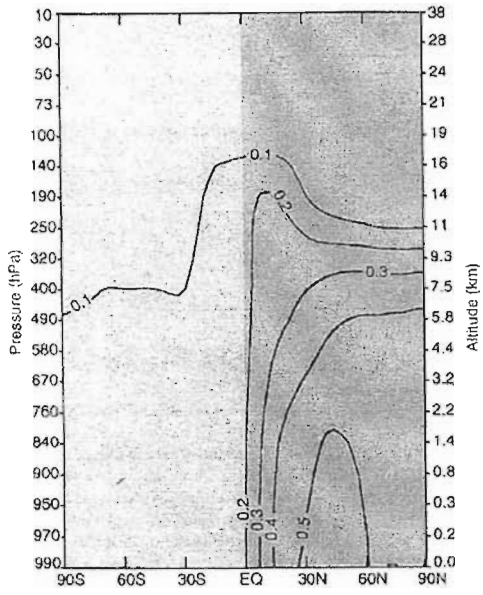

Figure 3.1: Calculated zonal and annual mean fractional contribution to tropospheric ozone by industrial emissions and all fossil-fuel-related sources for the present day atmosphere (Source: Lelieveld and Dentener, 2000: p 3545)

South African highveld possesses 8 large coal-fired power stations, 14 timber factories, 2 petrochemical operations, 10 smelters, 12 brick factories, and 15 coal and metal mines. These operations have an enormous influence on regional tropospheric ozone levels and urban smog, particularly during autumn (Kirkman *et al.*, 2000).

The source of precursor gases involved in the photochemical production of ozone are mainly concentrated in polluted urban environments where intense industrial activities and automobile emissions occur (Chameides and Walker, 1973; Crutzen *et al.*, 1985; Zunckel *et al.*, 1992b). Urban-industrial emissions of nitrogen oxides and hydrocarbons or volatile organic compounds (VOCs) are important in the production of photochemical smog, a major constituent of which is ozone (Stevens, 1987). The incomplete combustion of petroleum-based fuels in motor car engines and industrial machinery produces exhaust fumes which are high in hydrocarbons, CO, and CH_4 (Logan, 1985). Some of these hydrocarbons are partially combusted (Zeller and Moussiopoulos, 1986) and can produce peroxy radicals which then participate in the efficient production of photochemical ozone (Logan, 1985). Hydrocarbon emissions are accelerated largely due to peak hour traffic and poor engine combustion (Stevens, 1987). This was confirmed by Zeller and Moussiopoulos (1986) as they found that hydrocarbon emission factors showed a rapid increase in these conditions.

3.2.1.2 Biogenic Emissions

Harris *et al.* (1996) have shown that biogenic emissions make a significant contribution to ozone enhancement. Although continuous throughout the year (Scholes and Andreae, 2000), biogenic emissions are most important in the month of October in the Southern Hemisphere (Diab *et al.*, 1996a). As these emissions are produced close to the surface, their effect on tropospheric ozone production is most prominent in the boundary layer (Diab *et al.*, 1996a). This observation is consistent with ozone profiles measured during the Amazon Boundary Layer Expedition (ABLE 2A) experiment in Brazil (Jacob and Wolfsy, 1988) and at Ethosa National Park (ENP) during the SAFARI-1992 period (Swap *et al.*, 1996)

According to Lelieveld *et al.* (1999), it is estimated that the amount of NO_x emitted from soil to the present-day atmosphere is ~5-12 Tg N per year. The injection of fresh biogenic NO_x emissions into an air mass already enriched with biomass burning emissions enhances ozone production, especially if most of the NO_x of biomass burning origin has already been converted to NO_y (Harris *et al.*, 1996).

Owing to high temperatures and their wide geographic coverage, savannas in the tropics and subtropics are one of the key source regions of global soil biogenic NO. According to modelling studies (Potter *et al.*, 1996; Yienger and Levy, 1995), since Africa is covered by 65% of tropical savannas (Huntley and Walker, 1982), they can be regarded as an important contributor to such emissions (Levine *et al.*, 1996; Scholes and Andreae, 2000). Recent measurements over west and southern African savannas indicated that NO emission rates vary widely (Harris *et al.*, 1996; Parsons *et al.*, 1996), in response to varying degrees of soil moisture and soil nutrient content (Parsons *et al.*, 1996; Scholes and Andrea, 2000).

Vast quantities of biogenic soil emissions are released following rainfall events (Anderson *et al.*, 1998; Harris *et al.*, 1996; Levine *et al.*, 1988; Swap *et al.*, 1996), particularly during the dry season or at the onset of the wet season (Harris *et al.*, 1996). Light rainfall (less than 25 mm) which occurs after long dry spells results in large increases in NO emissions (Levine *et al.*, 1996), while heavy rainfall (more than 25 mm), typical of the wet season has a dampening effect (Cardenas *et al.*, 1993). Maximum quantities of NO_x are emitted from savanna soils if the soil moisture content varies between 40-60% (Cardenas *et al.*,

1993). The observed high NO_x emissions over ENP were similarly linked to the light rainfall events that brought the soil moisture content into the above range (Harris *et al.*, 1996).

Burning also has the effect of enhancing biogenic soil emissions (Anderson *et al.*, 1988; Levine *et al.*, 1988; Levine *et al.*, 1990; Swap *et al.*, 1996). According to Levine *et al.* (1988), increases in the level of soil ammonium (a main constituent of ash) can trigger the release of higher quantities of NO and N_2O.

Harris *et al.* (1996) concluded that high levels of biogenic NO soil emissions may be a significant source on a regional scale, comparable to or higher than that attributable to savanna burning (Levine *et al.*, 1996), with important consequences for the regional production of tropospheric ozone. Scholes and Andrea (2000) suggested that these emissions may play an important role in the observed seasonal ozone enhancement over the South Atlantic Ocean.

According to Guenther *et al.* (1995) more than 90% of the global non-methane hydrocarbons (NMHCs) are produced by vegetation. Although large differences exist in the amount of NMHC emitted for different plant species (Scholes and Andreae, 2000), estimates based on savannas of southern African indicate that they have an isoprene and monoterpene emission capacity in the region of 10 mg C m^{-2} per hour and 0.5 mg C m^{-2} per hour respectively (Guenther *et al.*, 1995). Clearly, savannas in the tropics and subtropics are inclined to influence NMHC budgets on a global scale (Scholes and Andreae, 2000).

CO production results from chemical oxidation of soil organic matter (Conrad and Seiler, 1985), and biological oxidation of CO by soil microorganisms (Seiler and Conrad, 1987). However, it was found that CO was produced more efficiently from surface litter and nonliving grass as compared to soil (Zepp *et al.*, 1996). This source in African savannas and grasslands is mainly active during daylight hours and has the potential to reach very high levels (Scholes and Andreae, 2000).

3.2.1.3 Lightning

NO_x produced by lightning is a natural ozone precursor and therefore played an important role in the global *in situ* photochemical production of ozone in the pre-industrial era. Lightning NO_x-derived ozone still remains relatively important, particularly in tropical regions (Lelieveld and Dentener, 2000) and in the upper troposphere (Ridley *et al.*, 1996; Zhang *et al.*, 2000). However, NO_x emissions generated by lightning are the least understood of all tropospheric NO_x sources (Price *et al.*, 1997).

Bond *et al.* (2002) analysed measurements made by the Lightning Imaging Sensor (LIS) used to produce estimates of lightning-generated NO_x in the tropics. These estimates were then weighed against three other dominant sources of NO_x to determine the importance of lightning in tropospheric ozone formation.

Figures 3.2a-d and Figure 3.2e show the seasonal and annual distribution of lightning NO_x production in the tropics respectively. Most of the NO_x is produced over land where convection and lightning are enhanced due to higher solar heating than the ocean. Central Africa shows the greatest annual production while production over the Saharan and central Australian deserts occurs to a slightly lesser extent (Fig. 3.2e). NO_x production is also seasonally dependent, with highest concentrations over South America, Australia, and southern Africa during the Southern Hemisphere summer (Fig. 3.2a), and over North America, central Africa, and Asia during the Northern Hemisphere summer (Fig. 3.2c). NO_x production over ocean surfaces is also prevalent between 20°N-10°S.

Annual averages of NO_x emissions due to anthropogenic activity, biomass burning, soil release and lightning production are compared in Figure 3.3 (Bond *et al.*, 2002). It is noted that anthropogenic activity in the industrialized areas of the United States, India and China exhibit the highest production rates.

Figure 3.4 shows seasonal maps of the ratio of lightning NO_x production to the total from all four sources from where it is evident that lightning alone produces the same amount of NO_x as that from the other three sources combined. With the exception of ship routes (depicted as lines over the oceans in Figure 3.3a), all the NO_x over ocean surfaces has been attributed to lightning. Lightning accounts for less than 10% of the total NO_x, during the

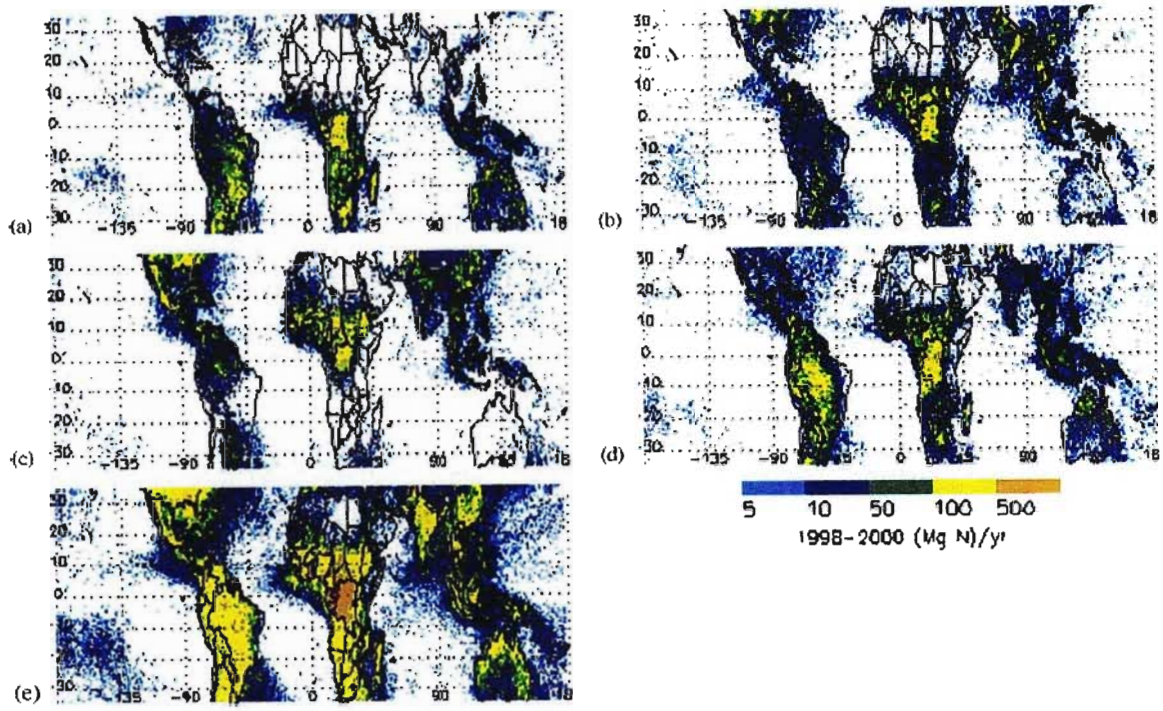

Figure 3.2: Global distribution of lightning generated NO_x (Mg N) for (a) DJF, (b) MAM, (c) JJA, (d) SON and (e) the entire year. Values are based on LIS lightning measurements from 1988-2000 data and have a 0.5° resolution (Source: Bond *et al.*, 2002: p 1511)

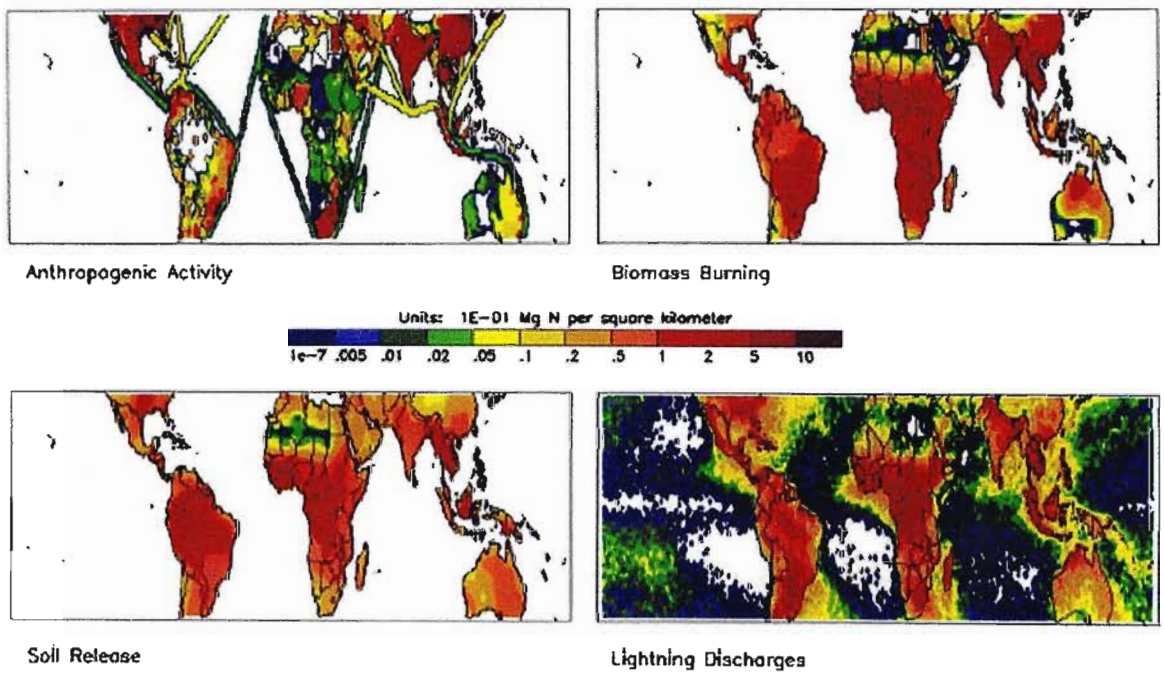

Figure 3.3: Comparison of annual averages of nitrogen oxide emissions due to anthropogenic activity, biomass burning, soil release and lightning production in the tropics (Source: Bond *et al.*, 2002: p 1514)

Northern Hemisphere winter over all continents in the Northern Hemisphere, and most of the Southern Hemisphere continents during the Southern Hemisphere winter. At least 40% of the NO_x during the Southern Hemisphere summer can be attributed to lightning over many regions in South America, southern Africa, and Australia. Lightning produces 10-90% of the NO_x over North America and northern Africa during the Northern Hemisphere summer (Bond *et al.*, 2002).

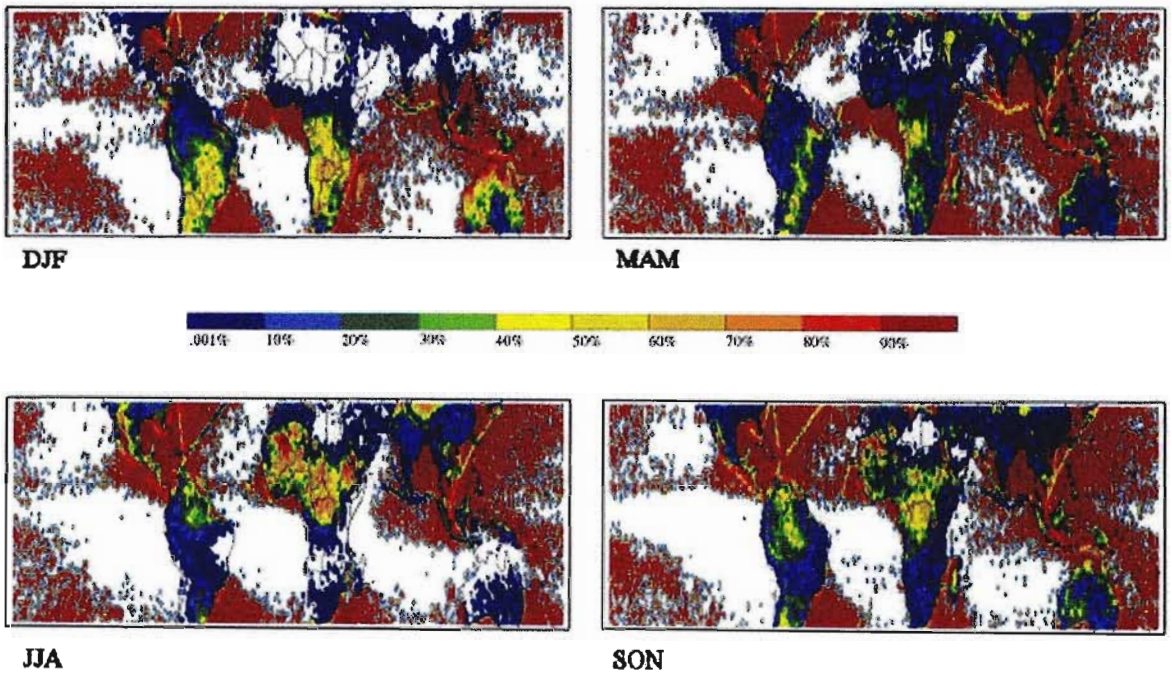

Figure 3.4: Seasonal maps of the ratio of lightning nitrogen oxide production to the total from all four sources (anthropogenic activity, biomass burning, soil release and lightning) in the tropics. The values are given in percentages (Source: Bond *et al.*, 2002: p 1515)

According to Bond *et al.* (2002) satellite data have shown that 76-85 % of global lightning occurs in the tropics making it the main source of lightning NO_x on a global scale. Lightning is the main source of NO_x that is directly released into the middle and upper troposphere (Bond *et al.*, 2002) and is therefore crucial to ozone production at these altitudes (Tie *et al.*, 2001). Ozone production in biomass burning plumes occurs mainly in the free troposphere and therefore relies heavily on NO_x produced by lightning (Lelieveld and Dentener, 2000) as surface-generated NO_x has a very short lifetime of a few hours at low altitudes (Bond *et al.*, 2002; Lelieveld and Dentener, 2000) and is destroyed before making it to the free troposphere by convective transport (Lelieveld and Dentener, 2000).

3.2.1.4 Biomass Burning

Biomass burning refers to the large scale burning of vegetation, which includes savanna, forests and grasslands, domestic fuels and agricultural wastes (Andreae, 1991; Crutzen and Andreae, 1990). It is a global phenomenon occurring in the tropics, temperate zones and in the boreal forest. According to Lelieveld and Dentener (2000) biomass burning has increased by 200% from the pre-industrial period to the present time, and has been accompanied by a shift in emissions from high to low latitudes. Present contributions of emissions from biomass burning at tropical latitudes are of the order of about 10-15 % to the tropospheric ozone column (Lelieveld and Dentener, 2000).

Fire is an important management tool and is used periodically in most ecosystems (Cofer *et al.*, 1996). Intentional burning is a traditional practice used in western and central Africa to improve game capture, discard useless bushes or foliage, and to regulate pests (Andreae, 1993; Cahoon *et al.*, 1992; Crutzen and Andreae, 1990). Prescribed burns and natural fires are employed by national parks and game reserves within southern and eastern Africa as management tools for the maintenance of forage for wildlife, whilst clearing and burning for cattle production and forestry activities are a global practice (Trollope, 1984). Although southern African fires are mainly due to human activities, a large number of fires are caused by lightning (Swap *et al.*, 1996).

Biomass burning occurs mainly during the dry season corresponding to the period from May to October in southern Africa (Cahoon *et al.*, 1996; Scholes *et al.*, 1996a, 1996b; Scholes and Andreae, 2000; Swap *et al.*, 1996). It is a significant source of tropospheric ozone precursors (Andreae, 1991; Crutzen and Andreae, 1990; Lacaux *et al.*, 1996; Levine, 1991) having a large effect on air pollution and global climate (Hao *et al.*, 1996; Ward *et al.*, 1996), as it occurs on an extensive scale. The biomass burning season is directly linked to the rainfall seasonality of the region. Rainfall during the growing season coupled with lower grazing due to a low palatability of the flora causes a build up of fuelwood which later becomes dry and prone to burning (Scholes and Andreae, 2000).

The tropics account for about 80-90% of the total global biomass burned (Crutzen and Andreae, 1990; Hao and Liu, 1994). Of this, savanna fires account for about 50-67% of fire emissions (Hao and Liu, 1994). The African continent alone holds at least half of the

world's savanna biome (Cofer *et al.*, 1996) and every year, 440 million hectares of this is burned (Hao *et al.*, 1996).

Emissions related to fire are mainly located between 5° and 20°S (Scholes *et al.*, 1996b; Swap *et al.*, 1996). This area experiences a subhumid, seasonal climate and is dominated by savannas and woodlands (Scholes *et al.*, 1996b). There is a shift in the dry season from the Northern to the Southern Hemisphere during the first half of the year, so fire activity in the tropics, especially that of savannas follows a north to south progression over the course of the year (Cahoon *et al.*, 1992). Satellite observations reveal that the Southern Hemisphere of Africa is characterised by a west-east progression of drier conditions accompanied by a shift of enhanced fire activity in the same direction. Thus western and interior countries such as Angola, Zambia, southern Zaire and Zimbabwe experience widespread burning by May while countries on the eastern coast of southern Africa such as Tanzania and Mozambique experience a peak in October. At the same time, burning activity diminishes in some western and interior countries from July to October (Cahoon *et al.*, 1992; Diab *et al.*, 1996a).

Peak tropospheric ozone concentrations over southern Africa and the south Atlantic Ocean were observed every year during August-October, using Nimbus 7/Total Ozone Mapping Spectrometer (TOMS) satellite imagery (Fishman *et al.*, 1986; 1990; 1991). Mean ozone profiles obtained during the SAFARI-92 period provided evidence of a general tropospheric enhancement at all stations, particularly at Okaukuejo and Brazzaville where it was manifest as an enriched upper tropospheric ozone layer with concentrations exceeding 80 ppbv (Diab *et al.*, 1996a). These observations suggested that this phenomenon was directly linked to the seasonality of South American and African biomass burning, coupled with meteorological transport (Zunckel *et al.*, 1996).

According to Scholes *et al.* (1996b), ~ 4% of the global NO_x budget is based on annual emissions from fires in southern Africa while the amount of CO emitted from this source is comparable to that released from global industries (Hao *et al.*, 1996). The annual observation of enhanced tropospheric ozone levels in the region is therefore most likely a product of reactions between pyrogenic NO_x, CO, and CH_4 (Scholes *et al.*, 1996b). Further, during the dry fire season, subsidence causes a low incidence of rain (Lelieveld and Dentener, 2000; Scholes and Andreae, 2000), thereby strengthening and enhancing the

atmospheric lifetime of emissions, and permitting them to be safely transported over enormous distances (Scholes and Andreae, 2000).

3.2.2 Sinks Contributing to the Tropospheric Ozone Budget

Ozone is destroyed through photolysis, HO_2/OH catalysis and surface deposition. Each of these processes will be examined in turn.

3.2.2.1 Photolysis

The photolysis of ozone is a destruction process and occurs through the photodissociation of ozone by short wave radiation (<340 nm):

(R10) $O_3 + hv \rightarrow O_2 + O(^1D)$ (adapted from Yienger *et al.*, 1999)
where hv is the product of the Planck constant and the frequency of light at wavelength λ (Lelieveld and Dentener, 2000).

The electronically excited $O(^1D)$ atoms from (R10) react with water vapor through:

(R11) $O(^1D) + H_2O \rightarrow 2OH$ (adapted from Yienger *et al.*, 1999)
forming OH (hydroxyl) radicals.

Thus the lifespan of ozone is limited by the concentration of water vapor present and the amount of solar radiation (Zachariasse *et al.*, 2000). Ozone thus has a very short lifetime of 2-5 days in the continental or marine boundary layer due to the high levels of water vapor and about 3 months in the middle and upper troposphere (Fishman *et al.*, 1991) due to the drier atmosphere.

3.2.2.2 HO_2/OH Catalysed Destruction

Ozone is subject to further destruction or chemical loss when it reacts with OH and HO_2 (hydroperoxy) radicals (Lelieveld and Dentener, 2000; Yienger *et al.*, 1999):

(R12) $O_3 + OH \rightarrow O_2 + HO_2$ (adapted from Yienger *et al.*, 1999)

(R13) $O_3 + HO_2 \rightarrow 2O_2 + OH$ (adapted from Yienger *et al.*, 1999)

3.2.2.3 Surface Deposition

Ozone is also destroyed at the earth's surface due to deposition (Thompson *et al.*, 1996a). It is thought that this sink has an effect on the diurnal variation of ozone (Staehelin *et al.*, 1994).

3.3 Dynamic Controls of Tropospheric Ozone Distribution

3.3.1 Stratospheric-Tropospheric Exchange

The aim of this section is to examine some of the most important mechanisms contributing to the exchange of air between the stratosphere and troposphere and vice versa. These include the mean meridional circulation, movement of the tropopause, tropopause folding and cut-off lows and are discussed below.

3.3.1.1 Mean Meridional Circulation

According to Tung *et al.* (1986), the zonal mean transport in the lower stratosphere assumes the form of a hemispheric two-cell circulation that causes air to rise vertically in the tropics and to subside near the poles.

The Hadley cell circulation which forms part of a three-cell pattern in the troposphere (except during summer) penetrates deep into the stratosphere and thus lifts a large quantity of tropical tropospheric air into the stratosphere through the rising branch. In a similar process, the same quantity of stratospheric air is returned to the troposphere in the middle and higher latitudes. According to the above principle, it is estimated that about 38% of the total volume of air in the stratosphere infiltrates into the stratosphere through the tropical branch of the Hadley cell and is subsequently restored to the troposphere through the subtropical branch, making it one of the most effective transport mechanisms (Reiter, 1975)

The upward flux of mass in the tropical branch of the Hadley cell does not occur in a

continuous slow moving process. Rather, it occurs within "hot tower" convective clouds which can penetrate the tropopause, thereby facilitating chemical exchange between the tropospheric and stratospheric air masses (Reiter, 1975).

3.3.1.2 Movement of the Tropopause

The height of the tropopause varies according to season (Reiter, 1975; Staley, 1962). This has important implications for the amount of ozone present in the troposphere. The upward movement of the tropopause during spring causes an outflow of ozone rich air into the troposphere and a subsequent reduction of the air mass in the stratosphere (Staley, 1962).

This process is reversed during autumn as the downward movement of the tropopause causes tropospheric air to flow into the stratosphere. These responses account for the observation of a spring maximum and an autumn minimum in ozone (Staley, 1962) at many locations. The net upward or downward flux of air (Staley, 1962) occurs due an imbalance in large scale processes such as the mean meridional circulation and eddy transport in the vicinity of the jet stream (Reiter, 1975).

Figure 3.5 and Table 3.1 portray the average seasonal fluctuation of tropopause height and stratospheric mass for a few North American stations and indicate that the middle and high latitude tropopause height varies substantially with season (Staley, 1962). Changes in stratospheric mass as a function of latitude is shown in Table 3.2 and corresponds well with data in Figure 3.5 and Table 3.1 (Reiter, 1975). The main features conveyed in Table 3.2 are that the stratosphere loses mass to the troposphere from winter to summer between 30-55°N, gains mass equatorward of 20°N and has no change poleward of 55°N as no significant variations were noted in the height of the tropopause (Reiter, 1975).

Table 3.1: Seasonal changes of stratospheric mass (Source: Staley, 1962: p 453)

		Tropopause pressure (mb)			
Station	Latitude	Jan 1957	July 1957	Change of areal stratospheric mass from January-July	Percentage change of stratospheric mass
Swan Island	17	94	105	+11	+10
Greensboro	36	224	131	-93	-42
Sault Sainte Marie	46.5	296	233	-63	-21
Port Harrison	58.5	325	250	-75	-23

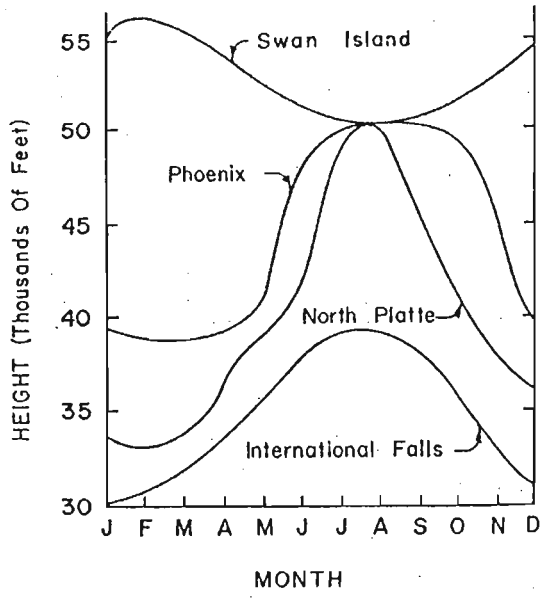

Figure 3.5: Dependence of tropopause height (average) on time of year at Swan Island (17°N), Phoenix (33°N), North Platte (41°N) and International Falls (49°N) for the period 1946-1956 (Source: Staley, 1962: p 453)

Table 3.2: Seasonal variation of median tropopause pressures (mb) over North America (Source: Reiter, 1975: p 462)

Latitude (°)	Winter	Summer	Change in pressure	Mass change (10^{17}g)
0			+ (25)	+ 28.4
5			+ (25)	+ 56.7
10			+ (25)	+ 55.6
15			+ (25)	+ 55.0
20	95	120	+ 25	+ 53.3
25	100	120	+ 20	+ 41.3
30	160	120	- 40	- 78.9
35	200	120	- 80	- 148.8
40	220	120	- 100	- 174.6
45	250	140	- 110	- 177.1
50	250	200	- 50	- 72.6
55	240	210	- 30	- 38.8
60	225	225	0	0
65	230	230	0	0
70	240	240	0	0
				Σ - 400.5

Based on the assumption that these changes are representative of the Northern Hemisphere, a net decrease of ~400 X 10^{17}g in stratospheric mass occurs from winter to summer. Seasonal variations in tropopause height over a period of 1 year thus account for a flux of ~10% of the stratospheric mass (Reiter, 1975).

3.3.1.3 Tropopause Folding

The idea of tropopause folding was first introduced by Reed (1955). This process is often associated with upper level frontogenesis near the tropopause and rapid surface cyclogenesis.

According to Danielsen (1968), the circulation accompanying a tropopause fold consists of a direct circulation cell centred on the warm side and an indirect circulation cell centred on the cold side of a tropopause break (Fig. 3.6). This two-cell circulation produces a confluence zone in the jet stream region. It is along the axis of this confluence zone, beneath the core of the jets where the folding process in initiated. The mean air flow shows the movement of tropospheric air into the stratosphere across the tropopause (Fig. 3.6). The resultant increase in the mass of the stratosphere due to this inflow is counterbalanced by a mass outflow of stratospheric air which accompanies tropopause folding. Trajectories showing the transport of stratospheric air from the region of the tropopause fold to the lower levels is shown schematically in Figure 3.7. A substantial amount of air reaching lower levels curves cyclonically and is unlikely to re-enter the stratosphere while the fraction of air remaining in the fold in the upper troposphere curves cyclonically and is drawn into the base of the lower stratosphere Danielsen (1968).

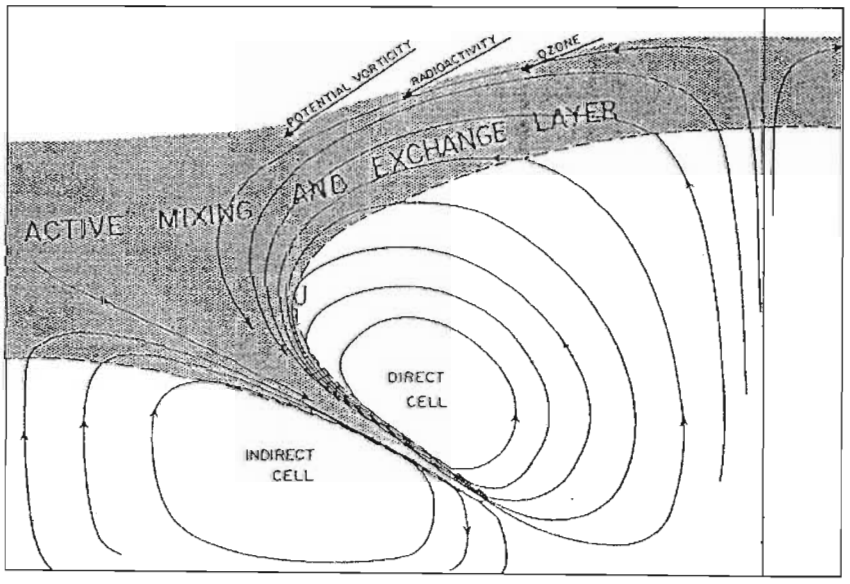

Figure 3.6: Schematic representation of the mean circulation relative to the tropopause in the jet stream region, including a folded tropopause. J indicates the position of the jet stream (Source: Danielsen, 1968: p 517)

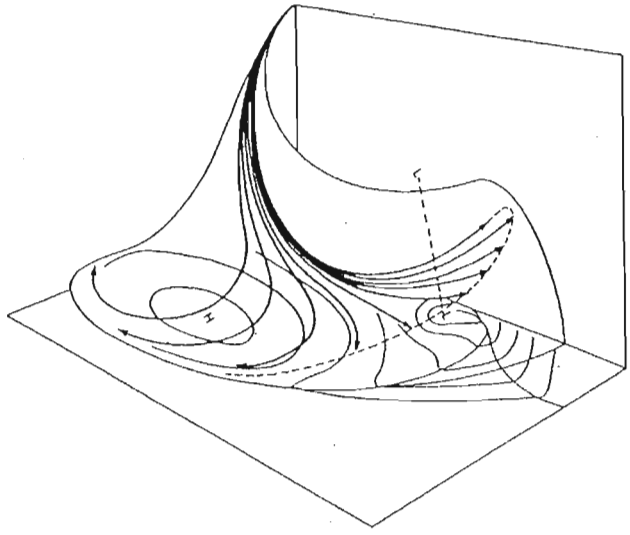

Figure 3.7: Conceptual model of the trajectories of ozone-rich air from the region of a tropopause fold in an upper-level trough behind a cold front and in the forward side of an anticyclone. L=low pressure; H=high pressure (Source: Danielsen, 1980: p 411)

3.3.1.4 Cut-Off Lows

Cut-off lows (COLs) are upper tropospheric cyclones (Price and Vaughan, 1992) and are associated with blocking patterns in tropospheric flow (Price and Vaughan, 1992; Vaughan and Price, 1991) and vertical transport (Preston-Whyte and Tyson, 1988; Tyson and Preston-Whyte, 2000). COLs generally arise when upper-air troughs extend far enough towards the equator such that a closed cyclonic circulation develops at the tip. Air in this low pressure system has a lower temperature than the air around it and usually comes from higher latitudes (Price and Vaughan, 1992).

COLs are active mixing zones between stratospheric and tropospheric air. Chemical characteristics of air in a COL system in the upper troposphere are intermediate between those of stratospheric and tropospheric air as it contains high levels of ozone and low values of chlorofluorohydrocarbons (CFCs). These measurements suggest that COLs play an integral role in STE (Bamber *et al.*, 1984).

Price and Vaughan (1992) identified 3 characteristic types of COL, namely polar, subtropical and polar vortex, which were based on different types of jet streams in the lower stratosphere and tropopause region (Fig. 3.8). Of the three, the polar type low which is characterised by cold polar air is the most effective contributor to STE. They form by

equatorward extensions of a strong polar jet and are often accompanied by tropopause folding (Price and Vaughan, 1992).

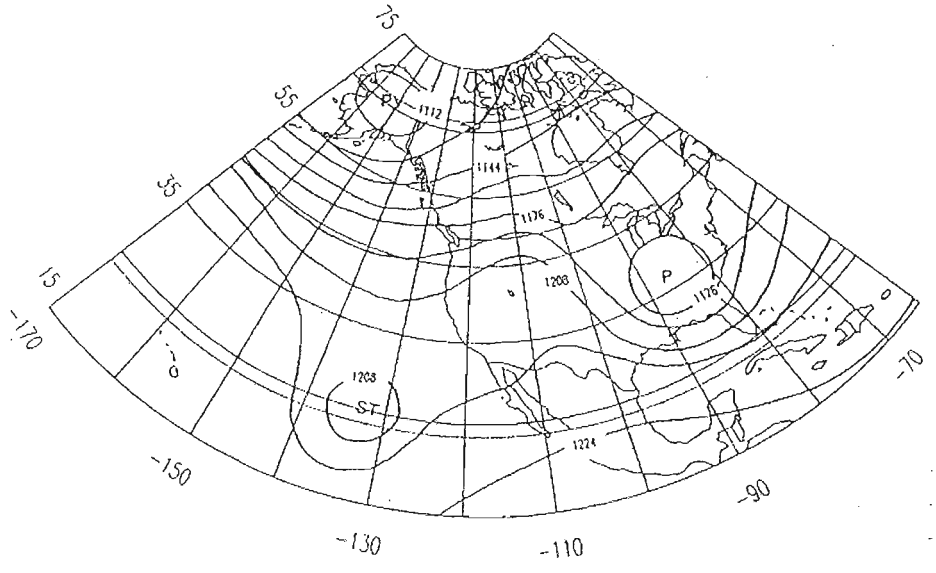

Figure 3.8: A typical 200 hPa synoptic chart showing three types of cut-off low types: polar (P), subtropical (ST) and polar vortex (PV) and related jet streams (Source: Price and Vaughan, 1992: p 97)

Three transfer mechanisms for the exchange of air between the stratosphere and troposphere (in association with COLs), namely convective erosion of the tropopause, erosion of the tropopause by turbulence and tropopause folding were proposed by Price and Vaughan (1993). Convective erosion of the tropopause arises when deep convection triggered by COLs over land surfaces in summer or warm oceans cause an indistinct tropopause. This facilitates mixing between the stratosphere and troposphere, leading to a band of air that shares characteristics of the troposphere and stratosphere. The tropopause is also disrupted by turbulence around the jet stream near the tropopause fold. Most of the air which helps form the COL, moves along the cyclonic side of the jet and is responsible for cross tropopause mixing. Air in the upper part of a tropopause fold usually forms the tropopause region within a COL and consequently contains a mixture of air originating from the stratosphere and troposphere. Transfer through tropopause folding which accompanies the formation of a COL is regarded as the most significant contributor as it causes transfer on a massive scale. Here, the returning branch of the fold which contains ozone-rich stratospheric air joins the tropopause region of a COL (Vaughan and Price, 1993).

Price and Vaughan (1993) suggested that subtropical COLs were smaller than the two other types, had a shorter lifetime and did not play a significant role in the tropospheric ozone budget. However, Barsby and Diab (1995) highlighted the importance of COLs in the day-to-day variation in ozone over southern Africa. More recently, Baray *et al.* (2003) documented a case study of a tropical COL, which occurred over South Africa during October 1996. In this study, the COL was completely separated from the main stratospheric air flow, in both the vertical and horizontal planes, with air being unable to return to the stratosphere even after a period of 6 days. This COL event had a long lifetime (~2 weeks) and a large horizontal extent (more than 15°), compared to the statistics presented by Price and Vaughan (1992). Many factors led Baray *et al.* (2003) to suggest that this COL could have a significant impact on tropospheric ozone over southern Africa as most of the stratospheric ozone remained in the troposphere. Although this investigation was based on only one case study, it is clear that the impact of subtropical COLs could be larger than previously thought, particularly in the overall ozone budget.

3.3.2 Synoptic Scale Circulations

This section deals with the influence of synoptic scale circulations, in particular anticyclones, on the distribution of ozone and its precursors in the troposphere of southern Africa. The role of convection is discussed separately.

3.3.2.1 Anticyclonic Circulations

The southern African subcontinent is (for most of the year) under the influence of a semi-permanent sub-tropical anticyclone. They dominate in mid-winter with a frequency of 80% but occur with a frequency of 20% in summer (Garstang *et al.*, 1996). These high pressure systems are associated with large-scale subsidence which has a considerable influence on the accumulation of trace gases (for example ozone) and aerosols in the troposphere (Garstang *et al.*, 1996; Swap and Tyson, 1999).

Other major circulation types over southern Africa were summarised by Tyson and Preston-Whyte (2000) and are displayed in Figure 3.9. Based on these dominant patterns, Garstang *et al.* (1996) identified five main horizontal transport modes which are depicted

in Figure 3.10. These include direct easterly or direct westerly transport, easterly advection or westerly advection and anticyclonic recirculation (Fig. 3.10) (Garstang *et al.*, 1996)

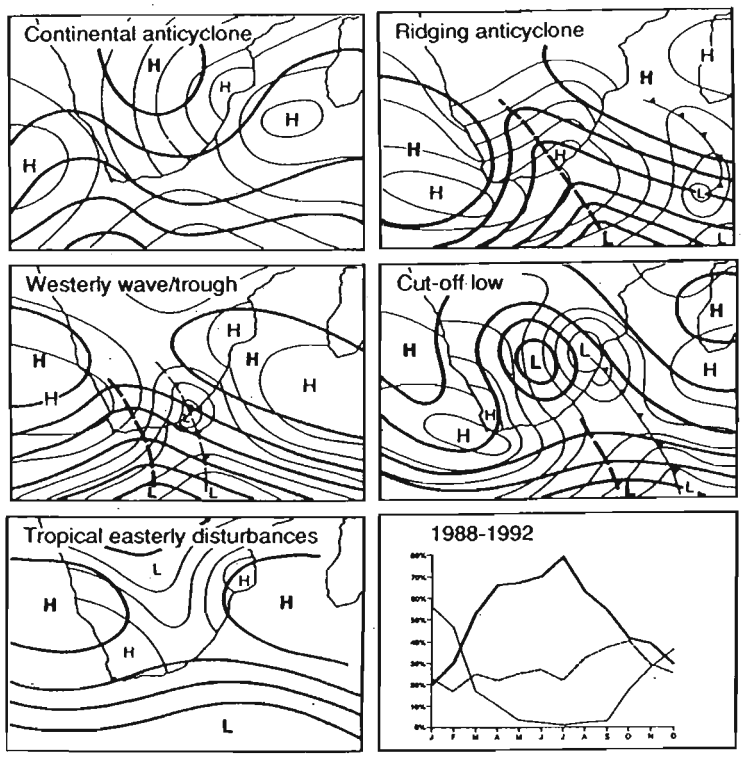

Figure 3.9: Major circulation types governing the transport patterns of aerosols and trace gases within over and out of the southern African troposphere, together with the frequency of occurrence (bottom right) over the period 1988-1992 of, first the combined continental and ridging anticyclone classes (heavy solid line), second, the combined westerly waves/troughs and cutoff lows (light solid line), and third, easterly wave disturbances (dashed line). Surface flow over the oceans are given in isobars at mean sea level while contours of the 850-hPa surface are used over the land (Source: Tyson and Preston-Whyte: p 184)

It is evident that anticyclonic circulation is thus the most important synoptic scale feature that influences the transport of atmospheric constituents over southern Africa (Garstang *et al.*, 1996). During SAFARI-92, anticyclonic conditions occurred on about 55% of occasions while westerly disturbances and wave disturbances in the tropical easterlies had a 41% and 4% occurrence respectively (Garstang *et al.*, 1996). Anticyclonic circulations and westerly disturbances favour transport out of southern Africa (in an easterly direction) over the Indian Ocean (Garstang *et al.*, 1996) through the Natal plume (Kirkman *et al.*, 2000). Anticyclonic flow of this nature can give rise to considerable recirculation (Kirkman *et al.*, 2000). Transport away from southern Africa (in a westerly direction) into the South Atlantic Ocean (Garstang *et al.*, 1996) in the Angolan plume (Kirkman *et al.*,

2000), is mainly limited to summer months when easterly waves propagate from the western side of southern Africa (Swap *et al.*, 1996).

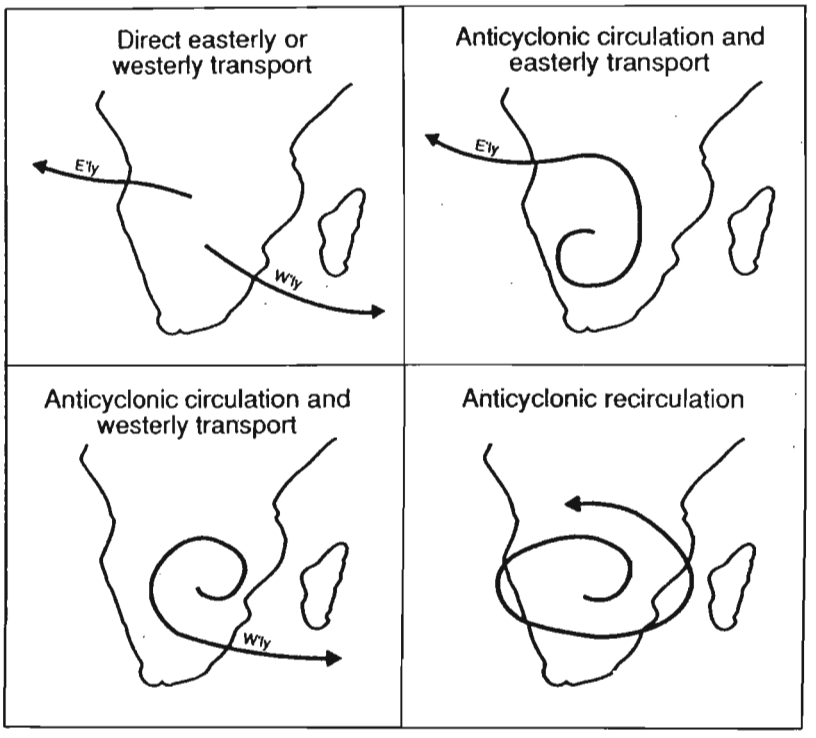

Figure 3.10: Major low level transport modes likely to result in easterly or westerly transport from southern Africa or in recirculation within the anticyclonic system (Source: Garstang *et al.*, 1996: p 23723)

The predominance of anticyclonic circulations means that southern Africa is characterised by a high frequency of subsidence inversions (Garstang *et al.*, 1996). Sinking promotes inversions and more importantly, has the effect of trapping aerosols and trace gases arising from boundary layer sources (Garstang *et al.*, 1996). It also promotes the downward movement of mid-tropospheric air into lower layers (Swap *et al.*, 1996). The southern African atmospheric environment is characterised by the frequent occurrence of multiple absolutely stable layers which are temporarily persistent and spatially continuous (Cosijn and Tyson, 1996; Garstang *et al.*, 1996; Swap and Tyson, 1999). Absolutely stable layers occur preferentially around the 700 hPa (3-km above mean sea level (asl)), 500 hPa (5-km asl) and 300 hPa (7-km asl) levels on most days throughout the year over southern Africa (Cosijn and Tyson, 1996; Swap and Tyson, 1999). A fourth stable layer is associated with the tropopause (Garstang *et al.*, 1996). Figure 3.11 shows the stability structure of the atmosphere over Pretoria between the late winter and early spring of 1992.

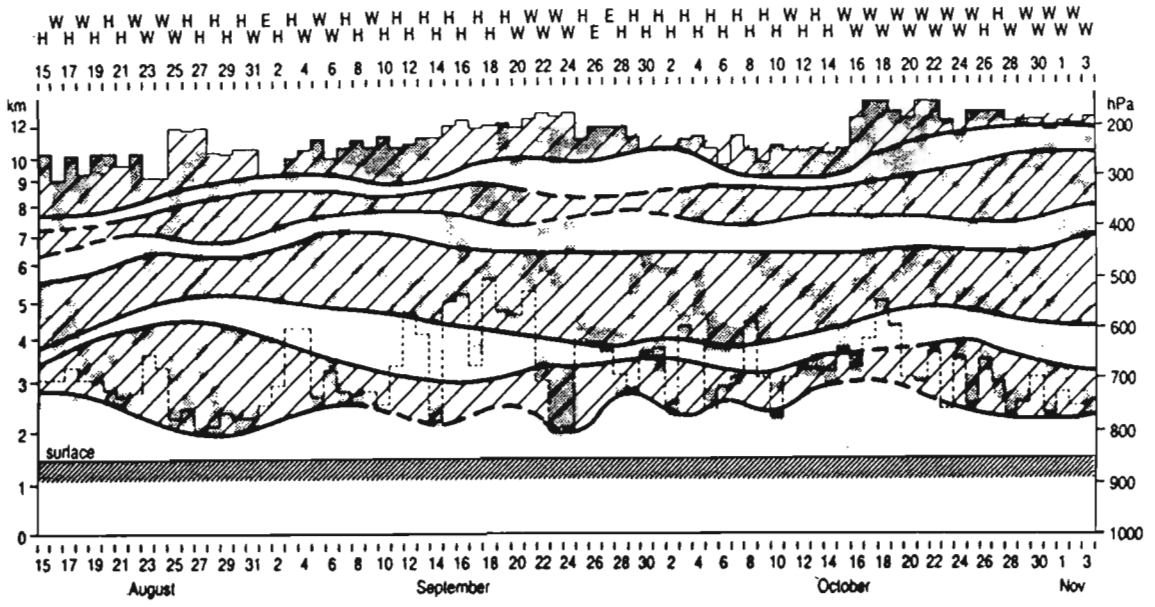

Figure 3.11: Daily variation of absolutely stable layers over Pretoria (southern Africa) during SAFARI-92. Stippled boxes indicate the height and depth of stable layers. Envelopes of continuous and discontinuous stable layers are indicated by cross-hatched regions enclosed by solid and dashed lines respectively. Light dashed lines depict the height of the 1200UT mixing depth. Circulation class for each day is shown by H (continental high), W (westerly disturbance) and E (easterly disturbance) (Source: Garstang *et al.*, 1996: p 23724)

The two lowest absolutely stable layers, which occur most frequently, exert the greatest control on the vertical and horizontal transport. The lowest stable layer which is usually associated with the top of the midday mixing layer is only disrupted by the passage of westerly disturbances at about weekly intervals, allowing the upward movement of pollutants by convective mixing. The 5-km absolutely stable layer which is associated with the main subsidence inversion is the most persistent and will only (on rare occasions) allow transport of pollutants to higher levels if it is absent or when deep convective lifting occurs. Figure 3.12 shows the extent to which vertical transport of air over the region is capped by the stable layers. In one case, the 5-km absolutely stable layer was observed to cover the whole of southern Africa (Fig. 3.12a), while in another, the 3-km absolutely stable layer formed along the south coast of Africa (Fig. 3.12b) (Garstang *et al.*, 1996).

When ozone precursors become trapped below the 3 and 5- km stable layers, they are subject to accumulation (for a period of 1-3 weeks) and optimum photochemical activity (Diab *et al.*, 1996b; Swap and Tyson, 1999). These air masses are also subject to massive scale recirculation (Swap and Tyson, 1999). The anticyclonic vortex of a recirculation may

be between a few hundreds or thousands of kilometres in diameter (Garstang *et al.*, 1996). It is possible that up to 44% of the total mass transport recirculates in an anticyclonic gyre and makes at least one complete revolution over central southern Africa (Tyson *et al.*, 1996). Recirculation provides additional time for photochemical ozone production and allows for the addition of fresh emissions (Swap *et al.*, 1996) from biomass, biogenic and industrial sources. According to Thompson *et al.* (1996b), ozone formation rates of 1-2 ppbv per day under these conditions can build up upper tropospheric ozone values to 20-30 DU in a matter of 1-2 weeks.

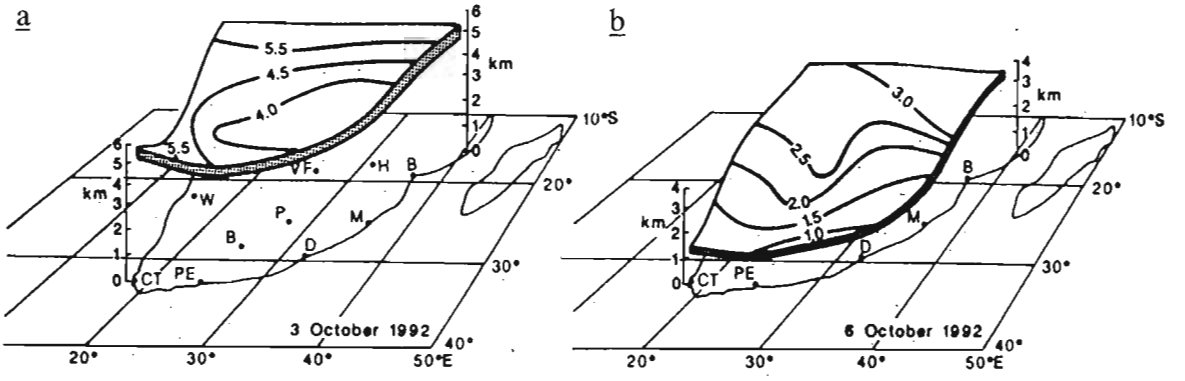

Figure 3.12: Diagrammatic representation of the spatial extent of the 5-km absolutely stable layer (3 October 1992) and 3-km layer (6 October 1992) over southern Africa (Source: Garstang *et al.*, 1996: p 23725)

Pollution plumes containing high ozone and ozone precursors produce well-defined layers of elevated ozone particularly if constrained by stable layers (Liu *et al.*, 1999). Swap and Tyson (1999) have shown that peaks and points of inflection in tropospheric ozone profiles are related closely to the occurrence of absolutely stable layers. Further, the existence of thin layers of absolutely stable air was also shown to have an effect on the microstructure of ozone profiles (Fig. 3.13a-d).

3.3.2.2 Convection

Deep convection is an effective mechanism for the rapid vertical transport (Dickerson *et al.*, 1987) and redistribution (Pickering *et al.*, 1992b) of ozone and ozone precursors from the boundary layer to the middle and upper troposphere. During normal atmospheric conditions, these gases will take a few months to spread to these altitudes (Dickerson *et al.*, 1987) but vertical transport is significantly speeded up during deep convective storm

events. Transport to the upper troposphere is accomplished in a few hours (Diab *et al.*, 1996b) or according to some authors (Pickering *et al.*, 1992b) in a few minutes. The atmosphere at these altitudes is very dry and therefore minimal destruction of ozone by the OH radical occurs, prolonging the lifetime of ozone (Liu *et al.*, 1987).

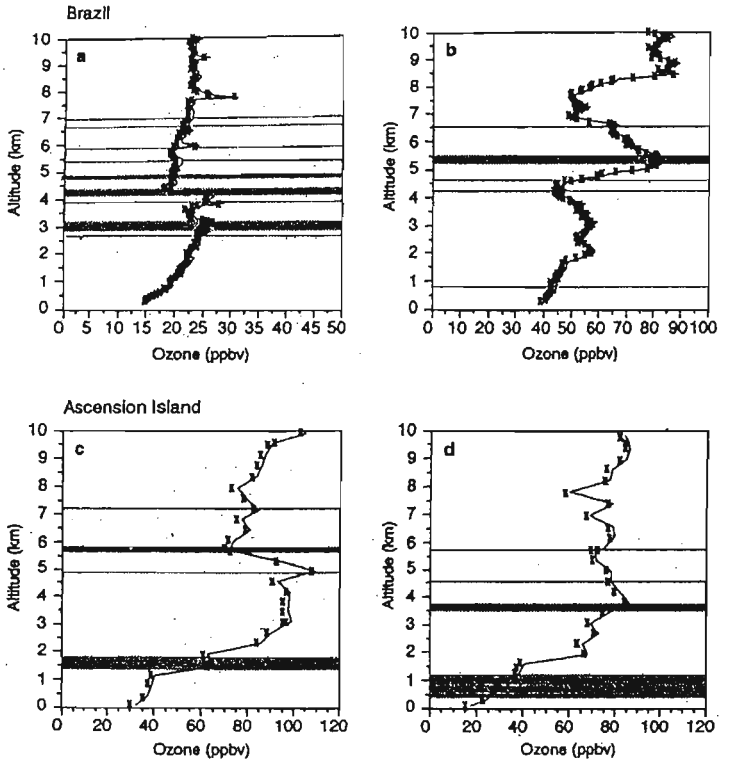

Figure 3.13: Ozone profiles observed at Cuiabá, Brazil, on (a) 18 September 1992 and (b) 2 October 1992 (after Kirchoff *et al.*, 1996) and at Ascension Island, South Atlantic Ocean, on (c) 9 September 1992 and (d) in September 1992 (after Thompson *et al.*, 1996). Absolutely stable layers are indicated by shading (Source: Swap and Tyson, 1999: p 68)

Turbulent mixing causes NO and other ozone precursor gases to become more diluted during convective transport to the free troposphere (Pickering *et al.*, 1990; 1992b) and thus enhances the production rate of ozone as it is formed more efficiently on a per molecule basis (Liu *et al.*, 1987). Ozone precursor gases transferred to the middle and upper troposphere in convective cloud outflow following a deep convective episode can also lead to substantial ozone production (Pickering *et al.*, 1992a; 1996), particularly if these regions have been enriched with lightning-produced NO_x (Pickering *et al.*, 1990). Depending on the amount of available NO_x as well as the scale and structure of cloud dynamics, ozone production rates can be intensified by a factor of 2-50 (Pickering *et al.*, 1992b) and can transform layers in the middle and upper troposphere from being a zone of net ozone destruction to net ozone production (Pickering *et al.*, 1991). The extent of ozone

production at these altitudes is also reliant on season, for example, the amount of NO_x available for convective transport during spring may be greater due to a higher occurrence of fire emissions (Pickering *et al.*, 1991). Enhanced ozone production is also noted downwind of convective cells (Pickering *et al.*, 1996) as photochemical ozone production continues in the cloud outflow region that is entrained in long range transport pathways.

3.4 Summary

It is clear that both photochemical and dynamic processes play a significant role in the tropospheric ozone budget. However, *in situ* photochemical production of ozone is regarded as a more dominant contributor in tropical and subtropical regions. The existence of a possible ozone maximum at any particular time and location will be a function of biomass burning, emissions from biogenic, urban/industrial and lightning sources and the prevailing meteorological conditions.

CHAPTER 4

TOTAL TROPOSPHERIC OZONE

4.1 Introduction

This chapter presents the results of TTO variations over Johannesburg for the period 1995-1998. Variations in TTO occur as a result of the downward flux of ozone from the stratosphere (STE), photochemical production/destruction of ozone and loss at the surface (Crutzen, 1973). It is valuable to examine TTO for many reasons. For example, a measure of TTO makes it easy to detect seasons and days of enhanced ozone. It is also a simple and useful way of comparing tropospheric ozone in different geographical locations (Baldy *et al.*, 1996; Browell *et al.*, 1996; Cros *et al.*, 1992; Diab *et al.*, 1996a; Fishman *et al.*, 1991, 1996; Krisnamurthi *et al.*, 1993; Logan, 1985; Olson *et al.* 1996; Thompson *et al.*, 1996a, 1996b, 2002; Thompson and Hudson, 1999) and for examining changes in ozone over time (Zunckel *et al.*, 1992a; 1992b).

An integrated measure of ozone in a column above the surface of the earth is also helpful in the validation of satellite data. For example, Cros *et al.* (1992), Thompson *et al.* (1996a; 1996b; 2002) and Thompson and Hudson (1999) compared ground-based and TOMS satellite-based measurements to determine the relative accuracy of measurements. In all cases, a high level of agreement was found.

Furthermore, a comparison between TTO and TO at a particular location permits an estimate of the percentage contribution of tropospheric ozone to the total amount of ozone in the atmosphere (Diab *et al.*, 1996; Fishman *et al.*, 1990; Lelieveld and Dentener, 2000; Thompson *et al*, 1996). When compared to expected background levels, this indicates whether ozone is increasing or decreasing in the troposphere.

An estimate of TTO is governed by the height of the tropopause which marks the top of the troposphere. It is well known that the tropopause varies as a function of latitude and season (Reiter, 1975; Staley, 1962) and also on a daily basis.

A number of methods exist for defining the height of the tropopause. Some studies define a

dynamic tropopause based on a change in potential vorticity (PV) (Danielsen, 1968; Reed, 1955), others define a thermal tropopause based on the vertical temperature gradient (WMO, 1986), and yet others a chemical tropopause based on the height at which ozone shows a sudden increase in values (Bethan *et al.*, 1996).

In this study a measure of TTO was obtained by integrating the ozone profiles between the surface and a predetermined height of 12 km since this was the maximum height reached by the MOZAIC aircraft, in accordance with air traffic regulations. In other studies over southern Africa, alternative methods of determining tropopause height have been adopted. For example, during SAFARI-92, Browell *et al.* (1996) used ozone data measured by the DIAL instrument to determine the point of inflection in the ozone profile where ozone concentrations showed a sudden sharp increase to signify the tropopause height. Thompson *et al.* (1996a) and Diab *et al.* (1996a) used a tropopause height of 15 km for Irene, which is at the same latitude as Johannesburg. Authors such as Cammas *et al.* (1998) and Thouret *et al.* (1998) applied an ozone threshold value of 100 ppbv to distinguish stratospheric air from tropospheric air. More recently, Thompson *et al.* (2003) have also used an approach based on the chemical tropopause, which is defined as the point at which extrapolation of the lower stratospheric ozone mixing ratios reach 100 ppbv. According to these authors it is usually within 10-15 hPa of the temperature based tropopause except at Irene where a double temperature-based tropopause is sometimes evident.

Hence, in this study, since TTO values are integrated to a height of only 12 km, the values are expected to be less than those presented in previous studies. However, while actual magnitudes may differ, seasonal trends are expected to be comparable.

Differences in TTO may also be attributed to differences in vertical height resolution and the number of measurements. Furthermore, ozone concentrations are generally lowest at night and early parts of the morning but increase during the morning after the break-up of the night-time inversion layer, resulting in a diurnal variation in surface ozone, with values peaking towards late afternoon. Thus, differences in the time of measurement could bear a significant influence on values (Thouret *et al.*, 1998).

4.2 Previous Research Results on TTO in Southern Africa

A comparison of ozone profiles measured at Pretoria (25° 44'S, 28° 11'E) for a background period (1965-1968) and a relatively recent period (1990-1991) indicates that there has been a substantial increase in tropospheric ozone over the years (Zunckel *et al.*, 1992a; 1992b). This increase has been related to increases in urban-industrial emissions in the region. Tropospheric ozone data derived from satellite measurements which showed a well-defined maximum in ozone of greater than 45 DU off the west coast of Africa during September and October was first detected by Fishman *et al.* (1990; 1991). These findings were subsequently confirmed by ozonesonde measurements. Fishman *et al.* (1991) attributed this maximum to pollution from widespread biomass burning in southern Africa but Krishnamurthi *et al.* (1993) later added that it also appears to be caused by horizontal and vertical advections and stratospheric influences.

Since these initial studies, a lot of work has been done on TTO over Southern Africa, particularly during the SAFARI-92, SAFARI 2000 and SHADOZ field campaigns. During the SAFARI-92 campaign, Diab *et al.* (1996) and Thompson *et al.* (1996a; 1996b) investigated the seasonal and interannual variability of integrated tropospheric ozone over Ascension Island (8°S, 14°W), Brazzaville (4°17'S, 15°15'E), Okaukuejo (19°11'S, 15°55'E) and Irene (25°52'S, 28°13'E) and noted that all stations exhibited a general springtime (September-October) enhancement. According to these authors, (Diab *et al.*, 1996; Thompson *et al.*, 1996a; 1996b) the seasonal pattern appears to be a reflection of seasonal burning pattern over Africa detected by satellite (Cahoon *et al.*, 1992) and the high ozone at these stations is due to biomass burning. This is confirmed by forward and backward trajectory analysis which suggest that southern Africa is supplied with ozone rich air and ozone precursors (Thompson *et al.*, 1996b) recirculating within stable layers (Garstang *et al.*, 1996). According to Diab *et al.* (1996) the extension of the ozone enhancement into summer suggests the forcing of a local urban-industrial source, as suggested by Zunckel *et al.* (1992a; 1992b).

These studies have concluded that the dynamics of the region (high ozone forming rates, extensive recirculation and stable layering) combined with abundant precursors from biomass burning, biogenic emissions and lightning play and important role in ozone buildup (Diab *et al.*, 1996; Thompson *et al.*, 1996a; 1996b). It was also revealed that TTO

accounts for up to 13-15% of the total ozone at Irene, 15% at Okaukuejo, 15-18% at Brazzaville and 18-19% at Ascension Island (Diab *et al.*, 1996; Thompson *et al.*, 1996a). A seasonal maximum in integrated tropospheric ozone at Ascension Island (50 DU), Brazzaville (45 DU), Okaukuejo and Irene (both 41 DU) was found during SAFARI (Thompson *et al.*, 1996a).

According to Diab *et al.* (1996), the mean integrated tropospheric ozone amount was in the region of 38 DU for Irene and 53 DU for Ascension Island. Tropospheric ozone is higher at Ascension Island and Brazzaville than the other two stations as the former were more directly affected by transport from biomass burning while the latter were removed from areas of burning. This is suggestive of a latitudinal gradient in tropospheric ozone (Diab *et al.*, 1996; Thompson *et al.*, 1996a; 1996b).

During SAFARI-2000, ozone measurements taken at Lusaka, Zambia (15.5°S, 28°E) during the burning season showed that column tropospheric ozone exceeded 50 DU and was higher than simultaneous measurements over Nairobi (1°S, 38°E, and Irene (25°S, 28°E). Thompson *et al.* (2002) thus concluded that Lusaka was a collection point for ozone-rich air originating from local and transboundary sources (i.e. from fire-rich rural areas of neighbouring countries). This is consistent with studies done by Browell *et al.* (1996) who detected elevated TTO of the order of 56 DU over the same region and season but using the airborne DIAL system. Browell *et al.* (1996) suggested that biomass burning was responsible for up to 50% of the TTO column across the region. The premise that biomass burning was responsible for the enhanced ozone in the mid-troposphere was confirmed by *in situ* measurements of high levels of CO, CH_4 and CO_2.

Thompson and Hudson (1999) noted that a distinctive feature of satellite based measurements over southern Africa (and the Atlantic) is a regular seasonal variation with tropospheric ozone maximizing in the latter half of the year than in the second quarter when ozone is at a minimum.

Cros *et al.* (1992) analysed 33 ozonesonde profiles in Brazzaville between June 1990 and May 1991 and compared it to the ozone measured by satellite. The seasonal cycle of ozone derived from ozonesondes and satellite-based data are in good agreement with each other, both peaking in September and both measurements showed that the highest integrated

tropospheric ozone were found between June and October, coincident with the dry season and widespread occurrence of biomass burning. However, the average integrated amount of ozone derived from ozonesonde and satellite data is 44 DU and 39 DU respectively. This study suggested that TOMS satellite-based measurements serves as a better indicator of integrated tropospheric ozone than ozonesondes.

4.3 Total Tropospheric Ozone (TTO) over Johannesburg

Daily values of TTO for the period 1995 to 1998 were computed according to the methodology described in section 2.3, and are presented as mean monthly values together with standard deviation bars in Figure 4.1. TTO values are highest during September and October (~32 DU) and lowest in autumn (~18 DU). This confirms the seasonal pattern noted by Combrink *et al.* (1995), Diab *et al.* (1992; 1996a), Logan (1999), Thompson *et al.* (1996a), Thouret *et al.* (1998) and Zunckel *et al.* (1992a; 1992b), which is indeed a well established Southern Hemisphere trend. Most studies have suggested that the main reason for this spring maximum is biomass burning, combined with prevailing anticyclonic circulation patterns which facilitate the build-up of ozone over the region (Diab *et al.*, 1996a; Thompson *et al.*, 1996a). The mean annual range is 14.9 DU, which is consistent with that derived for Irene, viz. ~13 DU, by Thompson *et al.* (1996a).

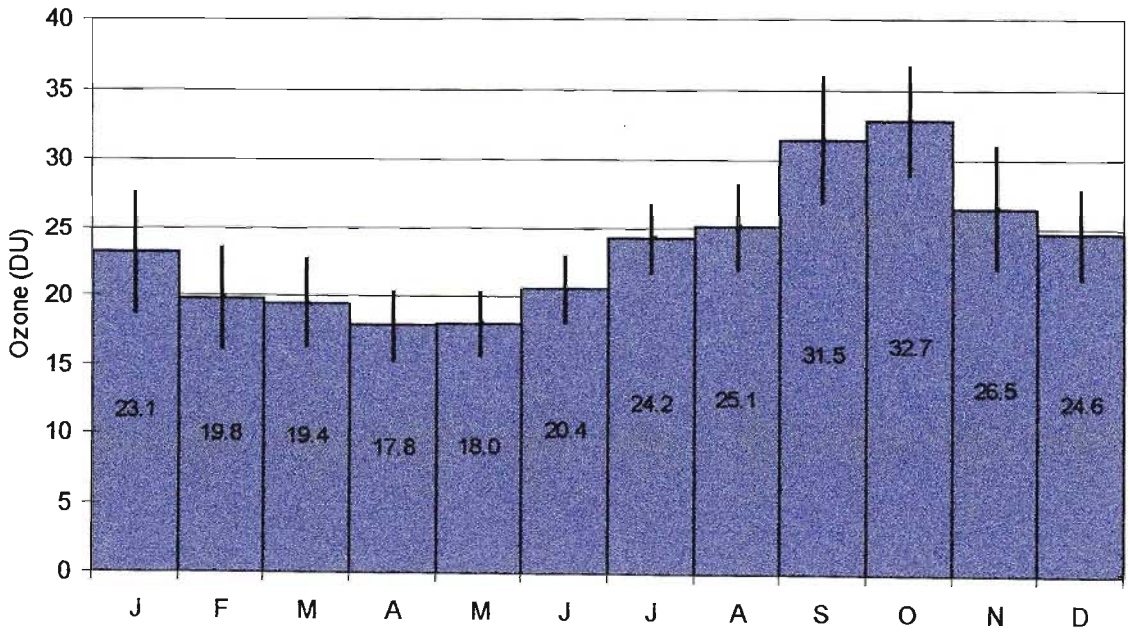

Figure 4.1: Mean monthly TTO (DU) above Johannesburg for the period 1995-1998 based on MOZAIC aircraft data. The vertical bars indicate two standard deviations on either side of the mean

Day-to-day fluctuations in TTO are expressed by the magnitude of the standard deviation bars shown in Figure 4.1. Variability is greatest in January, September and November, each with a standard deviation of ~4.5 DU and least during autumn and winter (April to July) when the standard deviation is between 2.3-2.5 DU. The lower day-to-day variability in autumn and winter is a reflection of the more settled weather at this time.

Figure 4.2 shows the inter-annual variability of TTO over the period 1995 to 1998. The seasonal forcing is well developed and consistent from year to year. TTO peaks either in September or October, while minimum values occur in late summer or autumn (February-May). Interannual variability is least in January and April to June. Again the autumn and winter ozone values are more consistent and appear to represent background tropospheric ozone loadings on which the dynamic and photochemical influences of other months are superimposed.

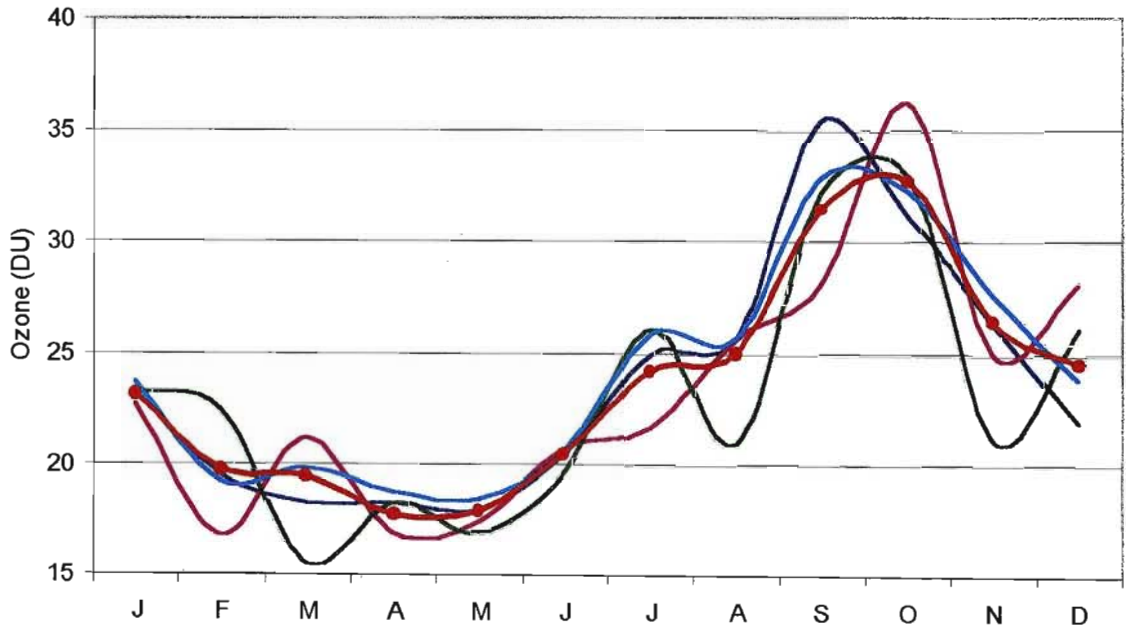

Figure 4.2: Inter-annual variation in mean monthly TTO for 1995-1998. Dark blue = 1995; pink = 1996; green = 1997; light blue = 1998; red = mean

4.4 Integrated Tropospheric Ozone in Layers

In order to investigate factors responsible for TTO variations, tropospheric ozone was integrated over 4 layers i.e. surface-3, 3-5, 5-7 and 7-12 km (Fig. 4.3). These layers were selected on the basis of the work of Cosijn and Tyson (1996), who identified that

absolutely stable layers occur preferentially at approximately 700 hPa (3 km), 500 hPa (5 km) and 300 hPa (7 km) levels over southern Africa. The same spring maximum is evident in each of the layers (Fig. 4.3). Below 5 km, the TTO minimum occurs in February and March, while above 5 km, the minimum occurs in April and May. These results are suggestive of a decoupling of the atmosphere and emphasize the role of the absolutely stable 5 km layer. The seasonal cycle is particularly well developed in the 7-12 km layer.

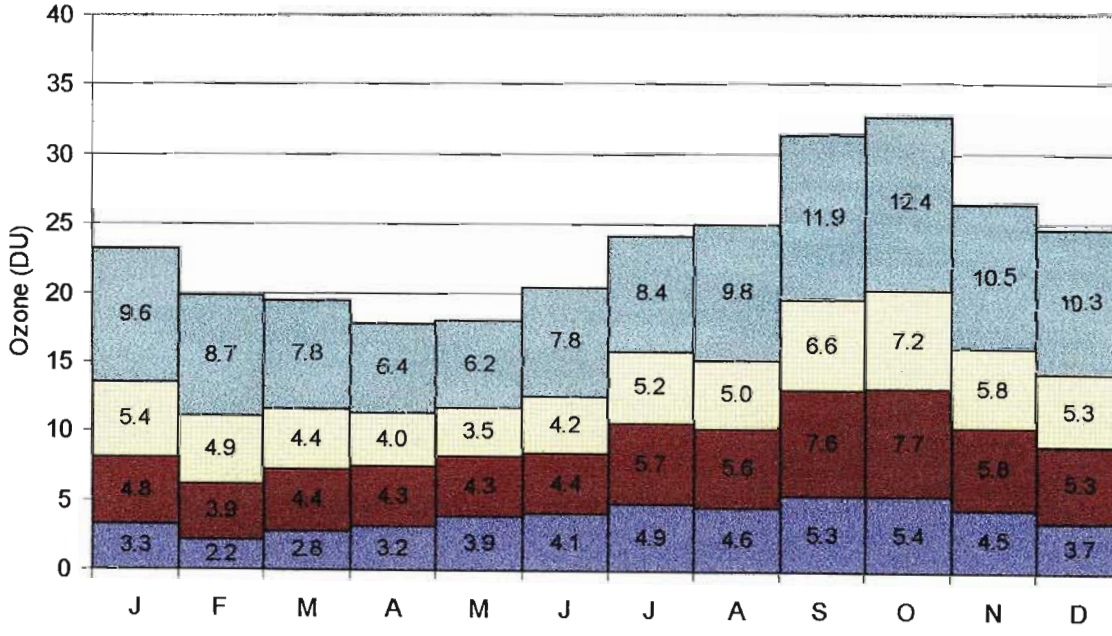

Figure 4.3: Monthly integrated TTO layers for 1995-1998. Dark blue = sfc-3 km; maroon = 3-5 km; cream = 5-7 km; light blue = 7-12 km layers

Taking these months as representative of background ozone loadings (i.e. February, March for layers below 5 km and April, May for layers above 5 km) the percentage increase observed in each month was computed. In each case the greatest enhancement occurred in October, with values of 143% in the surface to 3 km layer, 96% in the 3-5 km layer, 103% in the 5-7 km layer and 100% in the 7-12 km layer. This suggests that the October enhancement can be attributed to sources prevalent throughout the troposphere. It is not possible from this analysis to distinguish between surface based photochemical ozone production such as biomass burning and urban-industrial sources and upper tropospheric dynamical sources such as STE or long distance transport.

4.5 Elevated Ozone Events

A further analysis of days with highest TTO was undertaken to obtain greater insights. A

threshold value of 30 DU was selected arbitrarily to indicate an event of considerable ozone enhancement. Diab *et al.* (1996a) referred to events with TTO less than 30 DU as representative of unpolluted air, while Thompson *et al.* (1996b) used a value of 35 DU.

Figure 4.4 presents the breakdown of TTO into layers for individual days on which TTO exceeded 30 DU, while Figure 4.5 shows the corresponding percent contribution of each layer to TTO on a particular day. High TTO events occurred predominantly during September (16) and October (17), with the few remaining events scattered throughout the year.

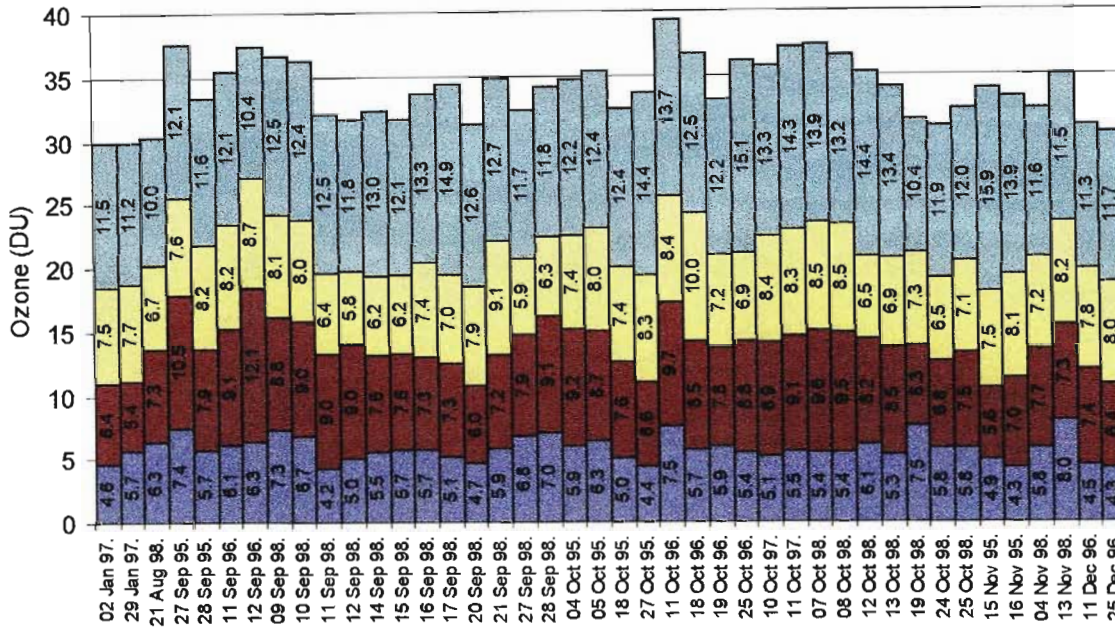

Figure 4.4: Ozone events with TTO greater than 30 DU. Dark blue = sfc-3 km; maroon = 3-5 km; cream = 5-7 km; light blue = 7-12 km layers

In order to separate events that were due to an increase in a particular layer, the percent contribution in each layer was compared with the mean percent contribution of that layer. These results are summarised in Table 4.1.

In the lower troposphere, 22 events showed enhancements in the sfc-3 km layer, while 23 events showed enhancements in the 3-5 km layer. Of these, 13 events were due to an increase in both layers. These enhancements seldom lasted for more than 1-2 consecutive days and occurred mostly in September. It is suggested that these events are most likely due to effects of local surface pollution sources, either localised biomass burning or urban-industrial effects.

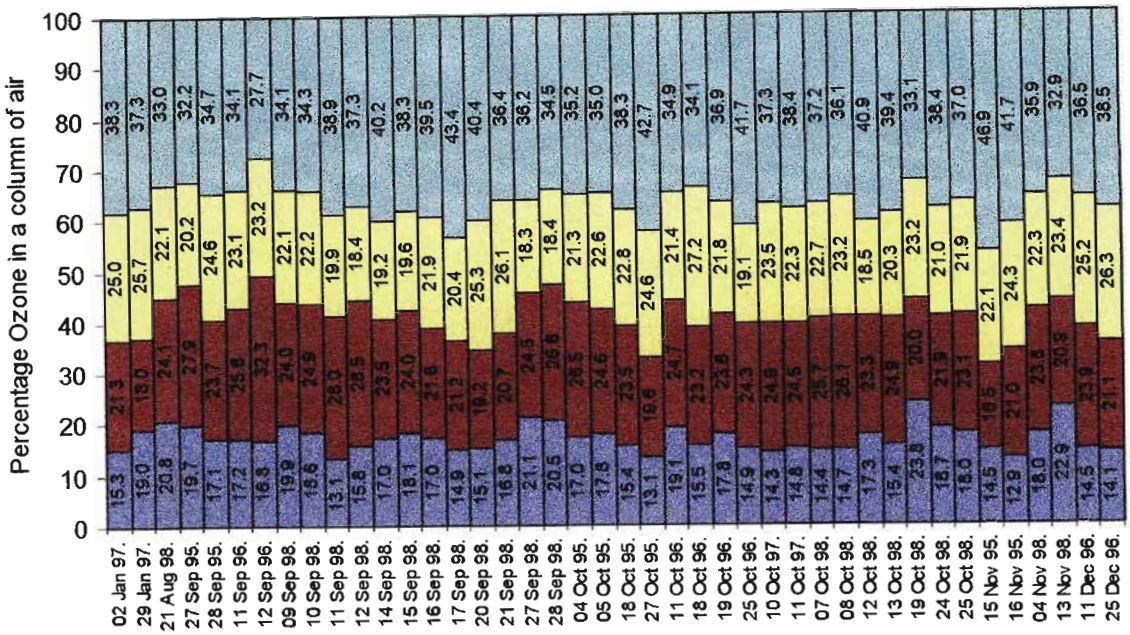

Figure 4.5: Percentage contribution of each layer for high ozone events with TTO greater than 30 DU. Dark blue = sfc-3 km; maroon = 3-5 km; cream = 5-7 km; light blue = 7-12 km layers

The number of events showing enhancements in the upper troposphere was similar, 20 in the 5-7 km layer and 21 events in the 7-12 km layer.

It is noted that an extended period of enhancement in the 7-12 km layer occurred from 14-17 September 1998 and again on 20 September 1998. The extended duration of this event suggests that it is due to an STE event. Confirmation of this was given in a case study of a particular MOZAIC flight on 16 September 1998 from Johannesburg to Cape Town by Mahumane (2002). It was concluded that the high ozone values (141 ppbv) at 11.5 km, the low relative humidity value (<20%) and the high potential vorticity value were evidence of this injection of stratospheric ozone rich air into the troposphere.

In summary the analysis of tropospheric ozone enhancements in layers have revealed that enhancements are due to processes operating throughout the troposphere and that the enhancements are an expression of a combination of factors.

Table 4.1: Events showing enhancements as a function of layer. X denotes an enhancement

Event	sfc-3km	3-5km	5-7km	7-12km
02 Jan 97			X	X
29 Jan 97	X		X	X
21 Aug 98	X	X		
27 Sep 95	X	X		
28 Sep 95	X	X	X	
11 Sep 96	X	X	X	X
12 Sep 96		X	X	X
09 Sep 98	X	X		
10 Sep 98	X	X		
11 Sep 98		X		
12 Sep 98		X		
14 Sep 98	X			X
15 Sep 98	X	X		X
16 Sep 98	X			X
17 Sep 98				X
20 Sep 98			X	X
21 Sep 98			X	
27 Sep 98	X	X		
28 Sep 98	X	X		
04 Oct 95	X	X		
05 Oct 95	X	X	X	
18 Oct 95			X	X
27 Oct 95			X	X
11 Oct 96	X	X		
18 Oct 96			X	
19 Oct 96	X			
25 Oct 96		X		X
10 Oct 97		X	X	X
11 Oct 97		X	X	X
07 Oct 98		X	X	X
08 Oct 98		X	X	
12 Oct 98	X			X
13 Oct 98		X		X
19 Oct 98	X		X	
24 Oct 98	X			X
25 Oct 98	X			
15 Nov 95				X
16 Nov 95			X	X
04 Nov 98	X	X		
13 Nov 98	X		X	
11 Dec 96		X	X	
25 Dec 96			X	X

4.6 Conclusion

The seasonal pattern in TTO, which is dominated by a spring maximum and autumn minimum, has been confirmed in the study. The seasonal forcing is consistent from year to year with TTO peaking either in September or October. The integration of tropospheric ozone into layers has provided valuable insights into some of the factors responsible for TTO variations. Below 5 km, the TTO minimum occurred in February and March, while above 5 km, the minimum occurred in April and May. These results are suggestive of a decoupling of the atmosphere and emphasize the role of the absolutely stable 5 km layer. The greatest enhancement occurred in October and was attributed to sources prevalent throughout the troposphere. Elevated TTO events occurred predominantly during September and October. Enhancements in the lower troposphere were most likely due to effects of local surface pollution sources, either localised biomass burning or urban-industrial effects. The extended duration of the enhancement in the upper troposphere (7-12 km layer) which occurred from 14-17 September 1998 and again on 20 September 1998 suggested that it was due to an STE event.

CHAPTER 5

VERTICAL DISTRIBUTION OF TROPOSPHERIC OZONE

5.1 Introduction

Knowledge of the vertical distribution of ozone is valuable for detecting layers of enhanced ozone and ozone minima. This offers important insights on possible mechanisms such as photochemical and dynamic processes which play a role in the tropospheric ozone budget. Vertical profiles at Johannesburg show considerable day-to-day variability in the vertical structure of ozone, evidenced by a large variation in the altitudes and magnitudes of maxima and minima. In some cases a profile exhibits marked stratification, with single or multiple peaks, and in other cases the profile is uniform with an absence of structure, indicative of a well-mixed atmosphere. Similar observations have been made at other locations.

Each ozone profile represents a unique response to photochemical and dynamic processes. Hence an in-depth study of the profiles with specific consideration of their structure, in particular the magnitude and altitudes of maxima and minima, depth of clearly defined layers and the vertical gradient of ozone is essential to provide meaningful insights into these processes.

Traditionally, studies on mean profiles averaged by season or year, together with some measure of variability about these means, have been carried out. Recent examples of studies in the literature, which have focused on the construction of an ozone climatology for specific locations include Kirchoff *et al.* (1991) who compiled an ozone climatology at Natal, Brazil, from *in situ* ozonesonde data, Diab *et al.* (1996a) for a set of four ozonesonde stations located at Ascension Island, Brazzaville, Okaukuejo, and Irene based on ozonesonde data, Fortuin and Kelder (1998) for 30 ozonesonde stations located around the world, based on ozonesonde and satellite measurements, Thouret *et al.* (1998a) for eight stations of the Ozone Sounding Network (OSN) using MOZAIC ozone data, Logan (1999) for 39 ozonesonde stations at various locations in the northern and southern hemisphere based on ozonesonde measurements, and Thompson *et al.* (2003) for a tropical ozone climatology.

In this study, mean ozone profiles were computed using 502 MOZAIC ozone profiles recorded over Johannesburg for the period 1995 to 2000. The mean annual tropospheric ozone profile over this period is shown in Figure 5.1e. There is a sharp increase in mean ozone from a near surface value of ~20 ppbv to ~45 ppbv within the lowest 2-3 km above sea level (asl). Thereafter, mean ozone values increase steadily throughout the troposphere to reach almost 70 ppbv by 12 km. Variability, as indicated by the standard deviation bars, is highest near the surface and in the upper troposphere. A study by Zunckel *et al.* (1992a) at Irene noted that the highest variability in ozone occurred near ground level, and attributed it to varying weather conditions and nearby ozone precursor sources. The greater variability which occurs in the upper troposphere (near the region of the tropopause) may be indicative of a more dynamic atmosphere due to the close proximity of Johannesburg to the mid-latitudes (Diab *et. al*, 1996a).

Seasonal trends in the vertical distribution of ozone (Fig. 5.1a-d) shows that there exists a large variability about the mean for all seasons, with an increasing trend with altitude. There is evidence of a clear seasonal pattern in tropospheric ozone with a spring maximum and an autumn minimum (Fig. 5.1f). This is consistent with other studies done by Diab *et al.* (1996a), Thompson *et al.* (1996a; 1996b) and Mari (2001), all who investigated the vertical distribution of ozone over Irene. Mari (2001) obtained spring near surface values of 40 ppbv compared with values of ~25 ppbv in other seasons and stated that spring values were generally greater than 10 ppbv than other seasons between the surface and 11 km asl. Diab *et al.* (1996a) obtained a near surface value of ~20 ppbv during the SAFARI-92 period. In this study, near surface values in spring is ~32 ppbv while values are between 17-24 ppbv in other seasons. Ozone values are generally greater than 15 ppbv in the mid-troposphere and 10 ppbv in the upper troposphere compared to other seasons. Whilst all mean seasonal profiles display a sharp increase in ozone between the surface to ~3km, the winter profile exhibits the greatest lower tropospheric enhancement of ~48 ppbv. This enhancement may be indicative of a local source as a contribution from biomass burning is minimal during this period.

Although much is gained from the analysis above, it is clear that calculation of a mean profile limits interpretation since the mean tends to mask the interesting and important micro-structure of individual profiles which is due to numerous counteracting influences present in the data.

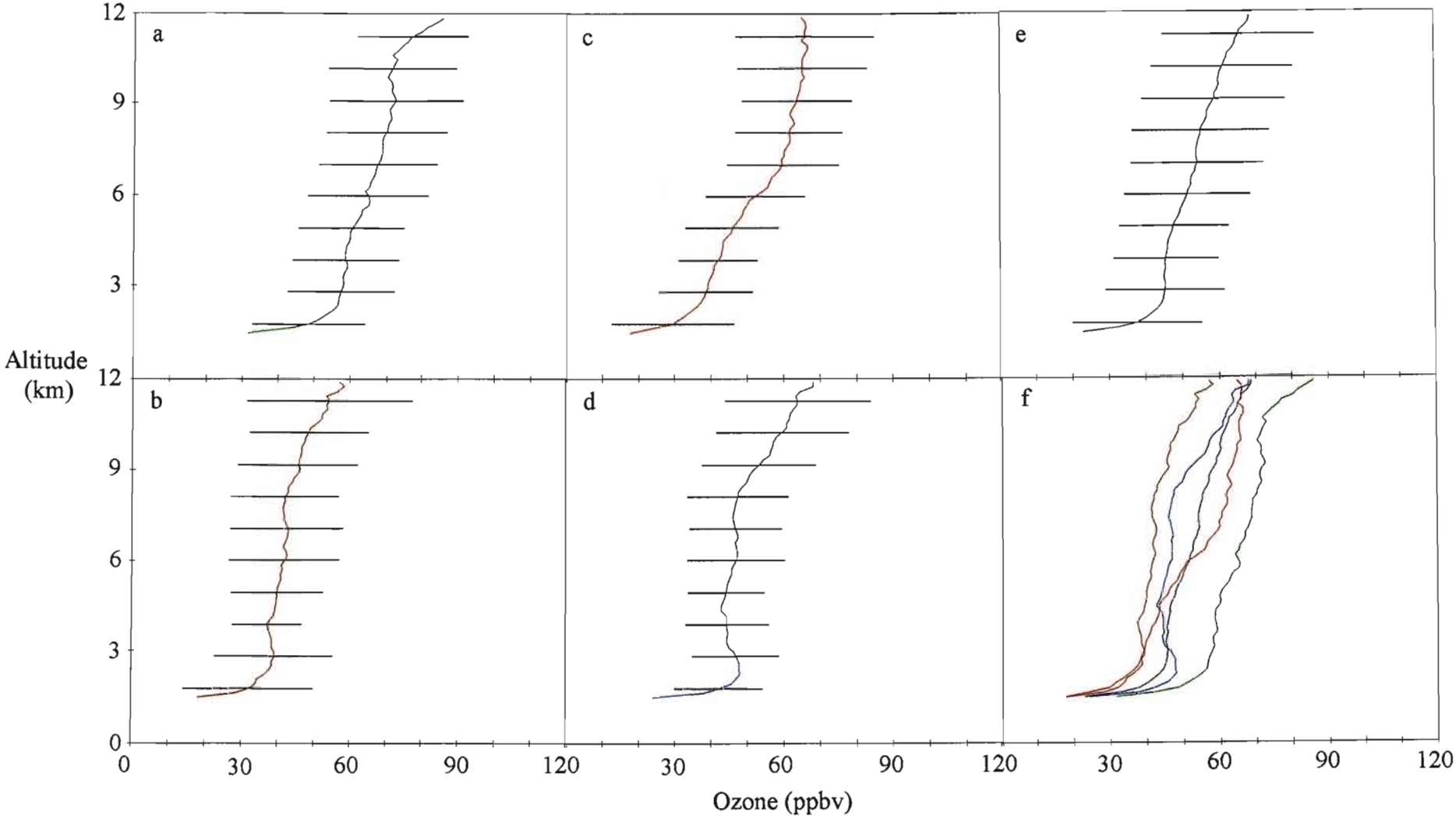

Figure 5.1: Mean vertical ozone concentration (ppbv) for the period 1995-2000: (a) spring, (b) summer, (c) autumn, (d) winter, (e) annual mean and (f) comparison of mean annual and seasonal profiles. Standard deviation bars for 150 m layers are given at 1050 m intervals.

An alternative approach is case study analysis, which has been used extensively to achieve a better understanding of specific processes that are in operation. Examples of studies that have centered on dynamic processes, particularly stratospheric-tropospheric exchange (STE) include, Merrill *et al.* (1996), Cooper *et al.* (1998), Folkins *et al.* (1999), Randriambelo *et al.* (1999), Zachariasse *et al.* (2000) and Kim *et al.* (2002). On the other hand, studies which document the presence of strong photochemical forcing include Fujiwara *et al.* (1999) and Longo *et al.* (1999). The advantage of case study analysis is that it greatly enhances the understanding of a particular process. On the contrary, a major deficiency of such studies is that they do not contribute significantly to our knowledge of the frequency of occurrence of such events or of their relative importance in the overall ozone budget.

In the light of these deficiencies a new approach to the analysis of ozone profiles is explored in this study. It is a classification of ozone profiles based on a cluster analysis technique.

5.2 Classification of Ozone Profiles

5.2.1 Classification Procedure

As an alternative to analyzing mean seasonal or individual profiles, ozone profiles are classified using a new approach based on a cluster analysis. In the quest for pattern and order in the structure of ozone profiles, the objective was to generate a classification of ozone profiles, which in turn could enhance our understanding of processes that govern the vertical distribution of ozone.

A number of authors have tried to group ozone profiles according to certain criteria, however, none has adopted an objective multivariate classification technique as has been done in this study. In one case, Newell *et al.* (1999) categorized fine laminar structures observed in ozone profiles into four layer types according to various combinations of ozone and water vapor characteristics, defined as either enhanced (+) or reduced (-). As each layer was assigned to a specific source, they were able to calculate the frequency of occurrence of each layer type as a percentage using vertical profile information obtained from the MOZAIC and PEM (Pacific Exploratory Mission) programs. The layer types are

defined as follows, with the percentage occurrence indicated in brackets after each type: O_3+/$H_2$0+ pointing toward continental pollution (11-15%); O_3+/H_2O- typical of stratospheric air or pollution (50-54%); O_3-/$H_2$0+ associated with convection from the moist boundary layer (15-19%); and O_3-/H_2O- characteristic of subsiding air initially lifted in deep convection above ocean surfaces (17-18%).

In another case, Cooper *et al.* (1998) grouped ozone profiles according to their geographic relationship to synoptic-scale weather systems i.e. pre-cold front, post-cold front, or cutoff low categories. This method was adopted in order to explain variations in the vertical distribution of ozone particularly influenced by atmospheric dynamics.

The classification scheme in this study was developed using 56 MOZAIC ozone profiles recorded over Johannesburg for the period 1995 to 2000. TWINSPAN (Two-Way Indicator Species Analysis) (Hill, 1979), was used to classify these profiles according to the magnitude and altitude of ozone concentration in a profile. Back trajectory modelling which was undertaken using the Hybrid Single-Particle Integrated Trajectory (HYSPLIT) model was used to provide evidence of the different origins of ozone enhancements in each of the classes.

5.2.2 Characteristics of Ozone Profiles used in the Classification

It is expected that the ozone profiles used in the classification will have been recorded at different times of the day and in different seasons. According to Thouret *et al.* (1998a), the recording times of profiles are highly dependent on the frequency of aircraft visits made to a city and on the strategy adopted by the airline. Figure 5.2a shows that Johannesburg profiles were recorded between 07:00-12:00 and 15:00-17:00, with most being recorded between 07:00-10:00. It is well known that there is a strong diurnal cycle in surface ozone (Combrink *et al.*, 1995; Fabian and Pruchniewicz, 1977; Lorenzi *et al.*, 1994; Marenco, 1986; Zeller and Moussiopoulos, 1986) and this should be considered when interpreting profiles in lower tropospheric layers. The distribution of profiles as a function of season is depicted in Figure 5.2b and shows that there is a relatively even spread of profiles across all seasons such that there is little room for bias in the classification.

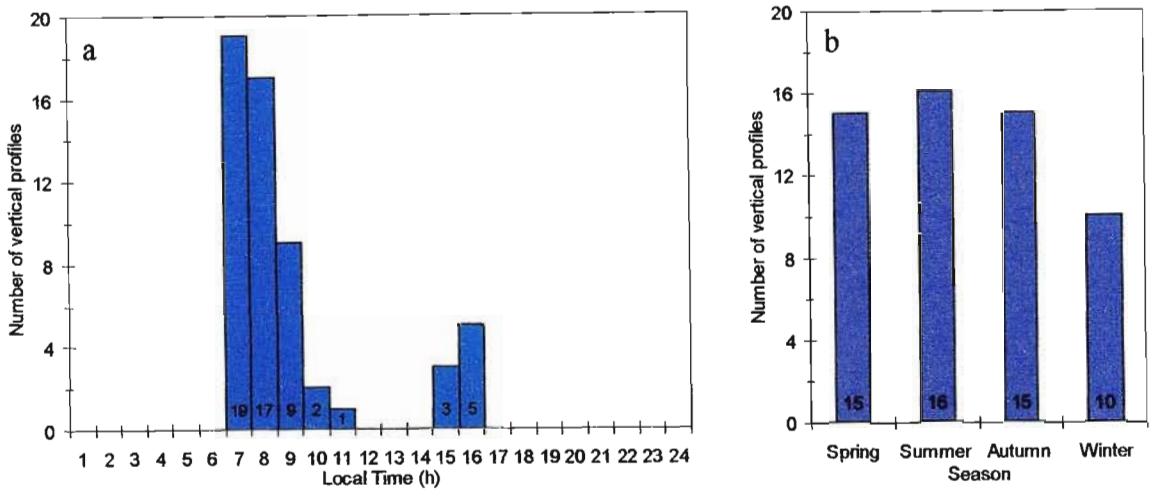

Figure 5.2: Distribution of ozone profiles at Johannesburg used in the TWINSPAN classification as a function of: (a) time of day and (b) season

5.2.3 Results of the Cluster Analysis

The breakdown of ozone profiles into classes is summarized by means of a dendogram presented in Figure 5.3. The dendogram is terminated after three levels of division as further division was regarded as meaningless (see below). Figures 5.4 to 5.6 shows the mean ozone profile and individual values at 150 m height intervals for all profiles within each group up to the third level of division, derived from the TWINSPAN cluster analysis.

At the first level of division, profiles were split into one group of 42 profiles (Group 1a), and a second group of 14 profiles (Group 1b) (Fig. 5.3). The mean profile in Group 1a (Fig. 5.4a) exhibits low ozone values (less than 40 ppbv) in the lower troposphere, while the mean profile in Group 1b (Fig. 5.4b) has an ozone value greater than 40 ppbv at the surface and ~70 ppbv in the lower troposphere. The first division has clearly singled out spring ozone profiles from those in other seasons, since the second group only contains two profiles that were not recorded in spring, when surface based emissions are known to maximise in this region (Justice *et al.*, 1996; Scholes and Andreae, 2000). A striking difference between both groups is also discernible at higher tropospheric altitudes. In the spring group (Group 1b), peaks in the middle troposphere are greater than 100 ppbv, whereas they seldom reach 90 ppbv in the first group (Group 1a).

At the second level of division, the first group (Group 1a) was divided again into one group of 15 (Group 2a) and a second group of 27 profiles (Group 2b) (Fig. 5.3). It is clear

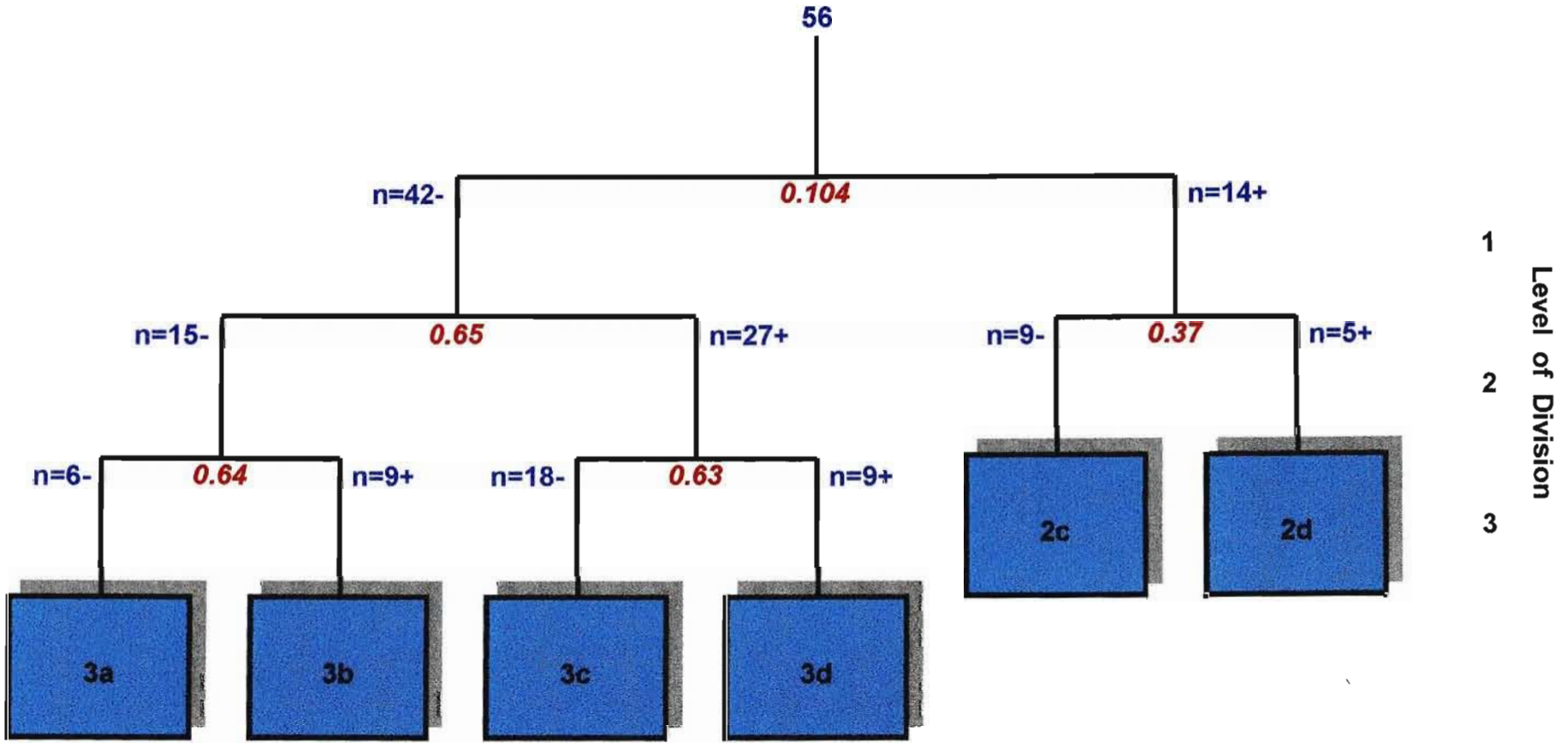

Figure 5.3: Dendrogram showing the hierarchical classification of ozone profiles derived from the TWINSPAN cluster analysis for the first three levels of division. n=number of profiles. Eigenvalues are given in italics. The main categories selected for analysis are: 3a = single mid-tropospheric peak; 3b = steady tropospheric increase; 3c = reduced tropospheric ozone; 3d = lower tropospheric enhancement; 2c = pronounced layering; 2d = considerable tropospheric enhancement

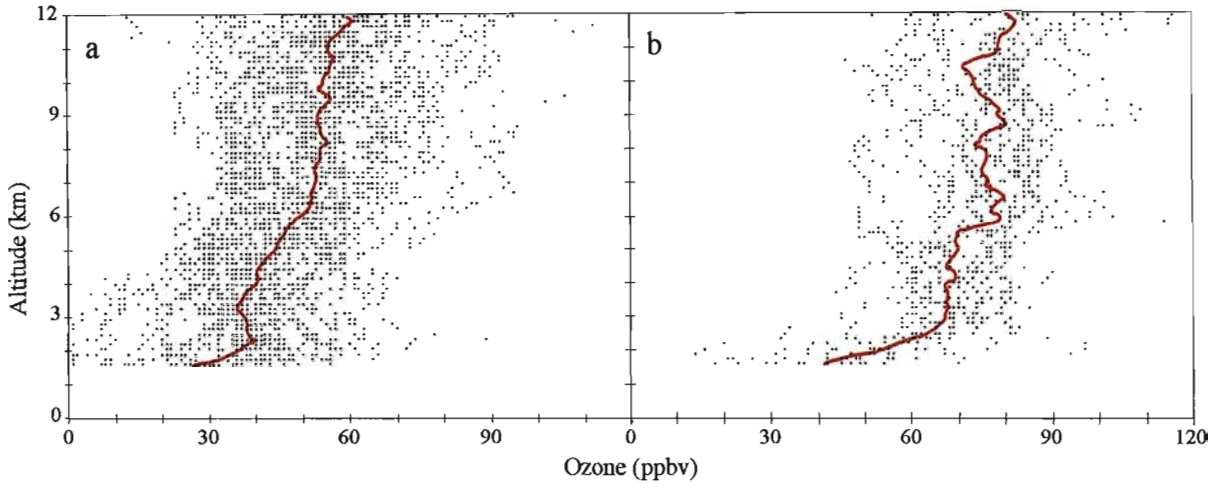

Figure 5.4: Mean (solid red line) and individual values at 150 m height intervals (black dots) for ozone profiles in each group derived from the TWINSPAN cluster analysis at the first level of division. (a) Group 1a and (b) Group 1b

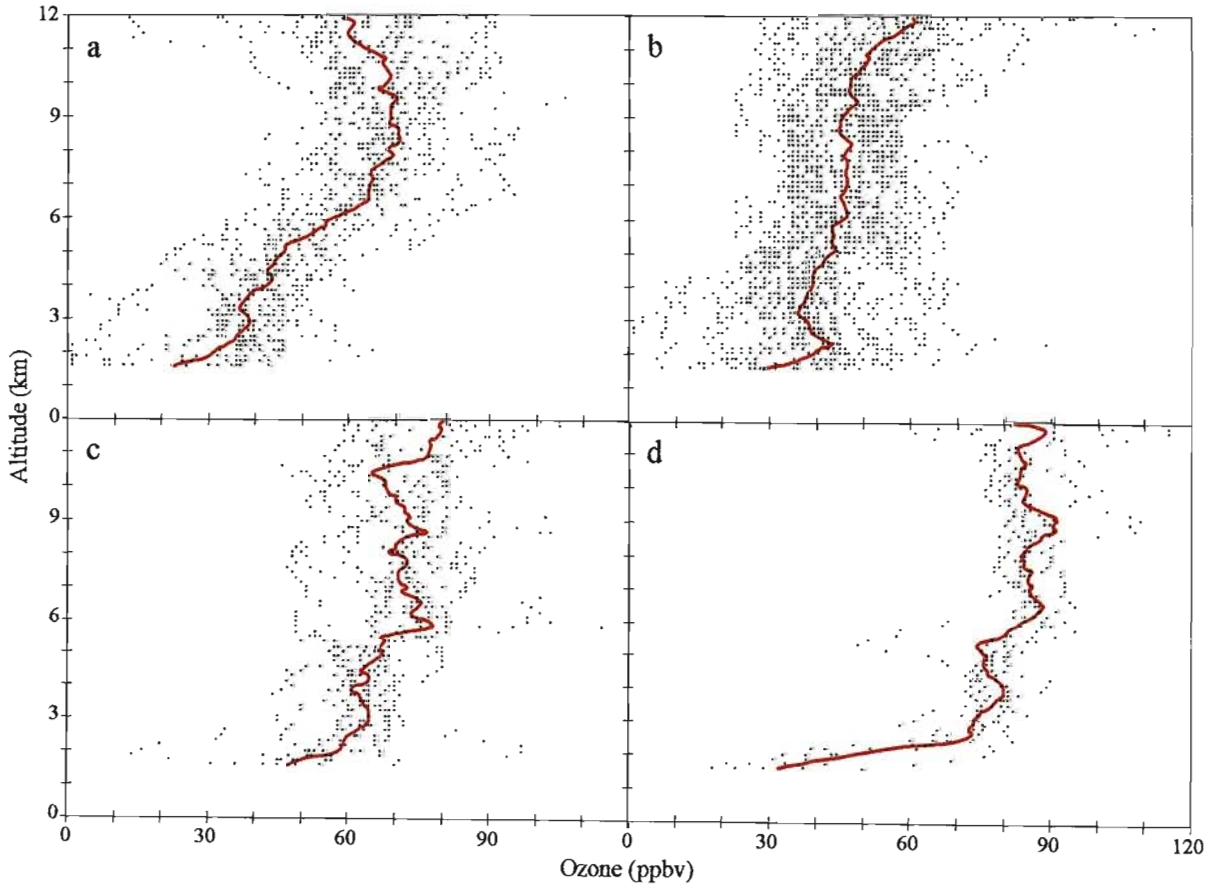

Figure 5.5: Mean (solid red line) and individual values at 150 m height intervals (black dots) for ozone profiles in each group derived from the TWINSPAN cluster analysis at the second level of division. (a) Group 2a, (b) Group 2b, (c) Group 2c and (d) Group 2d

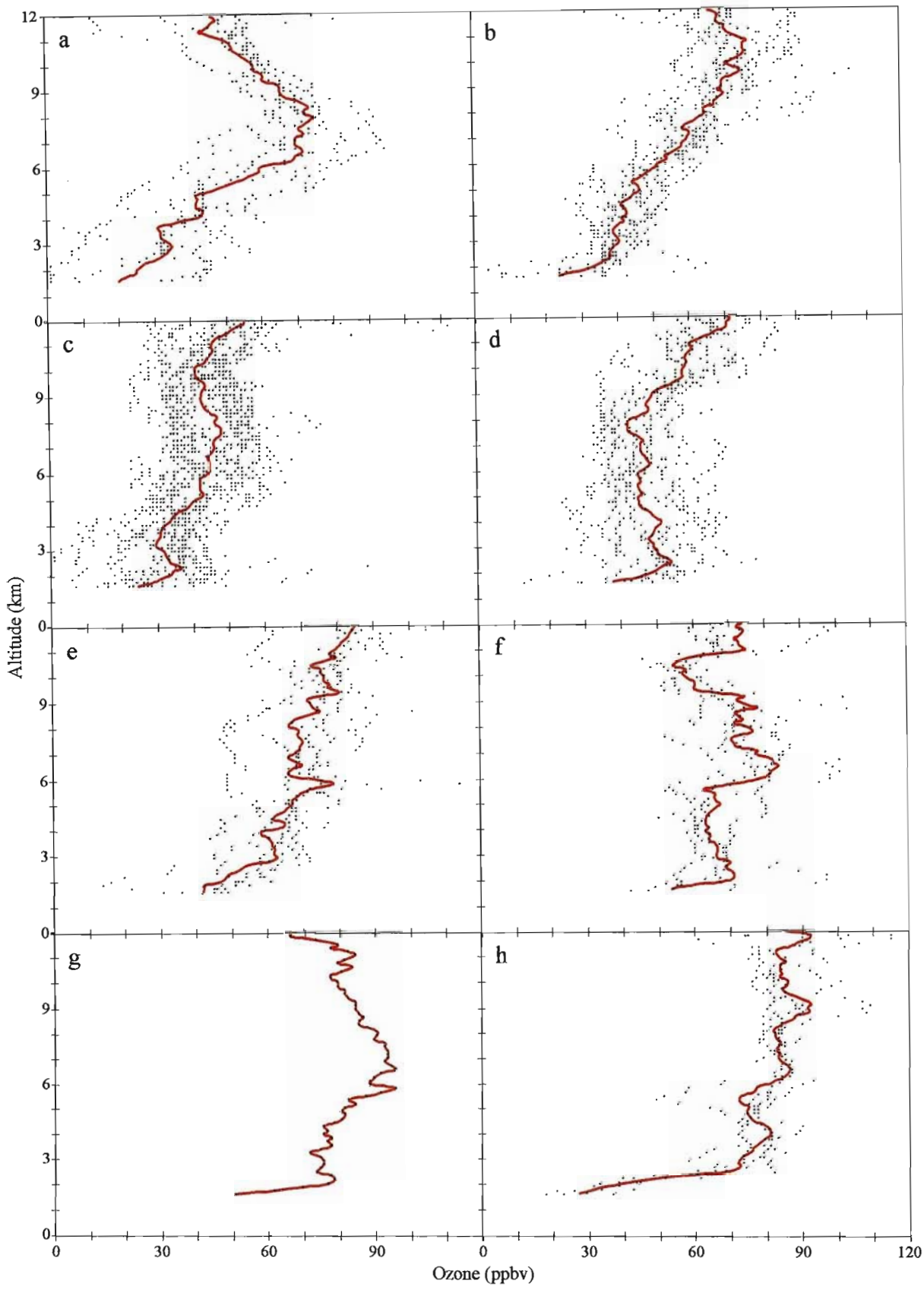

Figure 5.6: Mean (solid red line) and individual values at 150 m height intervals (black dots) for ozone profiles in each group derived from the TWINSPAN cluster analysis at the third level of division. (a) Group 3a, (b) Group 3b, (c) Group 3c, (d) Group 3d, (e) Group 3e, (f) Group 3f, (g) Group 3g and (h) Group 3h

that the division at this point has separated summer profiles from those in Group 2b which contains predominantly autumn and winter profiles, since the first group only contains 3 profiles that were not recorded in summer. Profiles in Group 2a (Fig. 5.5a) show a generally increasing trend in the lower to mid-tropospheric levels accompanied by an upper enhancement, usually above 8 km. There is no clear indication of an enhancement in the second group (Group 2b, Fig. 5.5b). The group containing predominantly spring profiles of the first level (Group 1b) is now further divided into one group of 9 profiles (Group 2c) and a smaller group of 5 profiles (Group 2d). Distinct layering patterns, with narrow peaks separated by bands of lower ozone characterize Group 2c (Fig. 5.5c). Group 2d (Fig. 5.5d) is characterized by a very sharp rise in ozone between the surface and just below 3 km, where values reach ~80 ppbv. Thereafter the distribution of ozone throughout the troposphere is uniform, with values fluctuating between 70-90 ppbv. The profiles in Group 2d do not show evidence of strong stratification.

The results of the third level of division are displayed in Figure 5.6. It is apparent that Group 3g consists of only one profile. Hence the final classification selected for in-depth analysis comprises a mixture of categories defined at level two and level three. There are six distinct categories, of which 4 were selected at the third level of division and 2 at the second level of division (Fig. 5.3). Each category has been named according to the structure of the characteristic profiles and are defined as follows: single mid-tropospheric peak (3a); steady tropospheric increase (3b); reduced tropospheric ozone (3c); lower tropospheric enhancement (3d); pronounced layering (2c) and considerable tropospheric enhancement (2d). Each category will be discussed in detail in the next section.

5.2.3.1 General Characteristics of Ozone Profiles in the Single Mid-Tropospheric Peak Category

Profiles in this category occur predominantly in summer (5), with 1 in winter, as is summarised in Table 5.1. The mean ozone profile of this category and values for individual profiles at each 150 m height interval are illustrated in Figure 5.7a. A typical profile within this group is best represented by a profile recorded on 25 December 1996 (Fig. 5.7b). All other individual profiles in this category are included in Appendix A.

The vertical distribution of ozone in this category is characteristic of a typical summer

pattern, where ozone values near to the surface are low, occasionally close to zero (Fig. 5.7a). This phenomenon is caused by ozone destruction in the moist boundary layer. According to Fishman *et al.* (1991), ozone has a fairly short atmospheric lifetime in the moist boundary layer, ranging from 2-5 days because of the high abundance of water vapor. Individual humidity profiles which are included in Appendix B show relative humidity values of up to 90% in the boundary layer. Further, removal mechanisms such as surface deposition (Liu *et al.*, 1987) in an unstable summertime boundary layer may also contribute to the low levels of ozone near the surface.

Table 5.1: Profiles in the single mid-tropospheric peak category as a function of season

Season	Spring	Summer	Autumn	Winter
Date		7 Feb 96 25 Dec 96 17 Jan 97 7 Feb 97 19 Feb 97		28 Aug 98
Total	0	5	0	1

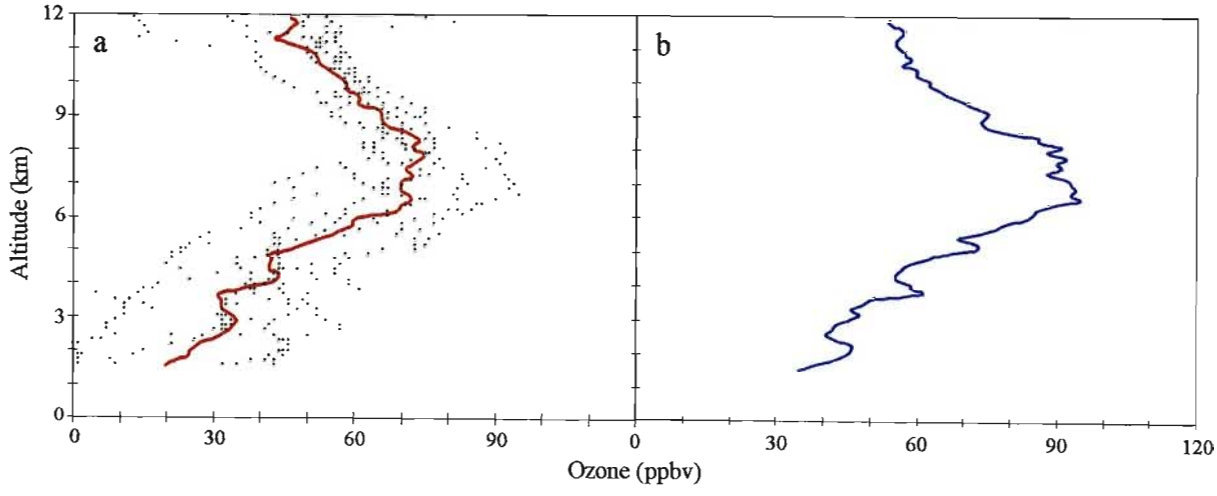

Figure 5.7: (a) Mean (solid red line) and individual values at 150 m height intervals (black dots) for ozone profiles and (b) a typical ozone profile (25 December 1996) in the single mid-tropospheric peak category

All profiles exhibit a single well-defined, broad mid-tropospheric ozone maximum located between 6-8 km, where peak values attain 80-100 ppbv. The mean value of this maximum is ~70 ppbv. This maximum is followed by a layer of comparatively lower ozone where values progressively drop from the peak to values of ~45 ppbv at 12 km. The reduced ozone in this upper layer is most likely due to convective outflow of ozone-poor air lifted

from the boundary layer. It also indicates that the tropopause is high at this time of year and consequently, there is an absence of the expected steep ozone increase in the vicinity of the tropopause.

- Two profiles that have outlying values have been identified in this category. The first occurs on 7 February 1996 (App. A), when two well-developed lower tropospheric peaks, each 1.5 km deep, occur at 3 and 4 km. These peaks are clearly related to the presence of absolutely stable layers (App. B). The 3 km peak is trapped below an inversion layer that corresponds to the lowest absolutely stable layer identified by Cosijn and Tyson (1996). The 4 km peak occurs above an isothermal layer.

The second profile is the only winter profile in this category, recorded on 28 August 1998 (App. A). While closely resembling the other summer profiles throughout most of the troposphere, it is the only profile that shows a sudden increase in ozone just below 12 km. This reflects the lower position of the tropopause during this season and the subsequent penetration of ozone-rich stratospheric air to these altitudes (see points on the extreme right of the mean in Fig. 5.7a).

Relative humidity (RH) profiles, and the occurrence of stable layers on individual days are displayed together with the ozone profiles in Appendix B. It was noted that there was considerable variability in RH within each category and even in the relationship between ozone and RH. Further analysis of RH profiles and stability layers was therefore excluded but they are included for the record in Appendix B.

5.2.3.2 Source Regions of Tropospheric Ozone for the Mid-Tropospheric Peak Category

In order to determine source regions of tropospheric ozone, back trajectory modelling using the HYSPLIT model was undertaken. On each day, trajectories were initiated at 2.5, 5, 7.5 and 10 km except for minor variations as discussed in the methodology (section 2.5).

Results of the 5-day back trajectory modelling for all days within this category are overlaid and depicted in Figure 5.8 Near-surface transport (back trajectory initialised at an altitude of 2.5 km) is from the northern and eastern sectors (red trajectories) and is associated with

anticyclonic circulation of moist maritime air. Trajectories generally originated over the Indian Ocean between the north-east and south-east, thus accounting for the high relative humidity recorded on these days and the low near-surface ozone values. Mid-tropospheric transport between 5 and 7.5 km (blue and green trajectories) was generally out of the west, although in two of the cases (7 February 1997 and 17 January 1997, App. C), easterly transport extended upwards from the surface.

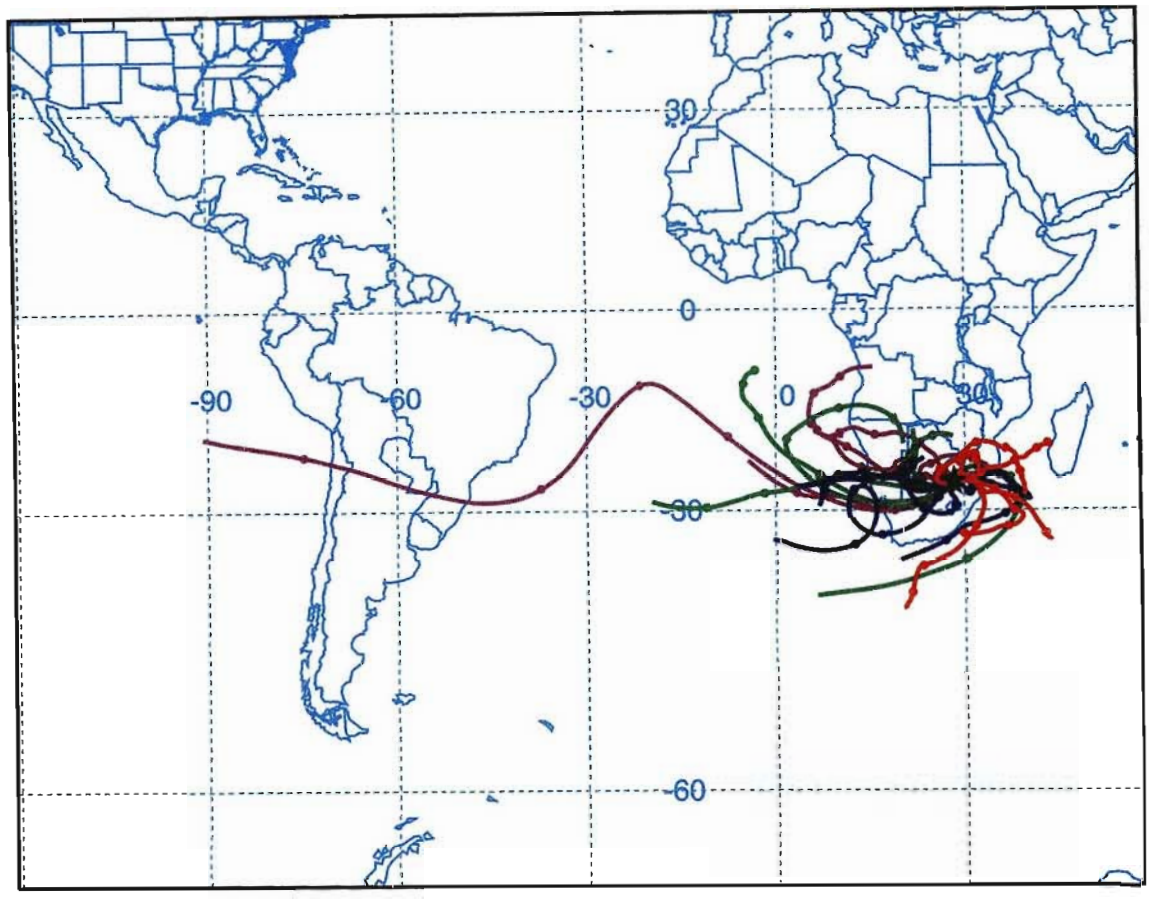

Figure 5.8: Composite of five-day back trajectory HYSPLIT model results for all days in the single mid-tropospheric peak category. Trajectories originating at 2.5 km are red, 5km blue, 7.5 km, green and 10 km, purple

The most distinguishing feature of this category is the descending movement of air in the upper troposphere (evident in the vertical cross sections shown in App. C) in a spiralling anticyclonic circulation, with trajectories generally originating over continental areas to the north rather than from the west. This feature is well represented by one case study (25 December 1996, App C), where air originated over the Democratic Republic of the Congo and descended from approximately 12 km to 8.7 km, most likely being responsible for the long-range transport of ozone-rich air from African countries to the north of Johannesburg.

Whilst this feature is clearly manifested in this case study (25 December 1996), it is generally evident in all other cases within this category (App. C). Strong summer convective activity in the lower latitudes would be able to mix surface generated ozone precursors (possibly from biomass burning which is known to exist at this time of year (Hao *et al.*, 1996) to higher altitudes where ozone has a longer lifetime (Liu *et al.*, 1987). Coupled with convective enhancement (Pickering *et al.*, 1990; 1992a; 1993) this would account for the relatively high ozone air transported southwards.

5.2.3.3 General Characteristics of Ozone Profiles in the Steady Tropospheric Increase Category

Profiles in this category occur predominantly in summer (7), with 2 in spring (Table 5.2). This group exhibits a generally increasing trend in ozone (Fig. 5.9a), with individual profiles characterized by the occurrence of multiple laminae ranging between 5-15 ppbv at variable altitudes (App. A). A typical ozone profile on 23 December 1995 that clearly depicts the layered structure is shown in Figure 5.9b. Newell *et al.* (1999) identified similar laminar structures between altitudes of 5.5-6.6 km and found that their thickness varied between 0.5-1.3 km. It is suggested that these fine laminar structures are generated by upward motion and lateral spreading associated with deep convection.

Table 5.2: Profiles in the steady tropospheric increase category as a function of season

Season	Spring	Summer	Autumn	Winter
Dates	17 Nov 98 18 Nov 98	23 Dec 95 16 Dec 98 22 Dec 98 23 Dec 98 30 Dec 98 6 Jan 99 5 Feb 99		
Total	2	7	0	0

It is noted that there is one case (5 February 1999) when a distinct near-surface peak (65 ppbv) at 2 km occurs in contrast to the generally increasing trend. The ozone peak coincides with high RH values and is most likely due to increased photochemical production of ozone typical of summer months, which has accumulated beneath an isothermal layer (App. B).

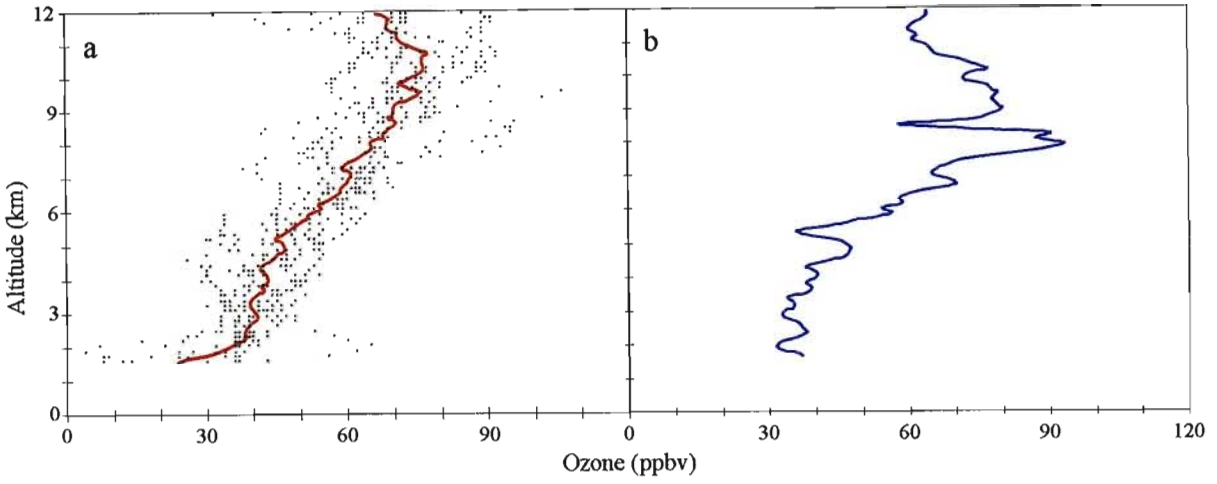

Figure 5.9: (a) Mean (solid red line) and individual values at 150 m height intervals (black dots) for ozone profiles and (b) a typical ozone profile (23 December 1995) in the steady tropospheric increase category

5.2.3.4 Source Regions of Tropospheric Ozone for the Steady Tropospheric Increase Category

Five-day back trajectory results for all days in this category are displayed in a composite map in Figure 5.10. The distinguishing feature of this category in terms of the source region of air masses is that most of the mid- to upper-tropospheric (5-10 km) trajectories (blue, green and purple) originate from the south-west over the Atlantic Ocean. There is evidence of relatively light winds over the subcontinent and stronger westerly winds over the Atlantic Ocean as indicated by the difference in the length of daily trajectories. The origin of near-surface air (red trajectories) is variable. Generally, winds are out of the east but may also be of continental origin, which accounts for the considerable variability indicated in near-surface ozone (Fig. 5.9a). Individual case studies are presented in Appendix C.

5.2.3.5 General Characteristics of Ozone Profiles in the Reduced Tropospheric Ozone Category

This category contains the largest number of profiles (18) and therefore does not display the coherence of other groups, evidenced by the relatively large spread of values about the mean (Fig. 5.11a) Profiles in this category occur predominantly in autumn and winter (16), with 2 in summer (Table 5.3).

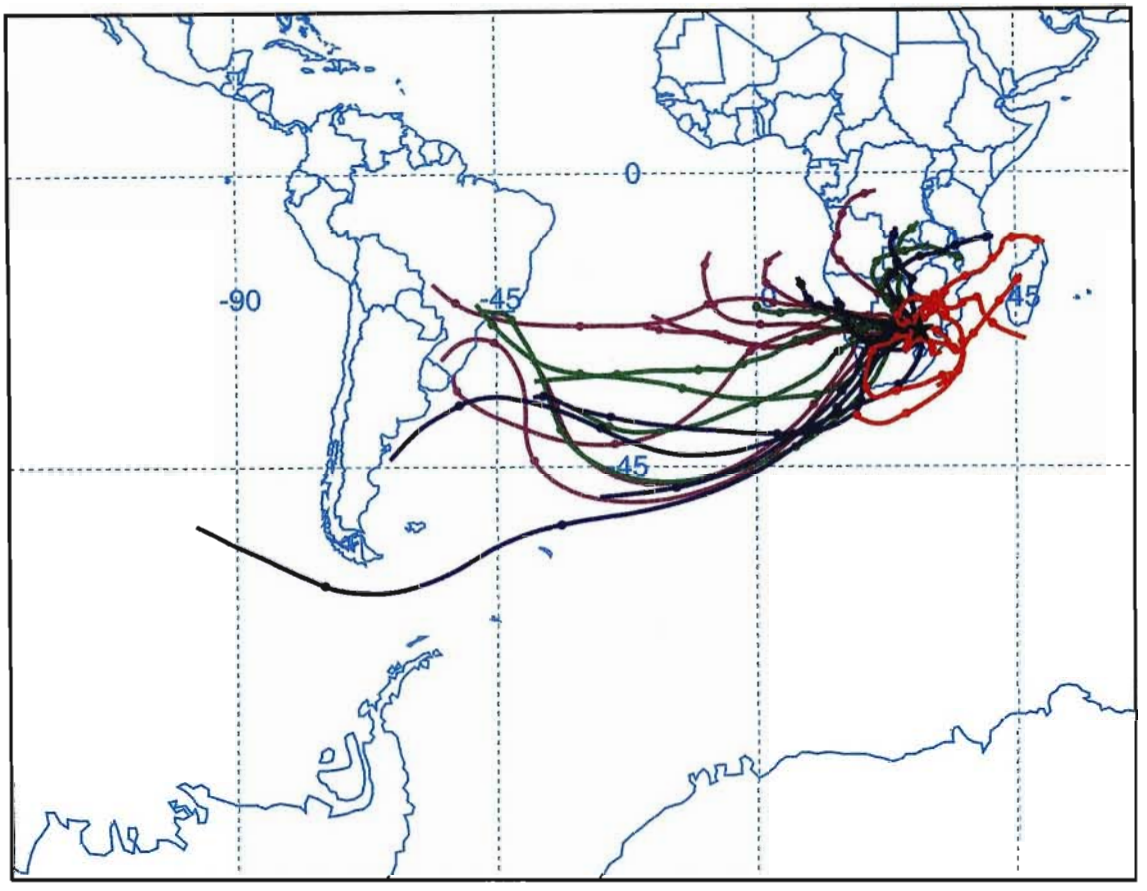

Figure 5.10: Five-day back trajectory HYSPLIT model results for the steady tropospheric increase category. Trajectories originating at 2.5 km are red, 5km blue, 7.5 km, green and 10 km, purple

Table 5.3: Profiles in the reduced tropospheric ozone category as a function of season

Season	Spring	Summer	Autumn	Winter
Dates		20 Feb 98	24 Apr 96	13 Jun 97
		29 Dec 98	1 May 96	12 Jun 98
			5 Mar 97	28 Jun 98
			26 Mar 97	6 Jul 98
			23 Apr 97	
			16 May 97	
			20 Mar 98	
			29 Mar 98	
			2 May 98	
			8 May 98	
			3 May 99	
			22 Mar 00	
Total	0	2	12	4

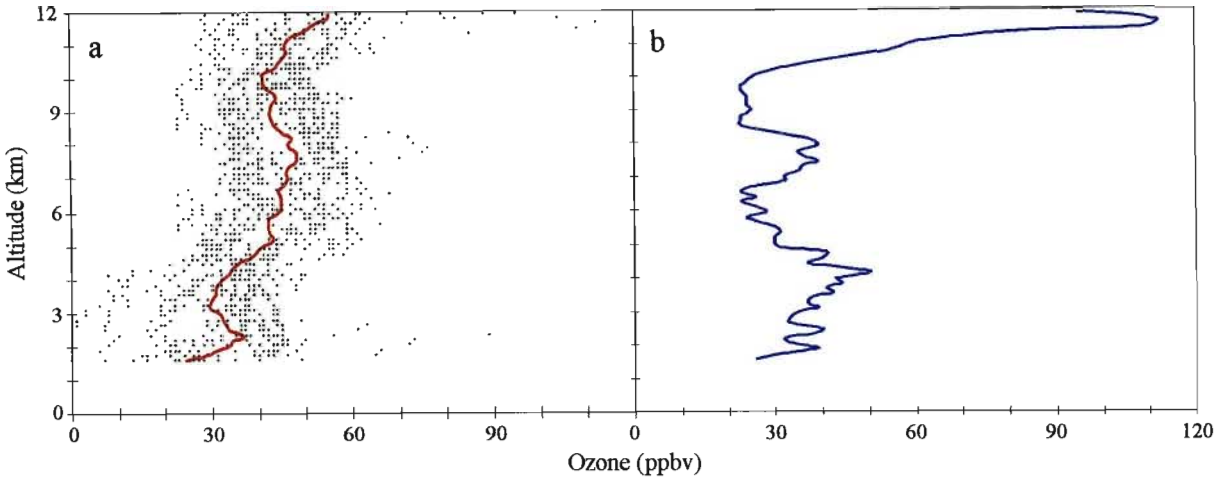

Figure 5.11: (a) Mean (solid red line) and individual values at 150 m height intervals (black dots) for ozone profiles and (b) a typical ozone profile (16 May 1997) for the reduced tropospheric ozone category

A distinguishing feature is the existence of relatively low ozone values throughout the troposphere. Values in the mean profile do not exceed 50 ppbv (Fig. 5.11a). The mean profile also exhibits a shallow near-surface enhancement (36 ppbv) up to 3 km, fairly low values (~30 ppbv) between 3-5 km and another broader mid-tropospheric enhancement between 5-8 km. Individual profiles in this group are also characterised by a generally increasing trend in ozone in the upper troposphere (App. A), reflecting the lower position of the winter tropopause and the penetration of stratospheric air that is richer in ozone. This is particularly evident in the individual ozone profile for 16 May 1997 (Fig. 5.11b). Most of these profiles (~90%) were recorded in either autumn or winter, when the northward displacement of the mean subtropical anticyclones permits the invasion of westerly winds through a deep layer of the atmosphere over southern Africa to a greater extent than at other times of the year. The penetration of maritime air from the west is likely to contribute to the relatively low ozone values found in this group.

5.2.3.6 Source Regions of Tropospheric Ozone for the Reduced Tropospheric Ozone Category

Back trajectory modelling reveals that westerly airflow dominates throughout the troposphere (Fig. 5.12) and is clearly evident in the typical case study (16 May 1997, App. C). The maritime origin of air over the Atlantic Ocean is responsible for the relatively low ozone values in these cases as noted above. At times, the origin of low-level air masses

(red trajectories) is from the south-east rather than the west, representing flow to the rear of the mid-latitude frontal system, but its maritime origin again gives rise to low ozone values. In a few cases, the low-level origin of air is over African countries (Botswana and Zimbabwe), however, the absence of significant biomass burning emissions during the autumn and winter seasons account for the comparatively low ozone levels.

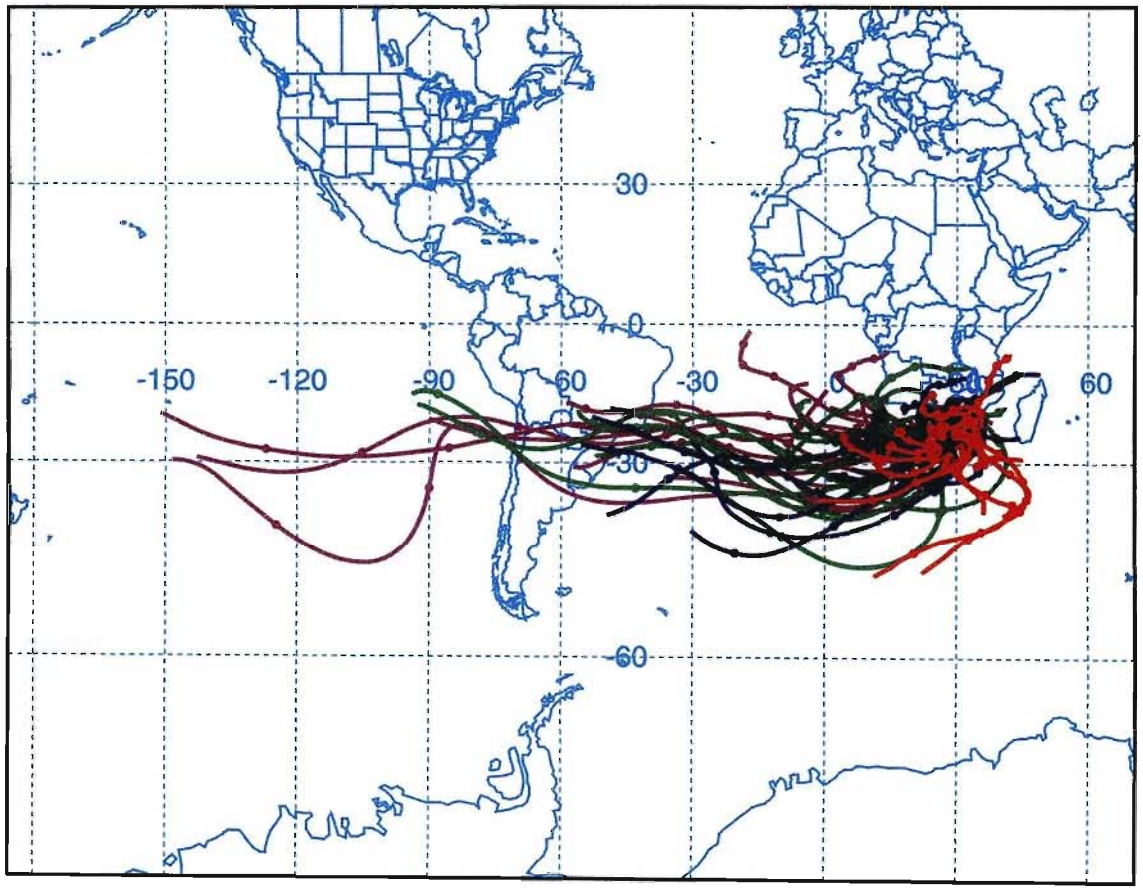

Figure 5.12: Five-day back trajectory HYSPLIT model results for the reduced tropospheric ozone category. Trajectories originating at 2.5 km are red, 5km blue, 8 km, green and 10 km, purple

5.2.3.7 General Characteristics of Ozone Profiles in the Lower Tropospheric Enhancement Category

Profiles in this category occur predominantly in winter (4), with 1 or 2 profiles in each of the other seasons (Table 5.4). The most prominent characteristic of this group is the occurrence of a lower tropospheric enhancement, where the mean ozone concentrations exceed 50 ppbv, followed by a deep layer of relatively lower ozone concentrations in the mid-troposphere (5-8 km) (Fig. 5.13a). Individual profiles show values in excess of 70

ppbv in the lower troposphere (App. A). The peak is generally confined below 5 km, which coincides with the height of the resilient and persistent absolutely stable layer described by Cosijn and Tyson (1996). The 5-km stable layer is a prominent feature and is known to exert an important influence on the vertical distribution of trace gases and aerosols over southern Africa (Tyson *et al.*, 1997). It restrains vertical mixing, trapping boundary layer photochemically-produced ozone within the lower troposphere. Most of the profiles in this group were recorded during autumn or winter when the absolutely stable layer is most prominent. The features of this group are well represented by an individual profile for 12 August 1998 displayed in Figure 5.13b.

Table 5.4: Profiles in the lower tropospheric enhancement category as a function of season

Season	Spring	Summer	Autumn	Winter
Dates	24 Nov 98	11 Dec 98 15 Dec 98	3 May 95 22 May 98	15 Jul 98 17 Jul 98 29 Jul 98 12 Aug 98
Total	1	2	2	4

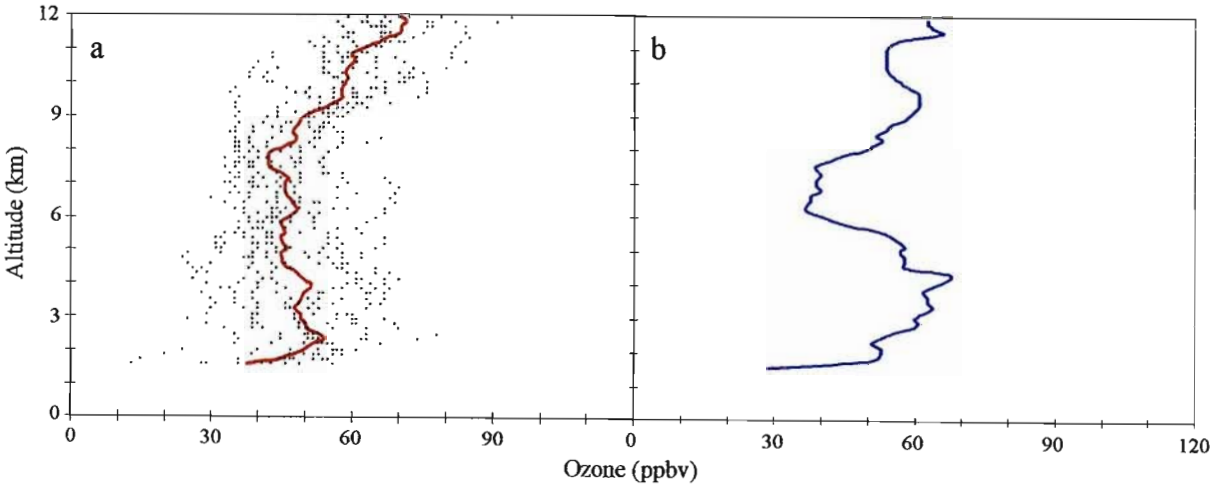

Figure 5.13: (a) Mean (solid red line) and individual values at 150 m height intervals (black dots) for ozone profiles and (b) a typical ozone profile (12 August 1998) for the lower tropospheric enhancement category

5.2.3.8 Source Regions of Tropospheric Ozone for the Lower Tropospheric Enhancement Category

Back-trajectory modelling confirms the presence of a strong discontinuity in the atmosphere (Fig. 5.14). Below 5 km, there is evidence of anticyclonic recirculation and

light winds (red trajectories), which are responsible for the build-up of lower tropospheric ozone (Fig. 5.13a). Above 5 km, air parcels have been advected in strong westerly flow from the Atlantic Ocean, bringing clean maritime air to the mid-troposphere over Johannesburg (blue, green and purple trajectories in Fig. 5.14). The increasing ozone between 9 and 12 km most likely reflects the lower altitude of the winter tropopause and the possible penetration of stratospheric ozone-rich air to lower levels (Fig. 5.13a). Results of back-trajectory modelling for individual days in this category are presented in Appendix C.

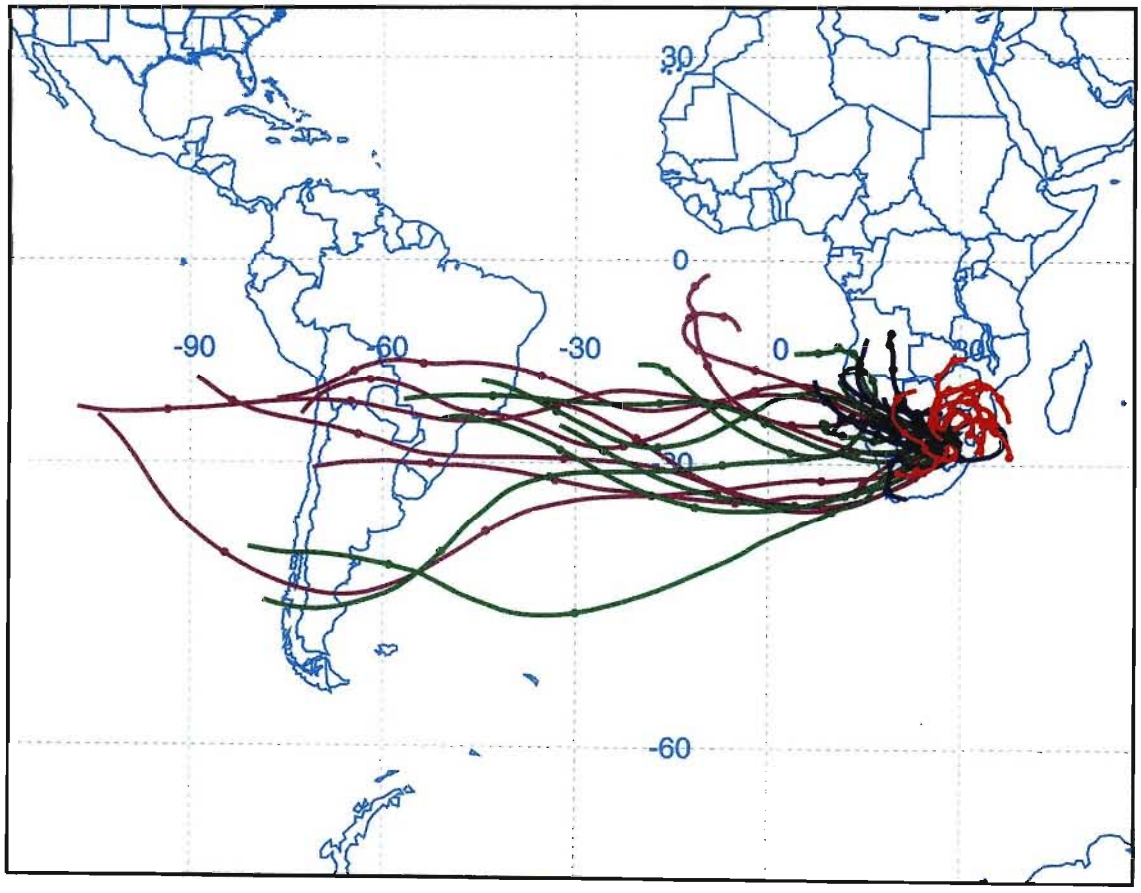

Figure 5.14: Five-day back trajectory HYSPLIT model results for the lower tropospheric enhancement category. Trajectories originating at 2.5 km are red, 4km blue, 7.5 km, green and 10 km, purple

5.2.3.9 General Characteristics of Ozone Profiles in the Pronounced Layering Category

Profiles in this category occur predominantly in spring (7), with 1 each in autumn and winter (Table 5.5). All profiles in this category display pronounced stratification, with

ozone differing by ~50 ppbv within a few hundred metres (App. A) and is well represented by the typical profile (Fig. 5.15b). There is thus considerable variation about the mean (Fig. 5.15a), which obscures the marked layering exhibited by individual profiles, for example 2 October 1998 (Fig. 5.15b). The peaks are narrow, occur at different altitudes and on some days reach ozone concentrations of up to 115 ppbv. All profiles with the exception of 2 were recorded in spring, a season when tropospheric ozone values are known to maximise (Diab *et al.*, 1996a; Thompson *et al.*, 1996b).

Table 5.5: Profiles in the pronounced layering category as a function of season

Season	Spring	Summer	Autumn	Winter
Dates	10 Sep 98 14 Sep 98 15 Sep 98 20 Sep 98 2 Oct 98 25 Oct 98 13 Nov 98		9 Mar 99	21 Aug 98
Total	7	0	1	1

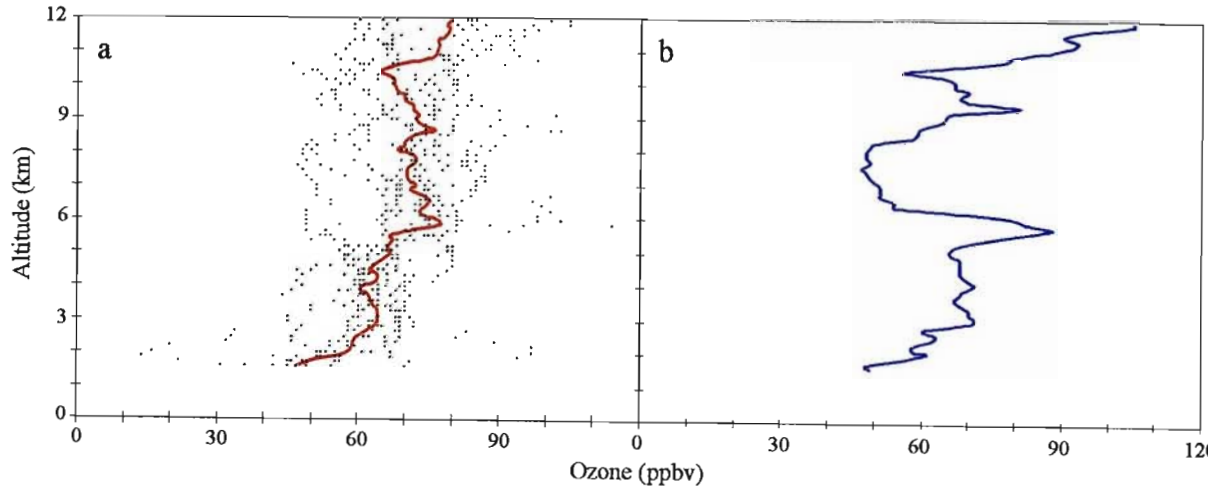

Figure 5.15: (a) Mean (solid red line) and individual values at 150 m height intervals (black dots) for ozone profiles and (b) a typical ozone profile (2 October 1998) for the pronounced layering category

5.2.3.10 Source Regions of Tropospheric Ozone for the Pronounced Layering Category

Back trajectory modelling (Fig. 5.16) confirms that air masses throughout the lower and mid-troposphere (up to ~5 km) originate predominantly over continental areas to the north

of Johannesburg (red and blue trajectories). Only in the upper troposphere (back trajectories originating at 7.5 and 10 km) is the source region from the west, with air masses characterized by cleaner maritime air (green and purple trajectories). Results for individual days are included in Appendix C.

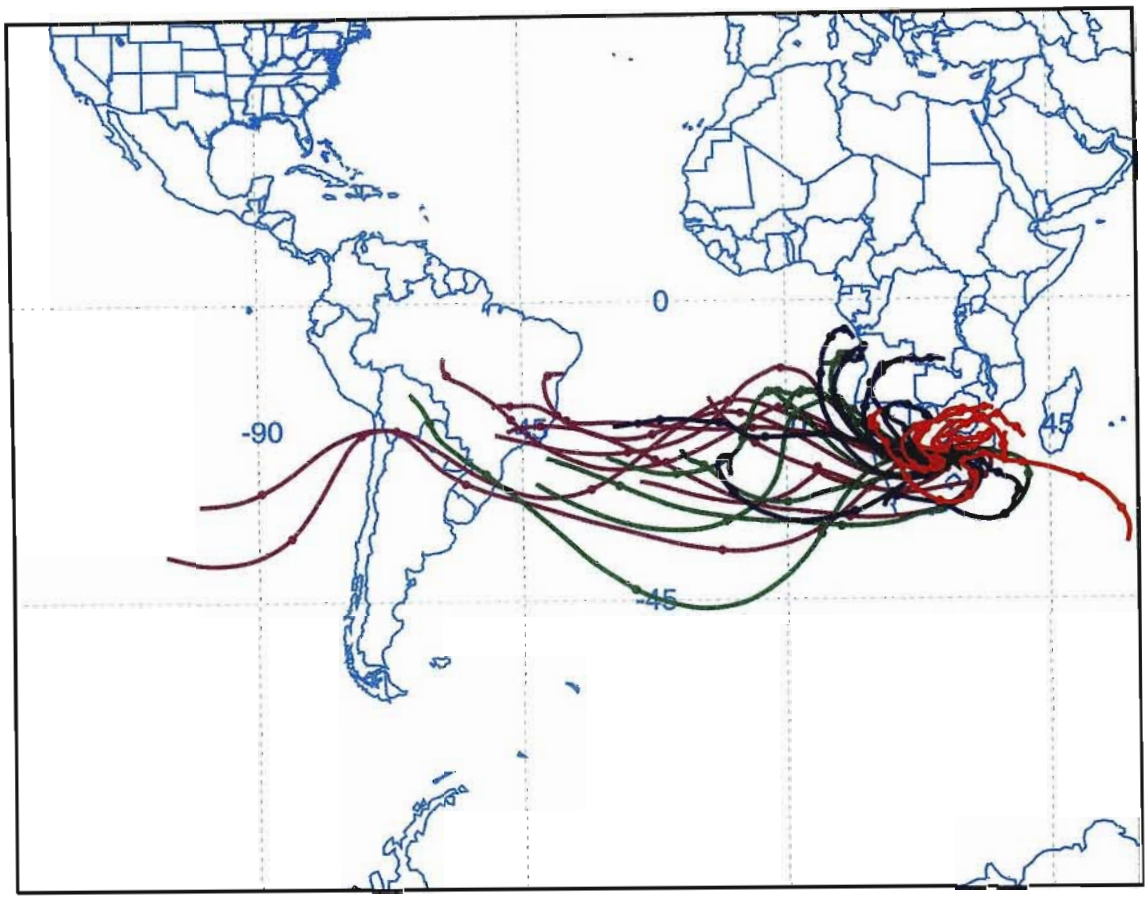

Figure 5.16: Five-day back trajectory HYSPLIT model results for the pronounced layering category. Trajectories originating at 2.5 km are red, 6km blue, 7.5 km, green and 10 km, purple

5.2.3.11 General Characteristics of Ozone Profiles in the Considerable Tropospheric Enhancement Category

All profiles in this category occur in spring (Table 5.6) and display a sharp increase in ozone from the surface-2.5 km, after which elevated ozone values (80-100 ppbv) predominate throughout the troposphere (Fig. 5.17a). These features are well represented by the typical profile displayed in Figure 5.17b. Further individual profiles are included in Appendix A. There is relatively little variation about the mean (Fig. 5.17a), which highlights the dominance of the springtime ozone enhancement. TTO for these days varied

between 35.7 and 39.3 DU and included some of the highest values recorded (section 3.5).

Table 5.6: Profiles in the considerable tropospheric enhancement category as a function of season

Season	Spring	Summer	Autumn	Winter
Dates	11 Oct 96 25 Oct 96 10 Oct 97 7 Oct 98 8 Oct 98			
Total	5	0	0	0

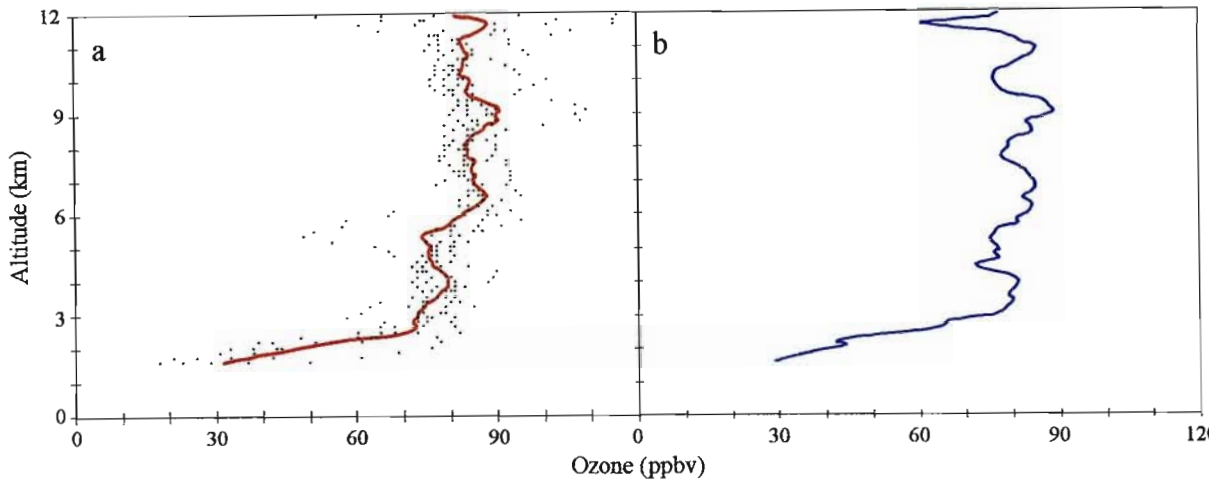

Figure 5.17: (a) Mean (solid red line) and individual values at 150 m height intervals (black dots) for ozone profiles and (b) a typical ozone profile (8 October 1998) for the considerable tropospheric enhancement category

5.2.3.12 Source Regions of Tropospheric Ozone for the Considerable Tropospheric Enhancement Category

Movement of air generally of continental origin in a large anticyclonic gyre over the subcontinent is responsible for the high ozone values recorded. Figure 5.18 displays the composite results of back trajectory modelling for this category. Trajectories frequently originate north of 15°S over locations which are widely acknowledged as key biomass burning regions at this time of year. Only at the highest level (10 km) is there evidence of the dominance of westerly flow (purple trajectories). Back trajectory modelling results for individual days in this category are included in Appendix C.

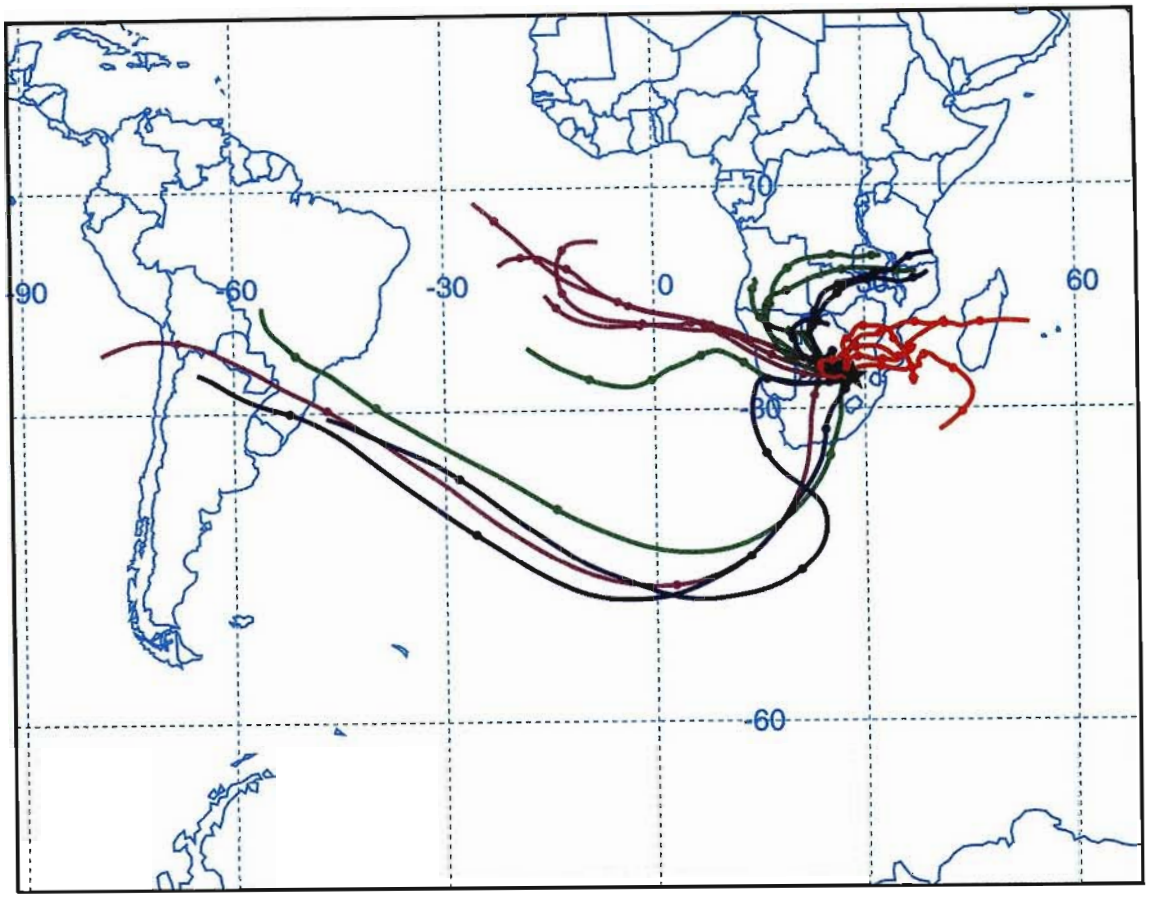

Figure 5.18: Five-day back trajectory HYSPLIT model results for the considerable tropospheric enhancement category. Trajectories originating at 2.5 km are red, 5km blue, 7.5 km, green and 10 km, purple

5.2.4 Comparison of Results as a Function of Category

5.2.4.1 Frequency Distribution of Ozone Values

The marked differences between groups are highlighted by ozone frequency distributions within each group (Fig. 5.19). Here ozone values (at 150 m height intervals) from individual profiles within each group have been binned into ozone classes, defined in intervals of 10 ppbv ranging from 0 to 120 ppbv, and expressed as percent frequencies.

Group 1 is characterised by a broad unimodal distribution, with most of the ozone values between 51-60 ppbv. In addition, it has a relatively higher frequency of very low values (less than 30 ppbv) than other groups, due to ozone destruction near the surface. Groups 2 and 4 exhibit similar frequency distributions with modal classes of 61-70 ppbv and 51-60 ppbv respectively. The third group displays a frequency shift to fairly low ozone values

(31-40 ppbv) and very few values (4.4 %) above 60 ppbv. Groups 5 and 6 display a frequency shift to much higher values and have modal classes of 61-70 and 81-90 ppbv respectively, reflecting the springtime ozone enhancement. They are also typified by an occurrence of low frequencies at lower end of the scale. In Group 6, less than 9% of the values are below 60 ppbv.

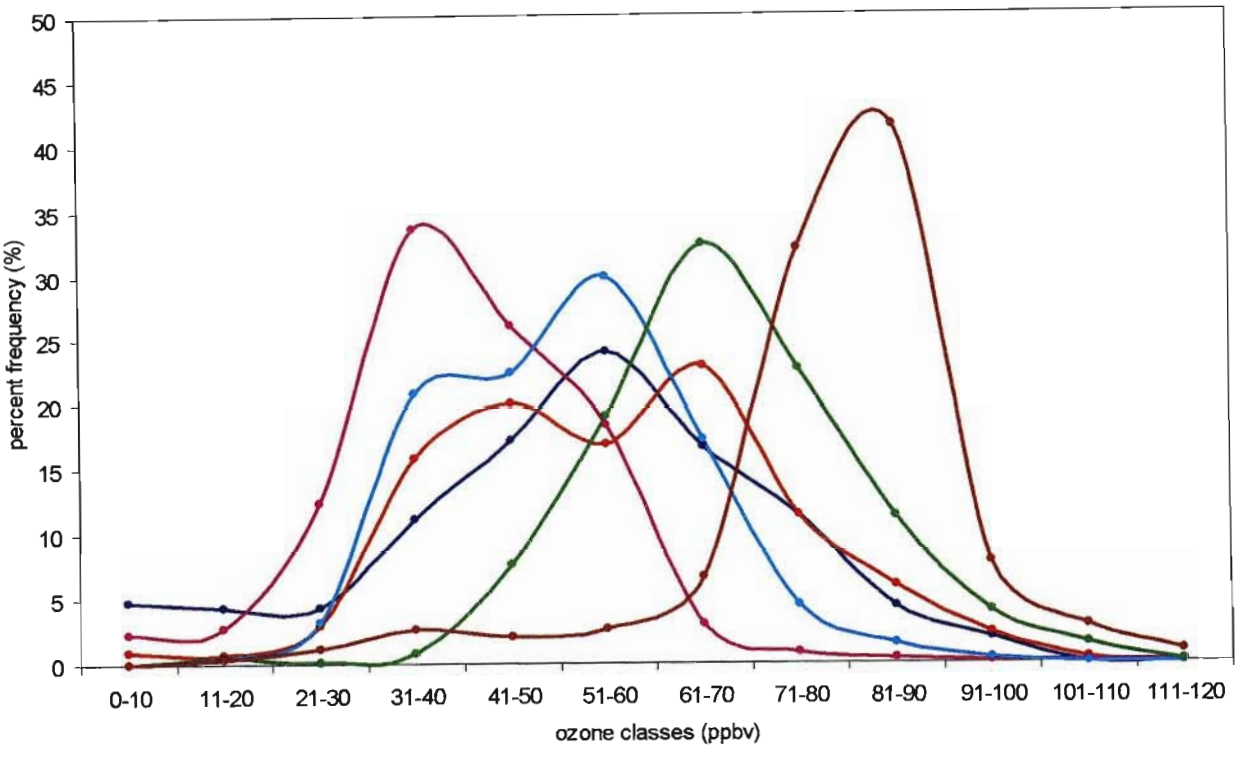

Figure 5.19: Frequency distribution of ozone values within each of the 6 defined profile categories. Dark blue = single mid-tropospheric peak; red = steady tropospheric increase; pink = reduced tropospheric ozone; light blue = lower tropospheric enhancement; green = pronounced layering; brown = considerable tropospheric enhancement

5.2.4.2 Seasonality of Ozone Profiles

The classification has clearly drawn attention to the distinct seasonality of ozone profiles (Table 5.7). Despite variation among groups, it is evident that seasons are dominated by distinct patterns and by inference, the processes and transport patterns that mould and define single profiles are seasonally dependent.

Spring is characterized by either 'pronounced layering' or 'considerable tropospheric enhancement', indicative of strong photochemical production from biomass burning and biogenic sources in this season. Summer profiles exhibit a 'mid-tropospheric peak' when

upper tropospheric air masses originate from continental areas to the north of Johannesburg, indicative of southward penetration of the Inter-Tropical Convergence Zone (ITCZ) or a 'steady tropospheric increase' when the troposphere is characterized by westerly flow originating over the Atlantic Ocean. Autumn profiles fall mainly into the 'reduced tropospheric ozone' group, caused by a dominance of westerly flow at all tropospheric levels. Winter profiles fall into both the 'reduced tropospheric ozone' and 'lower tropospheric enhancement' groups.

Table 5.7: Distribution of cases within each group by season

	Groups						
	1 Single mid-tropospheric peak	2 Steady tropospheric increase	3 Reduced tropospheric ozone	4 Lower tropospheric enhancement	5 Pronounced layering	6 Considerable tropospheric enhancement	Total
Spring	0	2	0	1	7	5	15
Summer	5	7	2	2	0	0	16
Autumn	0	0	12	2	1	0	15
Winter	1	0	4	4	1	0	10

Spring is widely acknowledged as the season during which tropospheric ozone maximizes, as confirmed by this study. However, the equally high summer mid-tropospheric peak as typified by the first category has not been identified in earlier studies. In an investigation of TTO, these cases would not have emerged as particularly high TTO days because of the counteracting influence of the particularly low near-surface ozone. Furthermore, summer is dominated by two patterns, viz. groups 1 and 2, and hence a study of mean seasonal profiles would have failed to reveal this particular pattern.

Johannesburg is situated at a latitude that is intermediate between tropical and mid-latitude meteorological regimes, making it an important location for an analysis of ozone profiles. Depending on the latitudinal position of the large scale pressure systems, so Johannesburg is dominated by circulation patterns characteristic of either mid-latitude or tropical latitudes. Thus, summer is dominated by tropical influences as the easterly waves and the ITCZ penetrate further south over the subcontinent, and winter by mid-latitude influences as the westerlies penetrate further north, particularly in the upper troposphere. Similar trends are also present at Irene (25.25°S; 28.22°E), which was noted by Thompson *et al.* (2003) to differ from other ozonesonde stations in the SHADOZ (Southern Hemisphere Additional Ozonesondes) network in that it did not always experience a typical tropical climate.

This conclusion has important implications for the computation of trends based on mean profiles at these intermediate latitudes. The mean comprises a mix of tropical and mid-latitude regimes, which are likely to differ in relative contribution from year to year as a function of dynamic factors, such as the latitudinal position of the jet stream. The meteorological regimes in turn may be characterized by different trends due to vastly different anthropogenic activities in tropical and mid-latitude regions. Hence it is suggested that for stations on the boundaries of zonally defined meteorological regimes that the computation of a mean profile and furthermore, extrapolation of trends based on a mean profile is meaningless.

5.2.4.3 Source Regions

The classification has also shown that trans-boundary sources contribute substantially to the tropospheric ozone enhancement observed at Johannesburg. Table 5.8 summarizes the source regions for each category as a function of atmospheric layer. The observed springtime enhancements are associated with transport of air masses over African countries to the north of Johannesburg. In a similar manner, the summertime mid-tropospheric peak is linked to long-range transport of air masses originating over central Africa in an anticyclonic circulation. The only peak that was found to originate locally is that of the 'lower tropospheric enhancement' group, where local anticyclonic circulation is accountable for the low level accumulation of ozone confined below the persistent 5 km absolutely stable layer. In general, maritime air carried by westerlies brings about comparatively lower ozone values. This is evidenced in the 'reduced tropospheric' ozone category, in which westerly winds prevail at all tropospheric levels.

5.3 Summary

The classification of ozone profiles using a multivariate cluster analysis technique known as TWINSPAN has permitted the identification of 6 categories, each of which possesses distinct attributes. Relating the profiles to the origin of air masses through back trajectory modeling has revealed clearly defined source regions. Continental areas over central Africa and long distance transport are thought to be responsible for the mid-tropospheric peak in summer and the low to mid-tropospheric enhancement in spring, whereas the winter low tropospheric enhancement is attributed to local sources. The dominance of westerly winds

through the troposphere gives rise to reduced ozone values. This investigation has emphasized the pronounced seasonality of tropospheric ozone vertical distribution suggesting that there are distinct tropical and mid-latitude influences which give rise to different vertical structures. The widely recognized spring maximum in tropospheric ozone has been endorsed in this classification, but a new summertime mid-tropospheric enhancement due to the penetration of tropical air masses from continental regions in central Africa has been identified. Drawbacks of focusing on mean profiles when estimating trends were highlighted.

Table 5.8: Source regions of air masses associated with each ozone profile category as a function of height

Category	Near-surface (2.5 km)	Mid-troposphere (5 km)	Mid-troposphere (7.5 km)	Upper troposphere (10 km)	Dominant season
1. Mid-tropospheric peak	East – Indian Ocean	West	West	North – continental Africa	Summer
2. Steady tropospheric increase	Variable, generally east	West	West	West	Summer
3. Reduced tropospheric ozone	West	West	West	West	Autumn
4. Lower tropospheric enhancement	Local, continental	West	West	West	Winter
5. Pronounced layering	North – continental Africa	North – continental Africa	West	West	Spring
6. Considerable tropospheric enhancement	North – continental Africa	North – continental Africa	North – continental Africa	West	Spring

CHAPTER 6

CONCLUSION

6.1 Summary

The aim of this thesis was to examine the nature and characteristics of tropospheric ozone over Johannesburg, with a focus on understanding the photochemical and dynamic processes operational in the atmosphere. The value of studying TTO and the vertical distribution of ozone has been highlighted.

Ozone, water vapor and meteorological profile data, which form part of the MOZAIC database for the period 1995 to 2000 were utilized in this study. The measurements were collected between the surface and 12 km and have a vertical resolution of 150 m.

Results of TTO variations over Johannesburg for the period 1995-1998 were presented in Chapter 4. In this study, a measure of TTO was obtained by integrating the ozone profiles between the surface and a predetermined height of 12 km. It was noted that Diab *et al.* (1996a) and Thompson *et al.* (1996a) obtained a measure of TTO by integrating profiles up to a height of 15 km for Irene, which is at the same latitude as Johannesburg. Hence, in this study, TTO values were less than those presented in these and other studies in the southern Hemisphere. However, while actual magnitudes differed, seasonal trends were comparable.

This study confirmed the seasonal pattern in TTO, which is dominated by a spring maximum and autumn minimum, and is indeed a well-established Southern Hemisphere trend. This seasonal forcing was consistent from year to year. TTO peaked either in September or October, while minimum values occurred in late summer or autumn (February-May). Interannual variability was least in January and April to June. The more consistent autumn and winter ozone values were attributed to background tropospheric ozone loadings upon which the dynamic and photochemical influences of other months are superimposed.

In order to investigate factors responsible for TTO variations, tropospheric ozone was integrated over 4 layers i.e. surface-3, 3-5, 5-7 and 7-12 km. The same spring maximum

was evident in each of the layers. Below 5 km, the TTO minimum occurred in February and March, while above 5 km, the minimum occurred in April and May. These results are suggestive of a decoupling of the atmosphere and emphasize the role of the absolutely stable 5 km layer. The greatest enhancement occurred in October and was attributed to sources prevalent throughout the troposphere. This analysis was unable to distinguish the relative importance of surface based photochemical ozone production, such as biomass burning and urban-industrial sources, and upper tropospheric dynamical sources such as STE or long distance transport.

Hence, a further analysis of days with highest TTO was undertaken to obtain greater insights. A threshold value of 30 DU was selected arbitrarily to indicate an event of considerable ozone enhancement. High TTO events occurred predominantly during September (16) and October (17), with the few remaining events scattered throughout the year. Enhancements in the lower troposphere occurred mostly in September and seldom lasted for more than 1-2 consecutive days. It was suggested that these events were most likely due to effects of local surface pollution sources, either localised biomass burning or urban-industrial effects.

An extended period of enhancement in the 7-12 km layer occurred from 14-17 September 1998 and again on 20 September 1998. The extended duration of this event suggested that it was due to an STE event. Confirmation of this was given in a case study analysis of a particular MOZAIC flight on 16 September 1998 from Johannesburg to Cape Town by Mahumane (2002).

The vertical distribution of tropospheric ozone was addressed in Chapter 5. In this study, mean ozone profiles were computed using 502 MOZAIC ozone profiles for the period 1995 to 2000. The mean annual tropospheric ozone profile over this period showed a sharp increase in ozone within the lowest 2-3 km asl. There was evidence of a spring enhancement in ozone and considerable variability about the mean in each season.

It is clear that calculation of a mean profile limits interpretation, since the mean tends to mask the interesting and important micro-structure of individual profiles. As an alternative to analyzing mean seasonal or individual profiles, ozone profiles were classified based on a cluster analysis. Thus, a classification scheme was developed using 56 MOZAIC ozone

profiles. A multivariate cluster analysis technique known as TWINSPAN which was used to classify these profiles has permitted the identification of 6 categories, each of which possesses distinct attributes. Each category was named according to the structure of the characteristic profiles and were defined as follows: single mid-tropospheric peak, steady tropospheric increase, reduced tropospheric ozone, lower tropospheric enhancement, pronounced layering and considerable tropospheric enhancement. The marked differences between groups were highlighted by ozone frequency distributions within each group.

This investigation has clearly emphasized the distinct seasonality of ozone profiles. It was evident that seasons were dominated by distinct pattern and by inference, the processes and transport patterns that define single profiles are seasonally dependent. Spring was characterized by either 'pronounced layering' or 'considerable tropospheric enhancement', indicative of strong photochemical production from biomass burning and biogenic sources in this season. Summer profiles exhibited a 'mid-tropospheric peak' when upper tropospheric air masses originate from continental areas to the north of Johannesburg, indicative of southward penetration of the ITCZ, or a 'steady tropospheric increase' when the troposphere was characterized by westerly flow originating over the Atlantic Ocean. Autumn profiles fell mainly into the 'reduced tropospheric ozone' group, caused by a dominance of westerly flow at all tropospheric levels, while winter profiles fell into both the 'reduced tropospheric ozone' and 'lower tropospheric enhancement' groups.

Spring is widely acknowledged as the season during which tropospheric ozone maximizes, as confirmed by this study. However, the equally high summer mid-tropospheric peak as typified by the first category has not been identified in earlier studies. Furthermore, summer was dominated by two patterns and hence a study of mean seasonal profiles would have failed to reveal this particular pattern.

Johannesburg is situated at a latitude that is intermediate between tropical and mid-latitude meteorological regimes and is dominated by circulation patterns characteristic of either mid-latitude or tropical latitudes, making it an important location for an analysis of ozone profiles. Thus, summer is dominated by tropical influences as the easterly waves and the ITCZ penetrate further south over the subcontinent, and winter by mid-latitude influences as the westerlies penetrate further north, particularly in the upper troposphere. This has important implications for the computation of trends based on mean profiles at these

intermediate latitudes. The mean comprises a mix of tropical and mid-latitude regimes, which are likely to differ in relative contribution from year to year as a function of dynamic factors, such as the latitudinal position of the jet stream. The meteorological regimes in turn may be characterized by different trends due to vastly different anthropogenic activities in tropical and mid-latitude regions. Hence it was suggested that for stations on the boundaries of zonally defined meteorological regimes that the computation of a mean profile and furthermore, extrapolation of trends based on a mean profile is meaningless.

Relating the profiles to the origin of air masses through back trajectory modeling has shown that trans-boundary sources contribute substantially to the tropospheric ozone enhancement observed at Johannesburg. Continental areas over central Africa and long distance transport are thought to be responsible for the mid-tropospheric peak in summer and the low to mid-tropospheric enhancement in spring, whereas the winter low tropospheric enhancement was attributed to local sources. The dominance of westerly winds through the troposphere gave rise to reduced ozone values.

6.2 Recommendations

In this study, TWINSPAN, a cluster analysis technique that is often used in ecological applications to classify vegetation into communities, was used to classify ozone profiles. Although this investigation has provided meaningful insights into the vertical distribution of tropospheric ozone, it is recommended that a more widely applicable and generic cluster analysis technique, such as SPSS, be applied in a future study. This would allow for a comparative study and verification of the results obtained by TWINSPAN.

In this study, only 56 profiles were selected for the development of the classification scheme on the basis that they had no missing values between the surface and 12 km. In future studies, it is recommended that data should be interpolated, perhaps using monthly averages, so that more profiles could be included in the classification scheme. It may also be useful to apply this technique to other tropospheric ozone data sets from programs such as SHADOZ, SAFARI-92 and SAFARI-2000.

Another suggestion is to undertake a classification of ozone profiles and to incorporate in some way simultaneous measurements of water vapor and other chemical species such as NO_y and CO. New MOZAIC sensors recording simultaneous measurements of NO_y, and CO have been installed aboard the respective MOZAIC aircraft since 2000 (http://www.aero.obs-mip.fr/mozaic/). This may provide an ideal opportunity for more in depth study into the origin of ozone peaks inherent in the datasets in future studies.

This is the first time that an attempt has been made to analyse ozone profiles by stratifying them into meaningful categories. It is hoped that this technique will be refined further in future studies and that greater insights into the photochemical and dynamic processes that are operating in the atmosphere will result.

REFERENCES

Anderson, B.E., Grant, G.L., Browell, E.V., Collins, J.E., Sachse, G.W., Bagwell, D.R., Hudgins, C.H., and Blake, N.J. (1996). Aerosols from biomass burning over the tropical South Atlantic region: distributions and impacts. **Journal of Geophysical Research**, 101 (D19), 24117-24137.

Anderson, I.C., Levine, J.S., Poth, M.A. and Riggan, P.J. (1998). Enhanced biogenic emissions of nitric oxide and nitrous oxide following surface biomass burning. **Journal of Geophysical Research**, 93, 3893-3898.

Andreae, M. O., Anderson, B. E., Blake, D. R., Bradshaw, J. D., Collins, J. E., Gregory, G. L., Sachse, G. W. and Shipham, M. C. (1994). Influence of plumes from biomass burning on atmospheric chemistry over the equatorial and tropical South Atlantic during CITE 3. **Journal of Geophysical Research**, 99 (D6), 12793-12808.

Andreae, M.O. (1991). Biomass burning: its history, use and distribution and its impacts on environmental quality and global climate. In **Global Biomass Burning: Atmospheric, Climatic, and Biospheric Implications**, (ed.) Levine, J.S., MIT Press, Cambridge, London, England, 3-21.

Andreae, M.O. (1993). The influence of tropical biomass burning on climate and the atmospheric environment. In **Biogeochemistry of Global Change: Radiatively Active Trace Gases**, (ed.) Oremland, R.S., Chapman and Hall, New York, 113-150.

Andreae, M.O., Fishman, J. and Lindesay, J. (1996). The Southern Atlantic Region Experiment (STARE): Transport and Atmospheric Chemistry near the Equator-Atlantic (TRACE-A) and Southern African Fire-Atmosphere Research Initiative (SAFARI): an introduction. **Journal of Geophysical Research**, 101 (D19), 23519-23520.

Baldy, S., Ancellet, G., Bessafi, M., Badr, A. and Lan Sun Luk, D. (1996). Field observations of the vertical distribution of tropospheric ozone at the island of Reunion (southern tropics). **Journal of Geophysical Research**, 101 (D19), 23835 – 23849.

Bamber, D.J., Healey, P.G.W., Jones, B.M.R., Penkett, S.A., Tuck, A.F. and Vaughan, G. (1984). Vertical profiles of tropospheric gases: chemical consequences of stratospheric intrusions. **Atmospheric Environment**, 18 (9), 1759-1766.

Baray, J.L., Baldy, S., Diab, R.D. and Cammas, J.P. (2003). Dynamical study of a tropical cut-off low over South Africa, and its impact on tropospheric ozone. **Atmospheric Environment** (in press).

Barsby, J., Diab, R. D. (1995). Total ozone and synoptic weather relationships over southern Africa and surrounding oceans. **Journal of Geophysical Research**, 100 (D2), 3023-3032.

Bethan, S., Vaughan, G. and Reid, S.J. (1996). A comparison of ozone and thermal tropopause heights and the impact of tropopause definition on quantifying the ozone content of the troposphere. **Quarterly Journal of the Royal Meteorological Society**, 122, 929-944.

Blake, N.J., Blake, D.R., Sive, B.C., Chem, T.Y., Rowland, F.S., Collins, J.E., Sachse, G.W. and Anderson, B.E. (1996). Biomass burning emissions and vertical distribution of atmospheric methyl halides and other reduced carbon gases during the Trace A experiment. **Journal of Geophysical Research**, 101 (D19), 24151-24-164.

Bond, D.W., Steiger, S., Zhang, R., Tie, X. and Orville, R.E. (2002). The importance of NO_x production by lightning in the tropics. **Atmospheric Environment**, 36 (9), 1509-1519.

Browell, E.V., Fenn, M.A., Butler, C.F., Grant, W.B., Clayton, M.B., Fishman, J., Bachmeier, A.S., Anderson, B.E., Gregory, G,L., Fuelberg, H.E., Bradshaw, J.D., Sandholm, S.T., Blake, D.R., Heikes, B.G., Sachse, G.W., Singh, H.B. and Talbot, R.W. (1996). Ozone and aerosol distributions and air mass characteristics over the South Atlantic Basin during the burning season. **Journal of Geophysical Research**, 101 (D19), 24043-24068.

Cahoon, D.R., Stocks, B.J., Levine, J.S., Cofer, W.R. and O'Neill, K.P. (1992). Seasonal distribution of African savanna fires. **Nature**, 359, 812-815.

Cammas, J.-P., Jacoby-Koaly, S., Suhre, K., Rosset, R. and Marenco, A. (1998). Atlantic subtropical potential vorticity barrier as seen by Measurements of Ozone by Airbus In-Service Aircraft (MOZAIC) flights. **Journal of Geophysical Research**, 103 (D19), 25681-25693.

Cardenas, L., Rondon, C., Johansson, C. and Sanhueza, E. (1993). Effects of soil moisture, temperature and inorganic nitrogen on nitric oxide emissions from acidic tropical savannah soils. **Journal of Geophysical Research**, 98, 14783-14790.

Chameides, W. and Walker, J.C.G. (1973). A photochemical theory of tropospheric ozone. **Journal of Geophysical Research**, 78 (36), 8751-8760.

Chameides, W.L. and Walker, J.C.G. (1976). A time-dependent photochemical model for ozone near the ground. **Journal of Geophysical Research**, 81, 413-420.

Cofer III, W.R., Levine, J.S., Winstead, E.L., Cahoon, D.R., Sebacher, D.I., Pinto, J.P. and Stocks, B.J. (1996). Source compositions of trace gases released during African savanna fires. **Journal of Geophysical Research**, 101 (D19), 23597-23602.

Combrink, J., Diab, R.D., Sokolic, F. and Brunke, E.G. (1995). Relationship between surface, free tropospheric and total column ozone in two contrasting areas in South Africa. **Atmospheric Environment**, 29(6), 685-691.

Conrad, R. and Seiler, W. (1985). Influence of temperature, moisture and organic carbon on the flux of H_2 and CO between soil and atmosphere: field studies in subtropical regions. **Journal of Geophysical Research**, 90, 5699-5709.

Cooper, O.R., Moody, J.L., Davenport, J.C., Oltmans, S.J., Johnson, B.J., Chen, X., Shepson, P.B. and Merrill, J.T. (1998). Influence of springtime weather systems on vertical ozone distributions over three North American sites. **Journal of Geophysical Research**, 103 (D17), 22001-22013.

Cosijn, C. and Tyson, P.D. (1996). Stable discontinuities in the atmosphere over South Africa. **South African Journal of Science**, 92, 381-386.

Cros, B., Nganga, D., Minga, A., Fishman, J. and Brackett, V. (1992). Distribution of tropospheric ozone at Brazzaville, Congo, determined from ozonesonde measurements. **Journal of Geophysical Research**, 97 (D12), 12869-12875.

Crutzen, P. J. (1973). A discussion of the chemistry of some minor constituents of the stratosphere and troposphere. **Pure Applied Geophysics**, 106-108, 1385 -1399.

Crutzen, P.J. (1974). Photochemical reactions initiated by and influencing ozone in unpolluted tropospheric air. **Tellus**, XXIV, 47-57.

Crutzen, P.J. and Andreae, M.O. (1990). Biomass burning in the tropics: impact on atmospheric chemistry and biogeochemical cycles. **Science**, 250, 1669-1678.

Crutzen, P.J. and Lelieveld, J. (2001). Human impacts on atmospheric chemistry. **Annual Revolutionary Earth Planetary Science**, 17-45.

Crutzen, P.J., Delany, A.C., Greenberg, J., Haagenson, P., Heidt, L., Lueb, R., Pollock, W., Seiler, W., Wartburg, A. and Zimmerman, P. (1985). Tropospheric chemical composition measurements in Brazil during the dry season. **Journal of Atmospheric Chemistry**, 2, 233-256.

Danielsen, E.F. (1968). Stratospheric-tropospheric exchange based on radioactivity, ozone and potential vorticity. **Journal of the Atmospheric Sciences**, 25, 502-518.

Danielsen, E.F. (1980). Stratospheric source for unexpectedly large values of ozone measured over the Pacific Ocean during Gametag, August 1977. **Journal of Geophysical Research**, 85 (C1), 401-412.

Diab, R., Barsby, J., Bodeker, G., Scourfield, M. and Salter L. (1992). Satellite observations of total ozone above South Africa. **South African Geographical Journal**, 74, 13-18.

Diab, R.D., Thompson, A.M., Zunckel, M., Coetzee, G.J.R., Combrink, J., Bodeker, G.E., Fishman, J., Sokolic, F., McNamara, D.P., Archer, C.B. and Nganga, D. (1996a). Vertical ozone distribution over southern Africa and adjacent oceans during SAFARI-92. **Journal of Geophysical Research**, 101(D19), 23823-23833.

Diab, R.D., Jury, M.R., Combrink, J. and Sokolic, F. (1996b). A comparison of anticyclone and trough influences on the vertical distribution of ozone and meteorological conditions during SAFARI –92. **Journal of Geophysical Research**, 101 (D19), 23809- 23821.

Dickerson, R.R., Huffman, G.J., Luke, W.T., Nunnermacker, L.J., Pickering, K.E., Leslie, C.D., Lindsey, C.F., Slinn, W.G.N., Kelly, T.J., Daum, P.H., Delany, A.C., Greenberg, J.P., Zimmerman, P.R. and Boatman, J.F. (1987). Thunderstorms: an important mechanism in the transport of air pollutants. **Science**, 235, 460-465.

Draxler, R.R. (1996). Boundary layer isentropic and kinematic trajectories duing the August 1993 North Atlantic Regional Experiment Intensive. **Journal of Geophysical Research**, 101(D22), 29255-29268.

Draxler, R.R. (1999a). Hysplit radiological transport and dispersion model implementation on the NCEP Cray, National Weather Service, Office of Meteorology, Technical Procedures Bulletin 458, July, 13 pp.

Draxler, R.R. (1999b). The Hysplit_4 User's Guide, NOAA Technical Memorandum ERL ARL-230, June 1999, 35p - Last Revised April 2000).

Draxler, R.R. and Hess, G.D. (1997). Description of the Hysplit_4 modeling system, NOAA Technical Memorandum ERL ARL-224, December, 24pp.

Draxler, R.R. and Hess, G.D. (1998). An Overview of the Hysplit_4 Modeling System for Trajectories, Dispersion, and Deposition. **Australian Meteorological Magazine**, 47, 295-308.

Everitt, B.S. (1978). **Graphical Techniques for Multivariate Data**. New York: North-Holland.

Fabian, P. and Pruchniewicz, P.G. (1977). Meridional distribution of ozone in the troposphere and its seasonal variation. **Journal of Geophysical Research**, 82, 2063-2073.

Fishman, J., Brackett, V.G., Browell, E.V. and Grant, W.B. (1996). Tropospheric ozone derived from TOMS/SBUV measurements during TRACE A. **Journal of Geophysical Research,** 101 (D19), 24069-24082.

Fishman, J., Fakhruzzaman, K., Cros, B. and Nganga, D. (1991). Identification of widespread pollution in the Southern Hemisphere deduced from satellite analyses. **Science**, 252, 1693-1696.

Fishman, J., Minnis, P. and Reichle Jr, H.G. (1986). The use of satellite data to study tropospheric ozone in the tropics. **Journal of Geophysical Research**, 91, 14451-14465.

Fishman, J., Watson, C.E., Larsen, J.C. and Logan, J.A. (1990). The distribution of tropospheric ozone determined from satellite data. **Journal of Geophysical Research**, 95, 3599-3617.

Folkins, I., Loewenstein, M., Podolske, J., Oltmans, S.J. and Profitt, M. (1999). A barrier to vertical mixing at 14 km in the tropics: Evidence from ozonesondes and aircraft observations. **Journal of Geophysical Research**, 104, 22095-22102.

Fortuin, J. P. F. and Kelder, H. (1998). An ozone climatology based on ozonesonde and satellite measurement. **Journal of Geophysical Research**, 105 (D24), 31709- 31734.

Fujiwara, M., Kita K., Ogawa, T., Kawakami, S., Sana, T., Komala, N., Saraspriya, S. and Suripto, A. (1999). Tropospheric ozone enhancements during the Indonesian forest fire events in 1994 and in 1997 as revealed by ground-based observations. **Geophysical Research Letters**, 26 (16), 2417-2420.

Garstang, M., Tyson, P.D., Swap, R., Edwards, M., Kållberg, P. and Lindesay, J.A. (1996). Horizontal and vertical transport of air over Southern Africa. **Journal of Geophysical Research**, 101 (D19), 23721-23736.

Gauch, H.G. (1982). **Multivariate Analysis In Community Ecology**. Cambridge University Press, Cambridge, chapters 1 and 5.

Gauch, H.G. and Whittaker, R.H. (1981). Hierarchical classification of community data. **Journal of Ecology**, 69, 135-52.

Gregory, G.L., Fuelberg, H.E., Longmore, S.P., Anderson, B.E., Collins, J.E. and Blake, D.R. (1996) Chemical characteristics of tropospheric air over the tropical South Atlantic Ocean: relationship to airmass source and trajectory history. **Journal of Geophysical Research**, 101 (D19), 23957-23972.

Guenther, A., Hewitt, C.N., Erickson, D., Fall, R., Geron, C., Graedel, T., Harley, P., Klinger, L., Lerdau, M., McKay, W.A., Pierce, T., Scholes, B., Steinbrecher, R., Tallamraju, R., Taylor, J. and Zimmerman, P. (1995). A global model of natural volatile organic compound emissions. **Journal of Geophysical Research**, 100, 8873-8892.

Hao, W.M. and Liu, M.H. (1994). Spatial and temporal distribution of tropical biomass burning. **Global Biogeochemical Cycles**, 8, 495-503.

Hao, W.M., Ward, D.E., Olbu, G. and Baker, S.P. (1996). Emission of CO_2, CO, and hydrocarbons from fires in diverse African savanna ecosystems. **Journal of Geophysical Research**, 101 (D19), 23577-23584.

Harris, G.W., Wienhold, F.G. and Zenker, T. (1996). Airborne observations of strong biogenic NO_x emissions from the Namibian Savanna at the end of the dry seasons. **Journal of Geophysical Research**, 101 (D19), 23707-23711.

Heffter, J.L. (2002). Running HYSPLIT on the READY Website. http://www.arl.noaa.gov/ready/.

Heikes, B., Lee, M., Jacob, D., Talbot, R., Bradshaw, J., Singh, H., Blake, D., Anderson, B., Fuelberg, H. and Thompson. (1996). Ozone, hydroperoxides, oxides of nitrogen, and hydrocarbon budgets in the marine layer over the South Atlantic. **Journal of Geophysical Research**, 101 (D19), 24221-24234.

Helten, M., Smit, H.G.J., Sträter, W., Kley, D., Nedélec, P., Zöger, M., and Busen, R. (1998). Calibration and performance of automatic compact instrumentation for the measurement of relative humidity from passenger aircraft. **Journal of Geophysical Research**, 103(D19), 25643-25652.

Hill, M.O. (1979). TWINSPAN-A FORTRAN Program for Arranging Multivariate Data in an Ordered Two-Way Table by Classification of the Individuals and Attributes. Cornell University, Ithaca, New York.

Huntley, B.J. and Walker, B.H. (1982). **Ecology of Tropical Savannas, Ecology Studies**. Vol 42, Springer-Verlag, New York.

Jacob, D.J. and Wofsy, S.C. (1998). Photochemistry of biogenic emissions over the Amazon forest. **Journal of Geophysical Research**, 93, 1477-1486.

Junge, C.E. (1962). Global ozone budget and exchange between stratosphere and troposphere. **Tellus** XIV, 4, 363-377.

Jury, M.R., Brunke, E. and Schormann, M. (1996). Aircraft section measurements of meteorology and ozone in northern Namibia during SAFARI-92. **Journal of Geophysical Research**, 101 (D19), 23713-23720.

Justice, C.O., Kendall, J.D., Dowty, P.R. and Scholes, R.J. (1996). Satellite remote sensing of fires during the SAFARI campaign using NOAA advanced very high resolution radiometer data. **Journal of Geophysical Research**, 101 (D19), 23851-23863.

Kim, Y.K., Lee, H.W., Park, J.K. and Moon, Y.S. (2002). The stratosphere-troposphere exchange of ozone and aerosols over Korea. **Atmospheric Environment**, 36, 449-463.

Kirchoff, V.W.J.H., Barnes, R.A. and Torres, A.L. (1991). Ozone climatology at Natal, Brazil, from *in situ* ozonesonde data. **Journal of Geophysical Research**, 96 (D6), 10899-10909.

Kirkman, G.A., Piketh, S.J., Andreae, M.O., Annegarn, H.J. and Helas, G. (2000). Distribution of aerosols, ozone and carbon monoxide over southern Africa. **South African Journal of Science**, 96, 423-431.

Krishnamurti, T.N., Fuelberg, H.E., Sinha, M.C., Oosterhof, D., Bensman, E.L. and Kumar, V.B. (1993). The meteorological environment of the tropospheric ozone maximum over the tropical South Atlantic Ocean. **Journal of Geophysical Research**, 98 (D6), 10621-10641.

Krishnamurti, T.N., Sinha, M.C., Kanamitsu, M., Oosterhof, D., Fuelberg, H., Chatfield, R., Jacob, D.J. and Logan, J. (1996). Passive tracer transport relevant to the TRACE A experiment. **Journal of Geophysical Research**, 101 (D19), 23889-23907.

Lacaux, J.P., Delmas, R., Jambert, C. and Kuhlbusch, T.A.J. (1996). NO_x emissions from African savanna fires. **Journal of Geophysical Research**, 101 (D19), 23585-23595.

Le Canut, P., Andreae, M.O., Harris, G.W., Wienhold, F.G. and Zenker, T. (1996). Airborne studies of emissions from savanna fires in southern Africa 1. Aerosol emissions measured with a laser optical particle counter. **Journal of Geophysical Research**, 101 (D19), 23615-23630.

Leighton, P.A. (1961). **Photochemistry of Air Pollution**. Academic Press, San Diego, California, New York.

Lelieveld, J. and Dentener, F. J. (2000). What controls tropospheric ozone? **Journal of Geophysical Research**, 105 (D3), 3531-3551.

Lelieveld, J., Thompson, A.M., Diab, R.D., Hov, O., Kley, D., Logan, J.A., Nielsen, O.J., Stockwell, W.R. and Zhou, X. (1998). Tropospheric ozone and related processes. In **Scientific Assessment of Ozone Depletion**, Rep. 44, pp. 8.1-8.42, World Meteorological Organisation, Geneva.

Levine, J.S. (1991). Introduction. In **Global Biomass Burning: Atmospheric, Climatic, and Biospheric Implications**. (ed.) Levine, J.S., MIT Press, Cambridge.

Levine, J.S., Cofer, W.R., Sebacher, D.I., Winstead, E.L., Sebacher, S. and Boston, P.J. (1998). The effects of fire on biogenic soil emissions of nitric oxide and nitrous oxide. **Global Biogeochemical Cycles**, 2, 445-449.

Levine, J.S., Winstead, E.L., Parsons, D.A.B., Scholes, M.C., Scholes, R.J., Cofer III, W.R., Cahoon JR, D.R. and Sebacher, D.I. (1996). Biogenic soil emissions of nitric oxide (NO) and nitrous oxide (N_2) from savannas in South Africa: the impact of wetting and burning. **Journal of Geophysical Research**, 101 (D19), 23689-23697.

Levy II, H. (1971). Normal atmosphere: large radical and formaldehyde concentrations predicted. **Science**, 173, 141-143.

Levy II, H., Mahlman, J.D., Moxim, W.J. and Liu, S.C. (1985). Tropospheric ozone: the role of transport. **Journal of Geophysical Research**, 90 (D2), 3753-3772.

Lindesay, J.A., Andreae, M.O., Goldammer, J.D., Harris, G., Annegarn, H.J., Garstang, M., Scholes, R.J. and van Wilgen, B.W. (1996). International Geosphere-Biosphere Programme/International Global Atmospheric Chemistry SAFARI-92 field experiment: background and overview. **Journal of Geophysical Research**, 101 (D19), 23521-23530.

Liu, H., Chang, W.L. Oltmans, S.J., Chan, L.Y. and Harris, J.M. (1999). On springtime high ozone events in the lower troposphere from Southeast Asian biomass burnng. **Atmospheric Environment**, 33, 2403-2410.

Liu, S.C., Trainer, M., Fehsenfeld, F.C., Parrish, D.D., Williams, E.J., Fahey, D.W., Hubler, G. and Murphy, P.C. (1987). Ozone production in the rural troposphere and implications for regional and global ozone distributions. **Journal of Geophysical Research**, 92 (D4), 4191-4207.

Logan, J. A. (1985). Tropospheric ozone: seasonal behavior, trends, and anthropogenic influence. **Journal of Geophysical Research**, 90 (D6), 10463 – 10482.

Logan, J. A. (1999). An analysis of ozonesonde data for the troposphere: recommendations for testing 3 –D models and development of gridded climatology for tropospheric ozone. **Journal of Geophysical Research**, 104 (D13), 16115-16149.

Longo, K.M., Thompson, A.M., Kirchoff, V.W.J.H., Remer, L.A., de Freitas, S.R., Silva Dias, M.A.F., Artaxo, P., Hart, W., Spinhirne, J.D. and Yamasoe, M.A., (1999). Correlation between smoke and tropospheric ozone concentration in Cuiaba during Smoke, Clouds, and Radiation-Brazil (SCAR-B). **Journal of Geophysical Research**, 104 (D10), 12113-12129.

Lorenzi, G., Nali, C. and Panicucci, A. (1994). Surface ozone in Pisa (Italy): a six year study. **Atmospheric Environment**, 28(19), 3155-3164.

Mahumane, M.G. (2002). Analysis of high ozone events over Africa. Unpublished Masters Thesis, School of Life and Environmental Sciences, University of Natal, Durban.

Marenco, A. (1986). Variations of CO and O3 in the troposphere: evidence of photochemistry. **Atmospheric Environment**, 20(5), 911-918.

Marenco, A., Gouget, H., Nédélec, P., Pagés, J.P. and Karcher, F. (1994). Evidence of a long-term increase in tropospheric ozone from Pic du Midi data series: consequences: positive radiative forcing. **Journal of Geophysical Research**, 99 (D8), 16617-16632.

Marenco, A., Thouret, V., Nedélec, P., Smit, H., Helten, M., Kley, D., Karcher, F., Simon, P., Law, K., Pyle, J., Poschmann, G., Wrede, R.V., Hume, C. and Cook, T. (1998). Measurement of ozone and water vapour by Airbus in-service aircraft: the MOZAIC airborne program, an overview. **Journal of Geophysical Research**, 103(D19), 25631-25642.

Mari, K. (2001). Vertical distribution of ozone over Irene. Unpublished Honours Thesis, School of Life and Environmental Sciences, University of Natal, Durban.

Merrill, J. T., Moody, J. L., Oltmans, S. J. and Levy II, H. (1996). Meteorological analysis of tropospheric ozone profiles at Bermuda. **Journal of Geophysical Research**, 101(D22) 29201-29211.

Merrill, J.T. (1994). Isentropic airflow probability analysis. **Journal of Geophysical Research**, 99 (D12), 25881-25889.

Merrill, J.T., Bleck, R. and Boudra, D.B. (1986). Techniques of Lagrangian trajectory analysis in isentropic coordinates. **Monthly Weather Review**, 114, 571-581.

MOZAIC Readme_prof file (MOZAIC cd).

MOZAIC-II: Technical Final Report (1996-1999). (2000) January 2000, 88p, University of Paul Sabatier, Toulouse, France.

Newell, R.E., Thouret, V., Cho, J.Y.N., Stoller, P., Marenco, A. and Smit, H.G., (1999). Ubiquity of quasi-horizontal layers in the troposphere. **Nature**, 398, 316-319.

Olson, J.R., Fishman, J., Kirchhoff, V.W.J.H. Nganga, D. and Cros, B. (1996). Analysis of the distribution of ozone over the southern Atlantic region. **Journal of Geophysical Research,** 101 (D19), 24083-24093.

Otter, L.B., Scholes, R.J., Dowty, P., Privette, J., Caylor, K., Ringrose, S., Mukelabai, M., Frost, P., Hanan, N., Totolo, O. and Veenendaal, E.M. (2002). The southern African Regional Science Initiative (SAFARI 2002): wet season campaigns. **South African Journal of Science**, 98, 131-137.

Parsons, D.A.B., Scholes, M.C., Scholes, R.J. and Levine, J.S. (1996). Biogenic NO emissions from savanna soils as a function of fire regime, soil type, soil nitrogen, and water status. **Journal of Geophysical Research**, 101 (D19), 23683-23688.

Pickering, K.E., Thompson, A.M., Scala, J.R., Tao, W.-K., and Simpson, J. (1992a). Ozone production potential following convective redistribution of biomass burning emissions. **Journal of Atmospheric Chemistry**, 14, 297-313.

Pickering, K.E., Thompson, A.M., Scala, J.R., Tao, W.-K., Dickerson, R.R. and Simpson, J. (1992b). Free tropospheric ozone production following entrainment of urban plumes into deep convection. **Journal of Geophysical Research**, 97 (D16), 17985-18000.

Pickering, K.E., Thompson, A.M., Wang, Y., Tao, W.-K., McNamara, D.P., Kirchoff, V.W.F.H., Heikes, G.W.S., Bradshaw, J.D., Gregory, G.L. and Blake, D.R. (1996). Convective transport of biomass burning emissions over Brazil during TRACE-A. **Journal of Geophysical Research**, 101 (D19), 23993- 24012.

Pickering, K., Thompson, A.M., Tao, W.-K. and Kucsera, T. (1993). Upper tropospheric ozone production following mesoscale convection during STEP/EMEX. **Journal of Geophysical Research**, 98 (D5), 8737-8749.

Pickering, K.E., Thompson, A.M., Dickerson, R.R, Luke, W.T., McNamara, D.P., Greenberg, J.P. and Zimmerman, P.R. (1990). Model calculations of tropospheric ozone production potential following observed convective events. **Journal of Geophysical Research**, 95 (D9), 14049-14062.

Pickering, K.E., Thompson, A.M., Scala, J.R., Tao, W., Simpson, J. and Garstang, M. (1991). Photochemical ozone production in tropical squall line convection during NASA global tropospheric experiment/Amazon boundary layer experiment 2A. **Journal of Geophysical Research**, 96 (D2), 3099-3114.

Potter, C.S., Matson, P.A., Vitousek, P.M. and Davidson, E.A. (1996). Process modeling of controls on nitrogen trace gas emissions from soils worldwide. **Journal of Geophysical Research**, 101, 1361-1377.

Preston-Whyte, R.A. and Tyson, P.D. (1988). **The Atmosphere and Weather of Southern Africa**. Oxford University Press, Cape Town, 374 pp.

Price, C., Penner, J. and Prather, M. (1997). NO_x from lightning 1. global distribution based on lightning physics. **Journal of Geophysical Research**, 102, 5929-5941.

Price, J. D. and Vaughan, G. (1993). The potential for stratosphere-troposphere exchange in cut-off low systems. **Quarterly Journal of the Royal Meteorological Society**, 119, 343-365.

Price, J.D. and Vaughan, G. (1992). Statistical studies of cut-off-low systems. **Annales Geophysicae**, 10, 96-102.

Ramdriambelo, T., Baray, J. L., Baldy, S., Bremaud, P., Cautenet, S. (1999). A case study of extreme tropospheric ozone contamination in the tropics using *in-situ*, satellite and meteorological data. **Geophysical Research Letters**, 26 (9), 1287-1290.

Reed, R. (1955). A study of a characteristic type of upper-level frontogenesis. **Journal of Meteorology,** 12, 226-237.

Reiter, E.R. (1975). Stratospheric-tropospheric exchange processes. **Reviews of Geophysics and Space Physics**, 13 (4), 459-473.

Ridley, B.A., Dye, J.E., Ealega, J.G., Zheng, J., Grahek, F.E., Rison, W. (1996). On the production of active nitrogen by thunderstorms over New Mexico. **Journal of Geophysical Research**, 101, 20985-21005.

Rolph, G.D., Draxler, R.R. and de Pena, R.G. (1992). Modeling sulphur concentrations and depositions in the United States during ANATEX. **Atmospheric Environment**, 26A (1), 73-93.

Rolph, G.D., Draxler, R.R. and de Pena, R.G. (1993). The use of model-derived and observed precipitation in long-term sulphur concentration and deposition modeling. **Atmospheric Environment**, 27A (13), 2017-2037.

Scholes, M. and Andreae, M.O., (2000). Biogenic and pyrogenic emissions from Africa and their impact on the global atmosphere. **Ambio**, 29 (1), 23-29.

Scholes, R.J., Kendall, J. and Justice, C.O. (1996a). The quantity of biomass burned in southern Africa. **Journal of Geophysical Research**, 101 (D19), 23667-23676.

Scholes, R.J., Ward, D.E. and Justice, C.O. (1996b). Emission of trace gases and aerosol particles due to vegetation burning in southern hemisphere Africa. **Journal of Geophysical Research**, 101 (D19), 23677-23682.

Seiler, W. and Conrad, R. (1987). Contribution of tropical ecosystems to the global budgets of trace gases, especially CH_4, H_2, CO and N_2O. In **The Geophysiology of Amazonia**. Dickinson, R.E. (ed.). John Wiley, New York.

Shea, R.W., Shea, B.W., Kauffman, J.B., Ward, D.E., Haskins, C.I. and Scholes, M.C. (1996). Fuel biomass and combustion factors associated with fires in savanna ecosystems of South Africa and Zambia. **Journal of Geophysical Research**, 101 (D19), 23551-23568.

Singh, H.B., Herlth, D., Kolyer, R., Chatfield, R., Viezee, W., Salas, L.J., Chen, Y., Bradshaw, J.D., Sandholm, S.T., Talbot, R., Gregory, G.L., Anderson, B., Sachse, G.W., Browell, E.V., Bachmeier, A.S., Blake, D.R., Heikes, B., Jacob, D. and Fuelberg, H.E. (1996). Impact of biomass burning emissions on the composition of the South Atlantic troposphere: reactive nitrogen and ozone. **Journal of Geophysical Research**, 101 (D19), 24203-24220.

Sneath, P.H.A. and Sokal, R.R. (1973). Numerical Taxonomy. W.H. Freeman: San Francisco.

Staehelin, J., Thudium, J., Buehler, R., Volz-Thomas, A. and Graber, W. (1994). Trends in surface ozone concentrations at Arosa (Switzerland). **Atmospheric Environment**, 258 (1), 75-87.

Staley, D.O. (1962). On the mechanism of mass and radioactivity transport from the stratosphere to troposphere. **Journal of the Atmospheric Sciences**, 19, 450-467.

Stein, A.F., Lamb, D. and Draxler, R.R. (2000). Incorporation of detailed chemistry into a three-dimensional Lagrangian-Eulerian hybrid model: application to regional tropospheric ozone. **Atmospheric Environment**, 34, 4361-4372.

Stevens, C.S. (1987). Ozone formation in the greater Johannesburg region. **Atmospheric Environment**, 21 (3), 523-530.

Stromgaard, P. (1985). A subsistence society under pressure: the Bemba of northern Zambia. **Africa**, 55 (1), 39-59.

Swap, R., Garstang, M., Macko, S.A., Tyson, P.D., Maenhaut, W., Artaxo, P., Kallberg, P. and Talbot, R. (1996). The long-range transport of southern African aerosols to the tropical south Atlantic. **Journal of Geophysical Research**, 101 (D19), 23777-23791.

Swap, R.J. and Tyson, P.D. (1999). Stable discontinuities as determinants of the vertical distribution of aerosols and trace gases in the atmosphere. **South African Journal of Science**, 95, 63-71.

Talbot, R.W., Bradshaw, J.D., Sandholm, S.T., Smyth, S., Blake, D.R., Blake, N.R., Sachse, G.W., Collins, J.E., Heikes, B.G., Anderson, B.E., Gregory G.L., Singh, H.B., Lefer, B.L. and Bachmeier, A.S. (1996). Chemical characteristics of continental outflow over the South Atlantic Ocean from Brazil and Africa. **Journal of Geophysical Research**, 101 (D19), 24187-24202.

Thompson, A.M., Diab, R.D., Bodeker, G.E., Zunckel, M., Coetzee, G.J.R., Archer, C.B., McNamara, D.P., Pickering, K.E., Combrink, J., Fishman, J. and Nganga, D. (1996a). Ozone over southern Africa during SAFARI-92/TRACE A. **Journal of Geophysical Research**, 101 (D19), 23793-23807.

Thompson, A.M., Pickering, K.E., McNamara, D.P., Schoeberl, M.R., Hudson, R.D., Kim, J.H., Browell, E.V., Kirchoff, V.W.J.H. and Nganga, D. (1996b). Where did tropospheric ozone over southern Africa and the tropical Atlantic come from in October 1992? Insights from TOMS, GTE TRACE A, and SAFARI 1992. **Journal of Geophysical Research**, 101, 24251-24278.

Thompson, A.M., Witte, J.C., Freiman, M. T., Phahlane, N.A. and Coetzee, G.J.R. (2002). Lusaka, Zambia, during SAFARI-2000: convergence of local and imported pollution. **Geophysical Research Letters**, 29 (20), 37–1-37–4.

Thompson, A.M., Witte, J.C., Oltmans, S.J., Schmidlin, F.J., Logan, J.A., Fujiwara, M., Kirchoff, V.W.J.H., Posny, F., Coetzee, G.J.R., Hoeger, B., Kawakami, S., Ogawa, T., Fortuin, J.P. F. and Kelder, H.M. (2003). Southern Hemisphere Additional Ozonesondes (SHADOZ) 1998-2000 tropical ozone climatology. 2. tropospheric variability and the zonal wave-one. **Journal of Geophysical Research**, 108 (D2), 8241-8262.

Thomspon, A.M. and Hudson, R.D. (1999). Tropical tropospheric ozone (TTO) maps from Nimbus 7 and Earth Probe TOMS by the modified-residual method: evaluation with sondes, ENSO signals, and trends from Atlantic regional time series. **Journal of Geophysical Research**, 104 (D21), 26961-26975.

Thouret, V., Marenco, A., Logan, J.A., Nedélec, P. and Grouhel, C. (1998a). Comparisons of ozone measurements from the MOZAIC airborne program and the ozone sounding network at eight locations. **Journal of Geophysical Research**, 103(D19), 25695-25720.

Thouret, V., Marenco, Nedélec, P. and Grouhel, C. (1998b). Ozone climatologies at 9-12 km altitude as seen by the MOZAIC airborne program between September 1994 and August 1996. **Journal of Geophysical Research**, 103(D19), 25653-25679.

Tie, X.X., Zhang, R., Brasseur, G., Emmons, L., Lei, W. (2001). Effects of lightning on reactive nitrogen and nitrogen reservoir species in the troposphere. **Journal of Geophysical Research**, 106, 3167-3178.

Trollope, W.S.W. (1984). Fire in savanna. In **Ecological Effects of Fire in South African Ecosystems**, (ed.) de van Booysen, P. and Tainton, N.M., Springer-Verlag, New York, 149-175.

Tung, K.K., Ko, M.K.W., Rodriguez, J.M. and Sze, N.D. (1986). Are Antarctic ozone variations a manifestation of dynamics or chemistry? **Nature**, 322, 811-814.

Tyson, P.D. and Preston-Whyte, R.A. (2000). **The Weather and Climate of Southern Africa**. Oxford University Press, Cape Town, 274 pp.

Tyson, P.D., Garstang, M. and Swap, R. (1996). Large-scale recirculation of air over southern Africa. **Journal of Applied Meteorology**, 35, 2218-2236.

Tyson, P.D., Garstang, M., Thompson, A.M., Diab, R.D., Browell, E.V., and D'Abreton, P.C. (1997). Correspondence between ozone measurements, transport and production of ozone over south central Africa. **Journal of Geophysical Research,** 102 (D9), 10623-10636.

Vaughan, G. and Price, J.D. (1991). On the relation between total ozone and meteorology. **Quarterly Journal of the Royal Meteorological Society**, 117, 1281-1298.

Ward, D.E., Hao, W.M., Susott, R.A., Babbitt, R.E., Shea, R.W., Kauffman, J.B. and Justice, C.O. (1996). Effect of fuel composition on combustion efficiency and emission factors for African savanna ecosystems. **Journal of Geophysical Research**, 101 (D19), 23569-23576.

World Meteorological Organisation (WMO) (1986). Atmospheric ozone. Report 36, Geneva.

Yienger, J.J. and Levy II, H. (1995). Empirical model of global soil-biogenic NO_x emissions. **Journal of Geophysical Research**, 100, 11447-11464.

Yienger, J.J., Klonecki, A.A., Levy II, H., Moxim, W.J. and Carmichael, G.R. (1999). An evaluation of chemistry's role in the winter-spring ozone maximum found in the northern midlatitude free troposphere. **Journal of Geophysical Research**, 104 (D3), 3655-3667.

Zachariasse, M., van Velthoven, P.F.J., Smit, H.G.J., Lelieveld, J., Mandal, T.K. and Kelder, H. (2000). Influence of stratosphere-troposphere exchange on tropospheric ozone over the tropical Indian ocean during the winter monsoon. **Journal of Geophysical Research**, 105 (D12), 15403-15416.

Zellner, K. and Moussiopoulos, N. (1986). Simulations of the ozone formation caused by traffic in urban areas. **Atmospheric Environment**, 20 (8), 1589-1596.

Zepp, R.G., Miller, W.L., Burke, R.A., Parsons, D.A.B., and Scholes, M.C. (1996). Effects of moisture and burning on soil-atmosphere exchange of trace carbon gases in a southern African savanna. **Journal of Geophysical Research**, 101 (D19), 23699-23706.

Zhang, R., Sanger, N.T., Orville, R.E., Tie, X., Randel, W., Williams, E.R. (2000). Enhanced NO_x by lightning in the upper troposphere and lower stratosphere inferred from the UARS global measurements. **Geophysical Research Letters**, 27, 685.

Zunckel, M., Scourfield, M.W.J. and Diab, R.D. (1992a). Vertical distribution of ozone above Pretoria from 1965 to 1968. **South African Journal of Science**, 88, 217-220.

Zunckel, M., Diab, R.D. and Scourfield, M.W.J. (1992b). Vertical distribution of ozone at Pretoria: comparisons between 1965-68 and 1990-1991. **The Clean Air Journal**, 8, 3-8.

Zunckel, M., Hong, Y., Brassel, K. and O'Beirne, S. (1996). Characteristics of the nocturnal boundary layer: Okaukuejo, Namibia, during SAFARI-92. **Journal of Geophysical Research**, 101 (D19), 23677-23682.

Internet Sources

http://www.aero.obs-mip.fr/mozaic/
http://www.arl.noaa.gov/slides/ready/traj/traj3.html

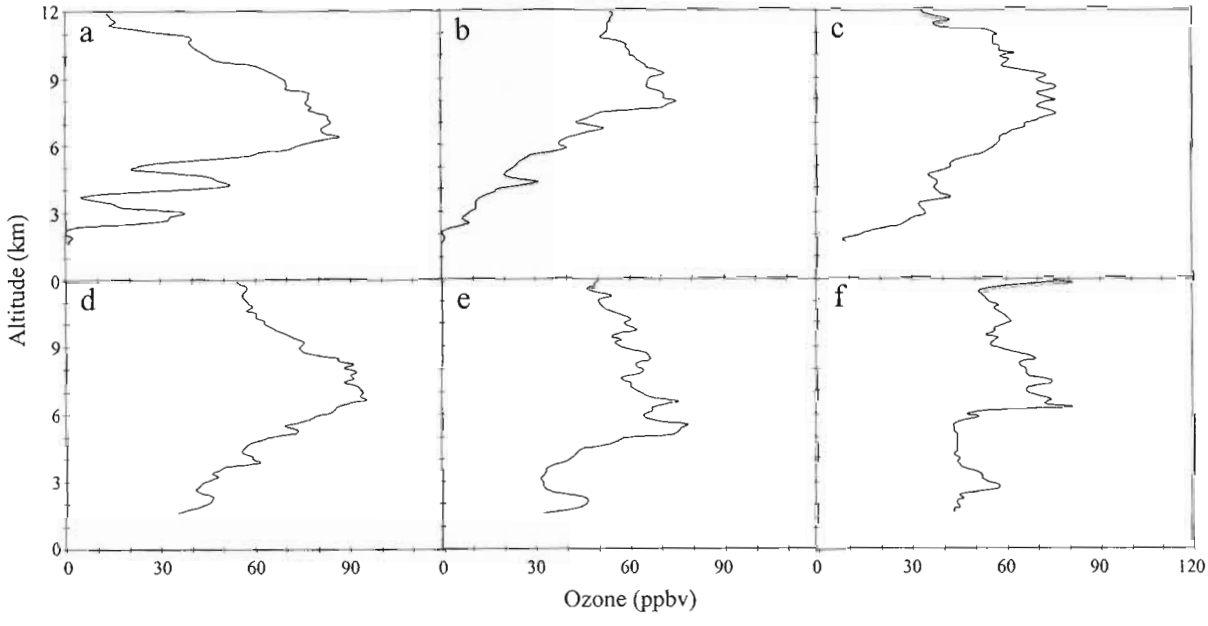

Figure A.1: Individual ozone profiles in the single mid-tropospheric peak category for (a) 7 February 1996, (b) 17 January 1997, (c) 7 February 1997 (d) 25 December 1996, (e) 19 February 1997 and (f) 28 August 1998

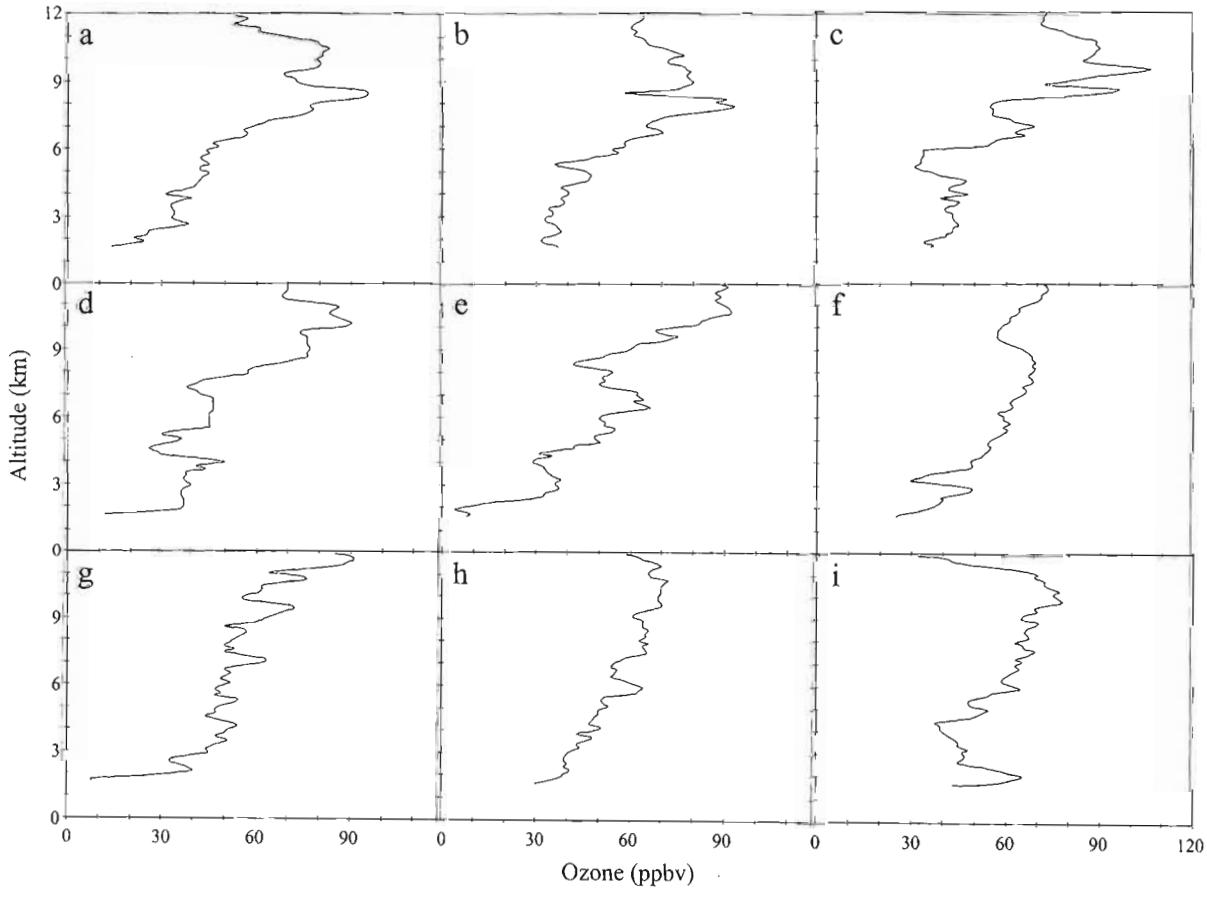

Figure A.2: Individual ozone profiles in the steady tropospheric increase category for (a) 30 December 1998, (b) 23 December 1995, (c) 6 January 1999 (d) 16 December 1998, (e) 22 December 1998, (f) 18 November 1998, (g) 23 December 1998, (h) 17 November 1998 and (i) 5 February 1999

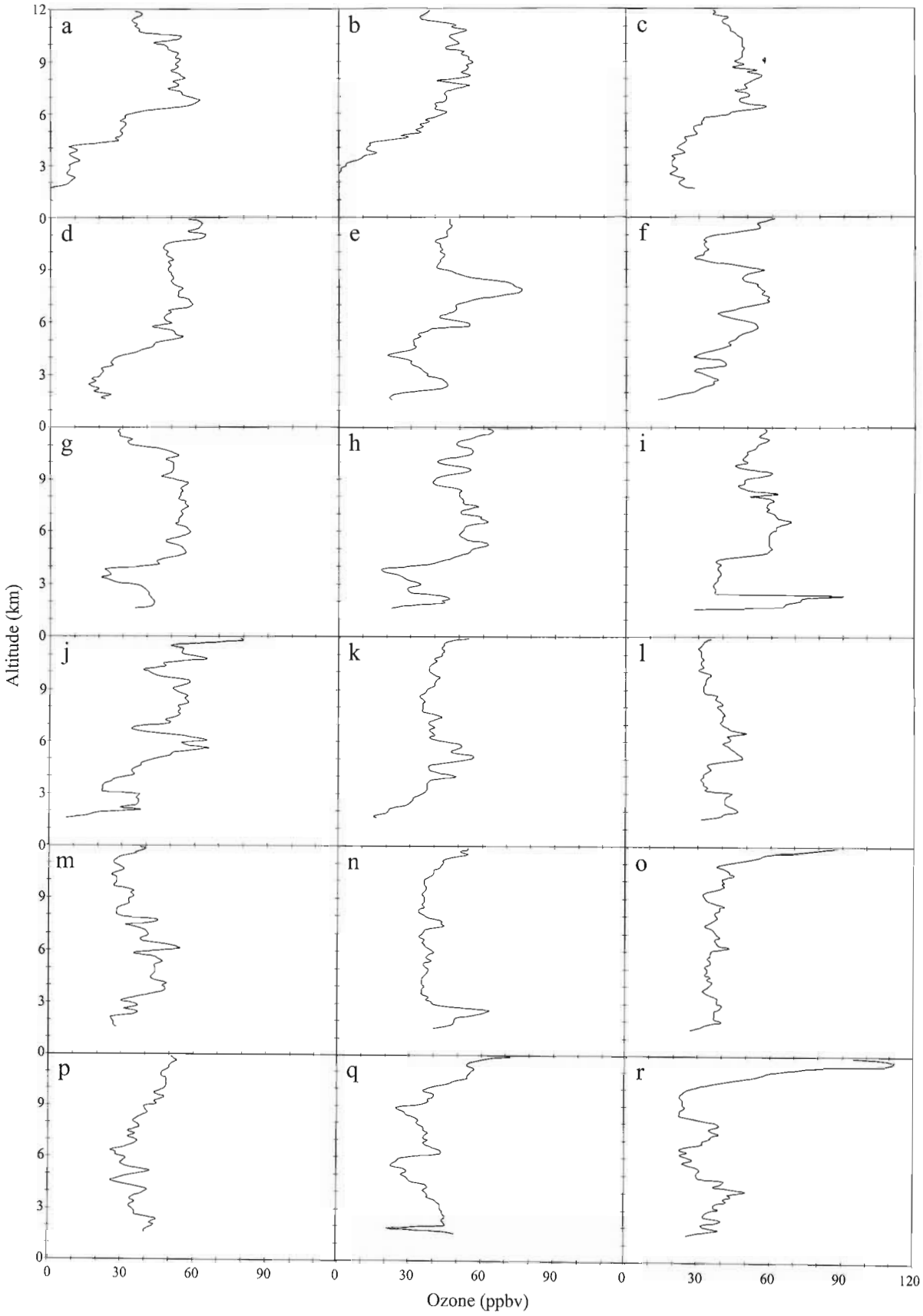

Figure A.3: Individual ozone profiles in the reduced tropospheric ozone category for (a) 26 March 1997, (b) 5 March 1997, (c) 8 May 1998, (d) 20 February 1998, (e) 29 March 1998, (f) 23 April 1997, (g) 3 May 1999, (h) 13 June 1997, (i) 6 July 1998, (j) 22 March 2000, (k) 29 December 1998, (l) 24 April 1996, (m) 1 May 1996, (n) 28 June 1998, (o) 12 June 1998, (p) 20 March 1998, (q) 2 May 1998 and (r) 16 May 1997

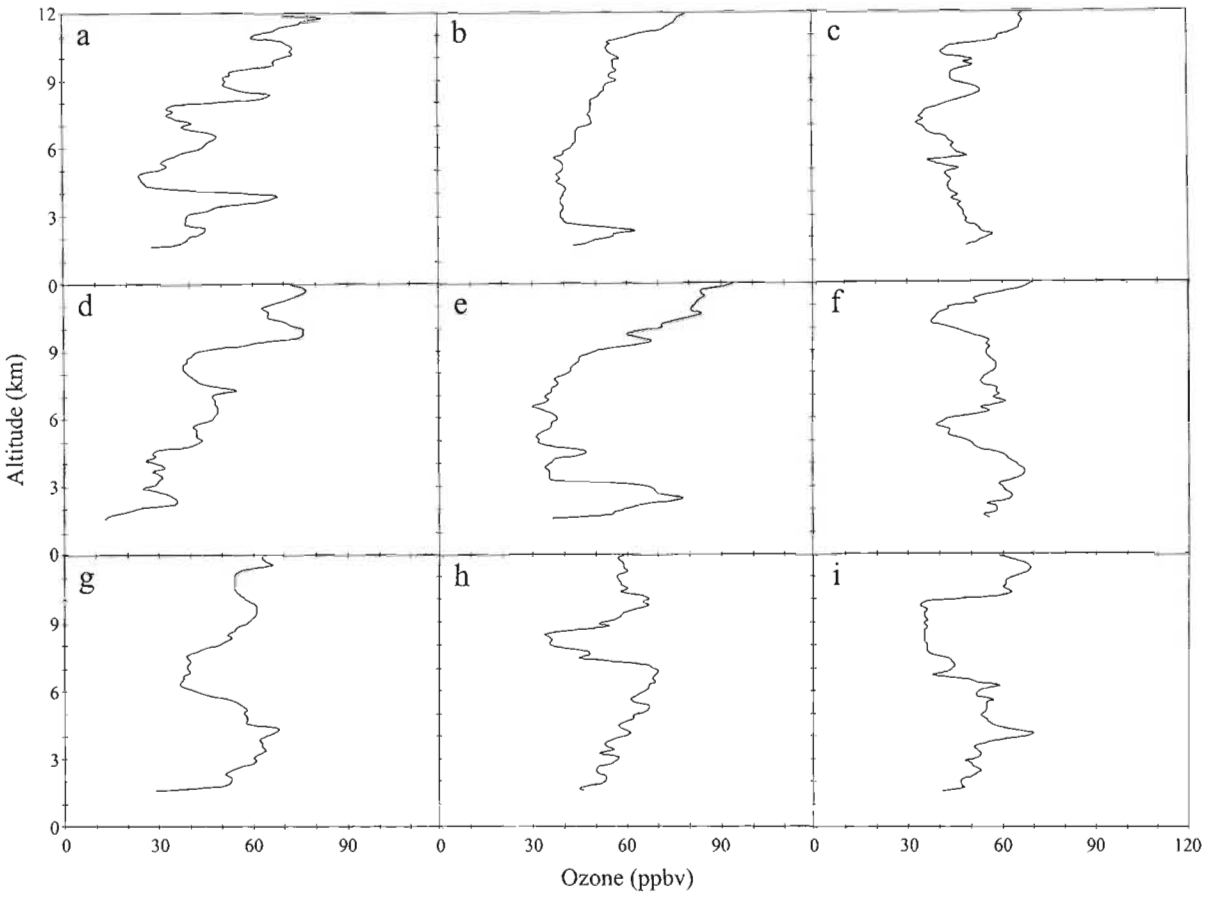

Figure A.4: Individual ozone profiles in the lower tropospheric enhancement category for (a) 15 December 1998, (b) 24 November 1998, (c) 11 December 1998, (d) 3 May 1995, (e) 22 May 1998, (f) 29 July 1998, (g) 12 August 1998, (h) 17 July 1998 and (i) 15 July 1998

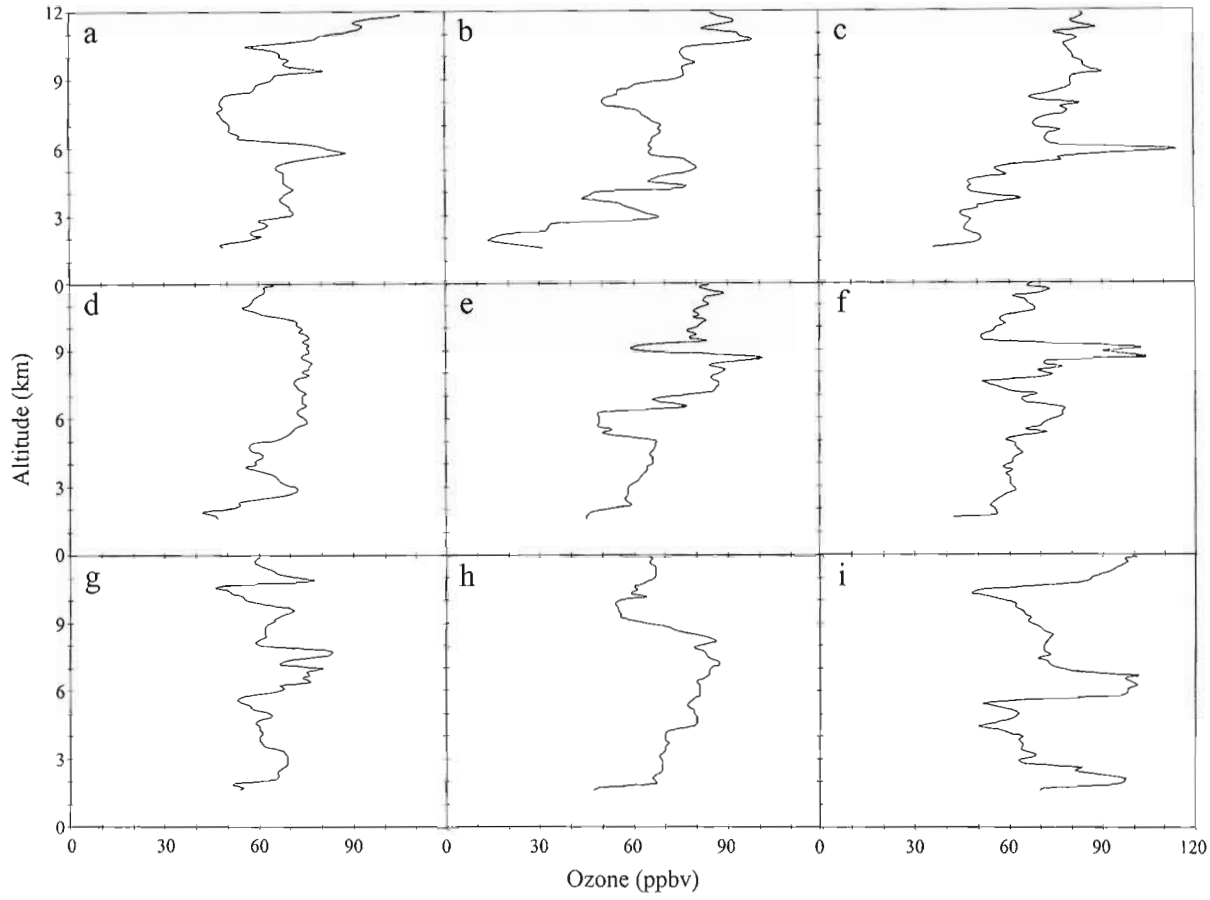

Figure A.5: Individual ozone profiles in the pronounced layering category for (a) 2 October 1998, (b) 9 March 1999, (c) 20 September 1998, (d) 15 September 1998, (e) 14 September 1998, (f) 25 October 1998, (g) 21 August 1998, (h) 10 September 1998 and (i) 13 November 1998

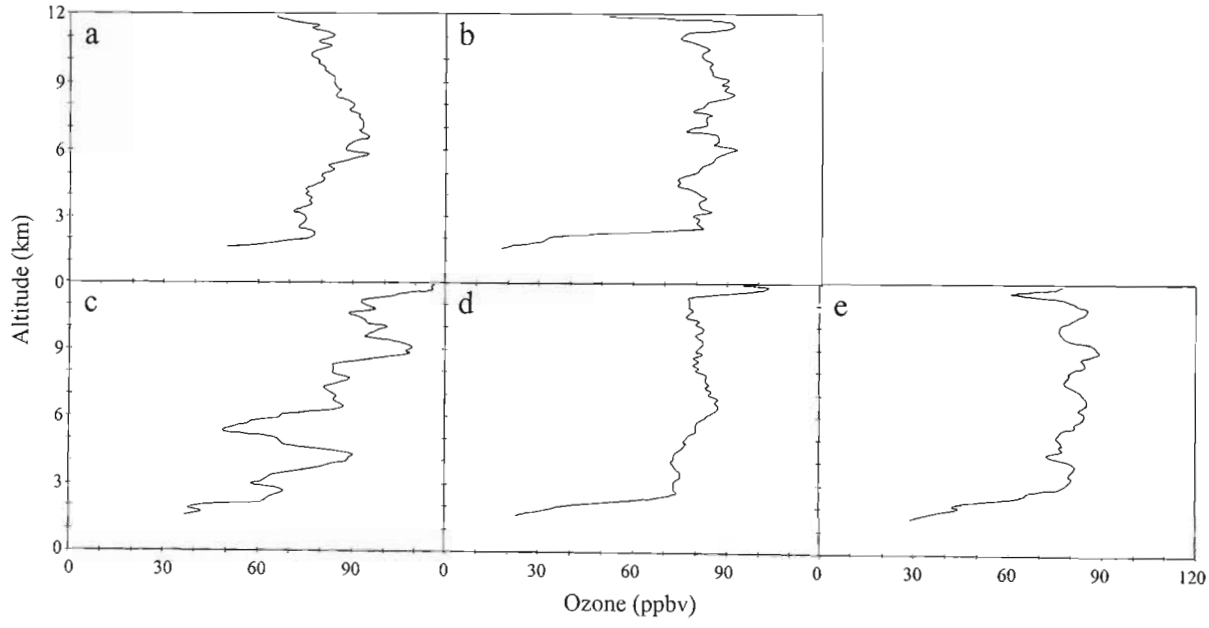

Figure A.6: Individual ozone profiles in the considerable tropospheric enhancement category for (a) 11 October 1996, (b) 7 October 1998, (c) 25 October 1996, (d) 10 October 1997 and (e) 8 October 1998

APPENDIX B

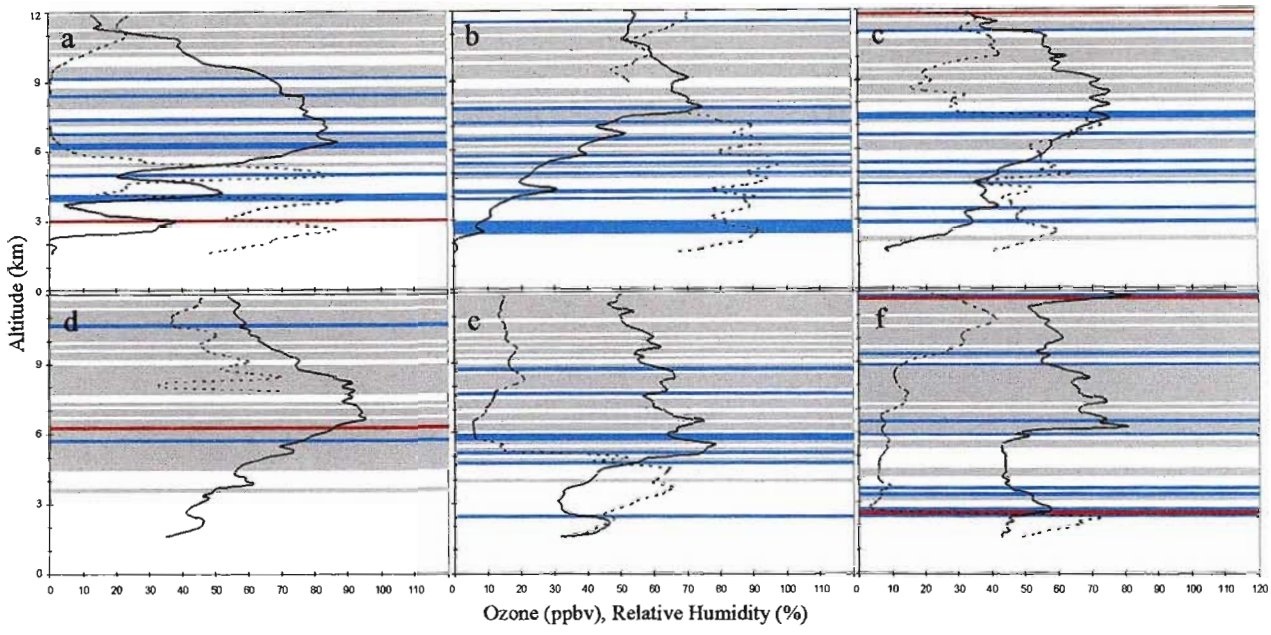

Figure B.1: Inversion (red), isothermal (blue) and stable layers (grey) for ozone (solid line) and relative humidity (dashed line) profiles in the single mid-tropospheric peak category for (a) 7 February 1996, (b) 17 January 1997, (c) 7 February 1997 (d) 25 December 1996, (e) 19 February 1997 and (f) 28 August 1998

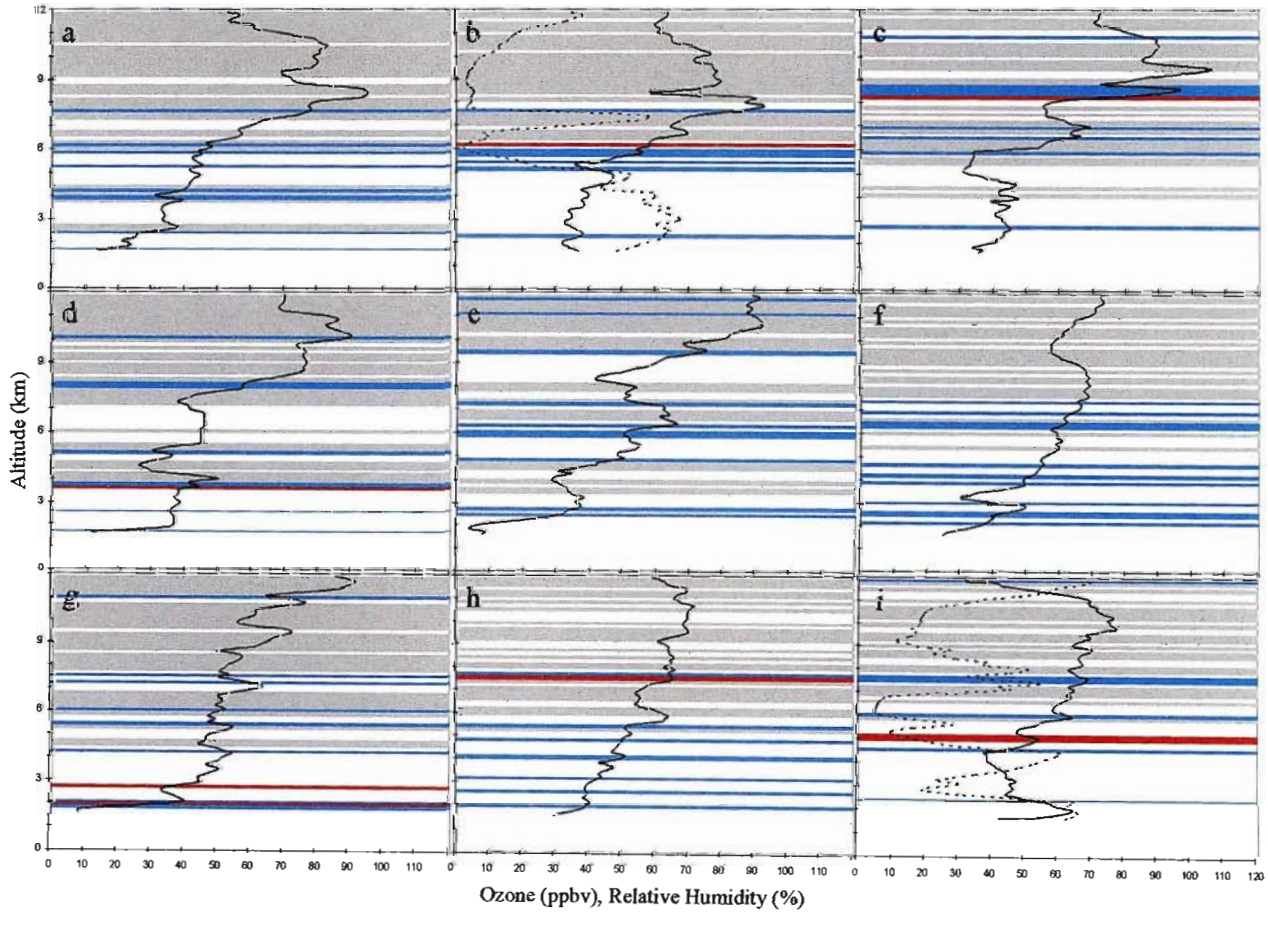

Figure B.2: Inversion (red), isothermal (blue) and stable layers (grey) for ozone (solid line) and relative humidity (dashed line) profiles in the steady tropospheric increase category for (a) 30 December 1998, (b) 23 December 1995, (c) 6 January 1999 (d) 16 December 1998, (e) 22 December 1998, (f) 18 November 1998, (g) 23 December 1998, (h) 17 November 1998 and (i) 5 February 1999

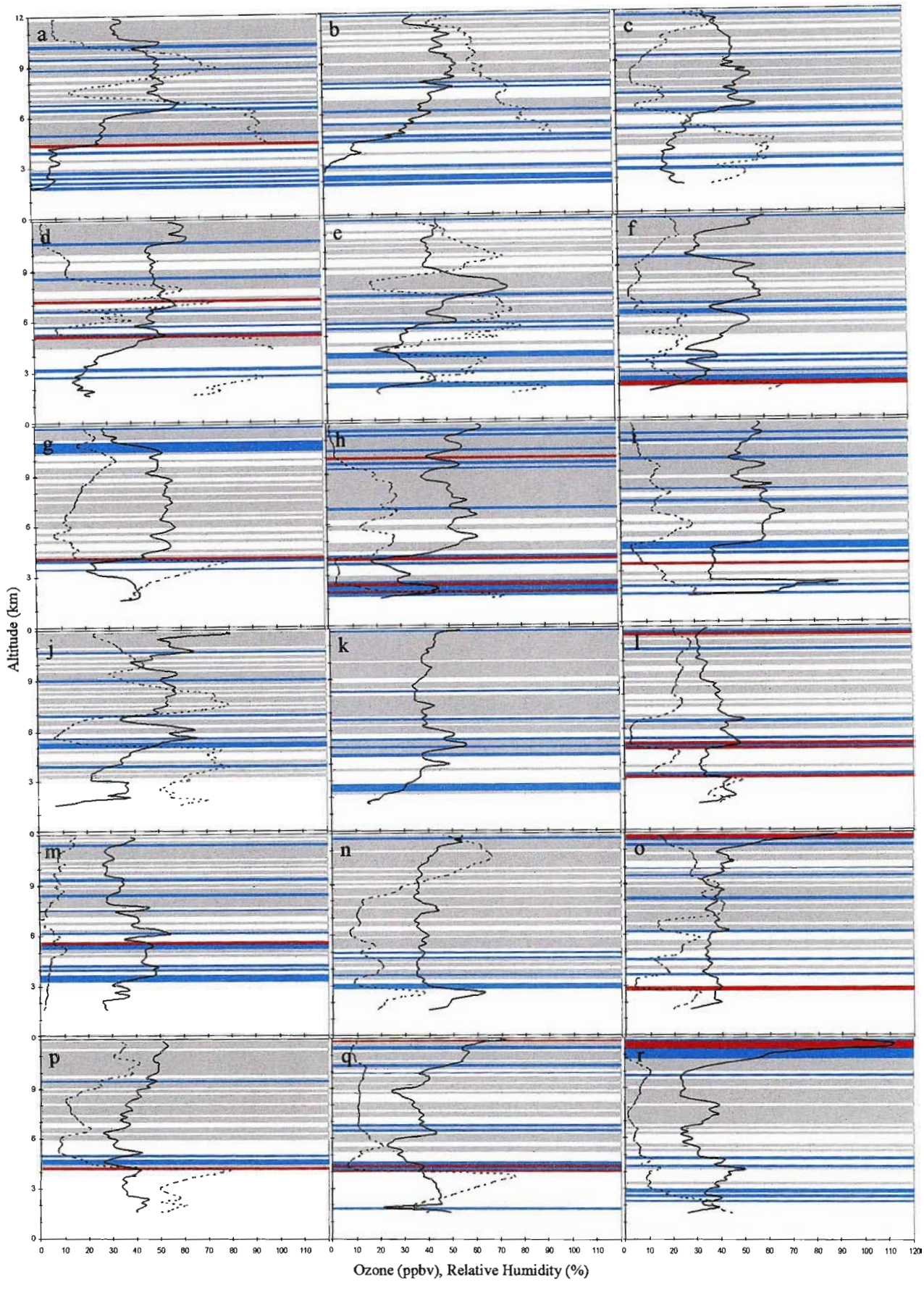

Figure B.3: Inversion (red), isothermal (blue) and stable layers (grey) for ozone (solid line) and relative humidity (dashed line) profiles in the reduced tropospheric ozone category for (a) 26 March 1997, (b) 5 March 1997, (c) 8 May 1998, (d) 20 February 1998, (e) 29 March 1998, (f) 23 April 1997, (g) 3 May 1999, (h) 13 June 1997, (i) 6 July 1998, (j) 22 March 2000, (k) 29 December 1998, (l) 24 April 1996, (m) 1 May 1996, (n) 28 June 1998, (o) 12 June 1998, (p) 20 March 1998, (q) 2 May 1998 and (r) 16 May 1997

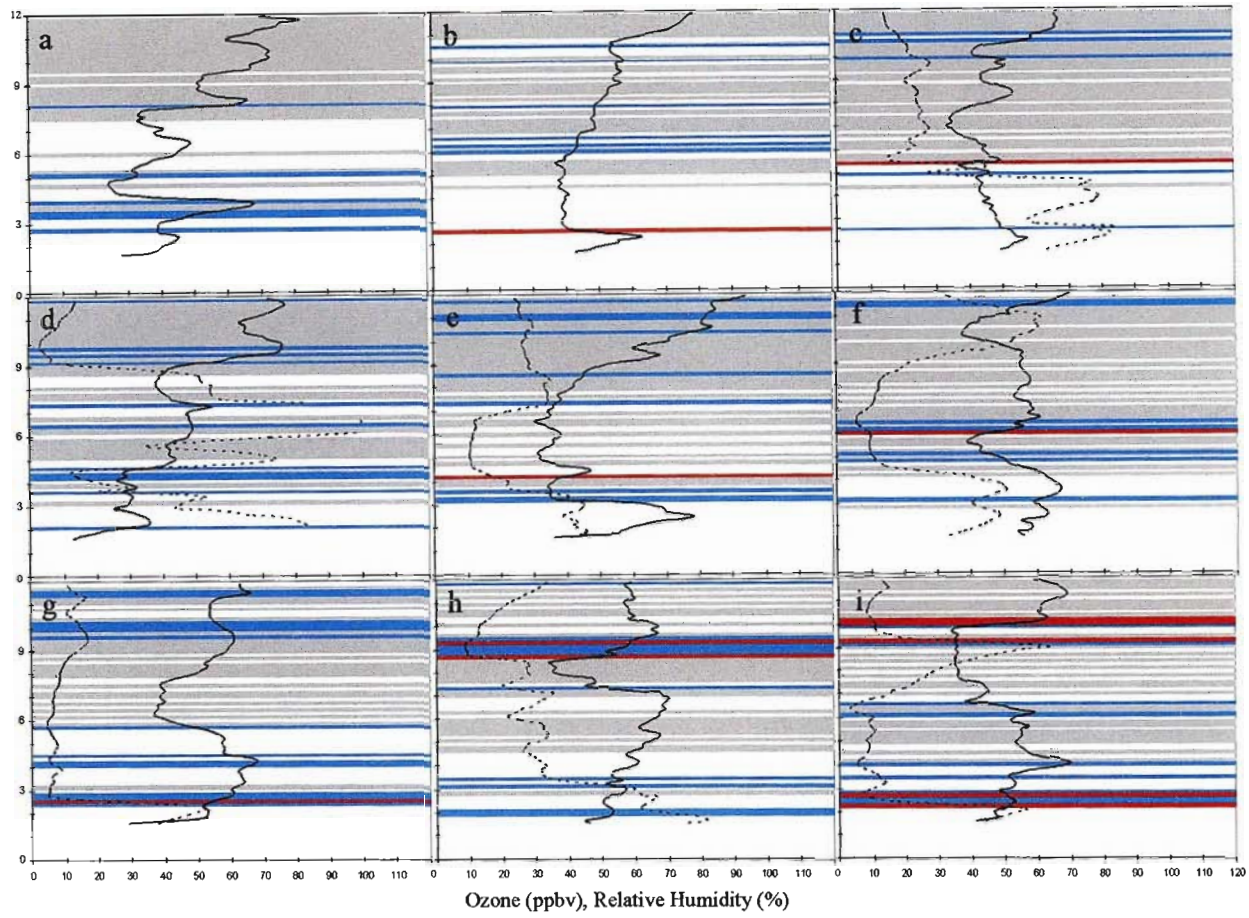

Figure B.4: Inversion (red), isothermal (blue) and stable layers (grey) for ozone (solid line) and relative humidity (dashed line) profiles in the lower tropospheric enhancement category for (a) 15 December 1998, (b) 24 November 1998, (c) 11 December 1998, (d) 3 May 1995, (e) 22 May 1998, (f) 29 July 1998, (g) 12 August 1998, (h) 17 July 1998 and (i) 15 July 1998

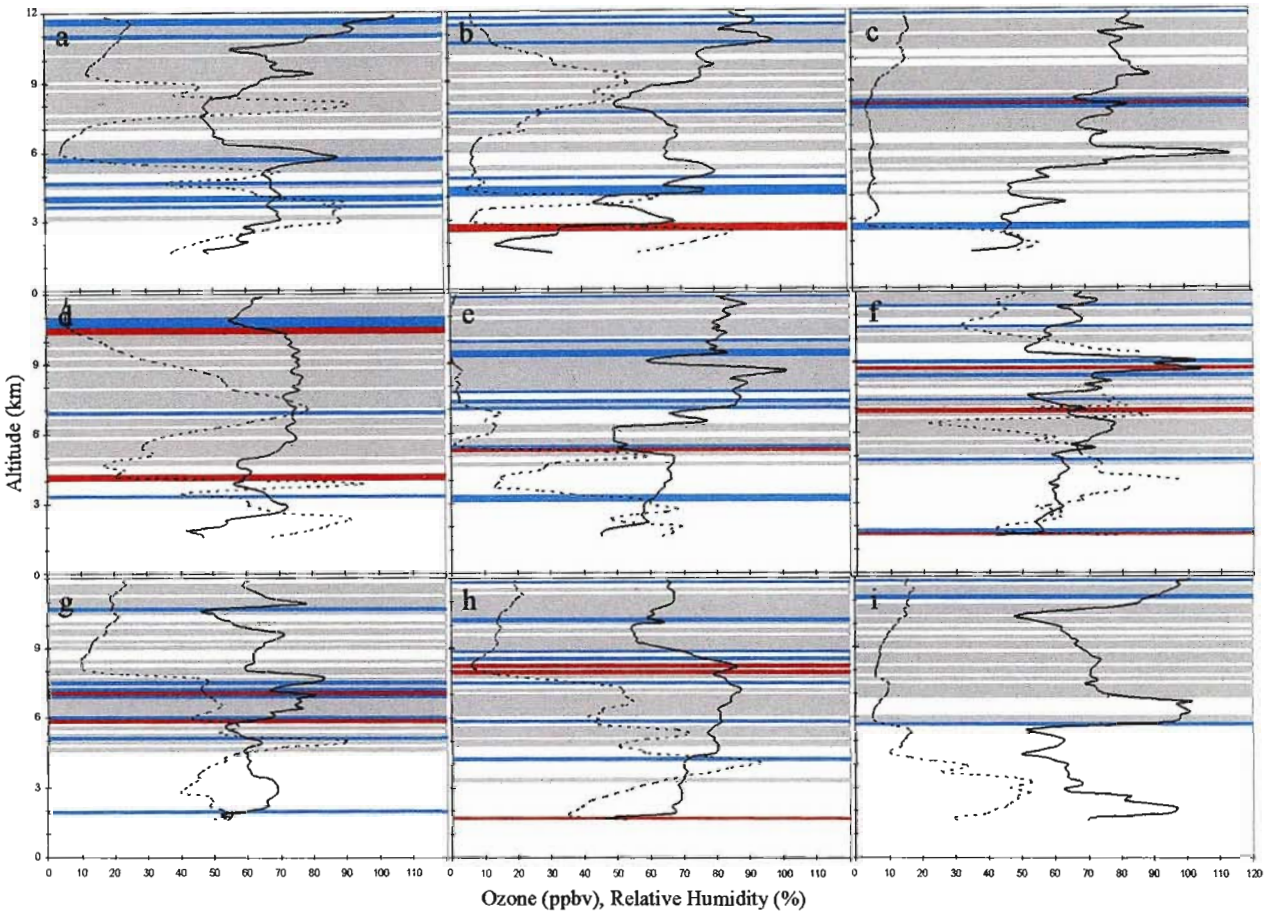

Figure B.5: Inversion (red), isothermal (blue) and stable layers (grey) for ozone (solid line) and relative humidity (dashed line) profiles in the pronounced layering category for (a) 2 October 1998, (b) 9 March 1999, (c) 20 September 1998, (d) 15 September 1998, (e) 14 September 1998, (f) 25 October 1998, (g) 21 August 1998, (h) 10 September 1998 and (i) 13 November 1998

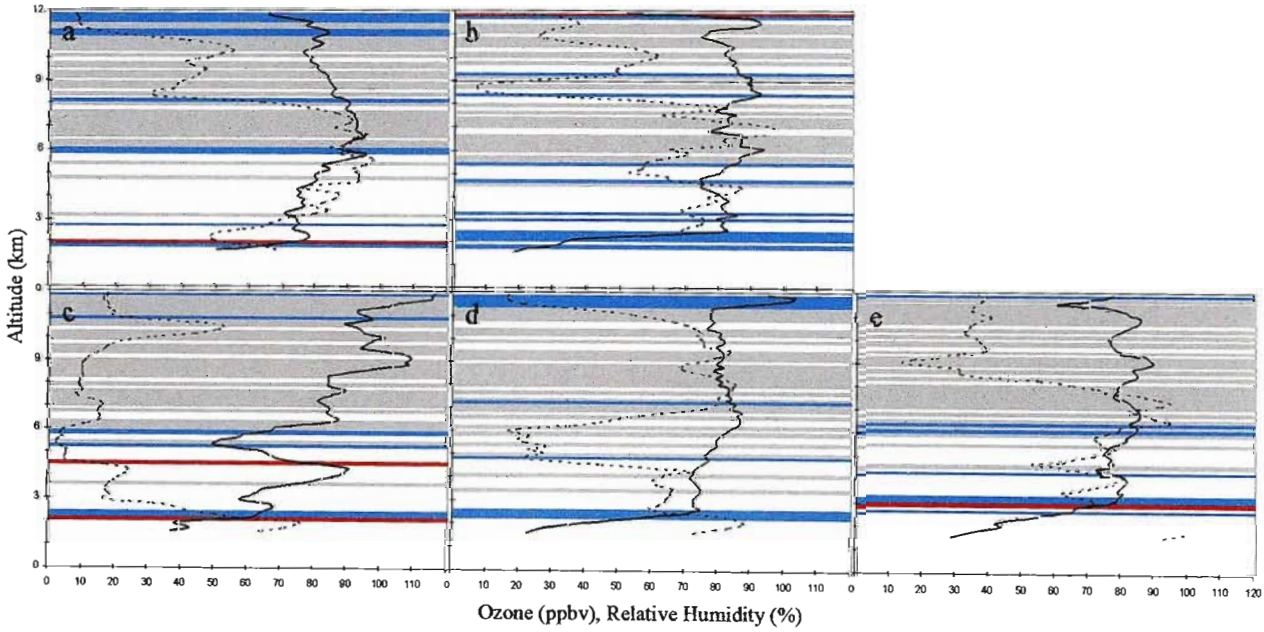

Figure B.6: Inversion (red), isothermal (blue) and stable layers (grey) for ozone (solid line) and relative humidity (dashed line) profiles in the considerable tropospheric enhancement category for (a) 11 October 1996, (b) 7 October 1998, (c) 25 October 1996, (d) 10 October 1997 and (e) 8 October 1998

APPENDIX C

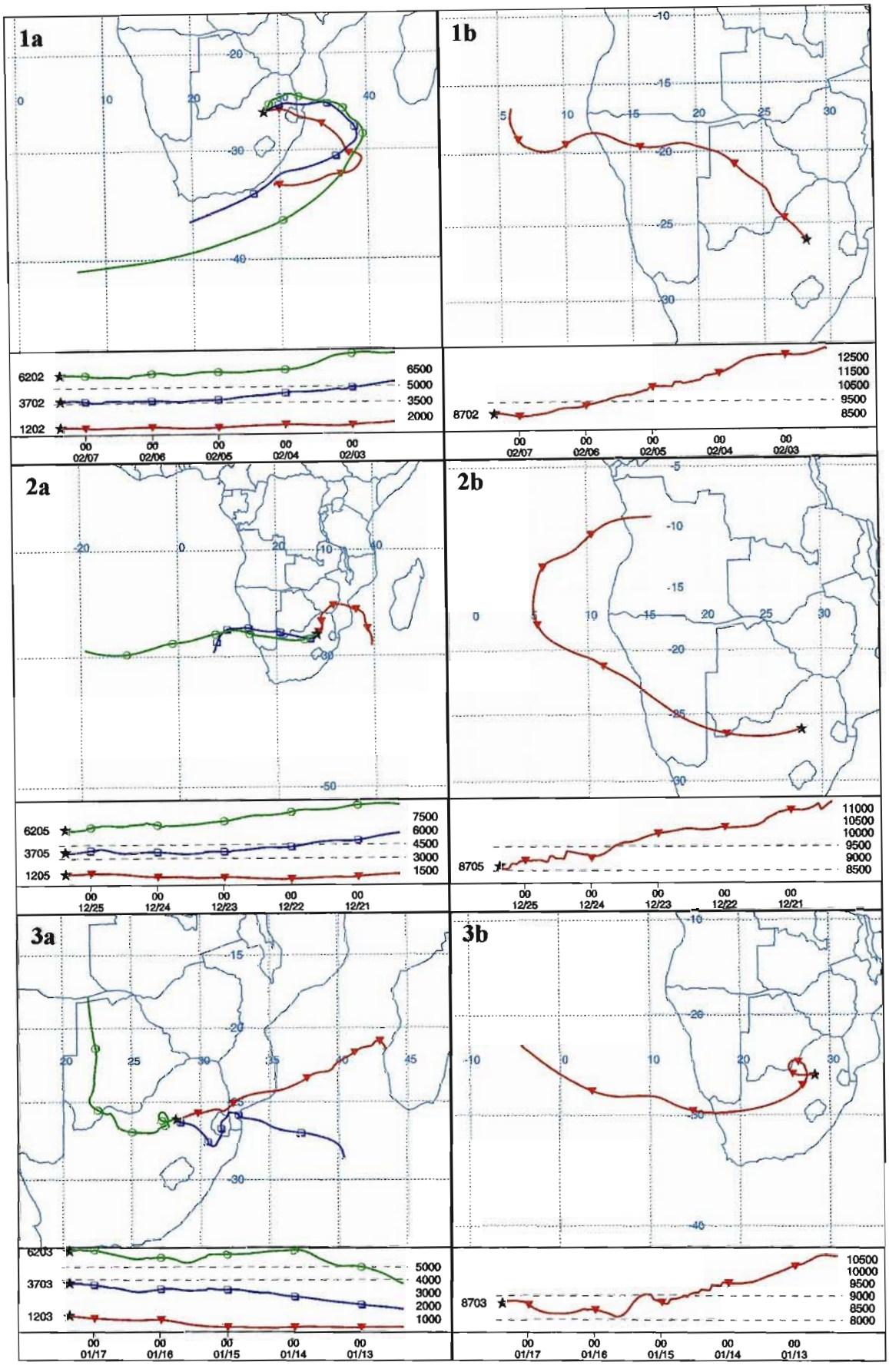

Figure C.1: 5-day back trajectory HYSPLIT model results for the single mid-tropospheric peak category for (1) 7 February 1996, (2) 25 December 1996 and (3) 17 January 1997.
(a) Horizontal and vertical plots of back trajectories originating at 2.5, 5 and 7.5 km
(b) Horizontal and vertical plots of back trajectories originating at 10 km

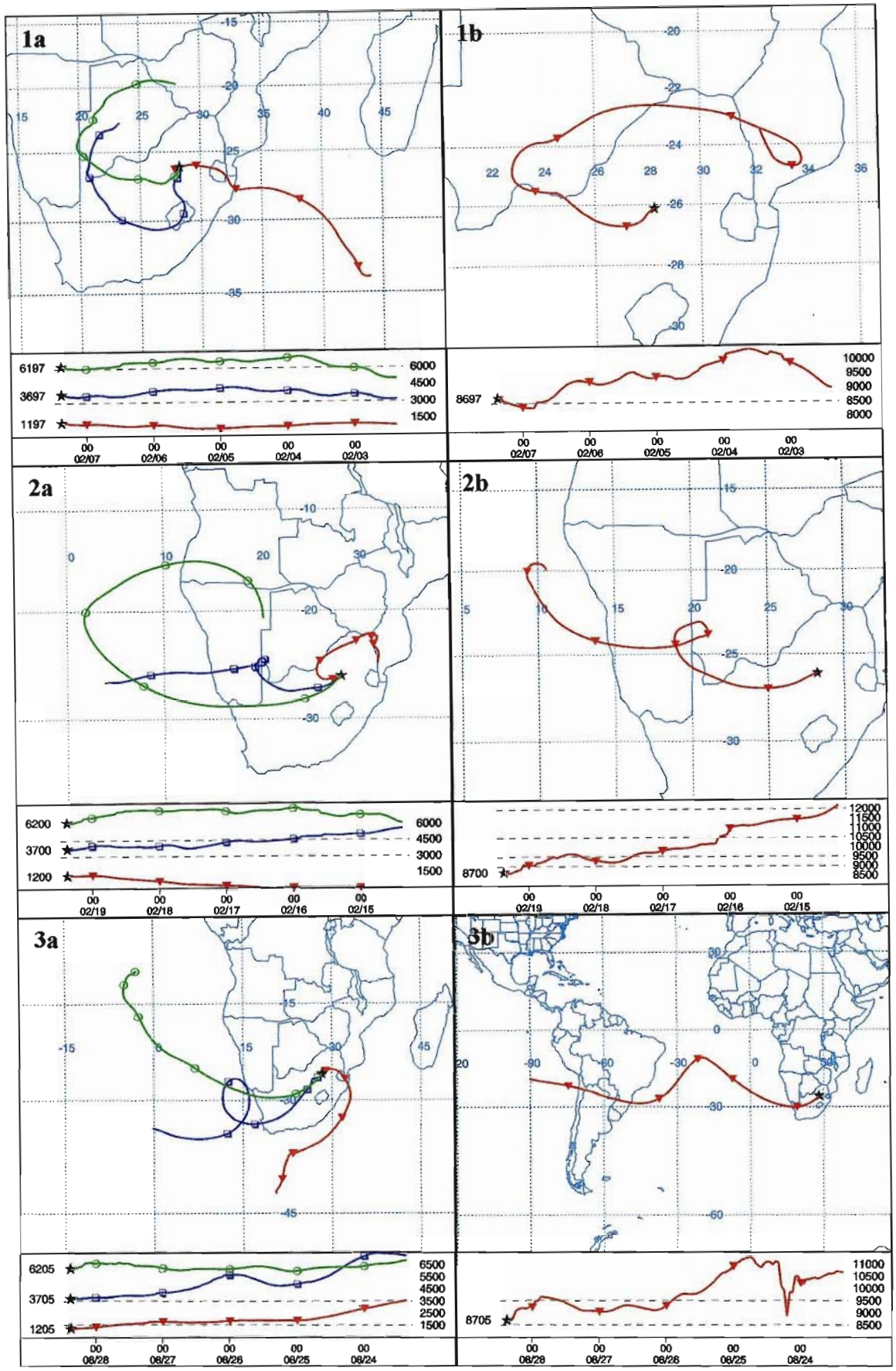

Figure C.1: continued (1) 7 February 1997, (2) 19 February 1997 and (3) 28 August 1998.
(a) Horizontal and vertical plots of back trajectories originating at 2.5, 5 and 7.5 km
(b) Horizontal and vertical plots of back trajectories originating at 10 km

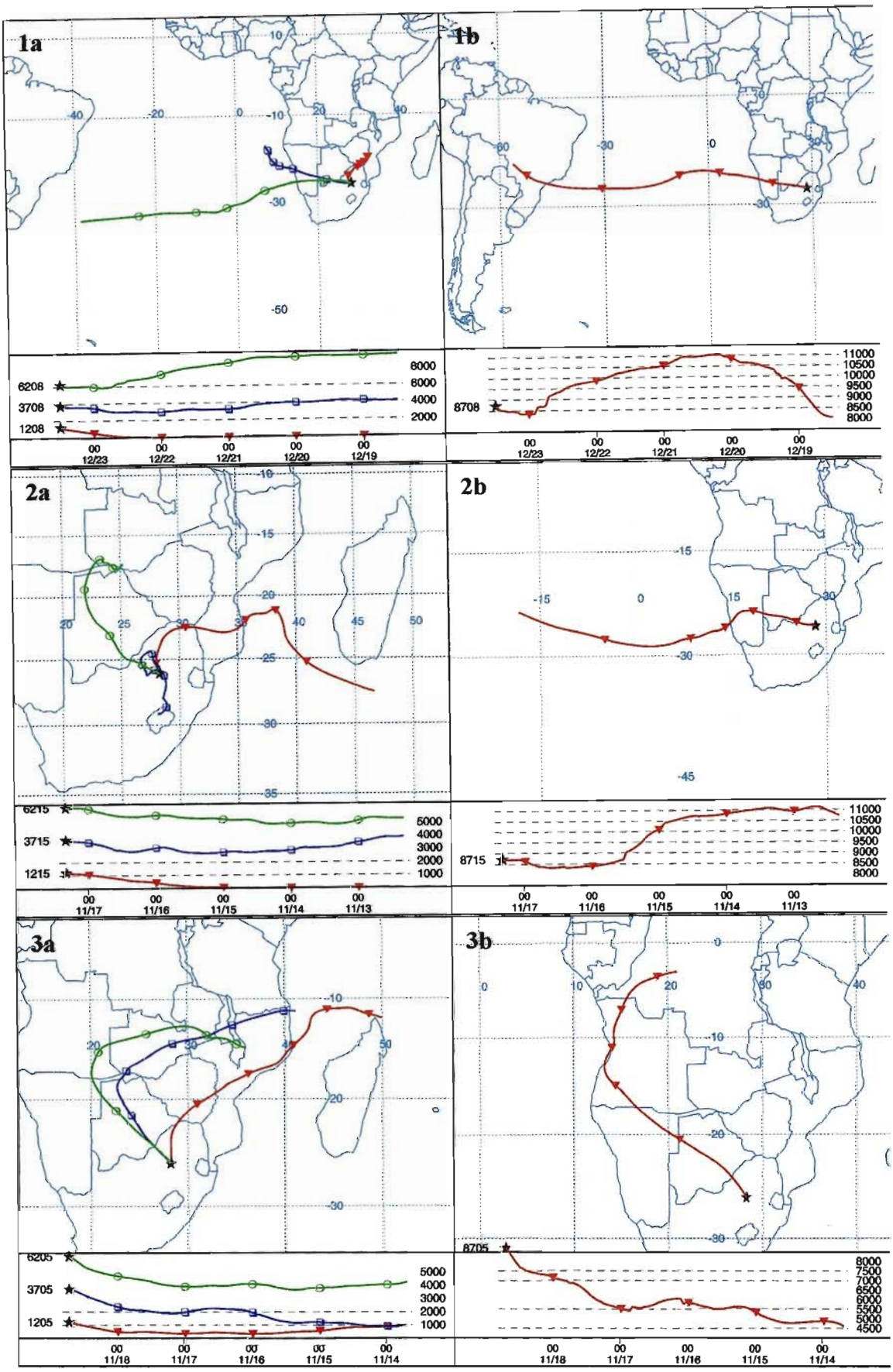

Figure C.2: 5-day back trajectory HYSPLIT model results for the steady tropospheric increase category for (1) 23 December 1995, (2) 17 November 1998 and (3) 18 November 1998. (a) Horizontal and vertical plots of back trajectories originating at 2.5, 5 and 7.5 km. (b) Horizontal and vertical plots of back trajectories originating at 10 km

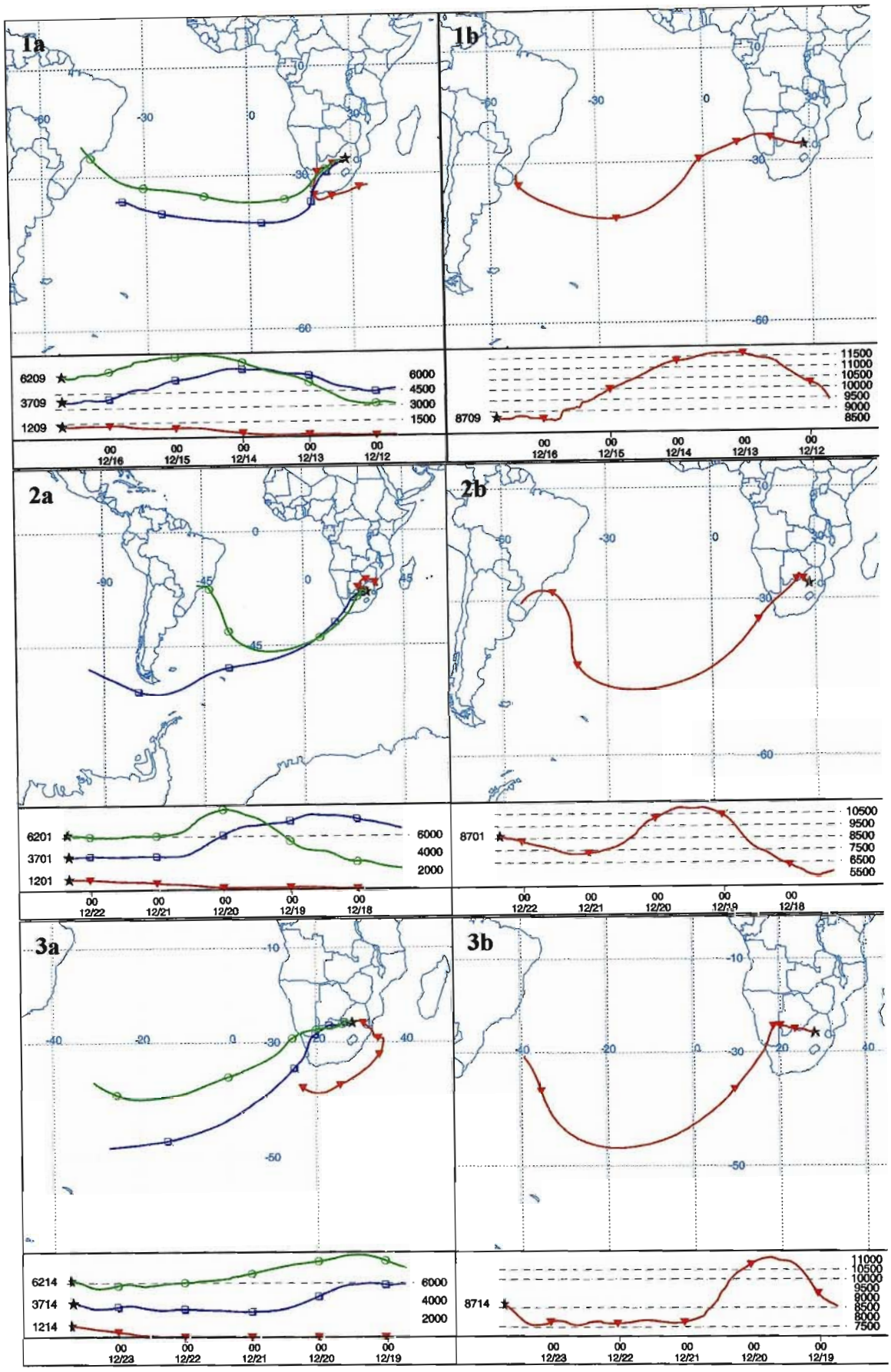

Figure C.2: continued (1) 16 December 1998, (2) 22 December 1998 and (3) 23 December 1998.
(a) Horizontal and vertical plots of back trajectories originating at 2.5, 5 and 7.5 km.
(b) Horizontal and vertical plots of back trajectories originating at 10 km

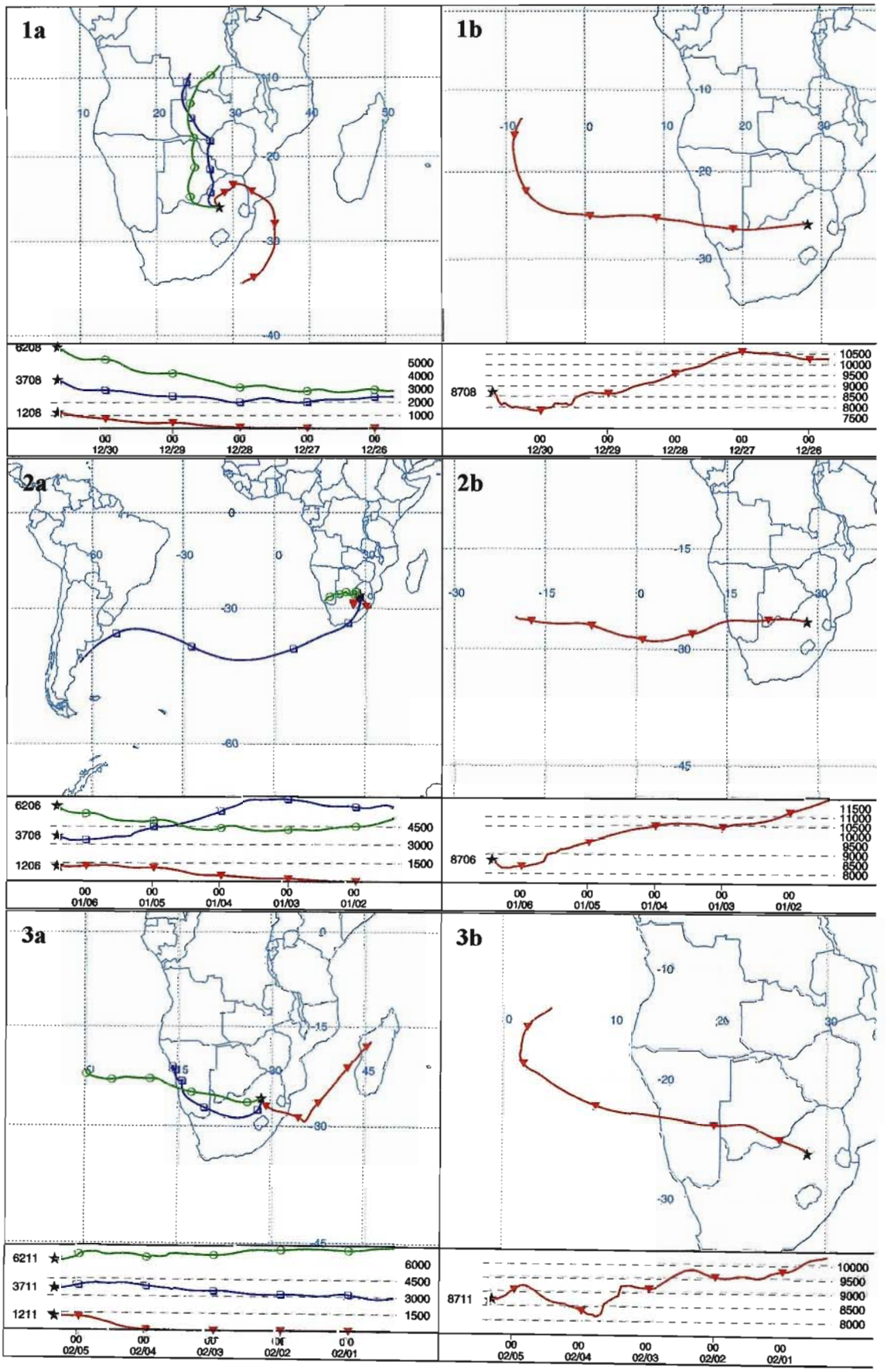

Figure C.2: continued (1) 30 December 1998, (2) 6 January 1999 and (3) 5 February 1999.
(a) Horizontal and vertical plots of back trajectories originating at 2.5, 5 and 7.5 km.
(b) Horizontal and vertical plots of back trajectories originating at 10 km

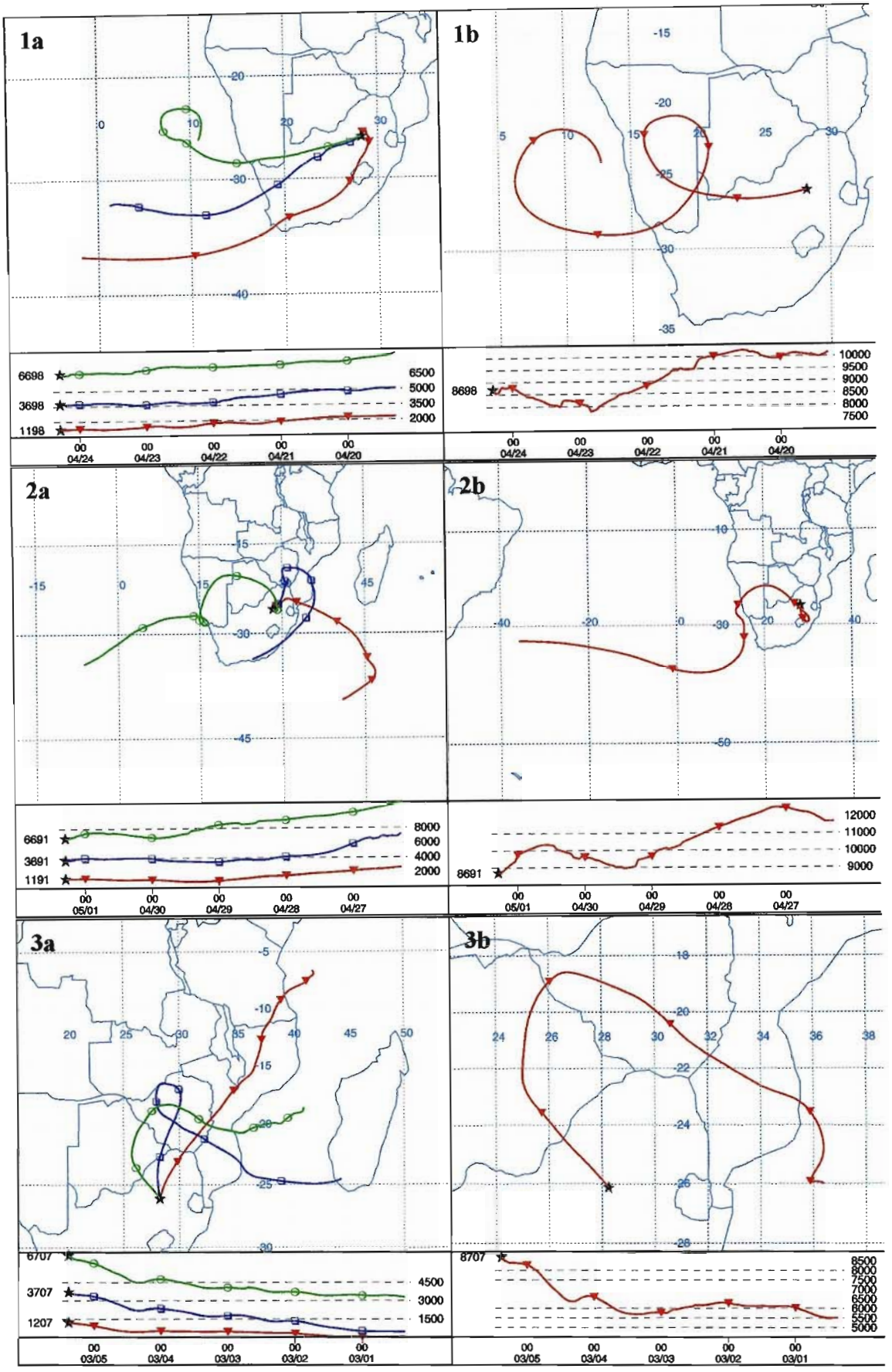

Figure C.3: 5-day back trajectory HYSPLIT model results for the reduced tropospheric ozone category for (1) 24 April 1996, (2) 1 May 1996 and (3) 5 March 1997.
(a) Horizontal and vertical plots of back trajectories originating at 2.5, 5 and 8 km.
(b) Horizontal and vertical plots of back trajectories originating at 10 km

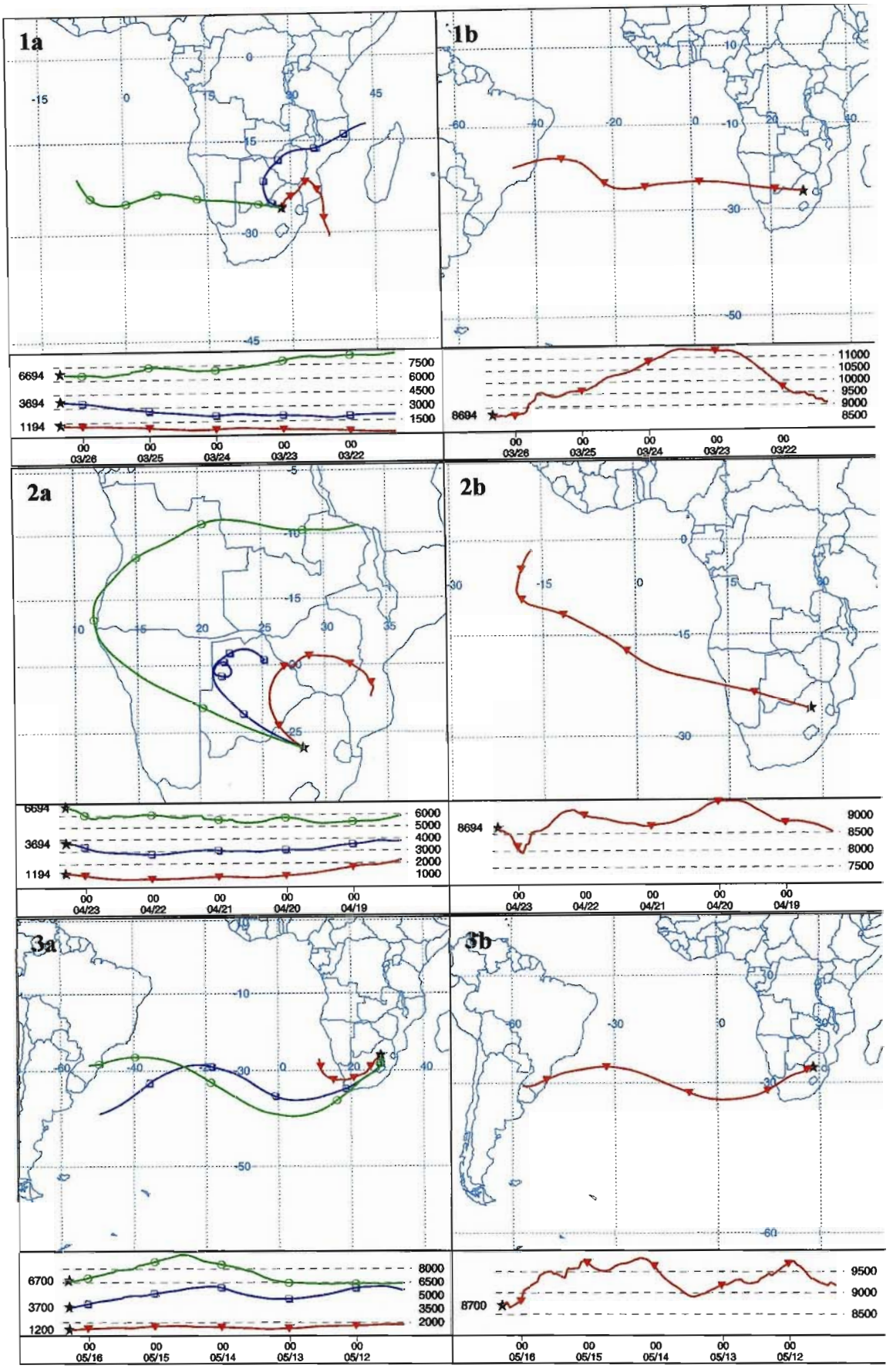

Figure C.3: continued (1) 26 March 1997, (2) 23 April 1997 and (3) 16 May 1997.
(a) Horizontal and vertical plots of back trajectories originating at 2.5, 5 and 8 km.
(b) Horizontal and vertical plots of back trajectories originating at 10 km

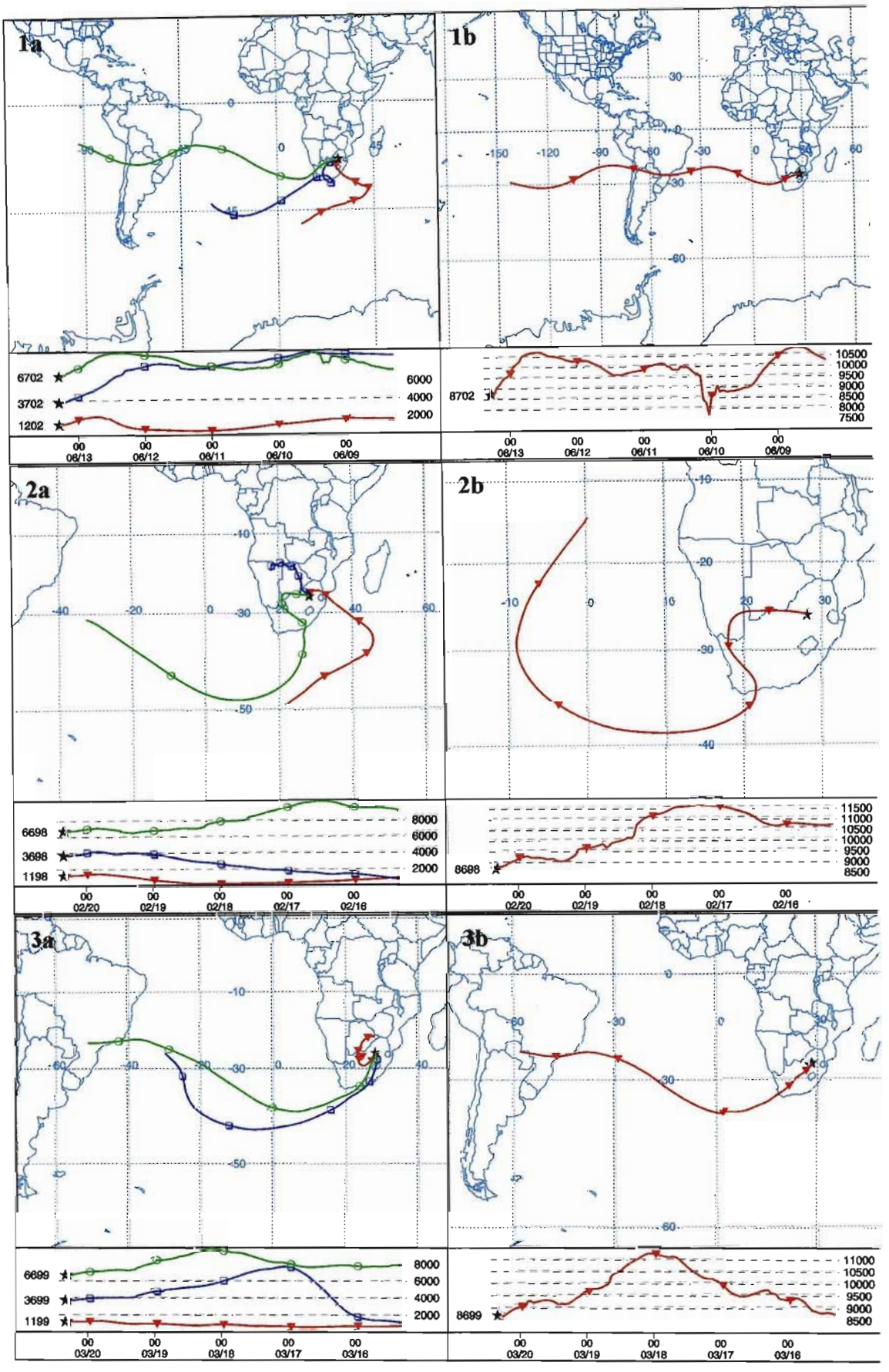

Figure C.3: continued (1) 13 June 1997, (2) 20 February 1998 and (3) 20 March 1998.
(a) Horizontal and vertical plots of back trajectories originating at 2.5, 5 and 8 km.
(b) Horizontal and vertical plots of back trajectories originating at 10 km

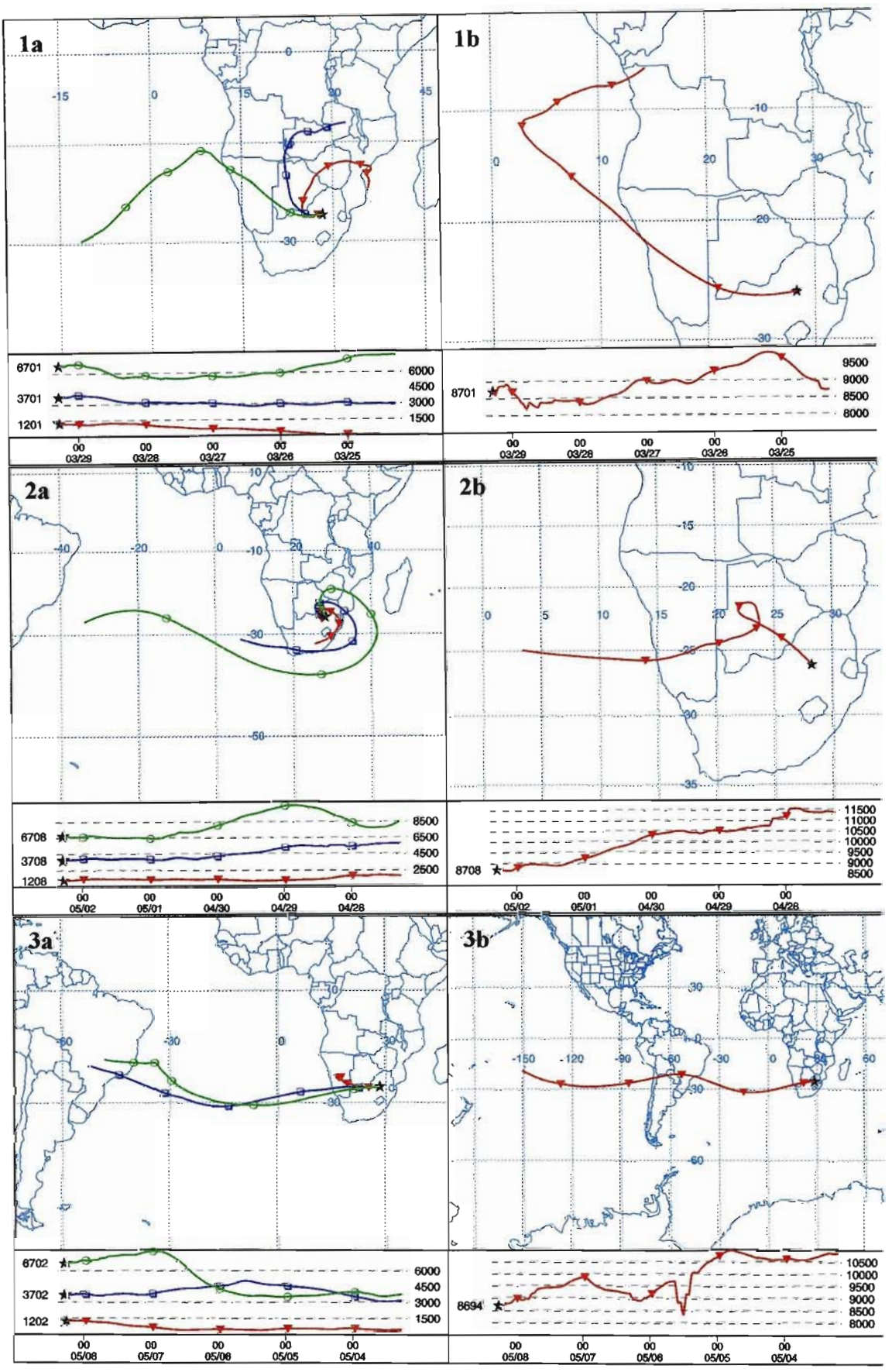

Figure C.3: continued (1) 29 March 1998, (2) 2 May 1998 and (3) 8 May 1998.
(a) Horizontal and vertical plots of back trajectories originating at 2.5, 5 and 8 km.
(b) Horizontal and vertical plots of back trajectories originating at 10 km

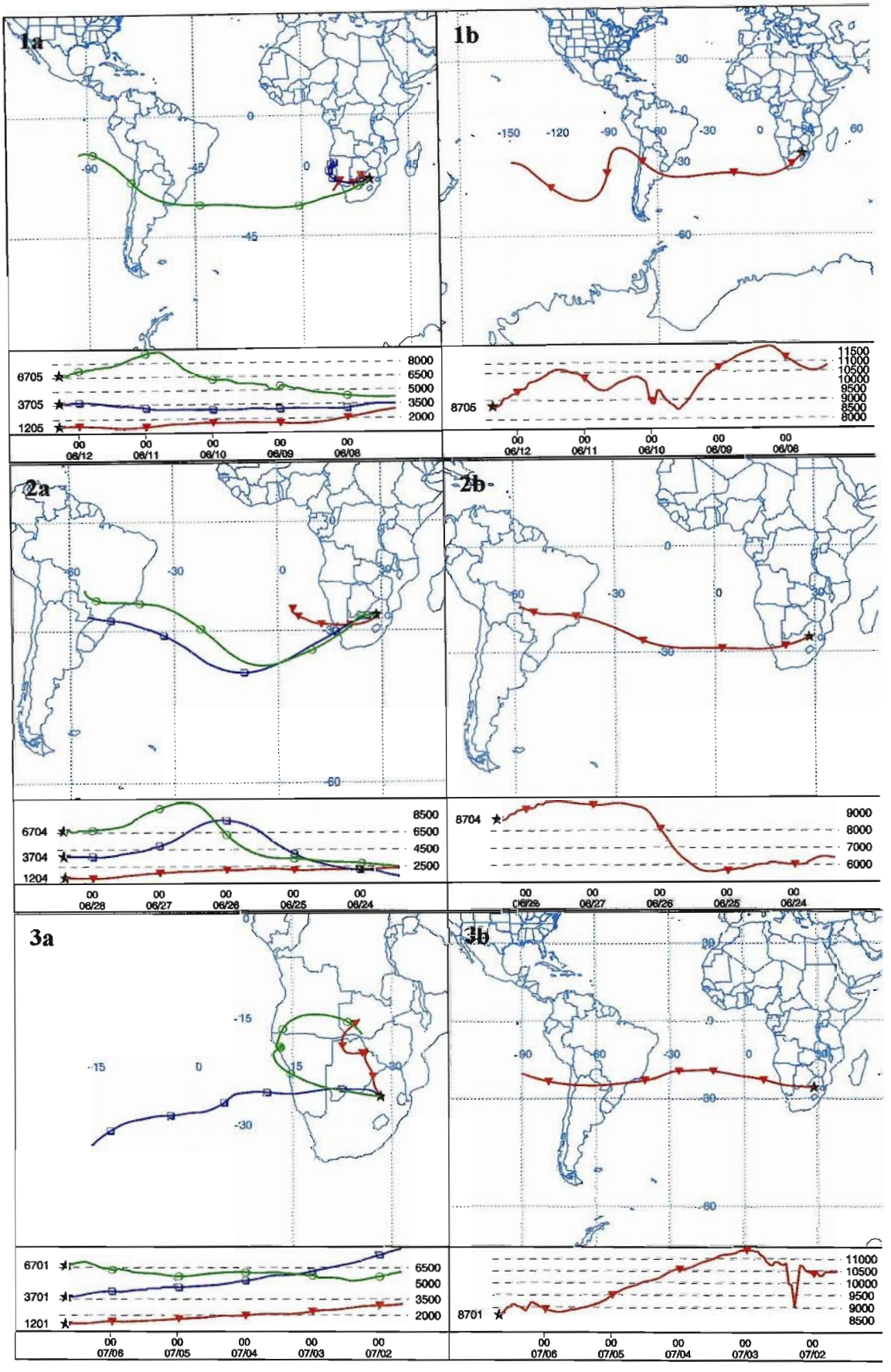

Figure C.3: continued (1) 12 June 1998, (2) 28 June 1998 and (3) 6 July 1998.
(a) Horizontal and vertical plots of back trajectories originating at 2.5, 5 and 8 km.
(b) Horizontal and vertical plots of back trajectories originating at 10 km

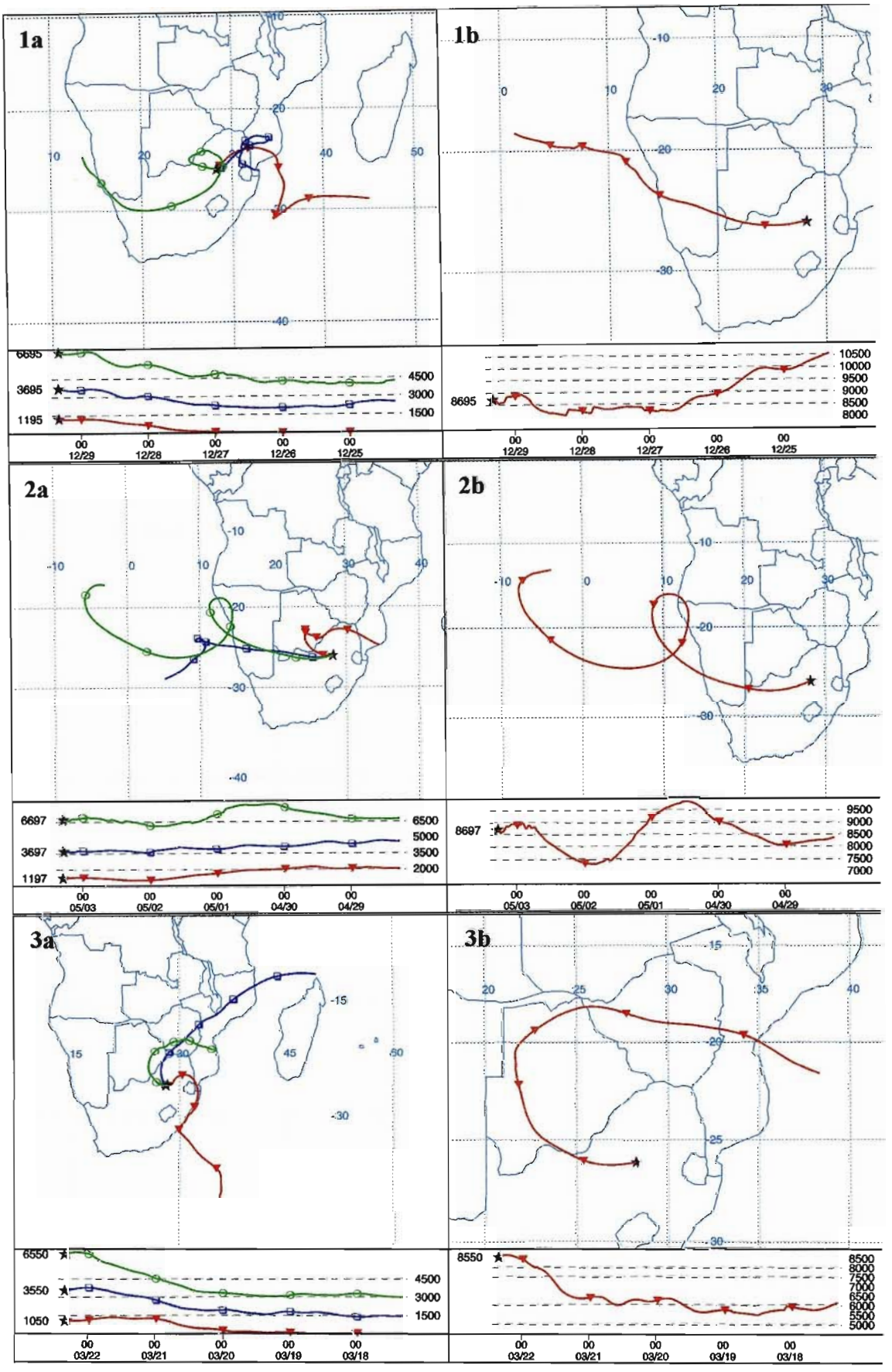

Figure C.3: continued (1) 29 December 1998, (2) 3 May 1999 and (3) 22 March 2000.
(a) Horizontal and vertical plots of back trajectories originating at 2.5, 5 and 8 km.
(b) Horizontal and vertical plots of back trajectories originating at 10 km

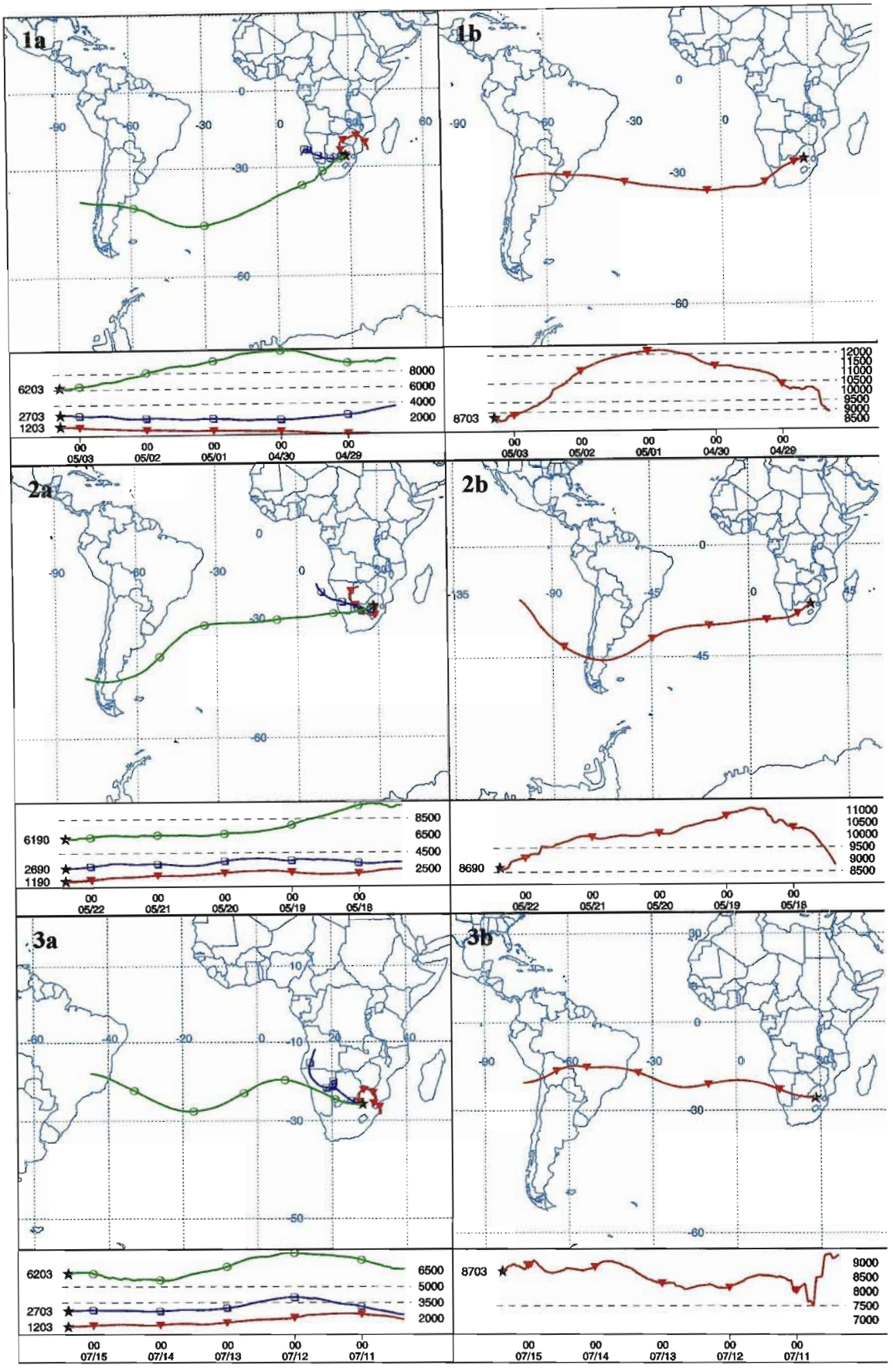

Figure C.4: 5-day back trajectory HYSPLIT model results for the lower tropospheric enhancement category for (1) 3 May 1995, (2) 22 May 1998 and (3) 15 July 1998. (a) Horizontal and vertical plots of back trajectories originating at 2.5, 4 and 7.5 km. (b) Horizontal and vertical plots of back trajectories originating at 10 km

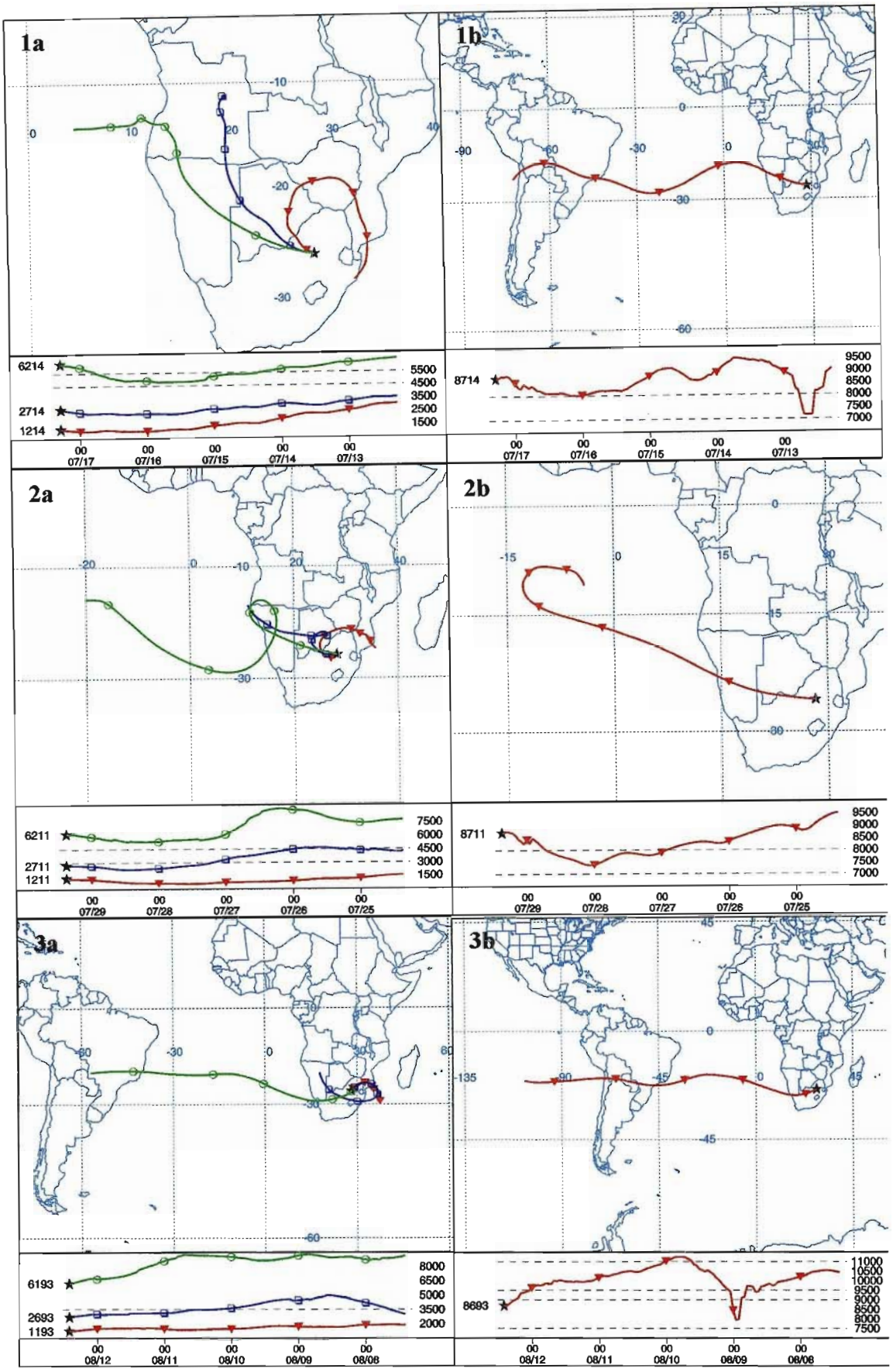

Figure C.4: continued (1) 17 July 1998, (2) 29 July 1998 and (3) 12 August 1998.
(a) Horizontal and vertical plots of back trajectories originating at 2.5, 4 and 7.5 km.
(b) Horizontal and vertical plots of back trajectories originating at 10 km

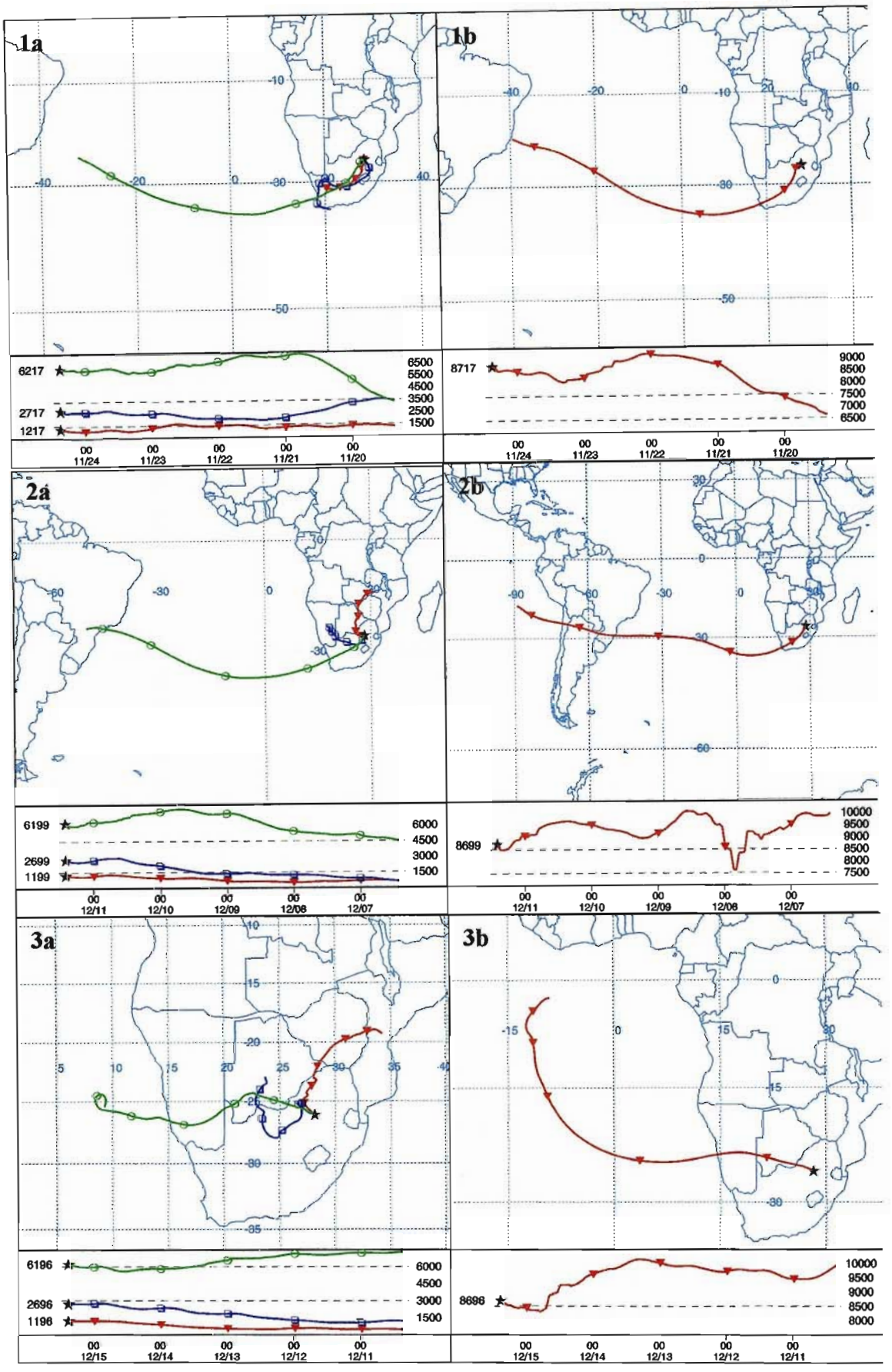

Figure C.4: continued (1) 24 November 1998, (2) 11 December 1998 and (3) 15 December 1998.
(a) Horizontal and vertical plots of back trajectories originating at 2.5, 4 and 7.5 km.
(b) Horizontal and vertical plots of back trajectories originating at 10 km

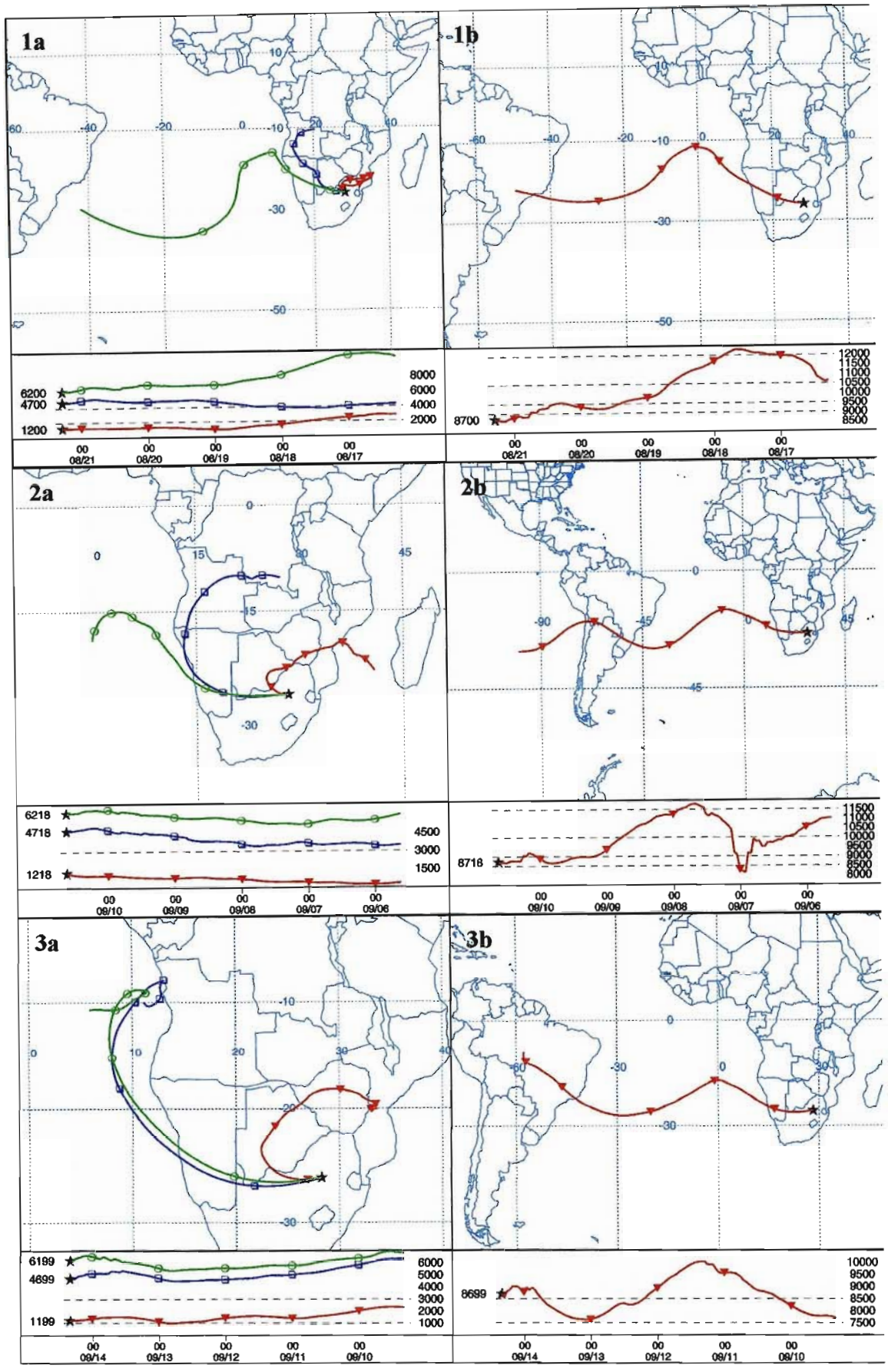

Figure C.5: 5-day back trajectory HYSPLIT model results for the pronounced layering category for (1) 21 August 1998, (2) 10 September 1998 and (3) 14 September 1998.
(a) Horizontal and vertical plots of back trajectories originating at 2.5, 6 and 7.5 km.
(b) Horizontal and vertical plots of back trajectories originating at 10 km

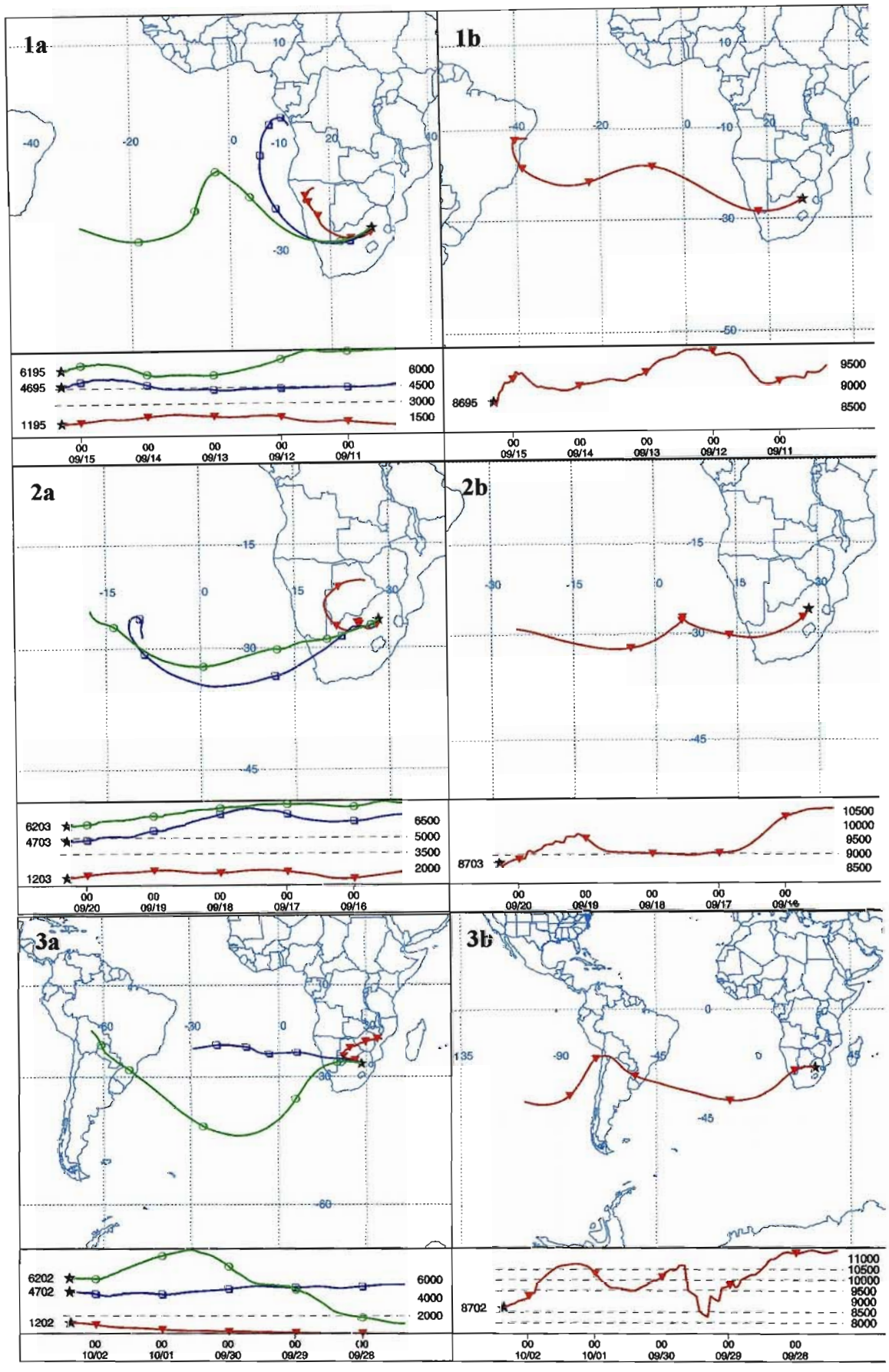

Figure C.5: continued (1) 15 September 1998, (2) 20 September 1998 and (3) 2 October 1998.
(a) Horizontal and vertical plots of back trajectories originating at 2.5, 6 and 7.5 km.
(b) Horizontal and vertical plots of back trajectories originating at 10 km

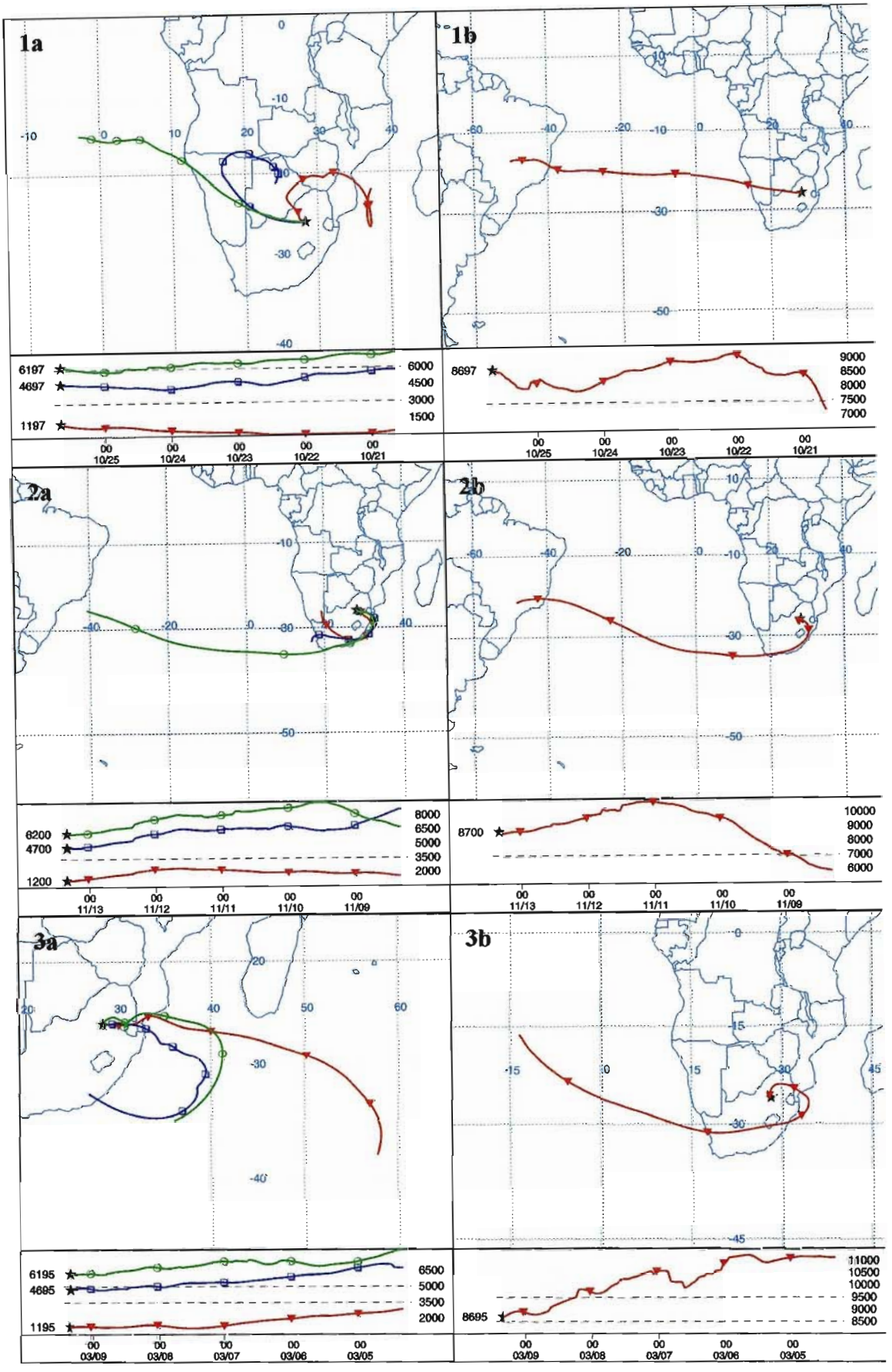

Figure C.5: continued (1) 25 October 1998, (2) 13 November 1998 and (3) 9 March 1999.
(a) Horizontal and vertical plots of back trajectories originating at 2.5, 6 and 7.5 km.
(b) Horizontal and vertical plots of back trajectories originating at 10 km

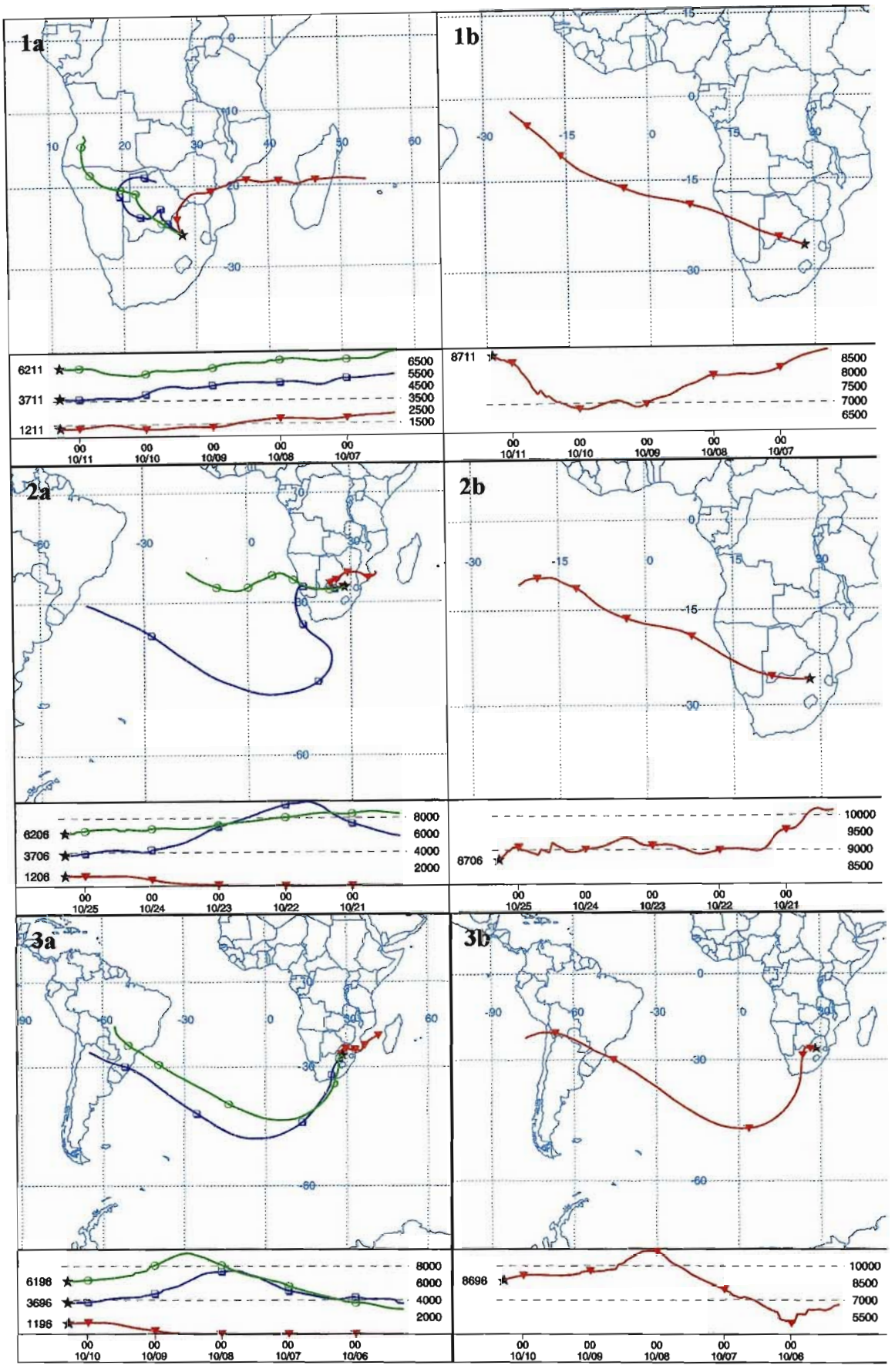

Figure C.6: 5-day back trajectory HYSPLIT model results for the considerable tropospheric enhancement category for (1) 11 October 1996, (2) 25 October 1996 and (3) 10 October 1997. (a) Horizontal and vertical plots of back trajectories originating at 2.5,5 and 7.5 km. (b) Horizontal and vertical plots of back trajectories originating at 10 km

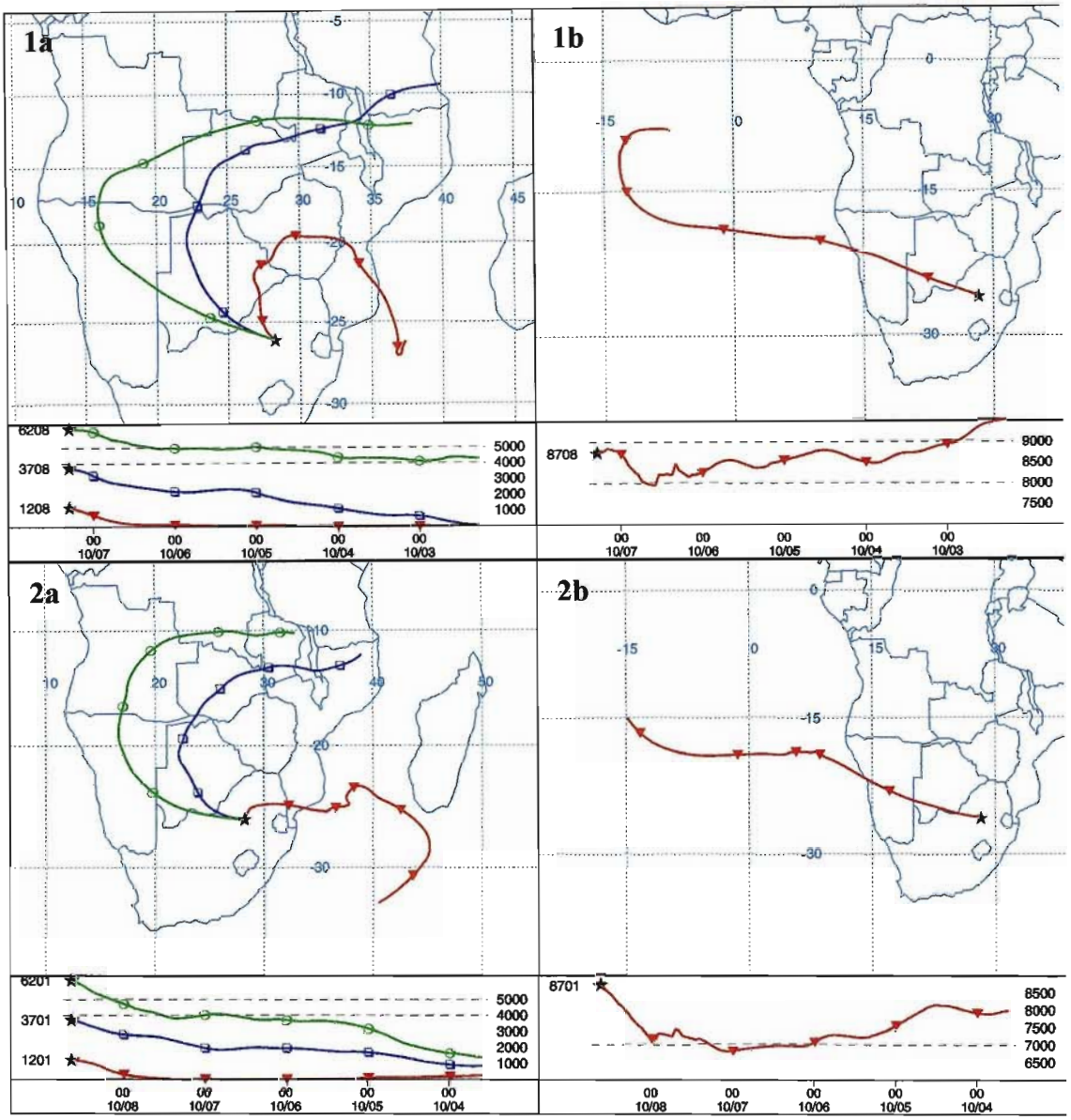

Figure C.6: continued (1) 7 October 1998 and (2) 8 October 1998.
(a) Horizontal and vertical plots of back trajectories originating at 2.5, 5 and 7.5 km.
(b) Horizontal and vertical plots of back trajectories originating at 10 km